TWR-5672

STUDY OF SOLID ROCKET MOTOR FOR SPACE SHUTTLE BOOSTER

VOLUME II TECHNICAL

BOOK 5 OF 5

APPENDICES E THRU H

by

Thiokol / WASATCH DIVISION

A DIVISION OF THIOKOL CHEMICAL CORPORATION

prepared for

NATIONAL AERONAUTICS AND SPACE ADMINISTRATION

George C. Marshall Space Flight Center

Contract NAS 8-28430
Data Procurement Document No. 314
Data Requirement MA-02

FINAL REPORT

STUDY OF SOLID ROCKET MOTOR FOR SPACE SHUTTLE BOOSTER

VOLUME II TECHNICAL

BOOK 5 OF 5

APPENDICES E THRU H

by

THIOKOL/WASATCH DIVISION
A Division of Thiokol Chemical Corporation
P.O. Box 524, Brigham City, Utah 84302

prepared for

NATIONAL AERONAUTICS AND SPACE ADMINISTRATION

15 March 1972

CONTRACT NAS 8-28430
Data Procurement Document No. 314
Data Requirement MA-02

George C. Marshall Space Flight Center
Marshall Space Flight Center, Alabama

Publications No. 0372-36175

APPENDIX E

RECOVERY SYSTEM CHARACTERISTICS FOR THIOKOL CHEMICAL CORPORATION SOLID PROPELLANT SPACE SHUTTLE BOOSTERS

GOODYEAR AEROSPACE
CORPORATION
AKRON, OHIO

RECOVERY SYSTEM CHARACTERISTICS FOR

THIOKOL CHEMICAL CORPORATION

SOLID PROPELLANT SPACE SHUTTLE

BOOSTERS

RSE-20207-24 February 17, 1972

GOODYEAR AEROSPACE CORPORATION
SPACE SHUTTLE BOOSTER RECOVERY

CODE IDENT NO. 25500

GOODYEAR AEROSPACE CORPORATION

AKRON 15, OHIO

RECOVERY SYSTEM CHARACTERISTICS FOR

THIOKOL CHEMICAL CORPORATION

SOLID PROPELLANT SPACE SHUTTLE

BOOSTERS

RSE-20207-24 February 17, 1972

TABLE OF CONTENTS

LIST OF FIGURES

LIST OF FIGURES (CONT.)

LIST OF FIGURES (CONT.)

LIST OF TABLES

SECTION I

INTRODUCTION AND SUMMARY

Preliminary parametric studies were performed by GAC to establish size, weight and packaging arrangements for aerodynamic decelerator devices that could be used for recovery of the expended solid propellant rocket motors used in the launch phase of the Space Shuttle System.

Computations were made using standard engineering analysis techniques. Terminal stage parachutes were sized to provide equilibrium descent velocities for water entry (V_T = 50,100,150 fps) that are presently thought to be acceptable without developing loads that could exceed the boosters structural integrity.

The performance characteristics of the aerodynamic parachute decelerator devices considered are based on analysis and prior test results for similar configurations and are assumed to be maintained at the scale requirements of the present problem. Weight relationships have been used which are based on the cube/square law of structural scaling, configuration geometry, material strength to weight ratios and empirical design and construction factors appropriate to the parachute configurations and operating environments of interest.

Representative base-line designs were selected to assess the requirements for ancillary equipment weights, bulk and packaging arrangements.

The effect of variations in the total system recovery weight and terminal descent velocity on the terminal stage parachute weight are graphically illustrated.

Preliminary analysis of an orientation system (uprighting and stabilization) has been conducted to establish basic design and weights. Several inflation system candidates are presented for relative comparison and evaluation.

The requirement for a refurbishment facility are presented and evaluate floor space and associated repair, and repack equipment, and a description of a refurbishment cycle.

Finally a top level program schedule, hardware quantity requirements, and cost has been created for a 445 launch operational schedule and associated Design Development, Test, and Evaluation program.

SECTION II

ANALYSIS

A. Terminal Stage Size Requirements

The aerodynamic performance characteristics for parachute decelerator devices appropriate to the present problem are shown in Figures 1, 2 and 3. Determination of the parachute size is obtained from the equation for equilibrium descent at standard sea level conditions which relates total system weight, decelerator size and terminal velocity by -

$$D_O = \frac{32.7}{V_T} \left[\frac{W_T}{(N)\ (\eta)\ C_{D_O}} \right]^{\frac{1}{2}} \qquad (1)$$

Where:

D_O is parachute reference (nominal) diameter, feet

V_T is system equilibrium descent velocity at sea-level, fps

W_T is total system weight, pounds

N is number of parachutes in a cluster

η is an efficiency factor that modifies the performance of a single parachute when operating in a cluster

C_{D_O} is the parachute nominal drag coefficient when operating as a single parachute.

For the relatively high canopy loadings (in the range of 3 to 30 psf) in equilibrium descent specified for the present applications, only ribbon or ring-slot type parachute canopies exhibit consistency of performance that is insensitive to canopy loading as shown in Figure 1. For this reason the ribbon-type parachute was selected for analysis.

Figure 2 illustrates the variation of the parachute performance efficiency term (η) as a function of the number of parachutes in a cluster. Figure 3 presents data indicating that under the specified canopy loading conditions for the present problem, the "decreasing factor" will have a value of about 1.0. This factor is of importance in establishing the strength and consequently the weight requirements for the parachute decelerators. Under lighter canopy-loading conditions, it accounts for the deceleration of a system during the inflation time of the canopy and would generally permit designs that require much less strength than that required to support a "steady" load at the initial deployment conditions. This would not be permitted in the present application as indicated by the trend of available data as shown in Figure 3. The means for limiting the magnitude of parachute loads at particular deployment conditions for the present application will be by the technique of reefing.

Figure 4 presents a plot of Equation 1 for the descent velocities of present interest and for several values for the number of parachutes in a cluster. The data of Figures 1 and 2 were considered in developing Figure 4. As noted on this figure, as the number of parachutes in a cluster exceeds 9 and the size of the parachute exceeds a nominal diameter of 135 feet, a higher technical risk for development must be expected since such configuration arrangements have not been practically demonstrated.

B. Parametric Weight Analysis

It can be shown that the weight for any structural device subjected to aerodynamic pressure loads (where minimum gage material thickness is not a limiting consideration) is related to the magnitude of the pressure loading, the cube of a characteristic reference dimension, the strength to weight ratio of the materials from which the device is manufactured, and the configuration geometry in relation to supporting the load. In terms of the several parameters, the weight relationship for a parachute system is -

$$W_{P_W} = (D.F)(N)(X)(R)(\eta)(C_{D_o})(S_o)(F)(q_D)(D_o)^3 \left[\frac{(C.F.)_1 \left(\frac{l_s}{D_o}\right)}{K_1} + \frac{(0.335)(C.F)_c \left(\frac{C_p}{C_{D_o}}\right)(\lambda)}{2K_c} \right] \quad (2)$$

For parametric analyses it is convenient to express equation (2) in the form of a weight fraction of total system weight as -

$$\frac{W_{P(N)}}{W_T} = (D.F.)(F)\left[\frac{\frac{q_o}{W_T}}{N \times R \eta C_{D_o} S_o}\right]^{g's} D_o \left[\frac{(C.F.)\ (1s/D_o)}{K} + \frac{(0.168)(C.F.)_c \left(\frac{C_p}{C_{D_o}}\right)(\lambda)}{K_c}\right] \quad (3)$$

It will be noted that the first bracketed quantity on the right-hand side of equation (3) corresponds to the loading conditions in terms of g's imparted to the system. It is thus convenient to relate this quantity in terms of the design maximum g-loads imparted to the system.

The several factors and coefficients of equations (2) and (3) are (with representative values appropriate for the selected ribbon-type parachute configuration) -

$W_{P_{(N)}}$ - weight of (N) number of parachutes, lbs.

W_T - Total recovered weight, lbs.

D.F. - Overall design factor including a margin of safety of 1.5; = 2.5

F - Factor to account for overloading of leading chute in a cluster; = 1.32: or opening shock factor for drogue parachutes; = 1.5

q_D - Dynamic pressure corresponding to maximum design g load imparted to system, e.g. at chute deployment, dis-reef or full-inflation stages.

N - Number of parachutes in a cluster.

χ - Decreasing factor; = 1.0 (see Figure 3)

R - Parachute reefed to full inflated drag area ratio.

η - Parachute cluster efficiency factor (See Figure 2).

C_{D_o} - Parachute nominal drag coefficient; = 0.5 for main parachutes, = 0.55 for drogue parachutes (see Figure 1).

S_o - Parachute nominal reference area ($= \frac{\pi}{4} D_o^2$), FT^2

D_o - Parachute nominal reference diameter, ft.

$(C.F.)_1$ Construction factor for parachute suspension lines; = 1.05.

$(1s/D_o)$ Ratio of parachute suspension line length to parachute nominal diameter; = 1.5 for main parachutes, = 2.0 for drogue parachute

K_1 - Suspension-line material strength to weight ratio; = 10^5 ft.

$(C.F.)_c$ Construction factor for parachute canopy accounting for seam overlaps, thread, re-inforcing, etc.; = 1.3

$C_{P_o/C_{D_o}}$ - Ratio of local (maximum) canopy pressure coefficient to nominal drag coefficient; = 2.0

λ - Ratio of canopy geometric cloth areas to nominal reference area; = 0.9.

K_c - Canopy material strength to weight ratio; = 10^5 feet (for ribbon construction)

Evaluating equation (3) for the numerical values indicated above where -

$$[G] \triangleq \left[\frac{q_D}{\frac{W_T}{N \times R \eta C_{D_o} S_o}}\right]_g$$

There is -

for the main parachutes -

$$\frac{W_P}{W_T}(N) = 6.5X10^{-5} [G](D_o)_{mains} \qquad (4)$$

for the drogue parachute

$$\frac{W_{P_d}}{W_T} = 9.83 \times 10^{-5} [G](D_o)_{drogue} \qquad (5)$$

Relationship (4) is used in conjunction with equation (1) or Figure 4 to establish the presentation of Figure 5 at a design load of 4 g's for the main parachutes.

Figure 6 illustrates the trend of recovery system weight fraction of total recovered weight as a function of design g-load for the main parachutes for representative recoverable space-shuttle booster applications. The ordinate scale has been adjusted by referencing the designs to their respective weight fraction value at the level of 4 g's. It can be seen that when a drogue deceleration stage is used the 4 g-design level for

the mains will result in a nearly optimum minimum parachute recovery system weight. Some improvement in recovery system weight can be realized with a drogue stage and 2-stages of reefing employed with the main at higher design-g-load. It is implicit, of course, that the basic booster (possibly using drag-flaps) would provide the proper deployment dynamic pressure conditions for the drogue.

To establish the size requirements for the drogue parachute it is necessary to determine the acceptable loading conditions at main parachute deployment. These are established as follows:

		MAINS AT 4g DESIGN LOAD	
$V_{T_{SL}}$ (fps) MAINS	q_T (psf)	1 STAGE REEFING	2 STAGE REEFING
50	2.975	47.6	190
100	11.89	190	650 (3.78g's/STAGE)
150	26.8	430	650 (2.5g's/STAGE)

It is appropriate that the drogue plus booster drag area provide a value for the terminal ballistic parameter that is at least 0.9 the permiseable main parachute deployment dynamic pressure, to assure deceleration to the required hand-off conditions within acceptable time and distance scales. The corresponding drogue deployment g's at a Mach number of 1.2 and altitude of 20,000 feet (q = 650 psi) are -

$V_{T_{MAINS}}$	g's AT DROGUE DEPLOYMENT 1 STAGE MAIN REEFING	g's AT DROGUE DEPLOYMENT 2 STAGE MAIN REEFING	Wp DROGUE (Eq 5) 1 STAGE MAIN REEFING	Wp DROGUE (Eq 5) 2 STAGE MAIN REEFING
50	14.28 (3.66-with 1 stage of drogue reefing)	3.58	$1.40X10^{-3}W_T$ D_{od} ($3.59X10^{-4}W_T$ D_{od})	$3.51X10^{-4}W_T D_{od}$
100	2.9	Drogue not Required	$2.85X10^{-4}W_T$	-
150	0.768	Drogue not Required	$0.767X10^{-4}W_T$ D_{od}	-

For the single booster configuration the calculated drag area is 222 ft^2 and for the 3 unit assembly 763 ft^2. The relationship for establishing the drogue parachute diameter is thus -

$$D_{od} = \left\{ \frac{4}{C_{D_O} \pi} \left[\frac{W_T}{q_{T_{\substack{\text{Booster} \\ \text{Drogue}}}}} - (C_D A)_{\text{Booster}} \right] \right\}^{\frac{1}{2}} \qquad (6)$$

Equation (6) can be substituted in relationship (5) and the drogue parachute weight can thus be determined directly in terms of the total recovered weight.

A riser line will usually be required to position the drogue parachute canopy at a distance aft of the booster base to assure adequate drag effectiveness. Experience has shown that for

drogue diameters equal to or greater than the forebody base diameter, a position 6.5 forebody base diameters aft will be adequate. The relationship for the riser line length used for the present analysis is thus -

$$I_R = 6.5\ d_B - 2\ D_{od} \tag{7}$$

The riser weight is obtained from -

$$W_R = (D.F.)\ (F)\ W_T\ \left[G\right] \cdot (l_R/K_1) \tag{8}$$

Where the terms and values are the same as those defined for relationships (3) and (5).

Figures 7, 8 and 9 present the combined drogue parachute and riser weight versus total recovered weight for the three desired terminal descent velocity conditions of interest and various combinations of main and drogue parachute reefing.

Figures 10 through 15 present the corresponding weight for the main parachutes.

Using the developed figures, representative recovery system characteristics are presented in Table I to assess requirements for ancillary equipments and packaging arrangements.

For reference purposes, terminal velocities of 50, 100 and 150 Ft/Sec will be referenced as A, B, C for Configuration I and II. Configuration II at 50 F/Sec has been eliminated from further consideration since parachute size is beyond the state of the art.

TABLE I - RECOVERY SYSTEM CHARACTERISTICS

SINGLE UNIT BOOSTER (CONFIGURATION I) PARALLEL BURN

CONFIGURATION	$V_{T_{SL}}$ (fps)	W_T (lbs)	W_P DROGUE / MAINS	N DROGUE / MAINS	D_O DROGUE / MAINS	G_S DROGUE / MAINS	q_∞ DROGUE / MAINS	R* DROGUE / MAINS
IA	50	160,000	2820 / 5550	1 / 9	40 / 136	3.58 / 4	650 / 190	NONE / 2 STAGES
IB	100	155,000	2175 / 3250	1 / 6	40 / 81	2.9 / 4	650 / 190	NONE / 1 STAGE
IC	150	150,000	535 / 2070	1 / 6	20 / 53	0.768 / 4	650 / 430	NONE / 1 STAGE
3 UNIT CLUSTER (CONFIGURATION(II) SERIES BURN								
IIA	50	585,000	11,180 / 39,000	1 / 9	79 / 260	1.79 / 4	650 / 47.6	1 STAGE / 2 STAGES
IIB	100	540,000	8,540 / 17,700	1 / 9	74 / 125	1.45 / 4	650 / 190	1 STAGE / 2 STAGES
IIC	150	520,000	3,840 / 11,500	1 / 9	38 / 83	0.768 / 4	650 / 430	NONE / 1 STAGE

*Loading conditions are defined to be balanced at each stage of operation.

C. Pilots, Risers, Mortars

Along with the drogues and main parachutes, additional components are required to deploy these devices into the airstream. Previous experience has shown that the most suitable method for this application is to utili › pilot parachutes to deploy the drogue and clusters of main parachutes. The pilot parachute will be deployed using a mortar device to eject it into the airstream. The following sub-sections present the criteria associated with pilot parachute, riser and mortar design criteria.

PILOTS

The pilot parachute is sized to provide an extraction force which will limit snatch forces of the parachute being deployed. Experience has shown that 10 g's acting on the packaging being deployed should be used as design criteria. The required extraction force is equated to be:

$$F_{EXT} = W_{PACK} \ (G'S) \qquad (9)$$

where:

F_{EXT} = Extraction Force

W_{PACK} = Weight of Package

G'S = Extraction Acceleration

the parachute size is related to this force by

$$F_{EXT} = qC_DA = qC_D \ \frac{\pi}{4} \ D_o^2 \qquad (10)$$

where q = free stream dynamic pressure

C_D = Drag Coefficient

A = Reference Area = $\pi/4\ D_o^2$

D_o = Nominal Reference Diameter

Figure 16 relates pilot D_o to the extraction force for a C_D = 0.55, 10 g's, and dynamic pressure of 47.6, 190, 430 and 650 PSF that are associated with drogue and main deployment conditions.

The weight of the pilots is given by

$$W_p = 6.5 \times 10^{-5} (G's)(W_{pack})(D_o) \qquad \text{(from Equation 4)}$$

Figure 17 shows pilot weight for varing diameters and four deployment dynamic pressures.

Based on weights for the drogue package and main packages, specific pilot size and weights have been defined for the two booster configurations and associated terminal velocities. This data is presented in Table II.

Risers

Parachute performance is dictated by two criteria. For single or clustered canopies, it is necessary to place the leading edge (shirt band) at a distance approximately 6.5 times the base diameter (max diameter) of the payload. For Configuration I and II the distance is 105 and 234 ft respectively. The riser length required is

$$L_R = X - L_S \qquad (11)$$

TABLE II - PILOT, RISER, MORTAR CONFIGURATION & WEIGHTS

SYSTEM CONFIGURATION	PILOT CONFIGURATION					RISER CONFIGURATION					
	DROGUE(1)		MAIN			PILOT				DROGUE	
						DROGUE		MAIN			
	DO (FT)	WGT (LBS)	QNTY	DO (FT)	WGT (LBS)	LENGTH (FT)	WGT (LBS)	LENGTH (FT)	WGT (LBS)	LENGTH (FT)	WGT (LBS)
IA	11.0	30	3	21	60	89.5	88.5	73.5	81.1	25	490
IB	9.0	20	2	19.6	45	91.5	88.3	75.6	72.2	25	357
IC	5.5	10	2	10	10	97.5	14.2	90	56.6	65	225
IIA	NOT CONSIDERED BECAUSE BEYOND STATE OF THE ART										
IIB	21	175	3	38.0	300	202.5	580	177	619	86	2260
IIC	13	45	3	20	100	214.5	217	204	450	158	1849

(1) 1 drogue pilot per booster

(2) Total weight for all risers required by cluster(6 or 9)

TABLE II (CONT.) - PILOT, RISER MORTAR CONFIGURATION & WEIGHTS

SYSTEM CONFIGURATION	MORTAR CONFIGURATION										
	MAIN		DROGUE PILOT[1]				MAIN PILOT				
	LENGTH (LBS)	WGT[2] (LBS)	DIAMETER (IN)	LENGTH (IN)	WGT (LBS)	MUZZLE VELOCITY FT/SEC	QTY	DIA (IN)	LENGTH (IN)	WGT (LBS)	MUZZLE VELOCITY FT/SEC
IA	88.5	1270	13.7	41.1	49.5	105	3	14.6	43.8	55.8	105
IB	20.2	291	13.2	39.6	46.9	105	2	13.7	41.1	48.6	105
IC	25.5	368	8.1	24.3	15.3	105	2	11.5	34.5	36.0	105
IIA	-	-	-	-	-	-	-	-	-	-	-
IIB	81.4	3990	25.9	77.7	735	235	3	27.5	82.5	827	235
IIC	109.5	54.00	18.2	54.6	409	235	3	23.3	69.9	610	235

Where L_R = riser length (ft

X = (6.5)(Base Diameter) (ft)

L_S = Suspension Line Length (ft) = 1.5 D_o

The riser length can be obtained directly from Figure 18 when the parachute D_o is known.

In addition to wake factors, for proper clustering riser length is dependent upon the number of canopies in the cluster and the relative size of the canopies. This criteria has been summarized in Figure 19 from Engineering Design Handbook - AMCD-706-130 for cargo delivery systems. For relation to this study, the data has been referenced to the nominal parachute diameter (D_o). The riser length required when 1.5 D_o suspension lines are used can be obtained directly as a percentage of the parachute D_o. For clusters of 6 and 9, optimistic values of this ratio are 0.25 and 0.65 respectively.

Riser weight is given by

$$W_R = (D.F.)(X)(W_p)(G's)\left(\frac{L_R}{K}\right) \qquad (12)$$

When D.F. = 2.5 - Design factors

X = 1.1 - Opening Shock

G's = 10.0

K = 10^5 Ft strength to weight ratio for nylon

$$W_R = 2.75 \times 10^{-4} (W) (L_R) \quad (13)$$

Riser lengths and weights for the pilot parachutes can be found in Table II.

For this main parachute the riser strength is given by Equation 12 except the X factor will reduce to 1.0 and G's = 4.0.

$$W_{R_{mains}} = 10^{-4} (W) (L) \quad (14)$$

Riser lengths and weights for both pilots and mains is presented in Table II for the respective sizes specified.

Mortar

The mortar size and weight is dependent upon two basic criteria:

1) Mass to be ejected
2) Muzzle velocity at mortar exit

The mass dictates the volume requirements and the mass and velocity provide strength requirements when the ejection energy is considered.

The mortar system defined in this report uses the Viking system mortar as a base of comparison. For its known weight, dimensions, ejected mass, muzzle velocity and internal pressure, scaled up criteria has been created for the booster recovery requirements. For a known ejected weight, mortar weight can be

obtained directly from Figure 20 for a muzzle velocity of 250 ft/sec., factor of safety equal to 20 and a length to diameter ratio of 3.0. The weight variation associated with changes in muzzle velocity are reflected in Figure 21

Using these two figures and muzzle velocities of 105 and 234 ft/sec for Conf I and II respectively, mortar weights for respective pilot sizes can be found in Table II.

Mortar size is dependent upon the mass to be ejected. For an assumed packing density of 35 pounds/ft^3, and an L/D = 3.0. The mortar diameter (D_m) can be shown to be

$$D_m = .230 \sqrt[3]{W} \tag{15}$$

and length is

$$L_m = .690 \sqrt[3]{W} \tag{16}$$

Mortar sizes have been established for the pilot parachute systems and is shown in Table II.

D. Orientation System

Orientation Device

The orientation device system is designed to rotate the booster after it is laying in the water to one of four roll positions. In each of the four positions a radio beacon and a flashing light will be visible from any approach direction. Positioning is accomplished by inflating 4 rows of inflatable spheres attached to the outside of the booster. The rows are located 90 degrees apart around the circumference. The locating beam and light are 180° apart from each other. The beacon and light are 45° from two of the rows of spheres, Figure 22.

Preliminary calculations indicated the water line will be 2.5 feet up for Configuration I and 4.0 feet up for Configuration II from the bottom of the cylindrical part of the booster and the booster will lie nearly level in the water. The minimum internal pressure necessary to maintain the shape of the spheres at a nominal depth of 4 feet is determined from the hydraulic head at the bottom of the sphere when it is underneath the booster, Figure 23.

The number of spheres of various diameters required to prevent the booster from rolling over in a sea state 4 condition with the row of spheres tending to right the booster completely submerged is presented in Figure 24.

Figure 25 presents the total weight of all four rows of sphere as a function of sphere diameter. This weight does not include the weight of the inflation system.

The results indicate that the 2-foot diameter sphere system is the lightest weight system, requiring 13 spheres in each row for Configuration I and 68 spheres in each row for Configuration II. Each row for Configuration II is 136 ft. long which seems impractical, and the larger numbers of spheres require more inflation hardware. Thus, it is recommended that two 3.6-foot dia. spheres per row be used on Configuration I and four 5-foot dia. spheres per row be used on Configuration II. The numbers recommended do not include allowances for damaged spheres.

Although spheres have been indicated in the above discussion, attachment considerations may result in modified configurations such as short cylinders curved about the booster periphery. Optimum longitudinal location of the orientation devices has not been determined at this time.

Inflation System

The orientation system, main parachute and drogue parachute all require inflation systems for their flotation bags. The three systems are essentially the same for Configuration I and II except they vary in size and weight. The preliminary requirements for the three systems are:

Inflated volume orientation system

- Configuration I — 49 cu ft at four positions
- Configuration II — 262 cu ft at four positions

Inflated volume main parachutes

- Configuration I — 5 cu ft for each of six parachutes
- Configuration II — 15 cu ft for each of nine parachutes

Inflated volume drogue parachute

- Configuration I — 11.4 cu ft
- Configuration II — 60 cu ft

Inflated pressure — 6 psig all units

Inflation initiation

- Orientation system - after water impact
- Drogue and main parachutes - after parachute deployment

Inflation time - not critical up to 5 minutes

Inflated life per cycle - 24 hours

Maximum storage temperature - 065 to 160°F

Maximum temperature in flight - +225°F

Deployment temperature limits

- air (ambient) — 40° to 95°F
- water (ambient) — 50° to 80°F

There are many candidate inflation systems that would meet the above requirements. Representative types are listed in Table III The systems shown in the table are not necessarily designed for the proposed system but the trends shown in the table are characteristic of each system. With this data and the selection criteria of high reliability and minimum development cost the possible system types can be reduced to either a gaseous nitrogen or gaseous nitrogen - carbon dioxide. Since weight is an important factor the potential system types can be reduced to a simple system, gaseous nitrogen carbon dioxide. The selection of this system type is tentative and must be reviewed in depth as additional design data becomes available and the selection criteria is specifically defined to meet the overall program philosophy.

Each of the gaseous nitrogen - carbon-dioxide systems would include 5000 psi gas storage cylinders, initiation valve, check valve on each bag for multiple bag systems, pressure relief valve, pressure regulator valve, recharging valve and associated plumbing. The storage cylinders are sized to provide make-up pressure for the 24 hour inflated life of each system.

The tentative weight for each inflation system is given in Table IV

TABLE IV INFLATION SYSTEM WEIGHT

	Configuration I	Configuration II
Orientation system (unit weight X 4 units)	120 LB	640 LB
Main Parachute (ea)	15 LB	20 LB
Drogue parachute	18 LB	40 LB

TABLE III - POTENTIAL INFLATION SYSTEM TYPES

SYSTEM TYPE	INFLATED VOL	INFLATED PRESS	INFLATION TIME	INFLATED LIFE	INFLATION GAS TEMP	SYSTEM WEIGHT	STORAGE PRESS	DEV STATUS	COMMENTS
Gaseous Nitrogen	195 cu ft	5 psig	≦ 4 sec	10 min	-311°F	≈200 lb	5000 psig	Developed	The system is heavy and the low gas inflation temperature causes fabric problems
Gaseous Nitrogen Carbon Dioxide Aspirated	195 cu ft	6 psig	≦ 4 sec	10 min	-80°F	117 lb	5000 psig	Developed	Induced air reduces storage vol and weight and also raised inflation gas temperature. CO_2 limits low temperature of inflation gas and increases storage density.
Chemically Heated Stored Gas	195 cu ft	6 psig	≦4 sec	10 min	300°F Max.	130 lb	5000 psig	Hardware Development Required	Inflation gas could be nitrogen or helium. Inflation gas temperature controlled by the amount of oxygen and nitrogen reacted by the catalyst.
Cool-Gas Generator	195 cu ft	6 psig	≦4 sec	10 min	200°F	≈66 lb	NH_3 -800 psia	Hardware Development Required	Initial inflation by NH_3 and propellant combustion. Pressure maintained by NH_3 gas. Pressure at inflation is approx. 1500 psia.
Gaseous Nitrogen Carbon Dioxide	139 cu ft	5 psig	≦7 sec	72 hrs	-80°F	86 lb	5000 psig	Developed	CO_2 limits low temperature of inflation gas and increases storage density.
Gaseous Nitrogen Carbon Dioxide	50 cu ft	5 psig	≦7 sec		-80°F	32 lb	5000 psig	Developed	CO_2 limits low temperature of inflation gas and increases storage density
Cool-Gas Generator	6 cu ft	300 psia	≦.050 sec		500°F	21 lb	Low Press	Hardware Development Required	Decomposition products are ammonia, carbon dioxide and steam
Cool-Gas Generator	12 cu ft	300 psia	≦.050		500°F	44 lb	Low Press	Hardware Development Required	Decomposition products are ammonia, carbon dioxide and steam

E. Sequencing System

A typical logic circuit schematic for a sequencer is presented in Figure 26 for reference only. This circuit is for an aerial retrieval type system and starts at a higher altitude than would be used for the present program. This typical recovery logic circuit consists of relays, barometric switches, pyrotechnic devices, resistors, diodes and associated electrical hardware. Two redundant, electrically isolated circuits, are used, although only one is shown in the sketch. The circuitry also provides additional reliability by including cross-overs between sequence channels. The recovery system is armed by a signal from the missile logic circuit, which energizes relays K1 and/or K2 in the recovery section. Then the signal from the missile logic circuit initiates booster separation and/or removes the recovery system cover.

The drogue chute or drogue pilot is mortared during missile descent when the barometric switch senses 30,000 feet attitude. The mortar circuit is initially locked out until the recovery system is armed and the vehicle is safely above 30,000 feet. The baroswitch is shown in the "less than 30,000 feet" position, and the open contact SQ9-3 prevents mortar firing. During vehicle flight above 30,000 feet, the baroswitch will be in the normally open position; if the recovery system is armed, pyroswitch SQ9 will be energized, closing contact SQ9-3, thereby enabling the mortar circuit. Upon descent to 30,000 feet, the baroswitch re-closes and fires the mortar cartridge initiator deploying the drogue.

After a half-second delay, the cartridge initiator circuit is cleared when SQ11-3 opens. At this time, SQ11-4 closes and a 20-second time delay (SQ-13) is energized (20 seconds is an approximate time for drogue chute operation prior to main chute deployment).

After the time delay, contact SQ13-3 closes and a heat shield shaped charge detonator SQ5 is energized. The heat shield is thus severed from the recovery section. Since the drogue is attached to the heat shield, which in turn is attached to the main chute deployment bag, the drag from the drogue parachute thus pulls out the main chute.

The circuit redundancy is illustrated in the sketch below.

Further reliability is achieved by employing cross-overs between sequence A and B, as illustrated by the use of contact K2 in sequence A and contact K1 in sequence B. By cross-over implementation, the operation of one sequence will not be completely lost if an early event is not obtained.

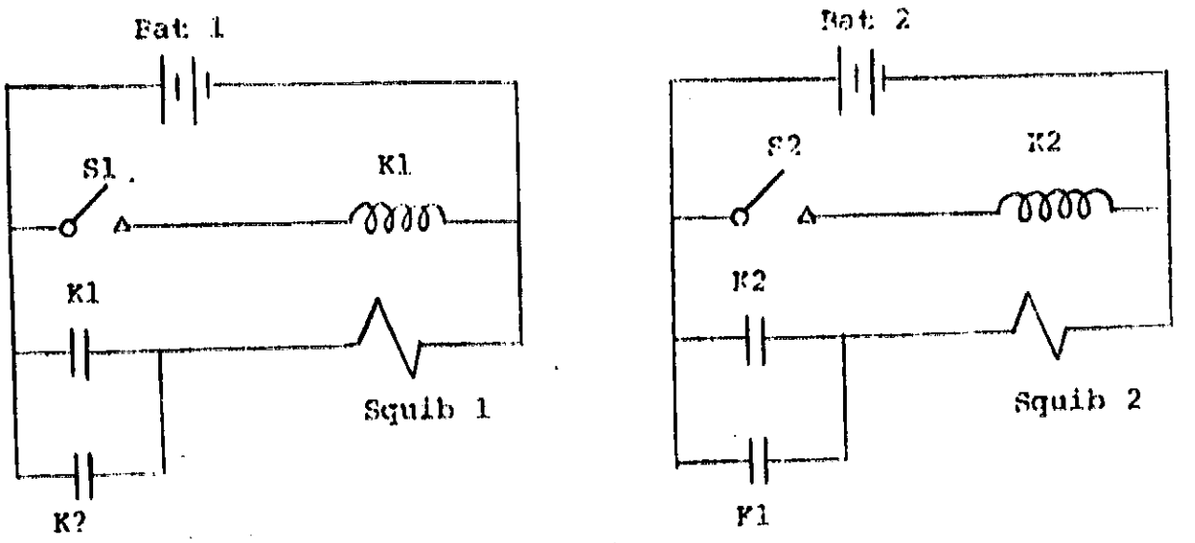

Sequence A

Sequence B

Each sequence has its own power supply. The choice of batteries will be determined considering the test facility requirements. The voltage and capacity rating will also be determined at that time and will be based on the recommended fire currents of the pyrotechnic devices, their resistance, circuit contact resistance, wiring resistance, current limiters and internal battery resistance.

The recovery section will contain a test, safe and arm connector as indicated by J1 on the sketch. Battery leads are also routed through an internally available connector for charging and checking the batteries.

To aid in locating the booster when it is in the water two radio beacons and flashing lights will be located 180 degrees apart on the body of the booster. The sequencer or mini-computer initiates the water retrieval aids system either at the start of recovery or water impact.

The radio beacon can be ordered for the desired frequency. A 1/4 wave stub antenna or flush antenna which operates on or near the standard Mayday frequency (243 MHz) is typical.

The flashing light emits flashes of 500,000 lumens intensity at the rate of 20 to 30 per minute and it and the beacon will operate for 36 hours on its own power supply. The duration of operation is a function of the battery furnished for the system.

F. Recovery System Weight Summary

Presented in Table V are weights for the Drogue, Main, and Orientation Sub-Systems. The weights are not the totals for the complete sub-system package but only those parts which have been defined in the preceeding sub-sections. Component weights which have been omitted are described in the foot notes at the bottom of the table.

The total weights which are presented are the assumed maximum anticipated and are obtained by applying experience factors to the weights for the mains and drogues.

More accurate total system weight estimates can be obtained after additional components have been established.

TABLE V - ESTIMATED RECOVERY SYSTEM TOTAL WEIGHT

SYSTEM CONFIGURATION	DROGUE SYSTEM WGT(1) (LBS)	MAIN SYSTEM WGT (2) (LBS)	ORIENTATION SYSTEM WGT(4) (LBS)	TOTAL RECOVERY SYSTEM WGT(3) (LBS)	% OF EMPTY BOOSTER WGT
IA	2988	7410	130	16,000	11.1
IB	2330.2	3872.6	130	11,000	7.75
IC	575	2643	130	6,000	4.2
IIB	10,030	26,928	680	49,000	10.0
IIC	4,511	20,380	680	29,000	5.9

(1) This weight does not include: Deployment Bags, Bridles, Riser Connectors, Bridle, Attachment/Disconnects, Flotation and Beacons.

(2) This weight does not include: Deployment Bags, Riser Connectors, Attachment/Disconnects, Reefing Systems, Flotation and Beacons.

(3) Assumed maximum weight and includes all items omitted in (1) and (2).

(4) Preliminary values based on optimum design considerations.

SECTION III
CONCEPT DESIGN

A. General

The parametric analysis as described in the preceeding section has provided basic sizes and weights for the primary components of the parachute recovery system required for proper deceleration to the desired terminal velocity conditions of 50, 100, and 150 Ft/Sec for both the parallel burn Configuration I and series burn Configuration II. Presented in Figures 27 and 28 are dimensional characteristics of Configuration I and in Figure 29 and 30 those of Configuration II as specified to Goodyear Aerospace Corporation by Thiokol Chemical Corporation. Presented in the following subsections are the deployment sequence for the recovery system and the preliminary approach to the packaging and stowage of the parachutes and mortar portions of the recovery system.

B. Deployment Sequence

Presented in Figures 31 , 32 , and 33 are a schematic representation of the anticipated recovery sequence for the Configuration I booster (2 required per launch) for a 100 Ft/Sec impact velocity. Figure 32 depicts the ejection of the drogue/pilot parachute from its mortar. The mortar imparts kinetic energy to the packaged pilot, sufficient to fully extend the pilot and its riser. As the bag detaches, the pilot is permitted to inflate, and in turn extract

the drogue parachute from its compartment. As the drogue bag detaches the apex of the drogue, the drogue inflates and decelerates the booster to a condition compatible with main parachute deployment

Because of the instability of the booster, prior to drogue deploy, it is assumed that a three legged bridle will be required to transfer load into the booster structure. This method will provide a straight line pull through the booster centerline.

After a predetermined time on the drogue, (compatible with proper deceleration to the main parachute deployment conditions) each leg of the drogue bridle will be severed at the vehicle with a pyrotechnic release mechanism. The drogue will separate from the booster. Shortly after separation 2 additional mortars will be simultaneously fired and each eject a main/pilot into the airstream(figure 32). These pilots will inflate and each extract a package containing a cluster of three main parachutes. As the main bag detaches the canopies apex, the parachutes will inflate to a reefed shape(figure 33). After a predetermined time, reefing cutters initiated during the bag stripping phase, severes the first stage reefing time and permits the canopies to inflate to a larger drag area. After an additional predetermined time this second stage of reefing is also severed, permitting the main parachute to fully inflate(figure 33) and achieve final deceleration to the desired impact velocity. Each cluster of three parachutes will have a single attachment point at the periphery of the booster base.

Although not shown, these main parachutes will disconnect from the booster at water impact. Flotation balloons inside the parachutes will inflate and location aid initiated for recovery and subsequent refurbishment of the main parachutes. A similar event is anticipated for the drogue.

Additionally, the booster orientation and location system(beacon) will be actuated and properly position the booster for acquisition and recovery.

A similar sequence of events will occur for the Configuration II booster as depicted in Figure 34, 35, and 36. The primary basic difference is that three main/pilots must be deployed to extract the three clusters of three main parachutes(Figure 35). Each cluster will attach at the booster base and be 120° apart.

C. Packaging/Stowage

Configuration I

Presented in Figure 37 is the presently anticipated approach to packaging of the pilot mortars, drogues, and main parachutes. In general the base diameter of the booster has been increased by approximately thirty inches and this diameter extended forward approximately 45 inches. A cone frustum will connect the 156 inch basic booster base, to the 225 inch cylindrical section.

This increase in base diameter is required to provide a straight line extraction of the drogue and main parachute package. The general sizes depicted for the drogue and main stowage compartments is approximately to scale for the weights presented in Section II.

Although not shown, the reaction loads of the mortars and deceleration loads of the parachute will be transferred into the basic booster structure through added metal structure.

It is presently assumed that the inflation system for the orientation system will be housed within the flare portion of the aft skirt.

Shown in Figure 38 is slightly more detail of aft end of the booster. Drogue bridle stowage and "hard point" load transfer locations are depicted.

Configuration II

Figure 39 presents the general approach for storage of the recovery system components. The "Clover Leaf" must be modified to provide stowage volume for the three groups of main parachutes, and their pilots and mortars. The drogue parachute and its pilot and mortar will be placed at the center of the three nozzles. It is assumed that the nozzles will be positioned at a zero angle prior to drogue/pilot mortar fire.
The shapesof the main packages have been established to provide a minimum increase in base area.

As with Configuration I additional structure will be required to transfer load from the mortars and parachutes into the basic booster structure.

Additional volume at the aft end or some other position along the boosters length can be used for orientation system and inflation system stowage.

Figure 40 provides more detail of hard point locations and drogue bridle routing for Configuration II.

SECTION IV

REFURBISHMENT AND TURN AROUND

Configuration I-B

A. Introduction

This refurbishment plan is based on the use of 12 each 81 Ft D_o main chutes; 4 each 20 Ft D_o pilot chutes (main); 2 each 40 Ft D_o drogue chutes; 2 each 9 Ft D_o pilot chutes (drogue), for each mission.

The assumption is made that 10 of the 12 main chutes will be refurbishable; that both drogues will be refurbishable; that all pilots and deployment bags are expendable.

Additionally it is assumed that all rigging and packing will be accomplished as part of the refurbishment plan. Thus:

10 Mains refurbish, rig and pack
2 mains new, rig and pack only
4 pilot chutes (main) rig and pack only
2 drogue chutes, refurbish, rig and pack
2 pilot chutes (drogue) rig and pack only

B. Scope

The scope of this plan includes off-loading of the recovered parachutes on the dock of the refurbishment facility through the parachute packing cycle and return to inventory awaiting delivery to the mission vehicle.

C. Requirements

The facility floor plan and equipment requirements are presented in Figure 41 and Table VI respectively. With certain notable exceptions the required equipment is comprised of "off the shelf" items. Where these exceptions exist they have been annotated TBD (To Be Designed)

D. Refurbishment Cycle

The following is a "walk through" in operation sequence from off loading through parachute packing, describing the planned methods and identifying the equipment, used for the main parachutes. This cycle is also presented in Schedule format in Figure 43.

1. (a) Remove chutes from transportation containers.

   (b) Engage hoisting hook through apex bridle.

   (c) Remove flotation gear.

   (d) Hoist each chute (of a cluster) and separate into individual chutes.

   (e) Untangle and defoul suspension lines

   Equipment:

   Electrically operated hoist, individually motorized, tracked to an over head monorail. Monorail will be of closed loop design. Ref.Figure 41. 1 hoist required per chute.

TABLE VI FACILITY AND EQUIPMENT REQUIREMENTS

Basic Facility:

400 Ft X 420 Ft, 100 Ft high (168,000 Ft^2)

Overhead lighting. 60 Ft candles

Environmental controls. $75^{\circ} \pm 10^{\circ}$(F) and 50 ± 20% R.H.

Air and electric outlets. 95 psi, 110/220/440V

Shop vacuum

Equipment:

Fork Lift 1 required

Overhead monorail system. Race track design with individually motorized, Electric hoists. 1 hoist required per parachute.

Washing containers. Volume of approx. 500 ft^3. 3 required (TBD)

Drying room/oven: Gas fired, floor ducted, forced air to maintain 160° to 180° (F). 1 required

Drop off table 220' x 10' (approx). 1 required

Inspection table 80' x 6' (approx). 1 required per chute

Work table 70' x 18' (approx). 1 required per chute

Packing table 150' x 6' (approx). 1 required per chute

Conveyor belt extension 50' x 6' (approx.) 1 required per chute (TBD)

Electric winch, reversible: capacity (to be determined)

1 required per packing table

1 required per inspection table

TABLE VI-(Cont)-FACILITY AND EQUIPMENT REQUIREMENTS

Sewing Machines:

2 each heavy duty Singer No. 97-10

3 each heavy duty Singer No. 114-204

3 each heavy duty Singer No. 144-204

3 each repair table Singer No. 111W-153

3 each repair table Singer No. 107W-3

3 each repair table Singer No. 17W-15

Overhead traveling crane system

Parachute packing press and fixture

1 required per cluster of main chutes (TBD)

Drogue and pilot chute packing press and fixture

2 required (TBD)

Y-Bar, floor stand mounted

2 per table inspection

2 per table packing

Suspension line combs

1 per packing table (TBD)

Tape Recorders

(TBD) To Be Designed

2. (a) Move hoist and chutes into wash area (3 at a time)

(b) Lower chutes into individual washing tanks

(c) Soak in fresh water, air agitated.

Equipment:

Three containers approx 500 Ft^3 each

Fresh water supply

Water drains

3. (a) Move hoist and chutes into drying room.

Dry in elevated temperature environment (160^{o}-$180^{o}F$

Equipment:

Forced air, floor ducted, gas furnace

4. (a) Move hoist and chutes to drop-off table.

(b) Use electric winch to stretch out and maintain tension on canopy and lines.

(c) Perform gore by gore and line by line inspection. Use voice recorders for initial documentation of damage; also flag the damaged areas.

(d) Transcribe on permanent records (damage report and damage chart) description and location of damage.

Equipment:

Drop off table 220' x 10 (approx.)

Inspection table 80' x 6' (approx.). 1 per chute.

Electric winch, mounted on flip up, flip down section of table top. 1 per table.

Y-Bar, mounted on floor stand 65 in. high. 2 per table.

5. Engineering decision:

   Repair or not repairable.

   If repair, engineering will furnish direction using a pre-planned set of repair procedures.

   If not repairable, use traveling crane to move chute to segregated area.

6. Use traveling crane to move repairable chute to repair area.

   Equipment:

   Traveling crane

7. Repair as necessary

   Equipment:

   Work table 70' x 18' (approx.)

   Standard Sewing Machines

8. Move repaired chute to ready area by traveling crane, or to packing table.

9. (a) Rig and install floatation

   (b) Install reefing system

   (c) Packing procedure. One cluster packed incrementally in a single compartmented deployment bag. Pressure pack 35 lb/Ft^3 (approx.)

   (d Equipment:

   Packing table 125' x 6' with conveyor

   Belt extension 50' x 6' 1 per chute

   Packing press and fixture 1 required per cluster

   Electric winch 1 per table

   Y-Bar 2 per table

10. Move parachute pack assy. to inventory stores. End of cycle

Configuration II-B

A. Introduction

This refurbishment plan is based on the use of 9 each 125 Ft D_o main chutes; 3 each 38.0 Ft D_o pilot chutes (main); 1 each 74 Ft D_o drogue chute; 1 each 21 Ft D_o pilot chute (drogue), for each mission.

The assumption is made that 7 of the 9 main chutes will be refurbishable; that the drogue will be refurbishable; that all pilots and deployment bags are expendable.

Additionally it is assumed that all rigging and packing will be accomplished as part of the refurbishment plan. Thus

7 Mains refurbish, rig and pack

2 mains new, rig and pack only

3 pilot chutes (main) rig and pack only

1 drogue chutes, rufirbish, rig and pack

1 pilot chutes (drogue) rig and pack only

B. Scope

The scope of this plan includes off-loading of the recovered parachutes on the dock of the refurbishment facility through the parachute packing cycle and return to inventory awaiting delivery to the mission vehicle.

C. Requirements

The facility floor plan and equipment requirements are presented in Figure 41 and Table VII respectively. With certain notable exceptions the required equipment is comprised of "off the shelf" items. Where exceptions exist they have been annotated TBD (To Be Designed).

D. Refurbishment Cycle

The following is a "walk through" in operational sequence from off-loading through parachute packing, describing the planned method and identifying the equipment used, for the main parachutes. This cycle is also presented in schedule format in Figure 44.

1. (a) Remove chutes from transportation containers.

   (b) Engage hoisting hook through apex bridle.

   (c) Remove flotation gear.

   (d) Hoist each chute (of a cluster) and separate into individual chutes.

   (e) Untangle and defoul suspension lines.

   Equipment:

   Electrically operated hoist, individually motorized, tracked to an over head monorail. Monorail will be of closed loop design. Ref. Figure 41.1 hoist required per chute.

TABLE VII FACILITY AND EQUIPMENT REQUIREMENTS

Basic Facility:

400 Ft x 350 Ft, 100 Ft high (140,000 Ft^2)

Overhead lighting. 50 Ft candles

Environmental controls. $75^{\circ} \pm 10^{\circ}$(F) and 50 ± 20% RH

Air and electric outlets - 95 psi, 110/220/440V

Shop vacuum

Equipment:

ForkLift 1 required

Overhead monorail system. Race track design with individually motorized, Electric hoists. 1 hoist required per parachute.

Washing containers. Volume of approx. 700 Ft^3. Fitted with water agitation system. 3 required (TBD)

Drying room/oven: gas fired, floor ducted, forced air to maintain 160° to 180°(F). 1 required

Drop off table 220' x 10' (approx.). 1 required

Inspection table 80' x 6 (approx.). 1 required per chute.

Work table 70' x 18'.(approx.). 1 required per chute.

Packing table 200' x 6' (approx.). 1 required per chute.

Conveyor belt extension 70' x 6' (approx.) 1 required per chute (TBD)

Electric winch, reversible, capacity(to be determined)

1 required per packing table
1 required per inspection table

Sewing Machines:

2 ea. heavy duty Singer No. 97-10
3 ea. heavy duty Singer No. 114-204
3 ea. heavy duty Singer No. 144-204
3 ea. repair table Singer No. 111W-153
3 ea. repair table Singer No. 107W-3
3 ea. repair table Singer No. 17W-15

TABLE VII -(Cont) - FACILITY AND EQUIPMENT REQUIREMENTS

Overhead traveling crane system

Parachute packing press and fixture. 1 required per cluster of main chutes (TBD)

Drogue and pilot chute packing press and fixture. 2 required (TBD)

Y-Bar, floor stand mounted

2 per table inspection

2 per table packing

Suspension line combs

1 per packing table (TBD

Tape Recorders

2. (a) Move hoist and chutes into wash area (2 at a time).

(b) Lower chutes into individual washing tanks.

(c) Soak in fresh water, air agitated.

Equipment:

Three containers approximately 700 Ft^3 each.

Fresh water supply

Water drains

3. (a) Move hoist and chutes into drying room.

Dry in elevated temperature environment (160° - $180^{\circ}F$)

Equipment:

Forced air, floor ducted, gas furnace.

4. (a) Move hoist and chutes to drop-off table.

(b) Use electric winch to stretch out and maintain tension on canopy and lines.

(c) Perform gore by gore and line by line inspection. Use voice recorders for initial documentation of damage; also flag che damaged areas.

(d) Transcribe on permanent records (damage report and damage chart) description and location of damage.

Equipment:

Drop off table 220' x 10' (approx.).

Inspection table 80' x 6' (approx).1 per chute.

Electric winch, mounted on flip up, flip down section of table top. 1 per table.

Y-Bar, mounted on floor stand 65 in. high. 2 per table.

5. Engineering decision:

   Repair or not repairable.

   If repair, engineering will furnish direction using a pre-planned set of repair procedures.

   If not repairable, use traveling crane to move chute to segregated area.

6. Use traveling crane to move repairable chute to repair area.

   Equipment:

   Traveling crane

7. Repair as necessary

   Equipment:

   Work table 70'x 18' (approx)

   Standard Sewing Machines

8. Move repaired chute to ready area by traveling crane, or to packing table.

9. (a) Rig and install flotation gear.

   (b) Install reefing system.

   (c) Packing procedure. One cluster packed incrementally in a single compartmented deployment bag. Pressure pack 35 lb/Ft^3 (approx).

   Equipment:

   Packing table 200' x 6' (approx) with conveyor.

   Belt extension 70' x 6'. 1 per chute.

   Packing press and fixture. 1 required per cluster.

   Electric winch. 1 per table

   Y-Bar

10. Move parachute pack assy. to inventory stores. End of cycle.

SECTION V HARDWARE REQUIREMENTS, SCHEDULE AND COSTS

Figure 45 Operational Hardware Requirements

The hardware required to support a 445 launch schedule is included for both configuration IB and IIB. It is believed that the drogues parachutes can be refurbished four (4) times and the main parachutes refurbished five (5) times before they are discarded. All pilot parachutes and associated equipment will be lost. It is planned to have at least one (1) new parachute for each launch cluster. Spares are not included.

Figure 46 Schedule

A very preliminary schedule is included. It is comparable to either configuration IB or IIB. It indicates that PDR is possible at the end of 12 months and CDR is possible by the end of 36 months. The first qualified launch set could be available within 5 years from contract go-ahead.

Figure 47 Rough Order of Magnitude (ROM) Estimate

The estimated price for furnishing the solid rocket motor recovery system was arrived at by using actual costs of much smaller but similar program conducted a: GAC. These costs were then ratioed upward to accommodate the new weights, sizes, complexity and quantities required. Also, the rates used for establishing the ROM were based upon 1970 actual rates. No attempt was made to esculate labor and material estimates over the proposed program calendar schedule.

DRAG COEFFICIENT VS TERMINAL CANOPY LOADING

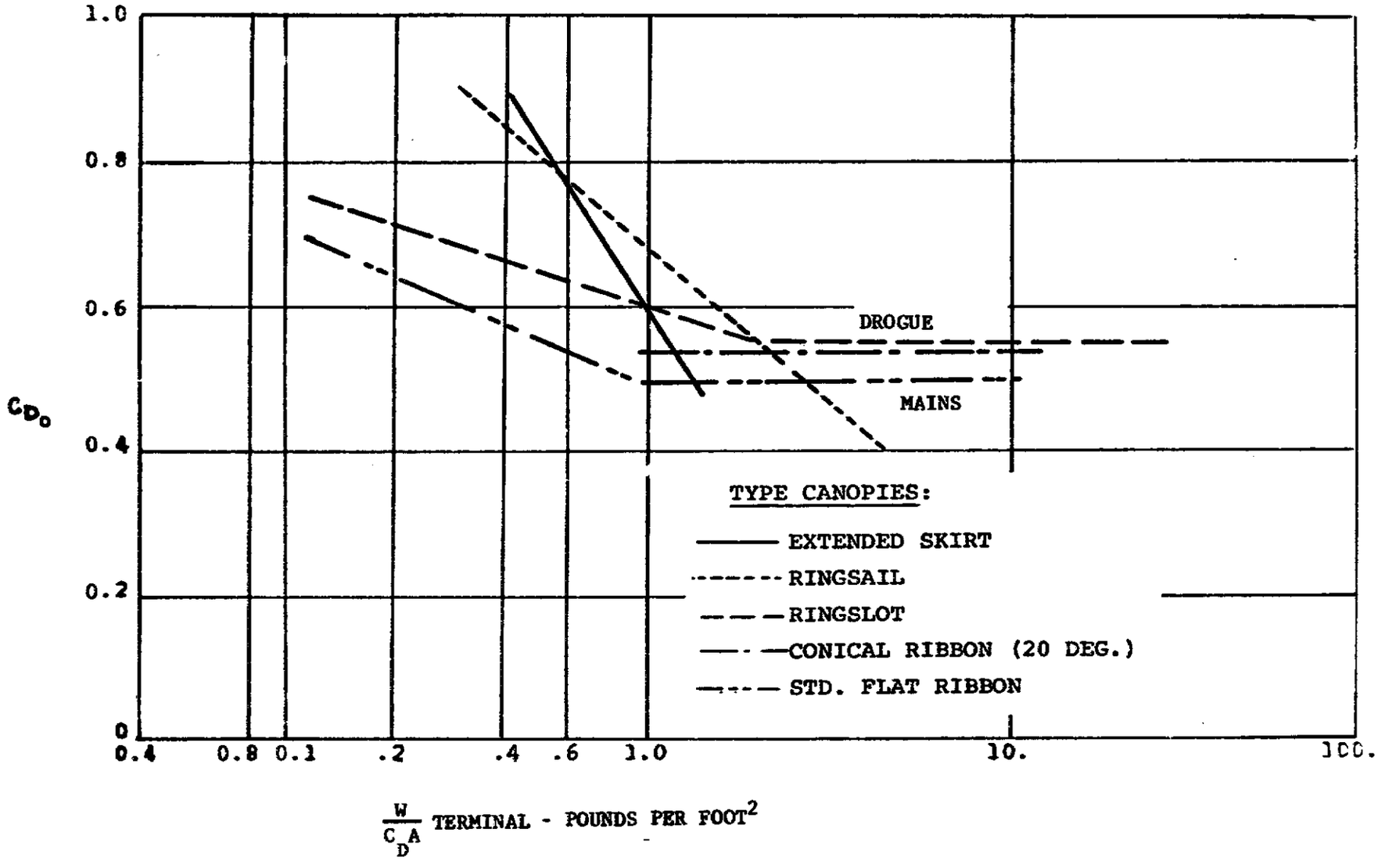

FIGURE 1

PARACHUTE CLUSTER EFFICIENCY

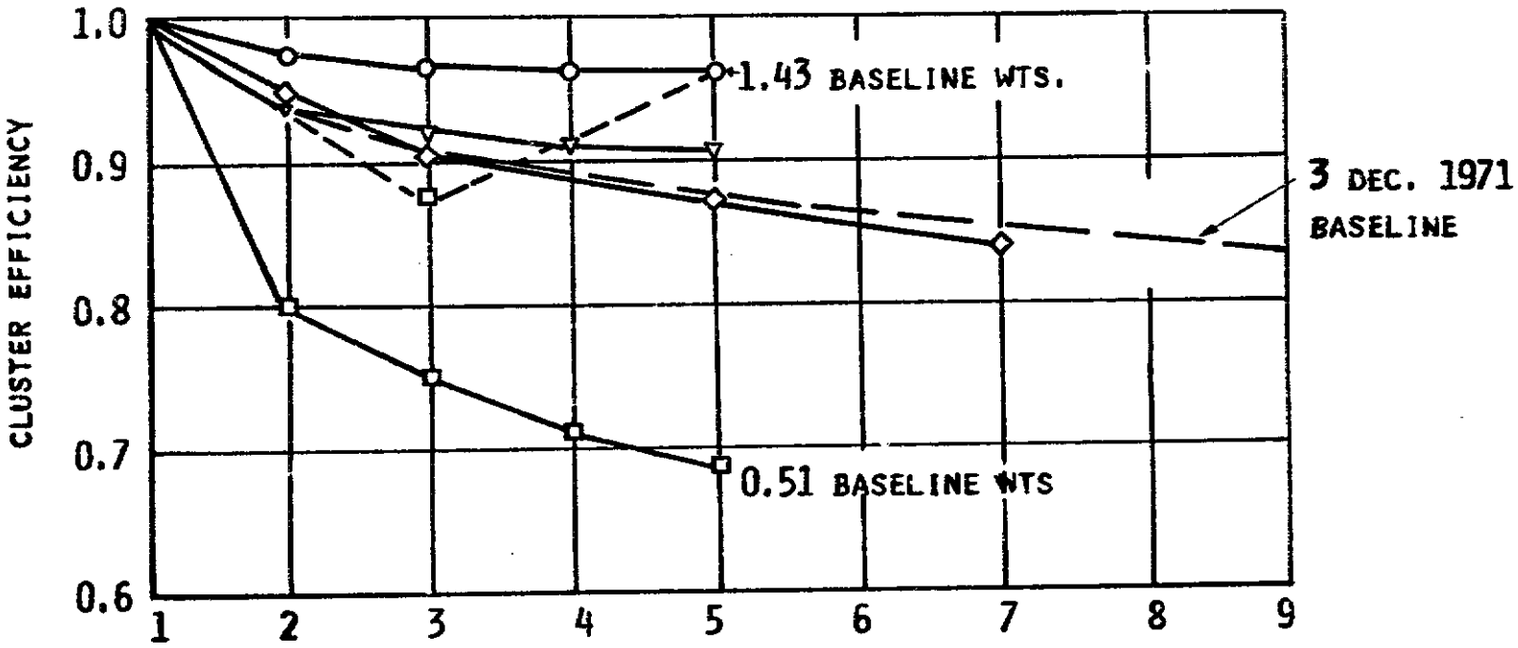

REF. - RAE TN AERO 1611, D_0 = 2.86 FT

- ○ RISER - 1.4 D_0, L_S=0.7 D_0
- ▽ RISER - 0.7 D_0, L_S=0.7 D_0
- □ RISER - NONE, L_S=0.7 D_0

REF. - ASD TDR 63-159, D_0 = 2.0 FT

- ◇ RISER - .5 D_0, L_S = 1.0 D_0

} WIND TUNNEL

REF - FTC TR-69-35, D_0 = 135 FT

- □ RISER - 1.25 D_0, L_S = 1.00 D_0

} PARACHUTE DROPS FROM 1800 FT ALT; 140 KNOTS UP TO 50,000 LB PAYLOAD

FIGURE 2

DATA REF.

T-1 - PARATROOPER
T-2 - SINGLE REEFED 135 FT D_0 STD FLAT (9000 LB PAYLOAD)
T-3 - REEFED CLUSTER OF 5 - 135 FT D_0 STD FLAT (50,000 LB PAYLOAD)
T-4 - SAME AS T-3 WITH ONE OR TWO LEADING CHUTES
T-5 - SINGLE REEFED 76 FT D_0 CONICAL RIBBON (35,000 LB PAYLOAD)
T-6 - SINGLE REEFED 76 FT D_0 CONICAL RIBBON (45,000 LB PAYLOAD)

BASELINE VALUES

D-1 - DISREEFED CLUSTER: 9-100 FT D_0 RIBBON
D-2 - REEFED CLUSTER: 9-100 FT D_0 RIBBON
D-3 - SAME AS D-1 FOR ONE LEADING CHUTE
D-4 - FULLY OPEN DROGUE: ONE 60 FT D_0 RIBBON
D-5 - SAME AS D-2 FOR ONE LEADING REEFED CHUTE

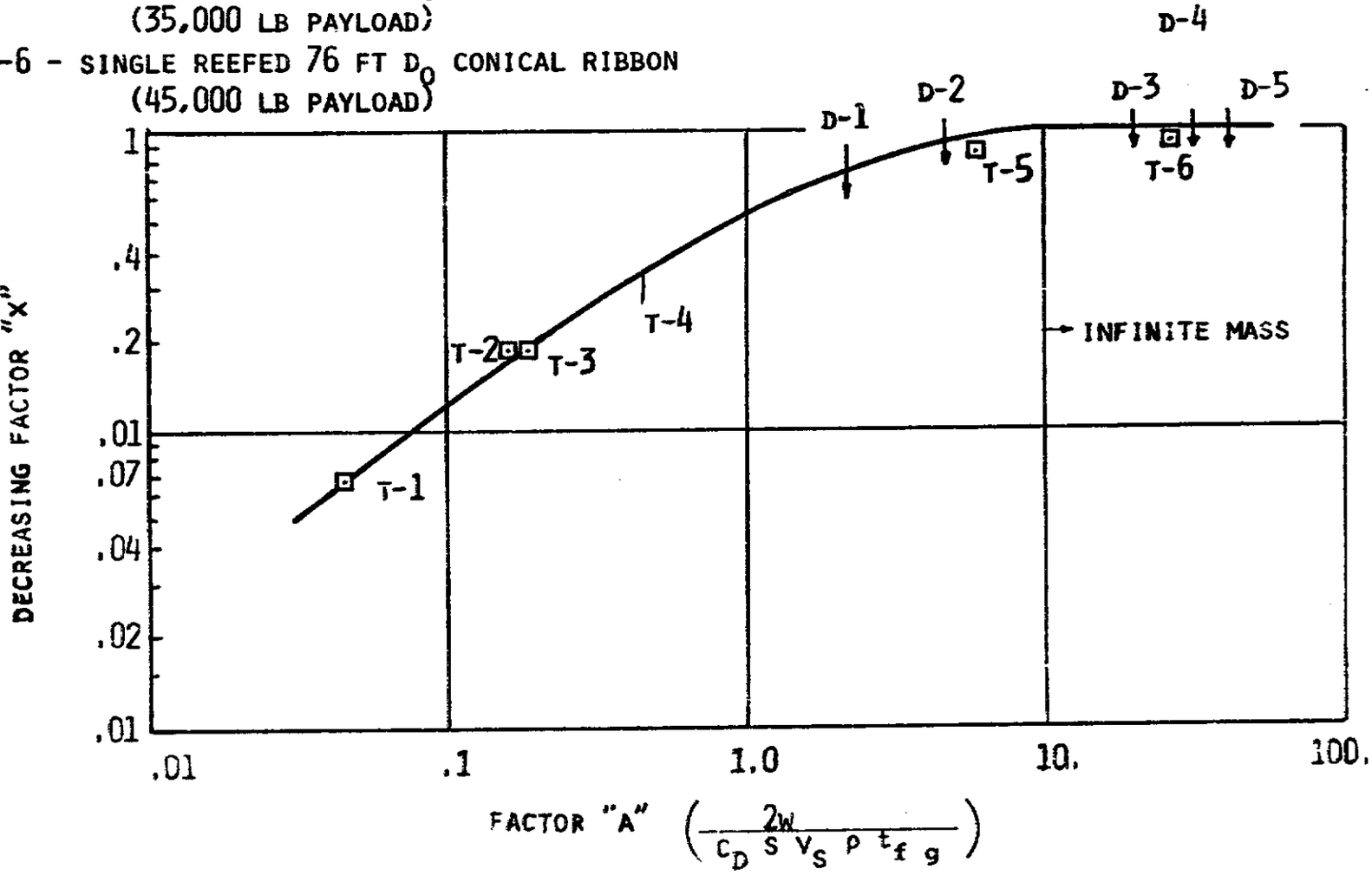

FIGURE 3

RIBBON-TYPE PARACHUTE NOMINAL DIAMETER VS TOTAL RECOVERY WEIGHT FOR SEA-LEVEL TERMINAL DESCENT VELOCITIES OF 50, 100 AND 150 FPS

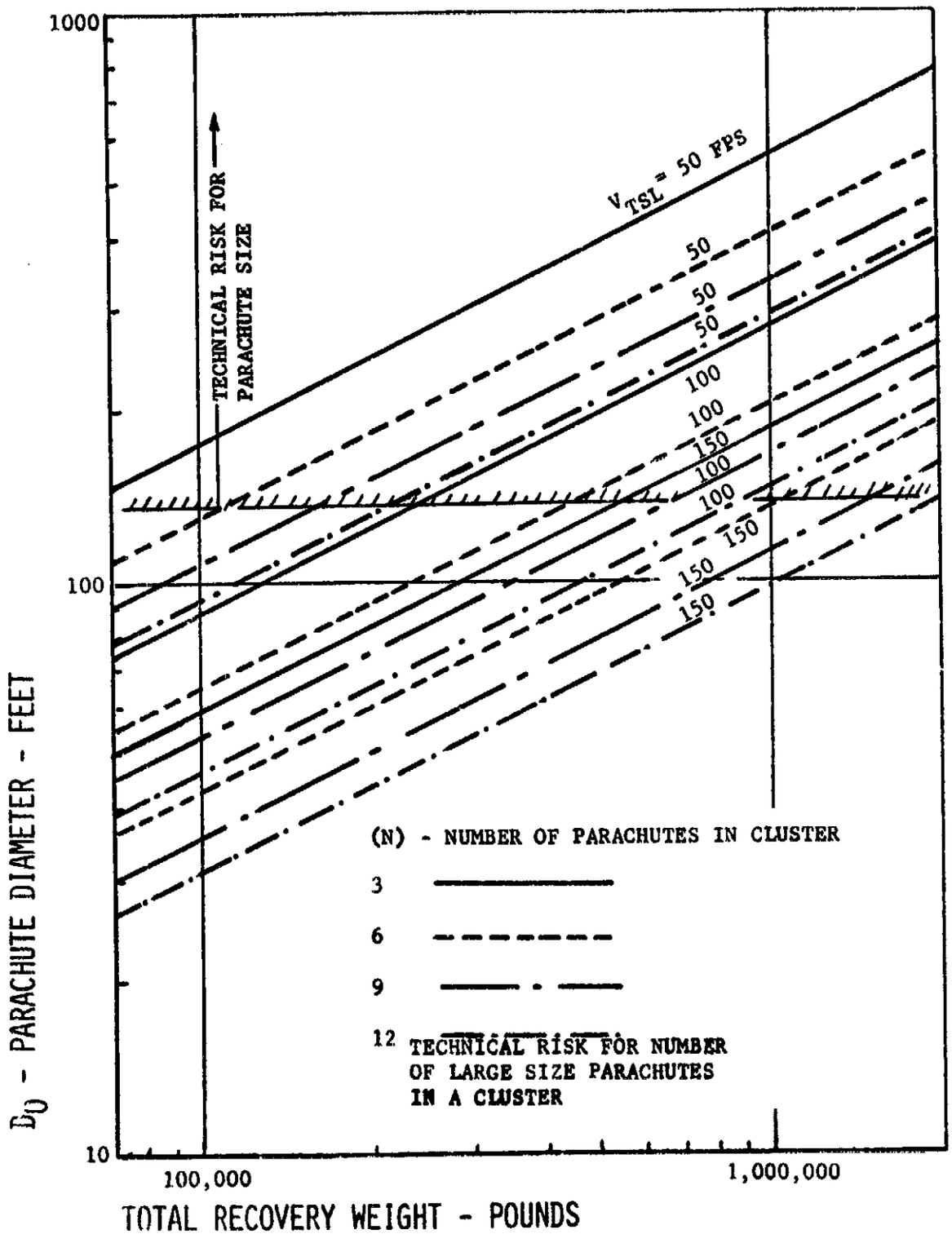

FIGURE 4

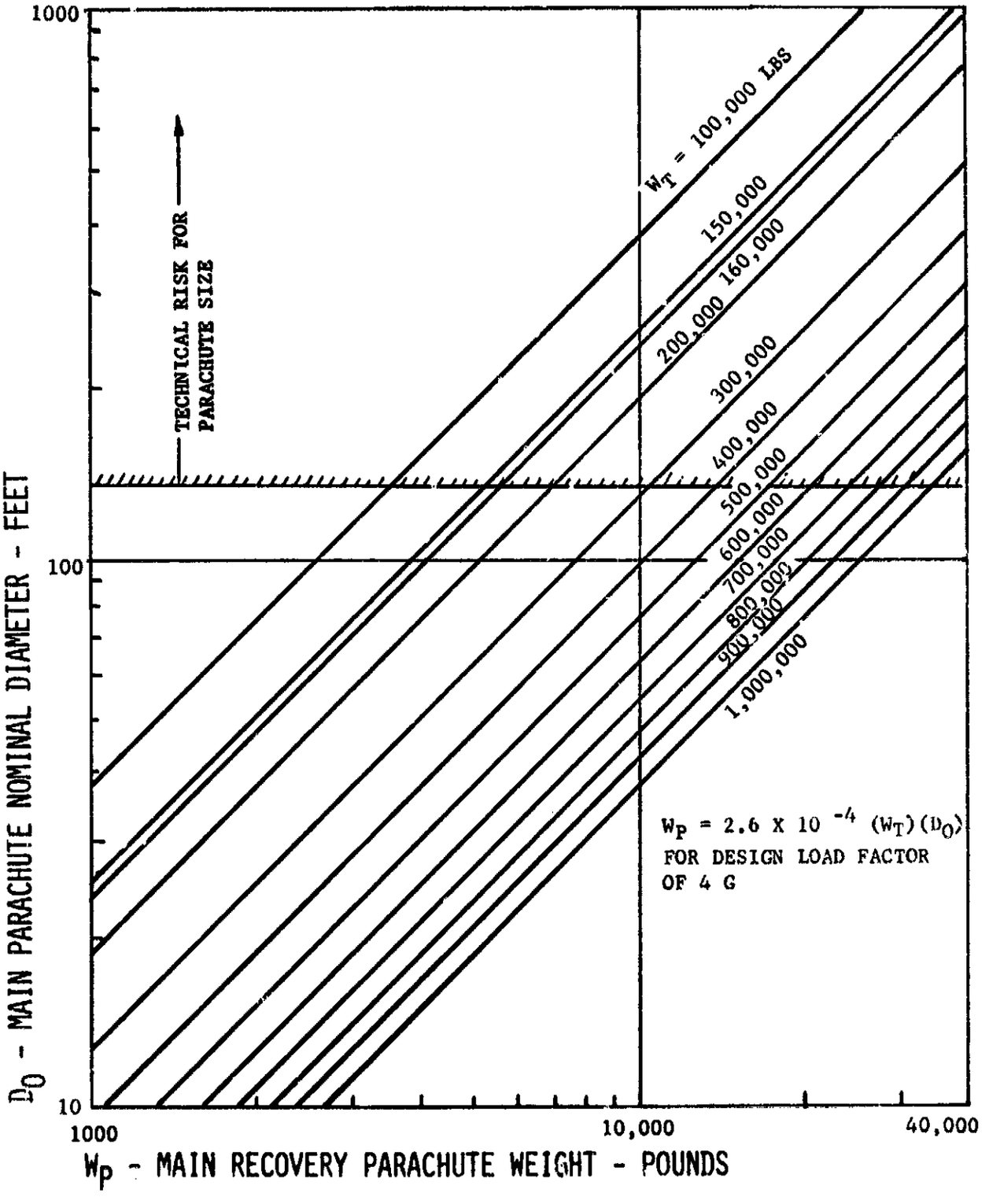
1000
100
10
1000
10,000
40,000
D_O - MAIN PARACHUTE NOMINAL DIAMETER - FEET
W_P - MAIN RECOVERY PARACHUTE WEIGHT - POUNDS
TECHNICAL RISK FOR PARACHUTE SIZE
W_T = 100,000 LBS
150,000
160,000
200,000
300,000
400,000
500,000
600,000
700,000
800,000
900,000
1,000,000
$W_P = 2.6 \times 10^{-4} (W_T)(D_O)$
FOR DESIGN LOAD FACTOR
OF 4 G

FIGURE 5

RECOVERY SYSTEM WEIGHT TREND AS A FUNCTION OF DESIGN G-LOAD ON MAIN PARACHUTES

NOTE: REFERENCED TO SYSTEM DESIGNED AT 4-G LOAD

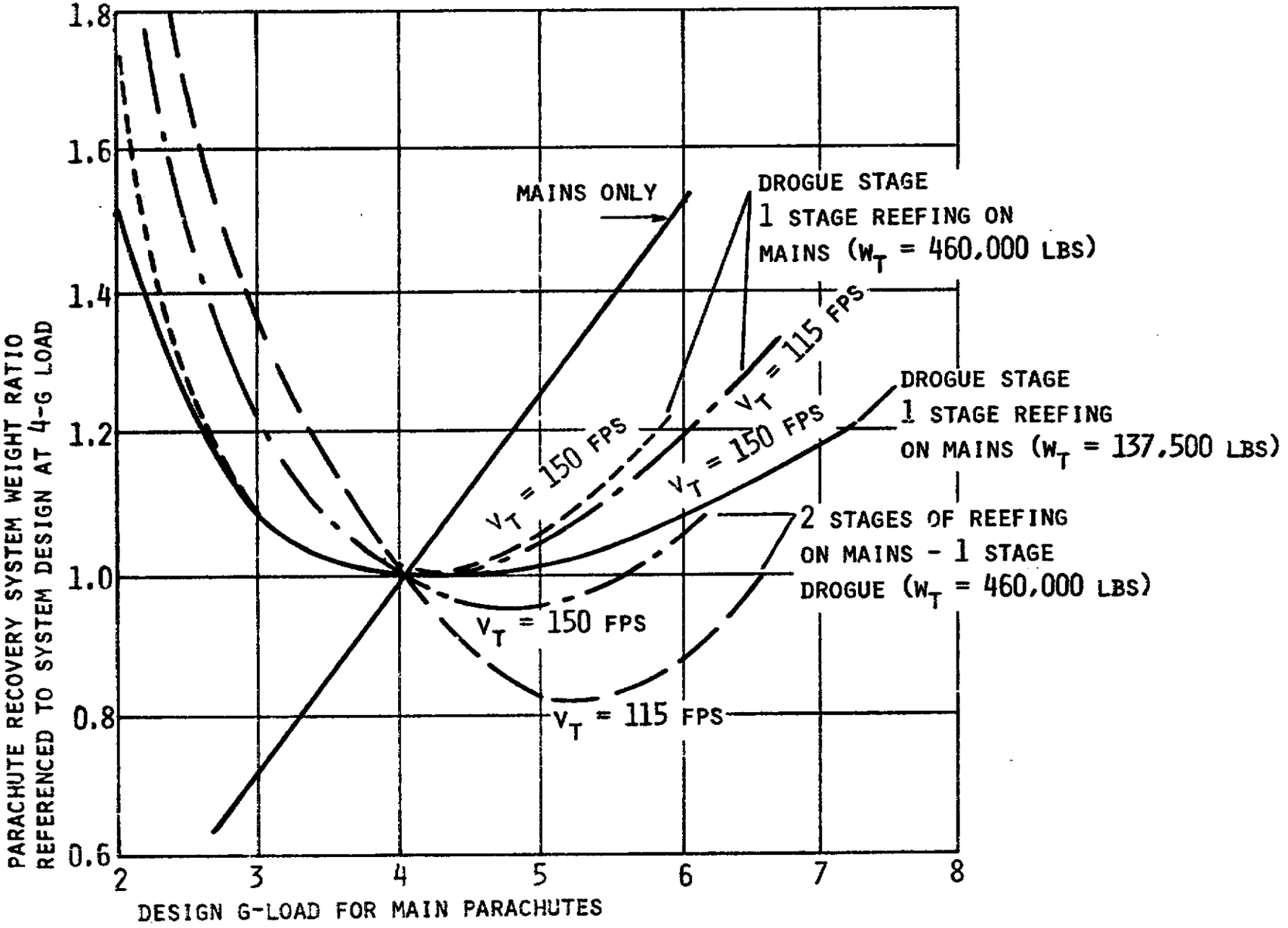

FIGURE 6

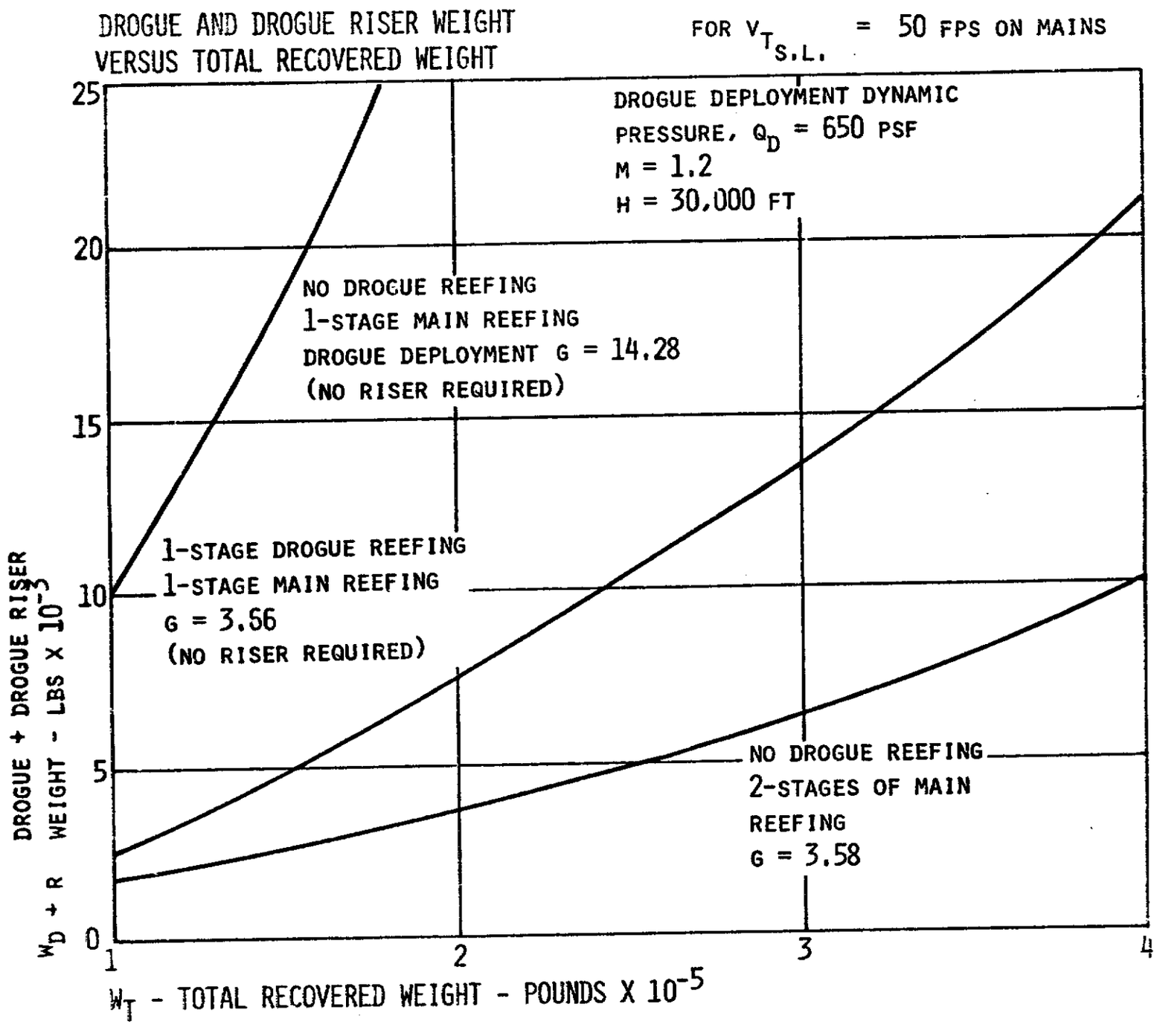
DROGUE AND DROGUE RISER WEIGHT
VERSUS TOTAL RECOVERED WEIGHT
FOR $V_{T_{S.L.}}$ = 50 FPS ON MAINS
DROGUE DEPLOYMENT DYNAMIC
PRESSURE, Q_D = 650 PSF
M = 1.2
H = 30,000 FT
NO DROGUE REEFING
1-STAGE MAIN REEFING
DROGUE DEPLOYMENT G = 14.28
(NO RISER REQUIRED)
1-STAGE DROGUE REEFING
1-STAGE MAIN REEFING
G = 3.66
(NO RISER REQUIRED)
NO DROGUE REEFING
2-STAGES OF MAIN
REEFING
G = 3.58
25
20
15
10
5
0
1
2
3
4
W_{D+R} DROGUE + DROGUE RISER WEIGHT - LBS X 10^{-3}
W_T - TOTAL RECOVERED WEIGHT - POUNDS X 10^{-5}

FIGURE 7

DROGUE AND DROGUE RISER WEIGHT
VERSUS TOTAL RECOVERED WEIGHT

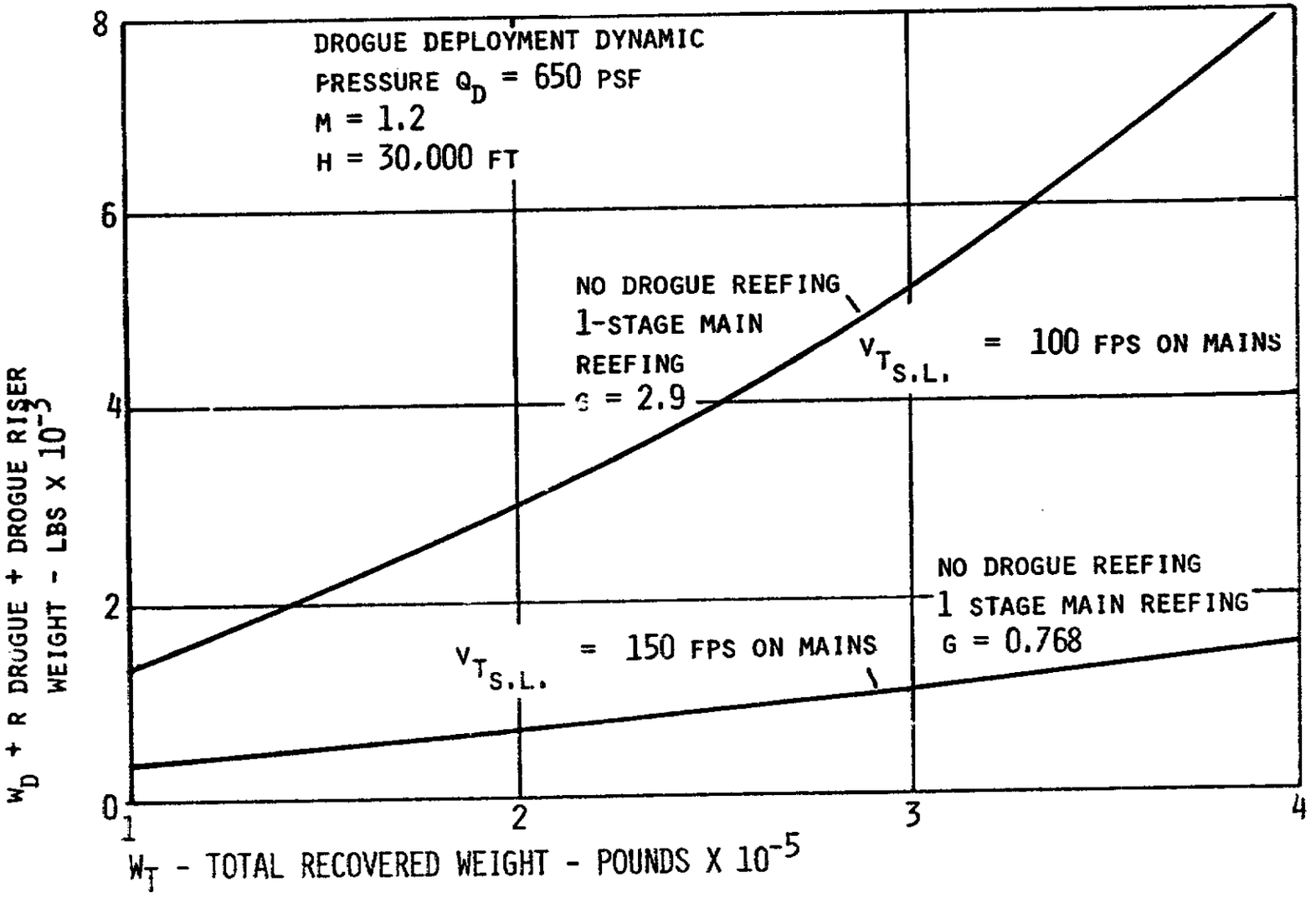

FIGURE 8

DROGUE AND DROGUE RISER WEIGHT
VERSUS TOTAL RECOVERED WEIGHT

DROGUE DEPLOYMENT DYNAMIC
PRESSURE, Q_D = 650 PSF
H = 30,000 FT
M = 1.2

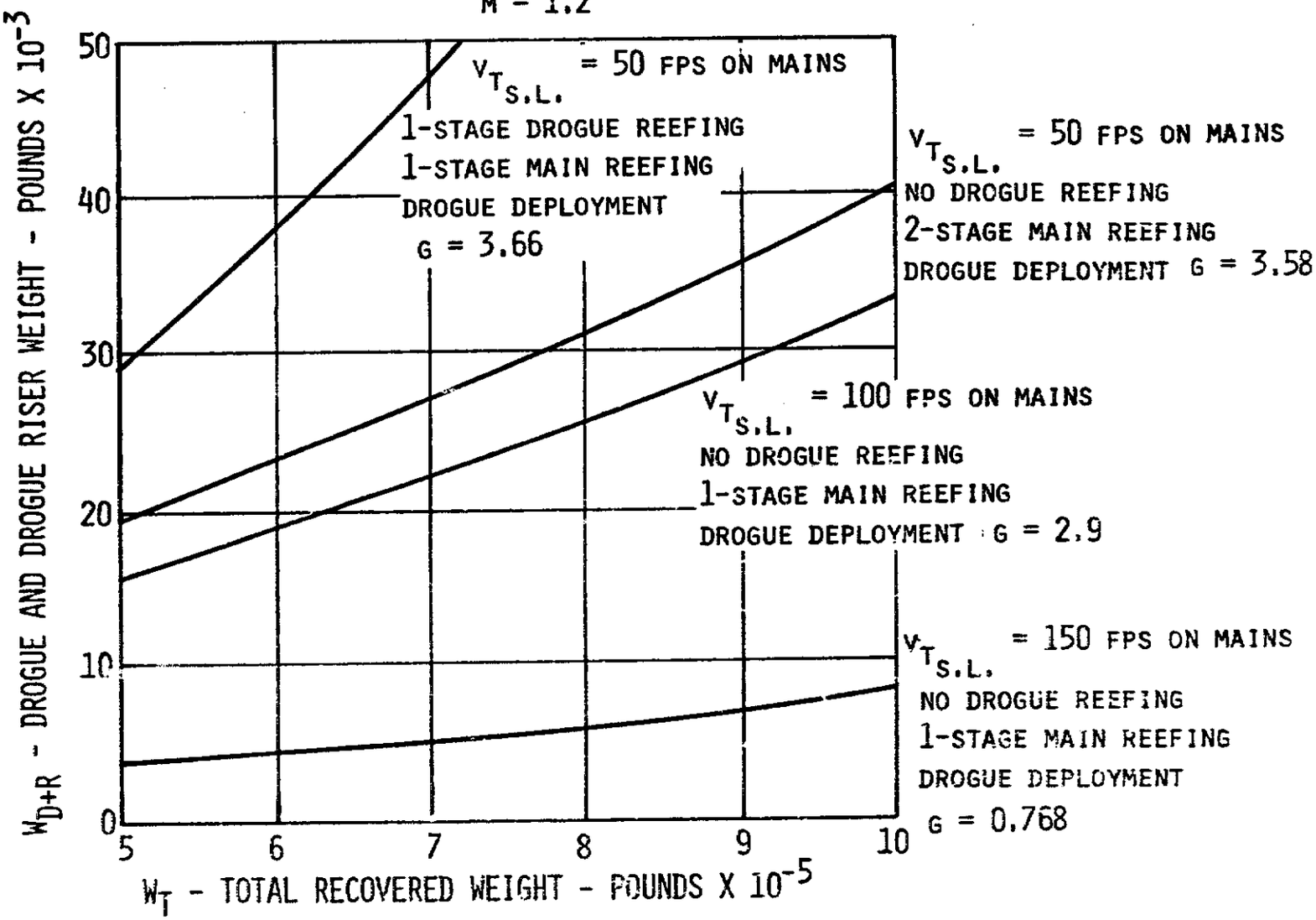

FIGURE 9

MAIN PARACHUTE WEIGHT VERSUS
TOTAL RECOVERED WEIGHT

FOR $V_{T_{S.L.}}$ = 50 FPS

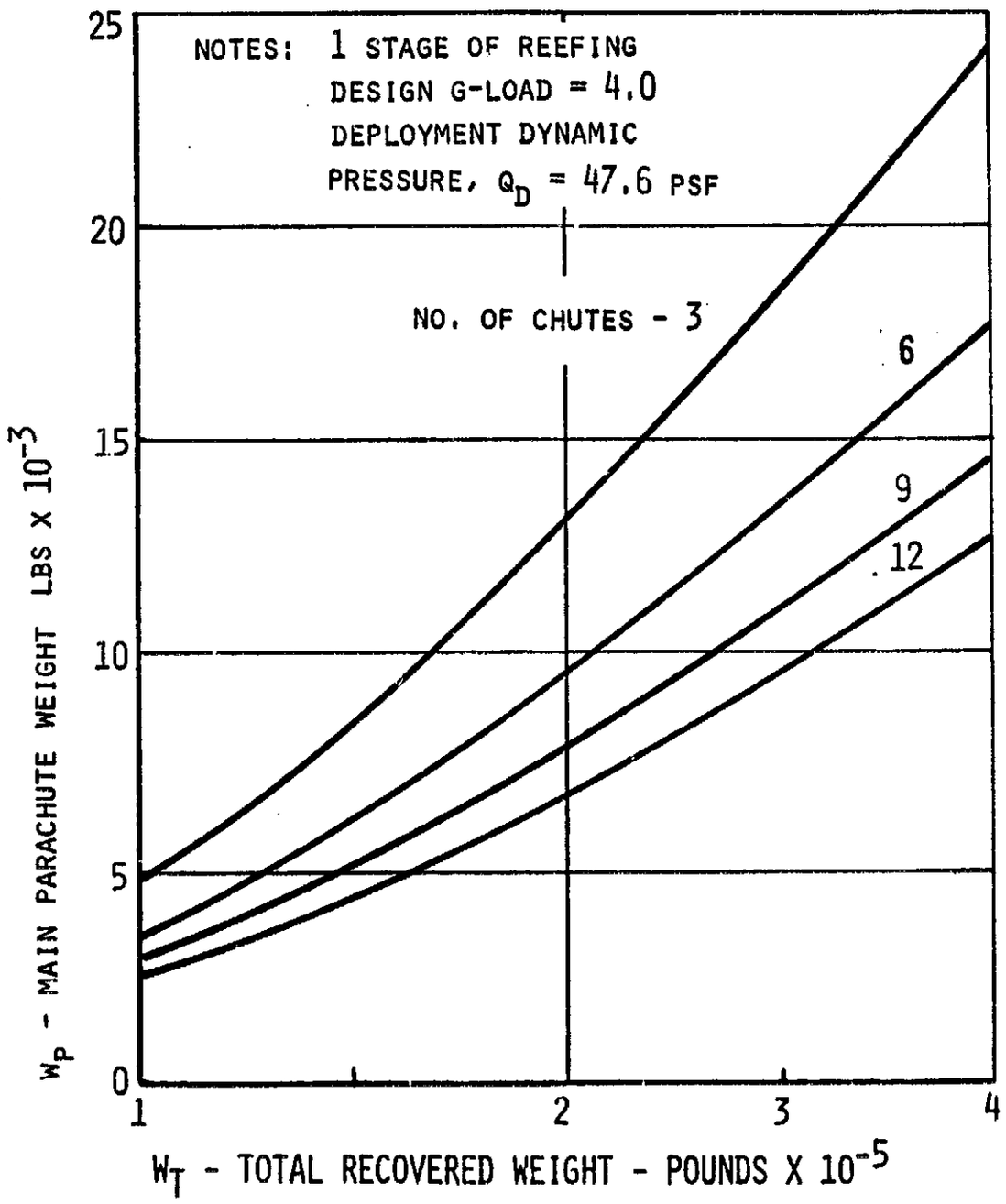

FIGURE 10

MAIN PARACHUTE WEIGHT VERSUS
TOTAL RECOVERED WEIGHT

FOR $V_{T_{S.L.}}$ = 100 FPS

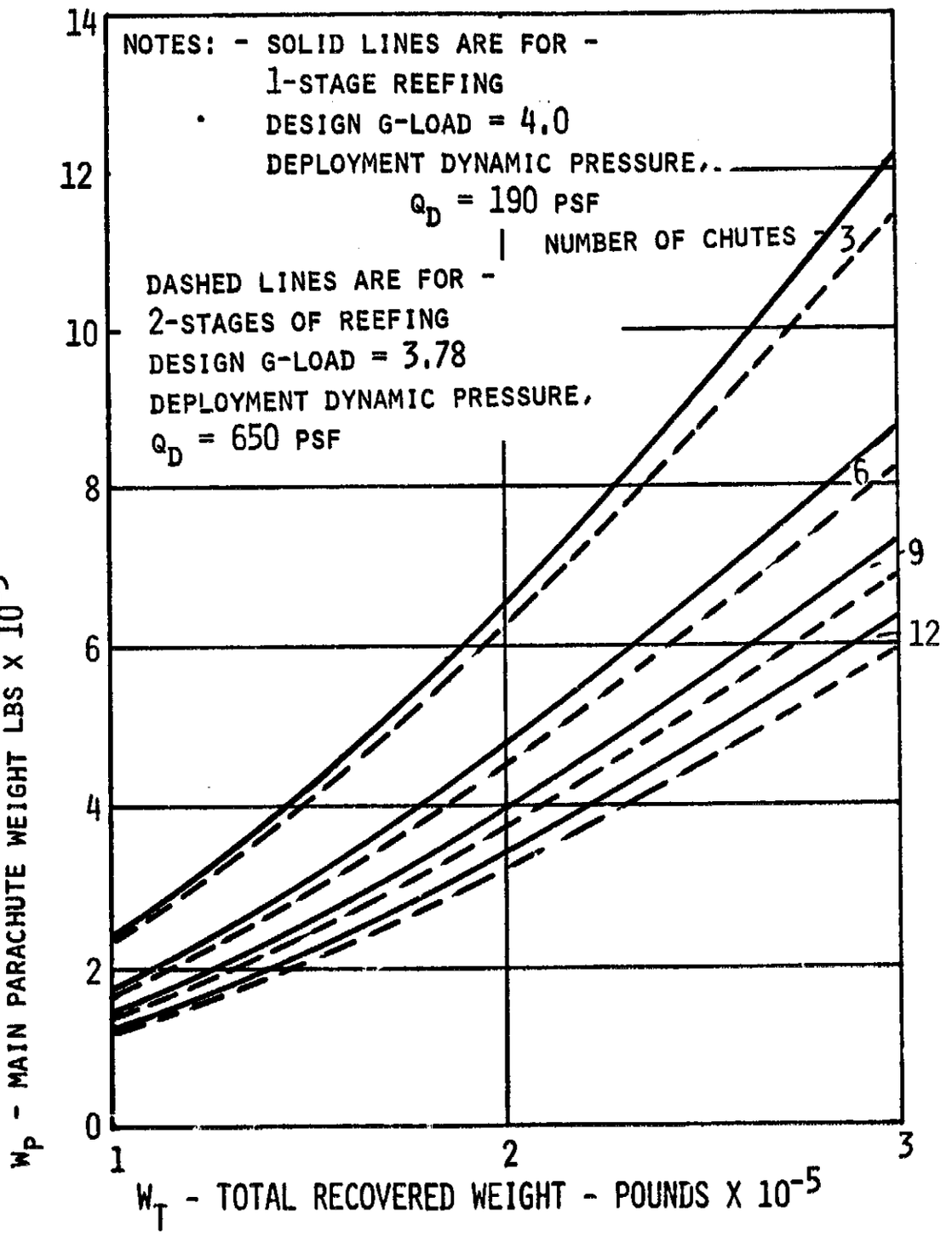

FIGURE 11

MAIN PARACHUTE WEIGHT VERSUS
TOTAL RECOVERED WEIGHT

FOR $V_{T_{S.L.}}$ = 150 FPS

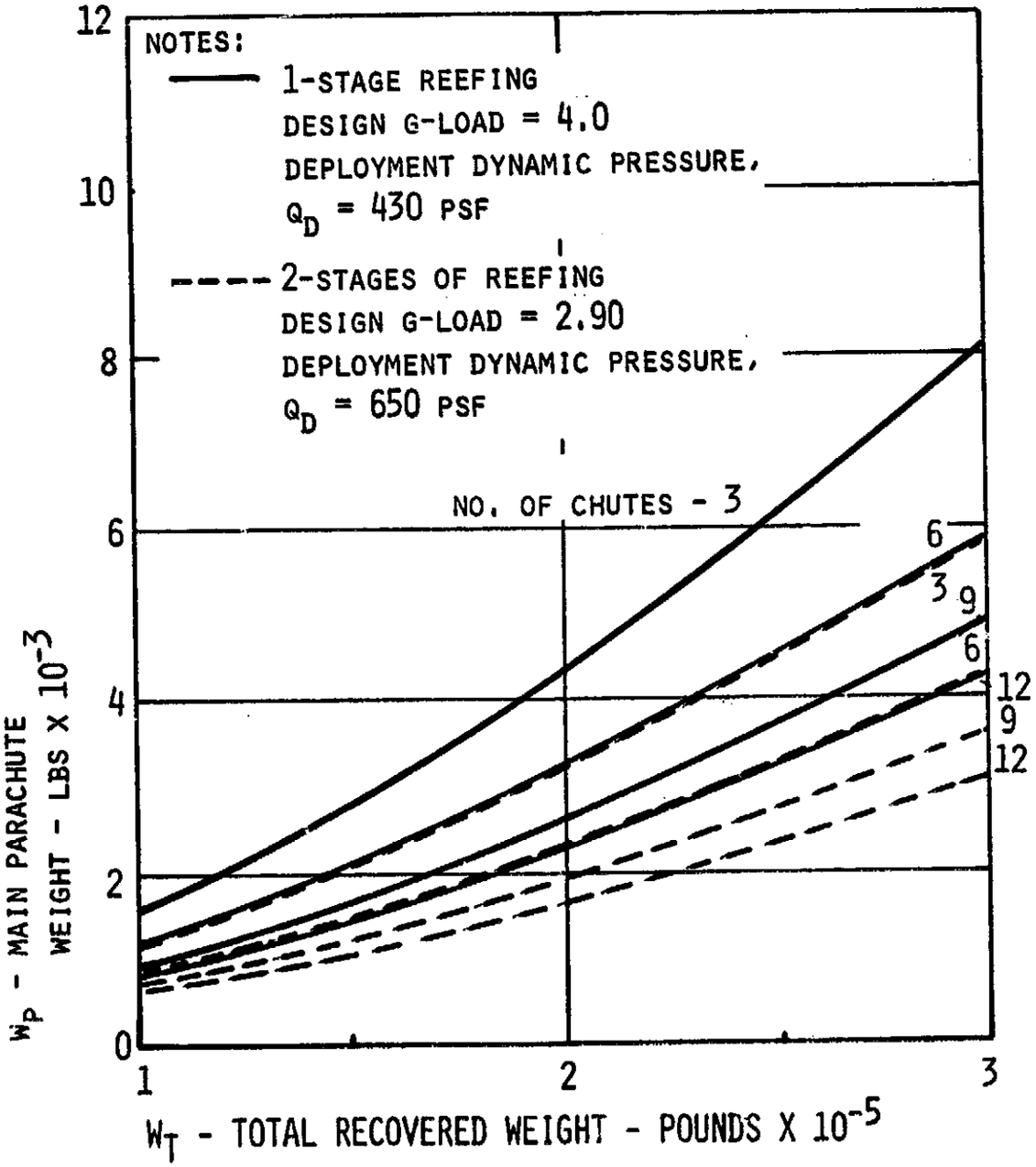

FIGURE 12

MAIN PARACHUTE WEIGHT VERSUS
TOTAL RECOVERED WEIGHT

FOR $V_{T_{S.L.}}$ = 50 FPS

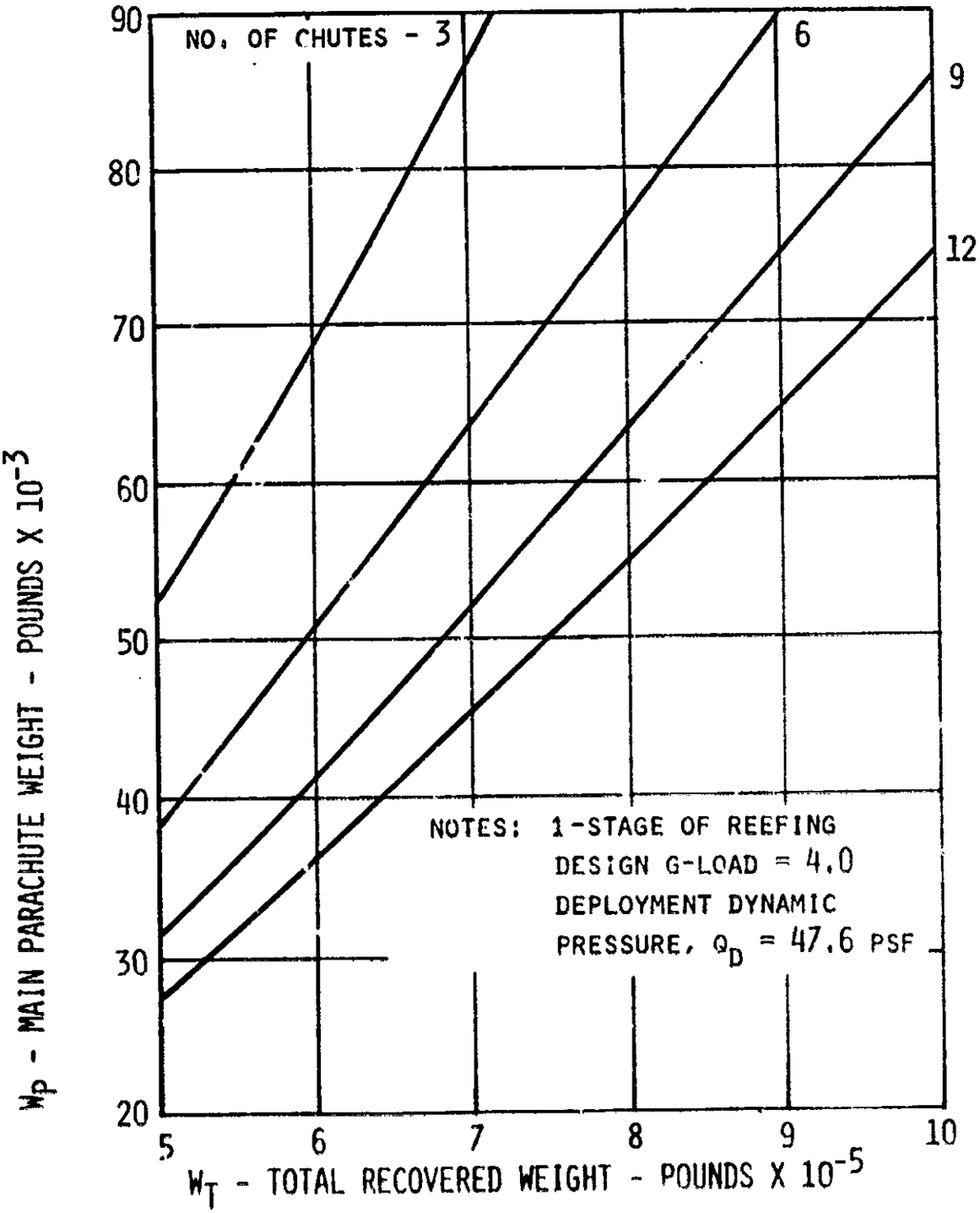

FIGURE 13

MAIN PARACHUTE WEIGHT VERSUS
TOTAL RECOVERED WEIGHT

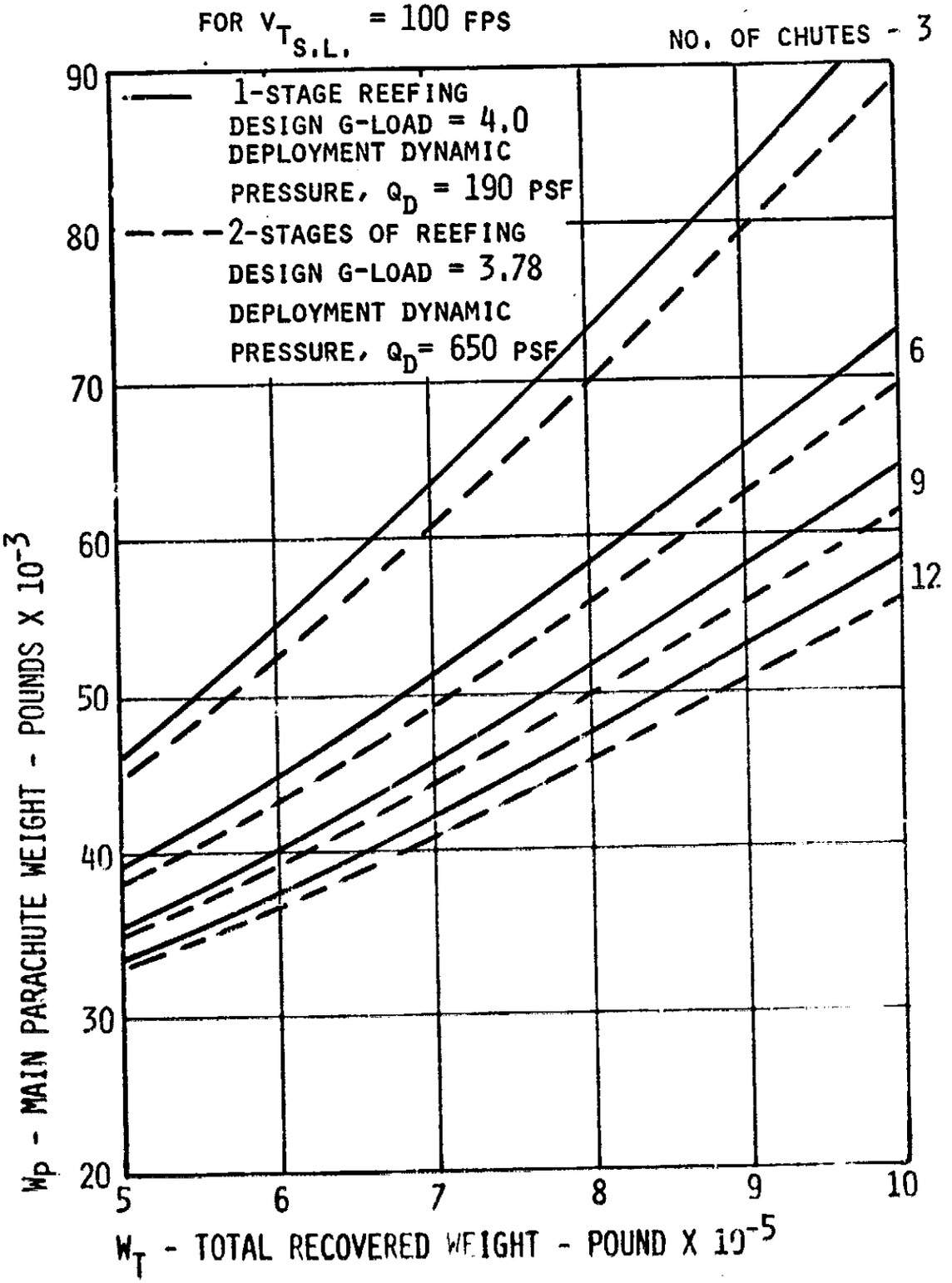

FIGURE 14

MAIN PARACHUTE WEIGHT VERSUS
TOTAL RECOVERED WEIGHT

FOR $V_{T_{S.L.}}$ = 150 FPS

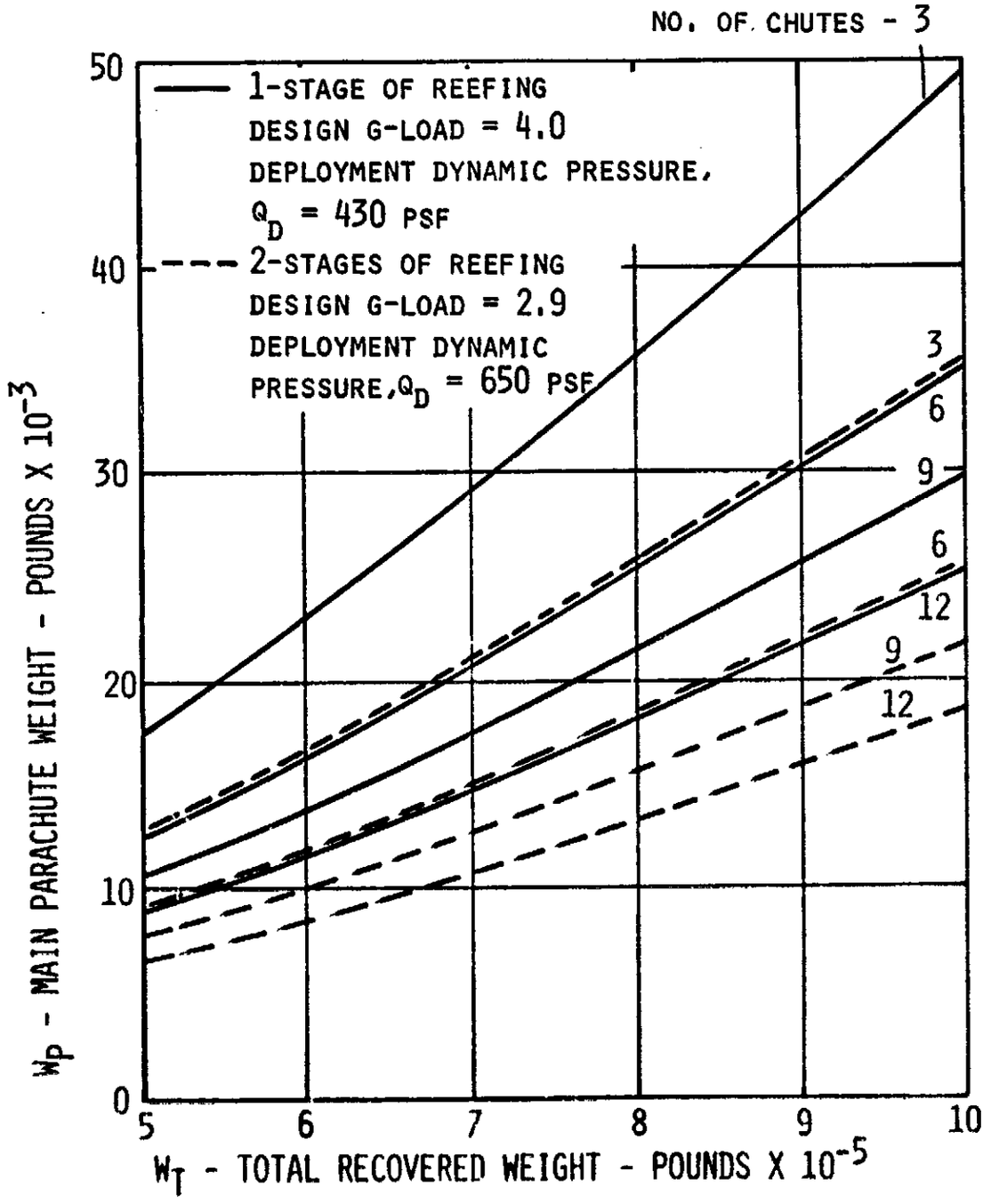

FIGURE 15

PILOT D_0 VS PACKAGE WEIGHT

1. $D_0 = \sqrt{\frac{40(W_p)}{\pi Q C_D}}$

2. FOR 10G EXTRACTION LOADS

3. $C_D = 0.55$

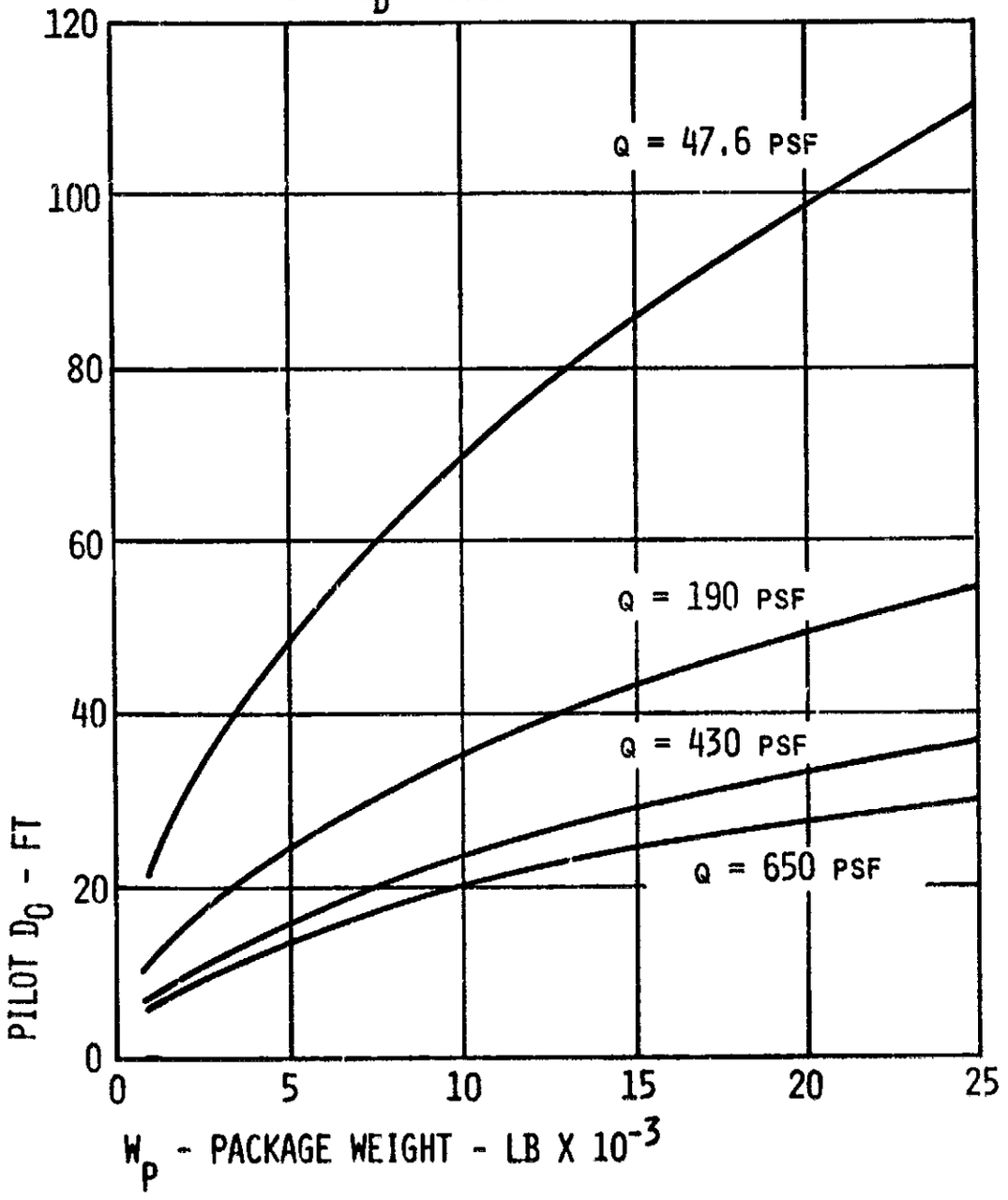

FIGURE 16

PILOT D_0 VS PILOT WEIGHT

1. EXTRACTION FORCE = 10G'S
2. $W_P = 6.5 \times 10^{-5}(G's)(W)(D_0)$

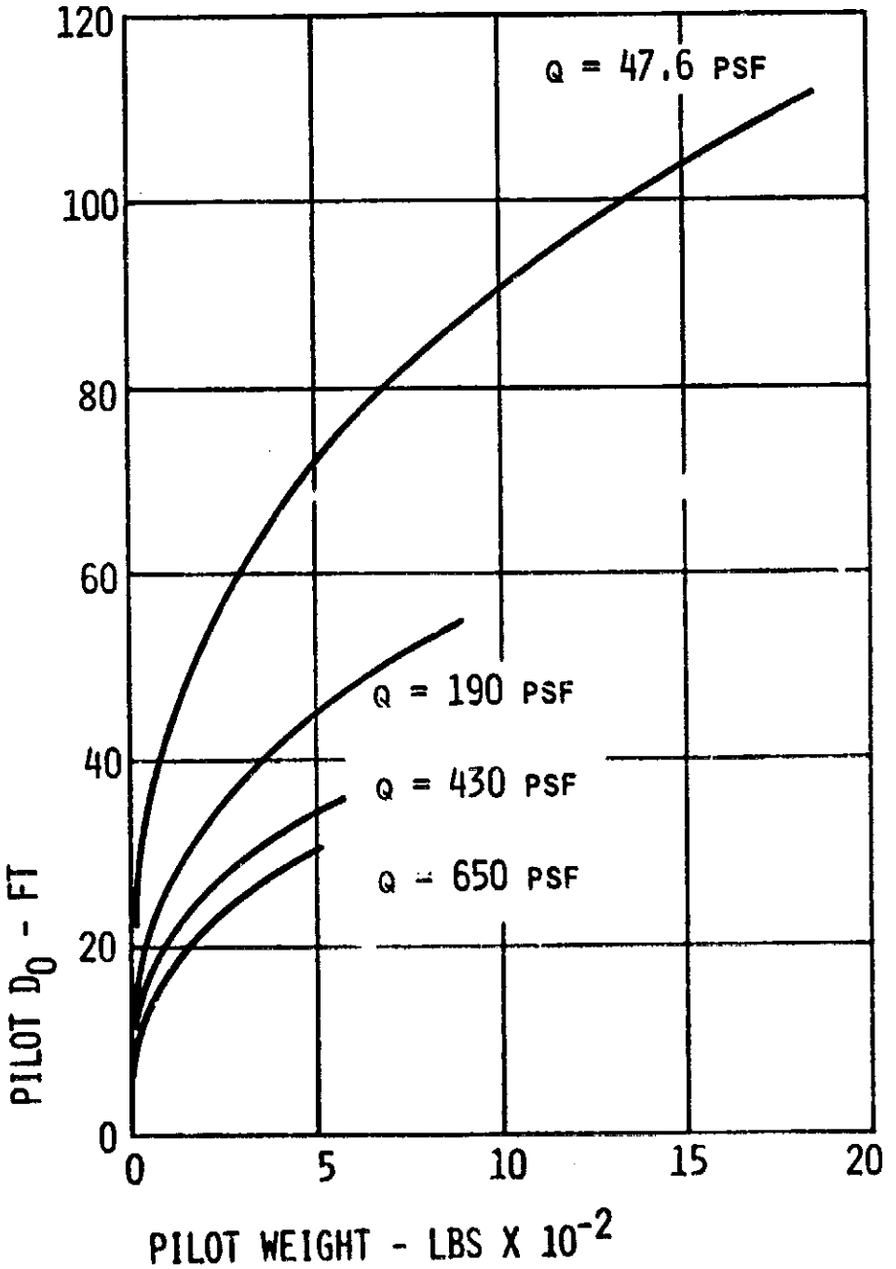

FIGURE 17

RISER LENGTH FOR VARIOUS DIAMETER PARACHUTES

1. X/D = 6.5

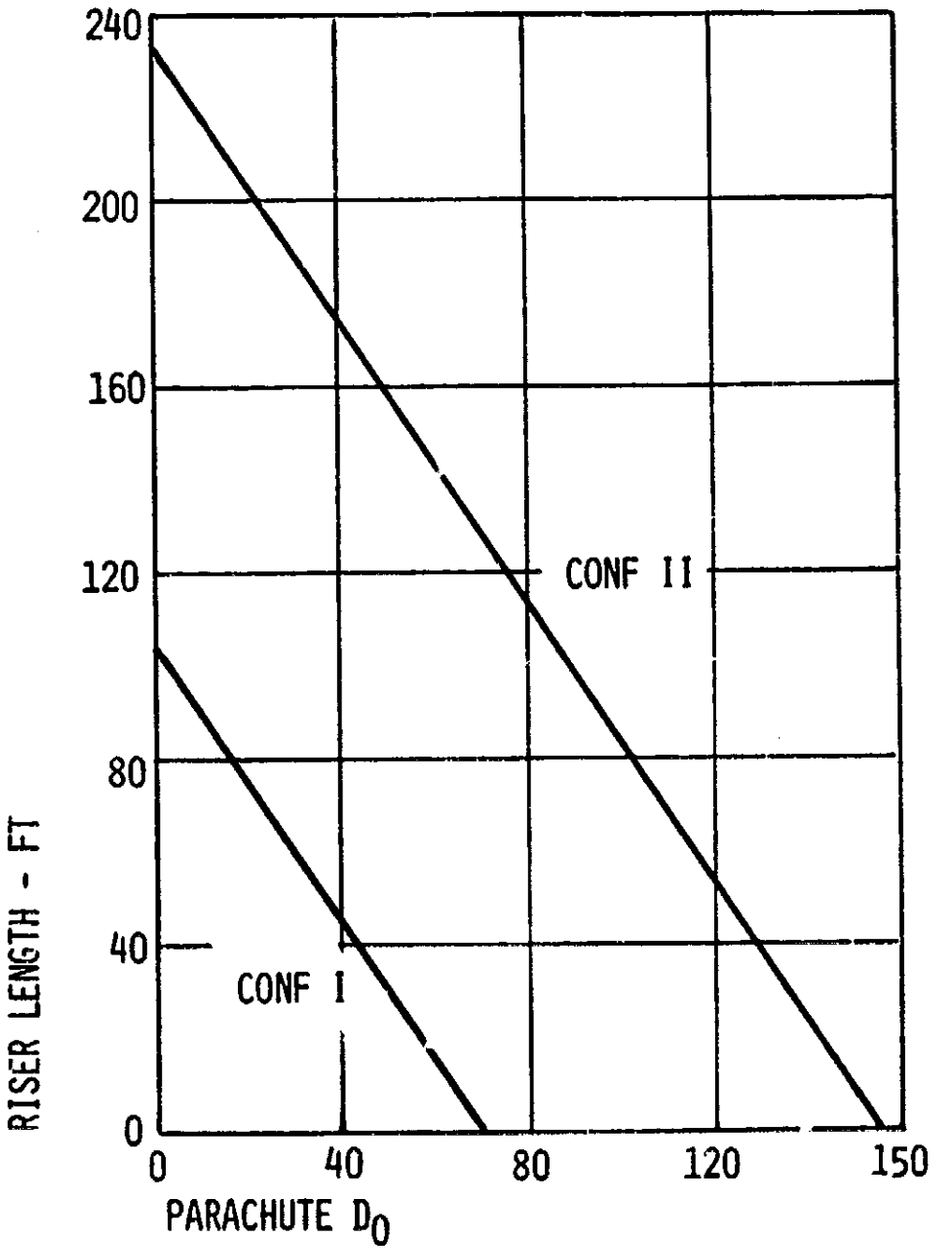

FIGURE 18

RISER LENGTH CRITERIA FOR PARACHUTE CLUSTERS

1. REF AMCP 706-130

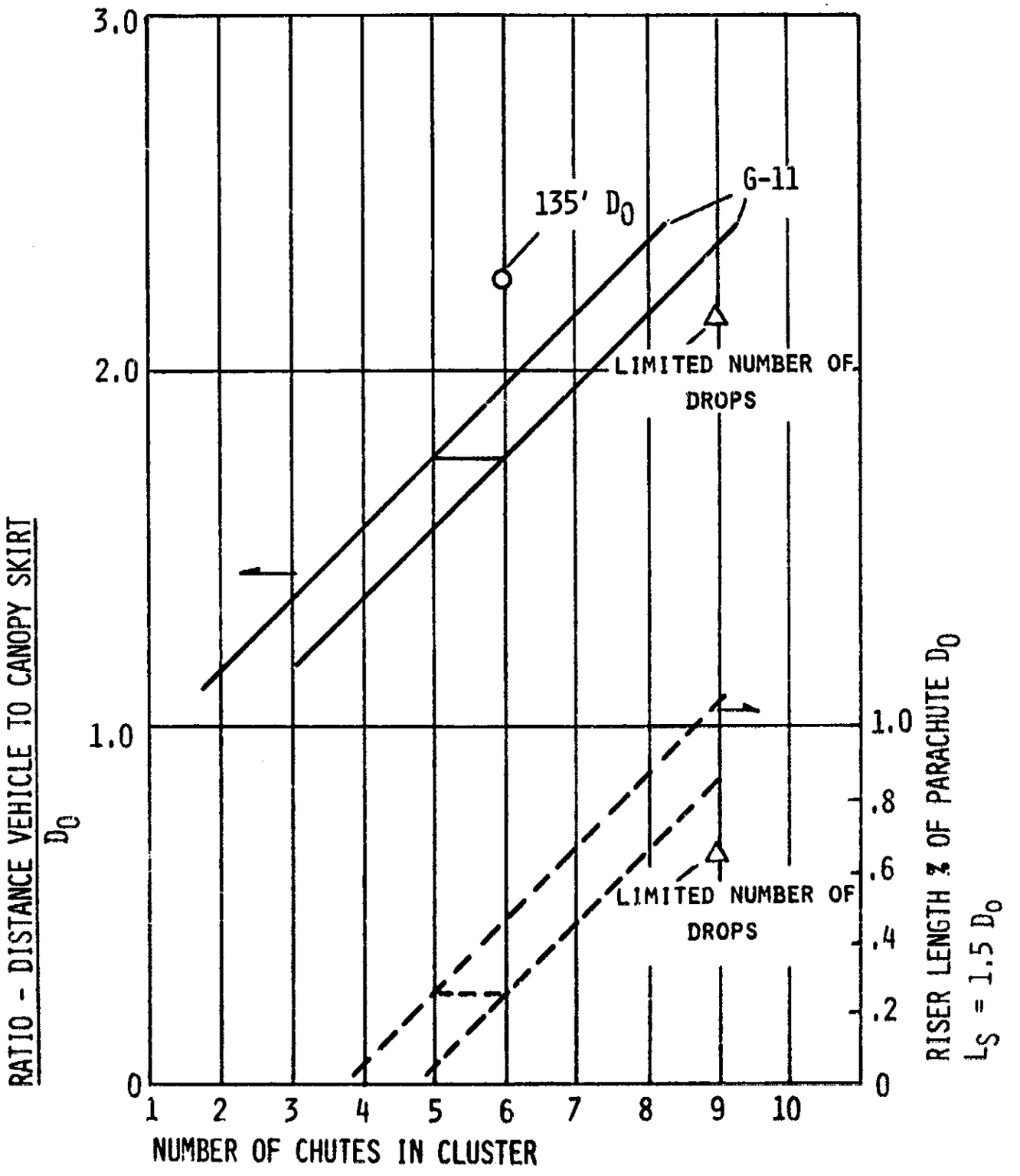

FIGURE 19

MORTAR WEIGHT VS EJECTED WEIGHT

1. F.S. = 2.0
2. MORTAR WGT - TUBE + BREECH PLATE + POWER UNIT + SABOT + COVER
3. $F_{MAX} = 1.18\ F_{AVG}$

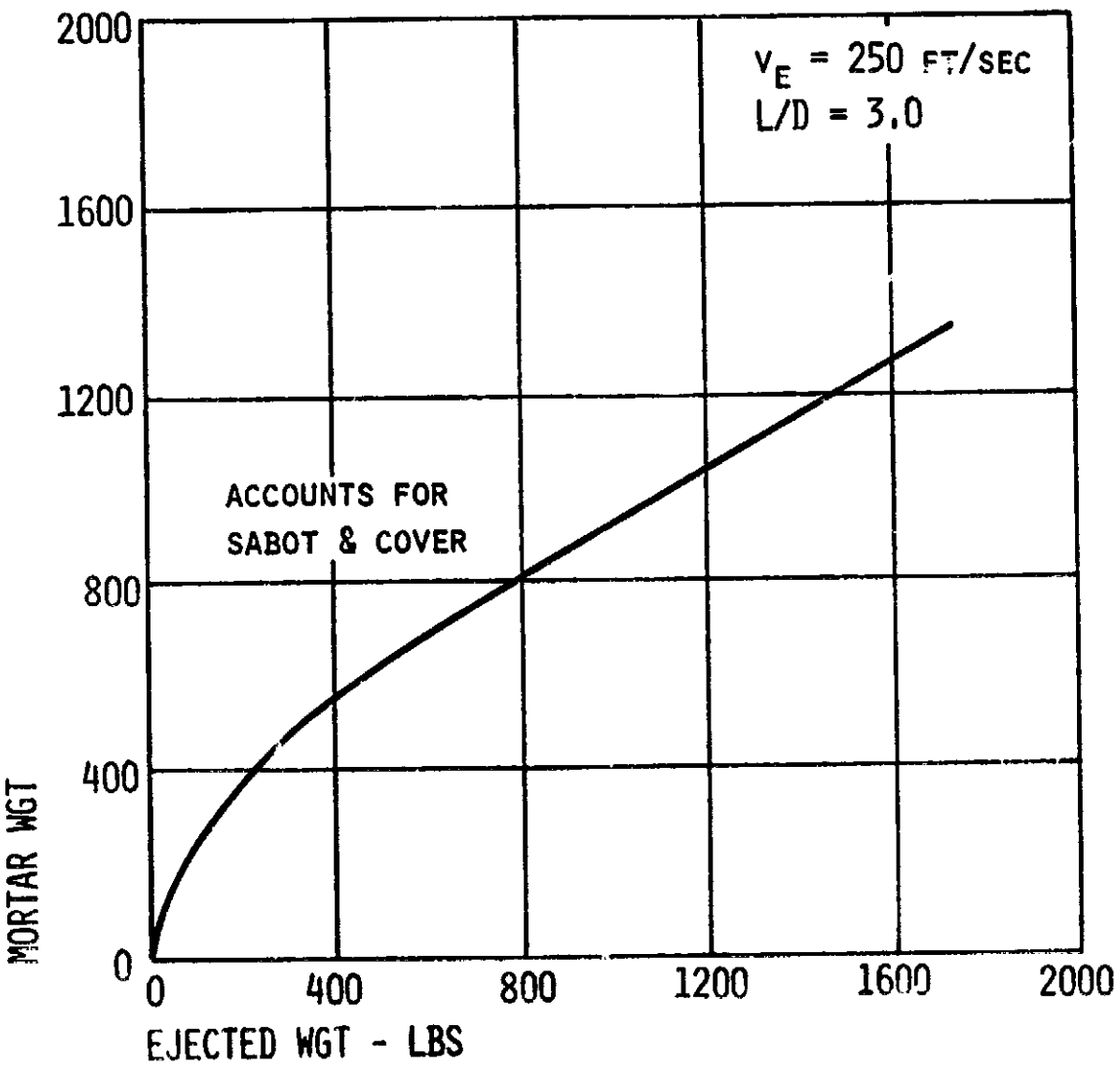

FIGURE 20

EFFECTS OF MUZZLE VELOCITY ON MORTAR WEIGHT

1. RELATIVE TO
250 FT/SEC WEIGHTS

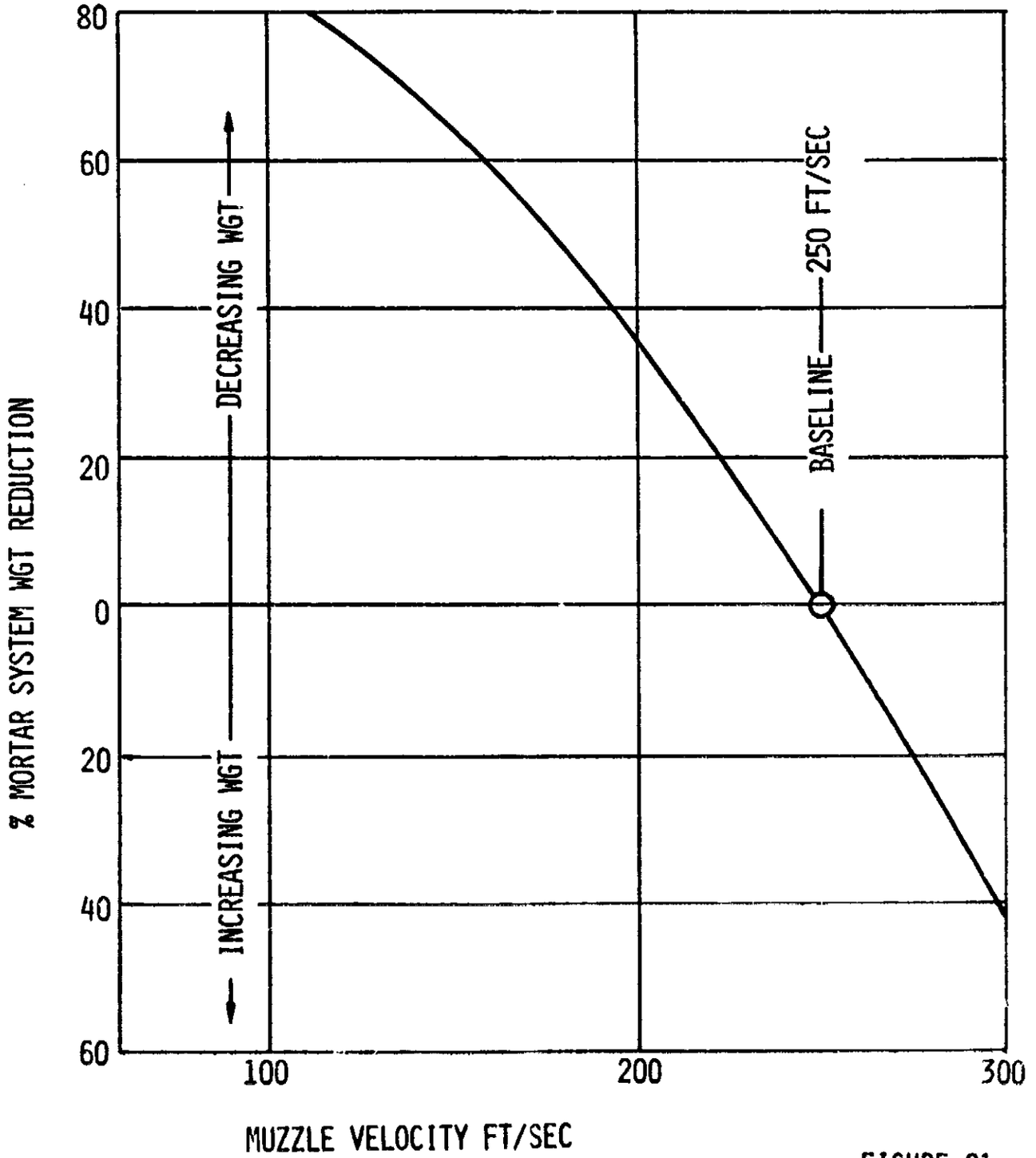

FIGURE 21

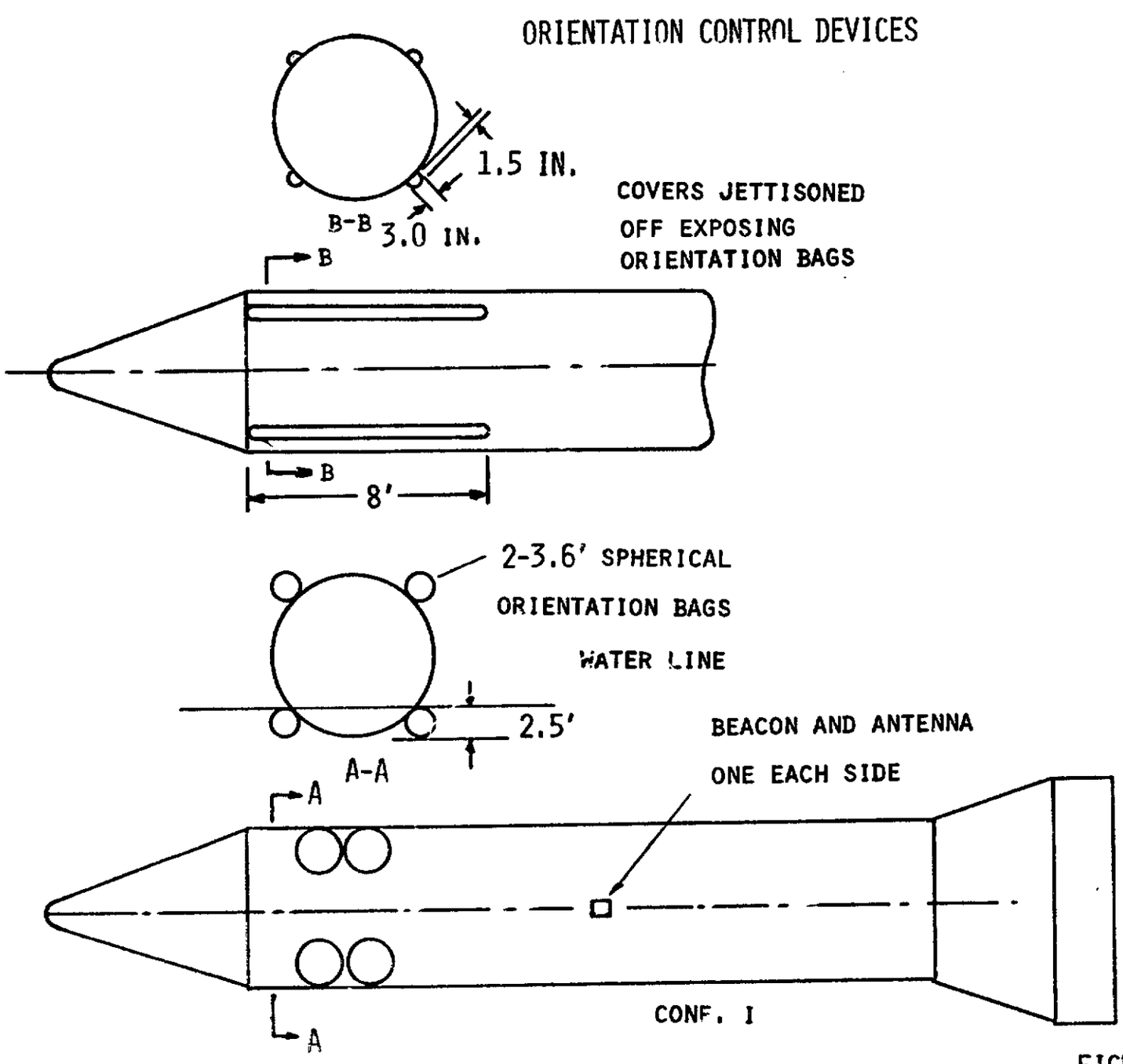
ORIENTATION CONTROL DEVICES
1.5 IN.
B-B 3.0 IN.
COVERS JETTISONED
OFF EXPOSING
ORIENTATION BAGS
B
B
8'
2-3.6' SPHERICAL
ORIENTATION BAGS
WATER LINE
2.5'
A-A
BEACON AND ANTENNA
ONE EACH SIDE
A
A
CONF. I

FIGURE 22

REQUIRED INTERNAL PRESSURE OF ORIENTATION SPHERE AS A FUNCTION OF DIAMETER - BASED ON W = 4.0 FT.

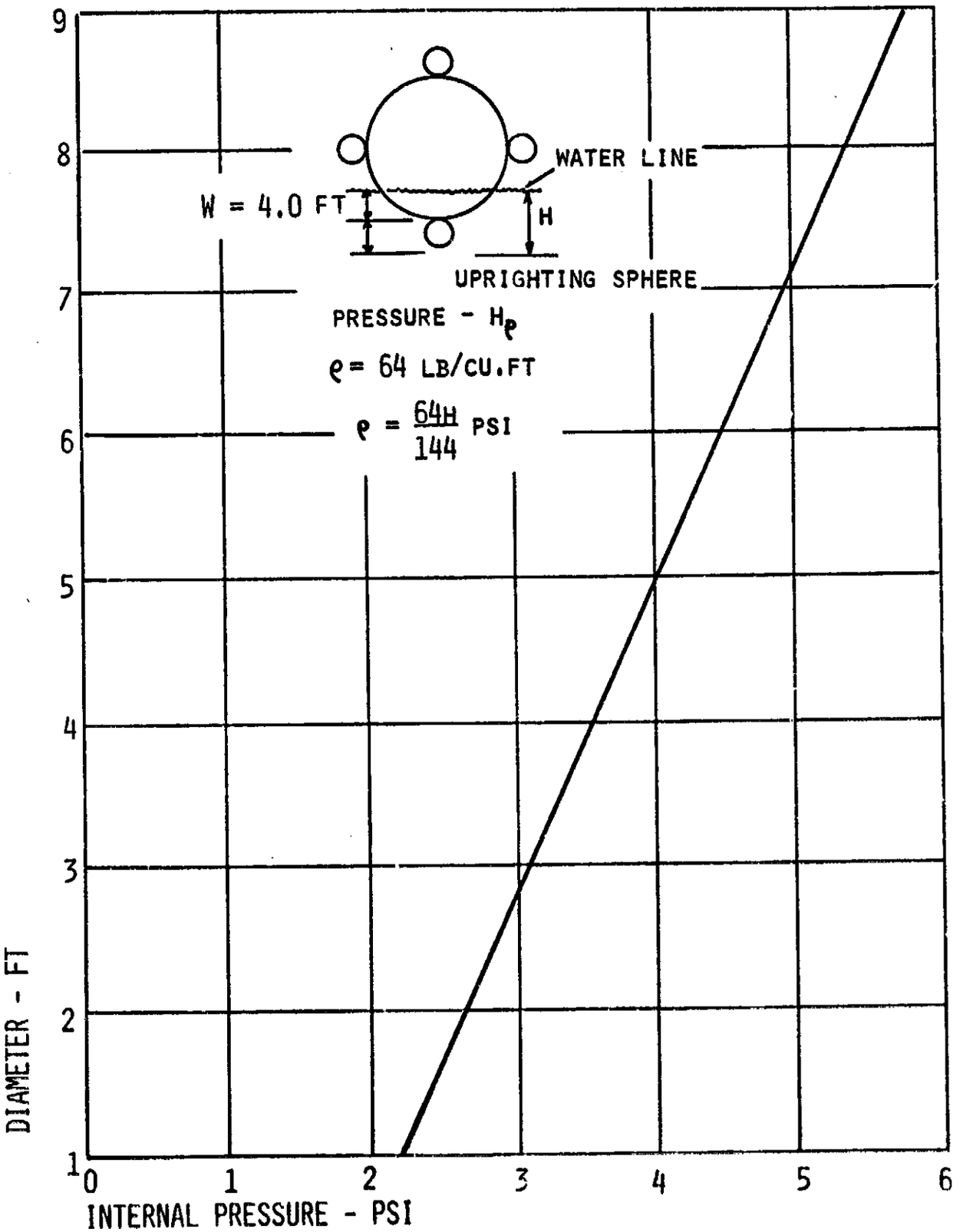

FIGURE 23

NUMBER OF ORIENTATION SPHERES PER ROW (4 ROWS) AS A FUNCTION OF DIAMETER TO PREVENT ROLLOVER IN SEA STATE 4

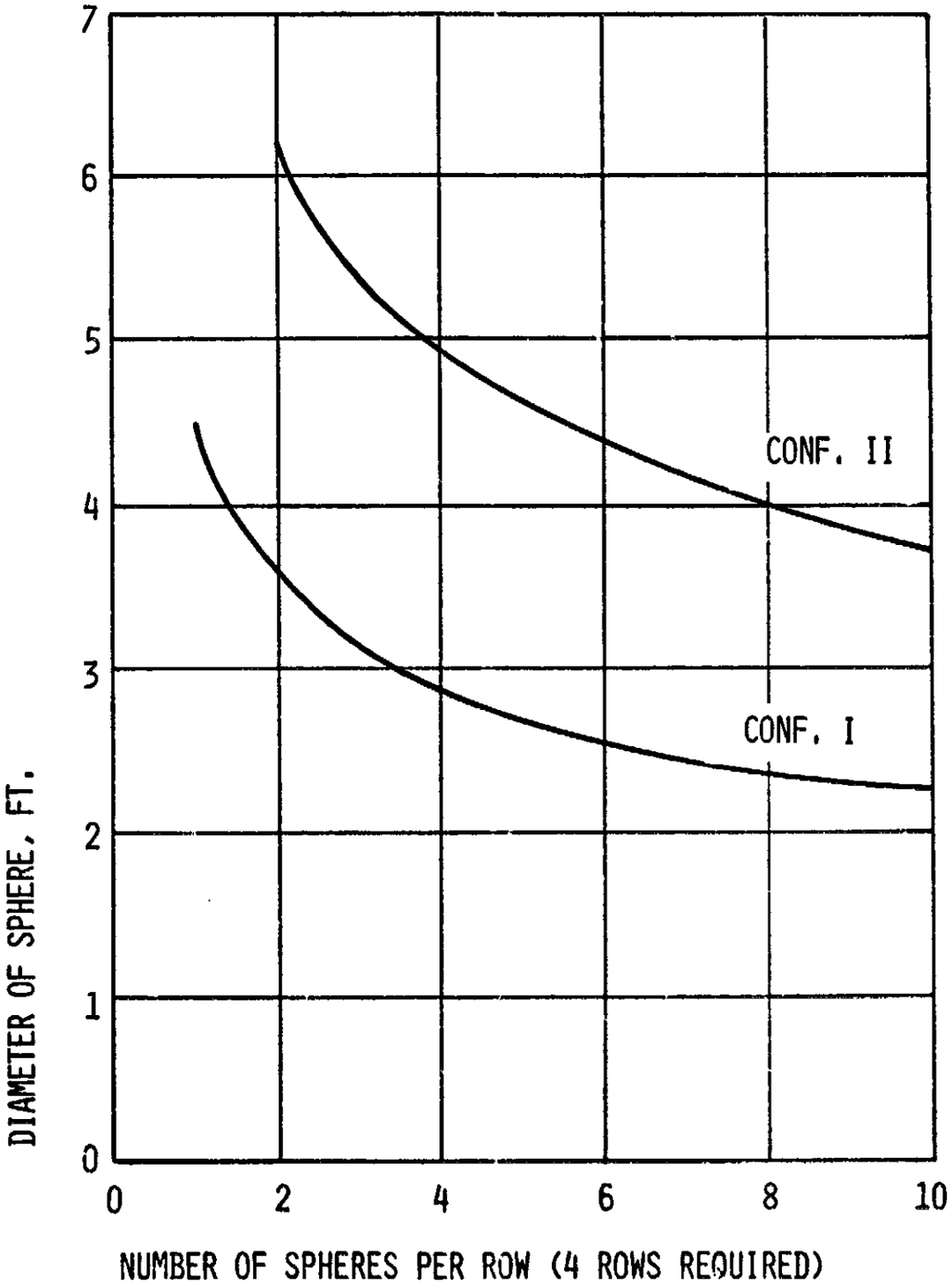

FIGURE 24

TOTAL WEIGHT OF ALL SPHERES AS A FUNCTION OF DIAMETER (DOES NOT INCLUDE INFLATION SYSTEM)

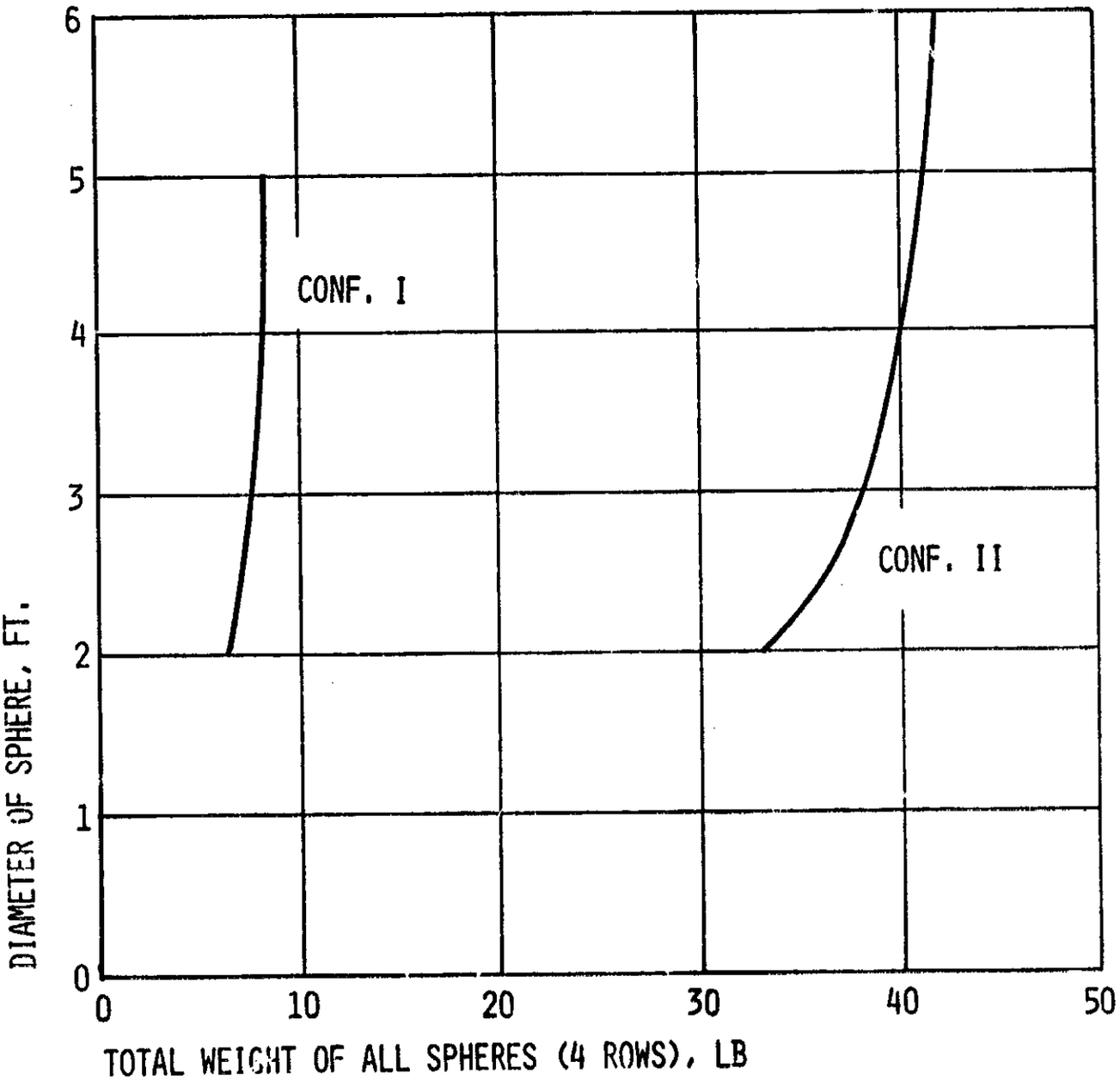

FIGURE 25

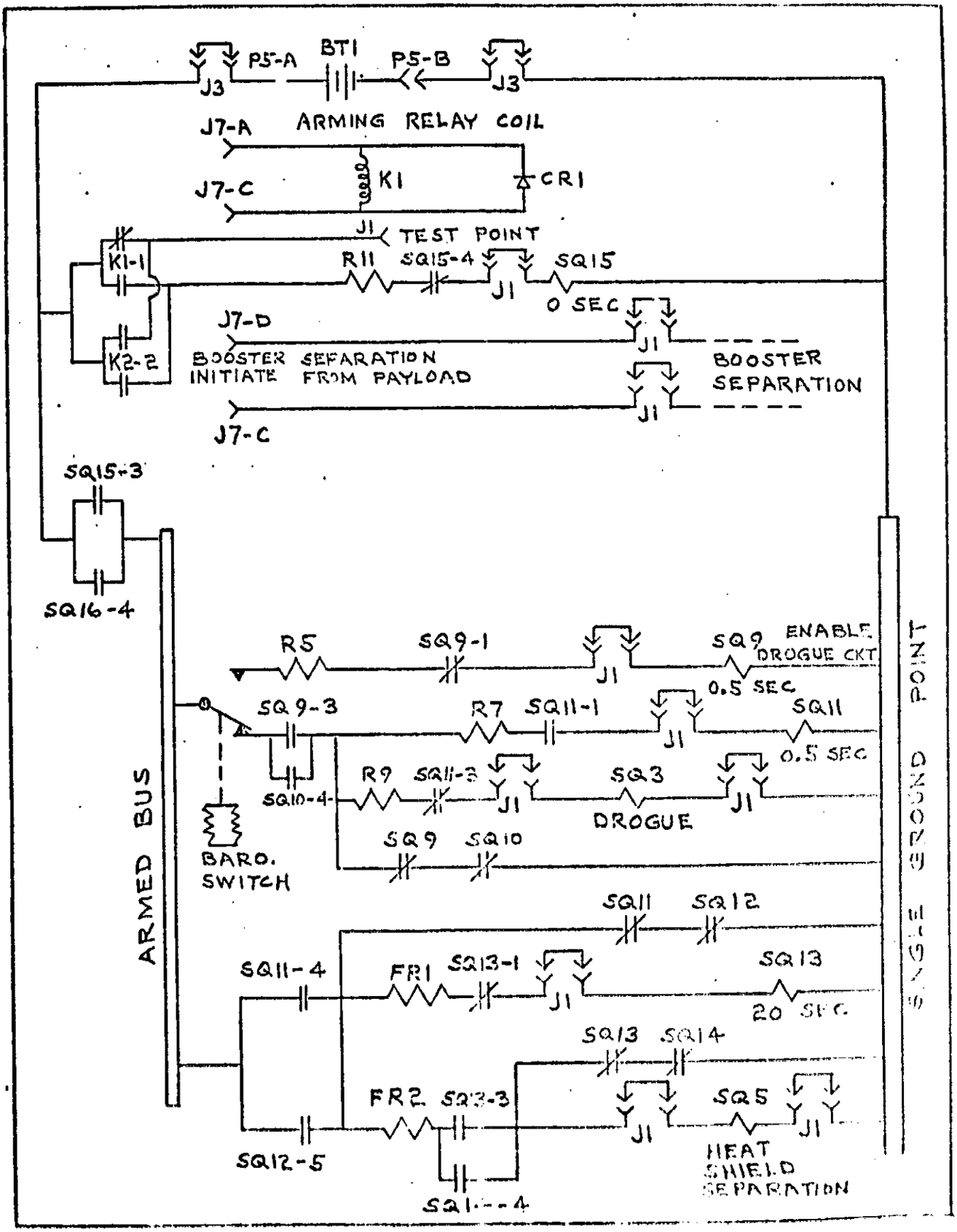

Figure 26 Logic Circuit Schematic

CONFIGURATION I

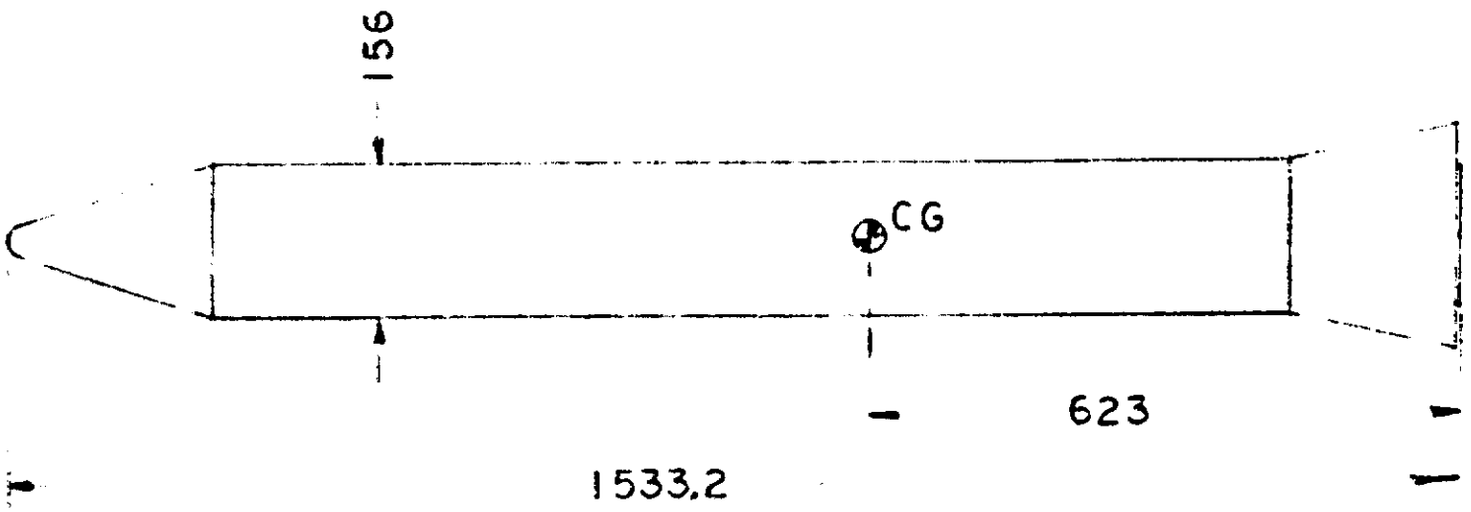

WEIGHT (EMPTY) 144,300 LBS

1" = 200"

FIGURE 27

CONFIGURATION I AFT END

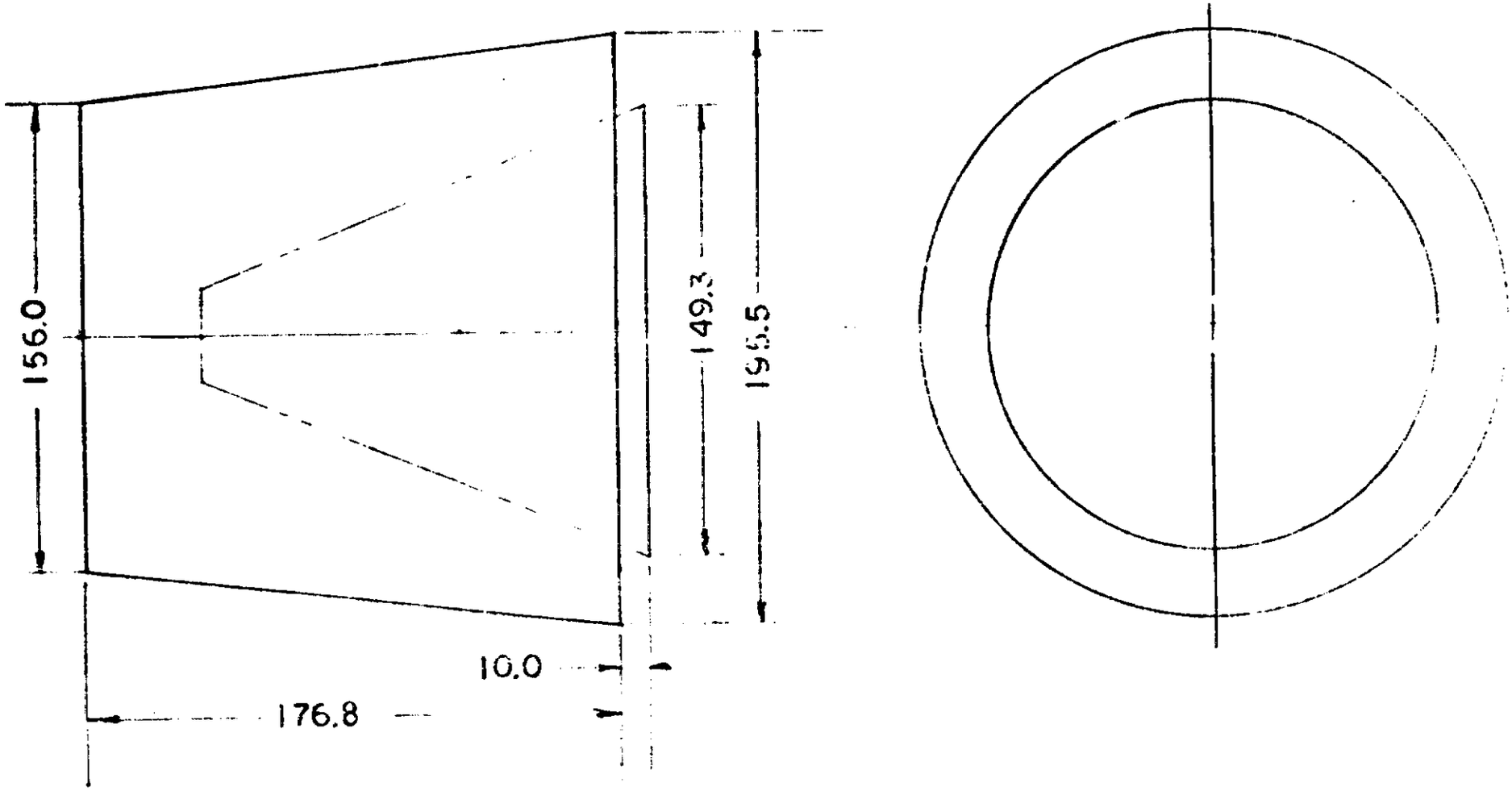

1" = 50"

FIGURE 28

CONFIGURATION II

WEIGHT (EMPTY) 491,566 LBS

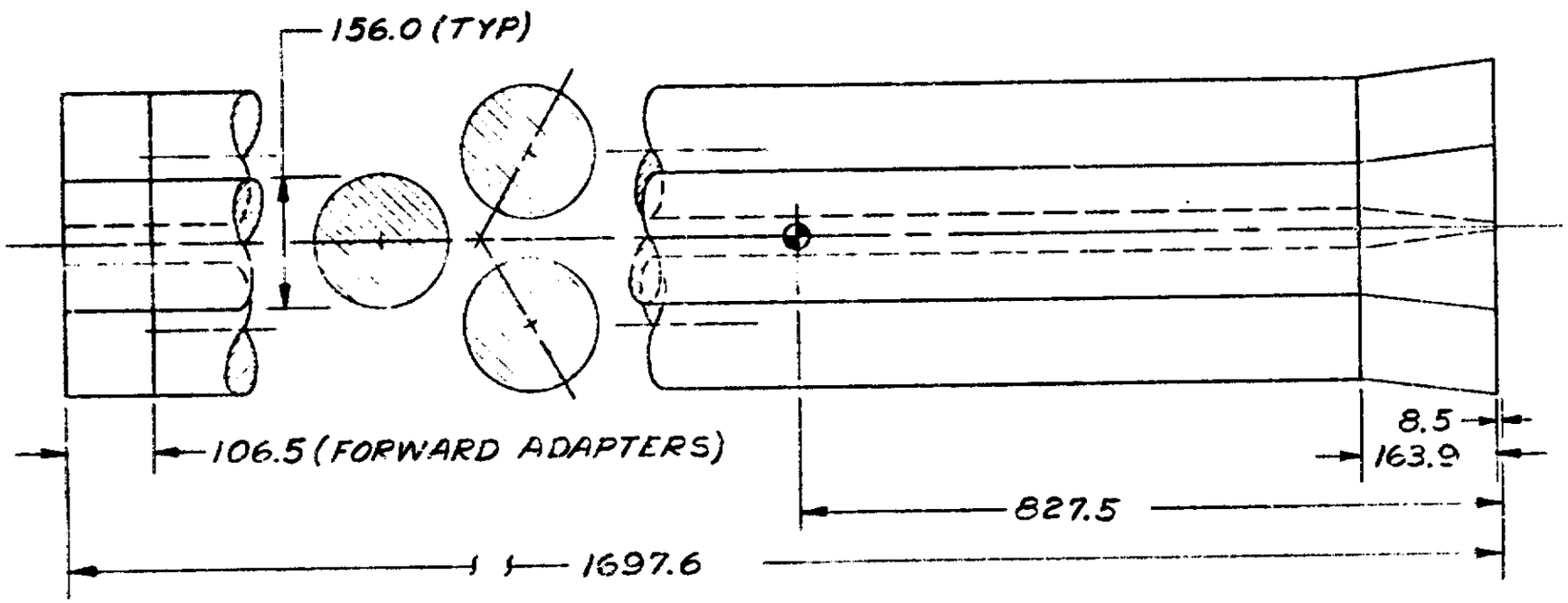

1" = 200"

FIGURE 29

CONFIGURATION II AFT END

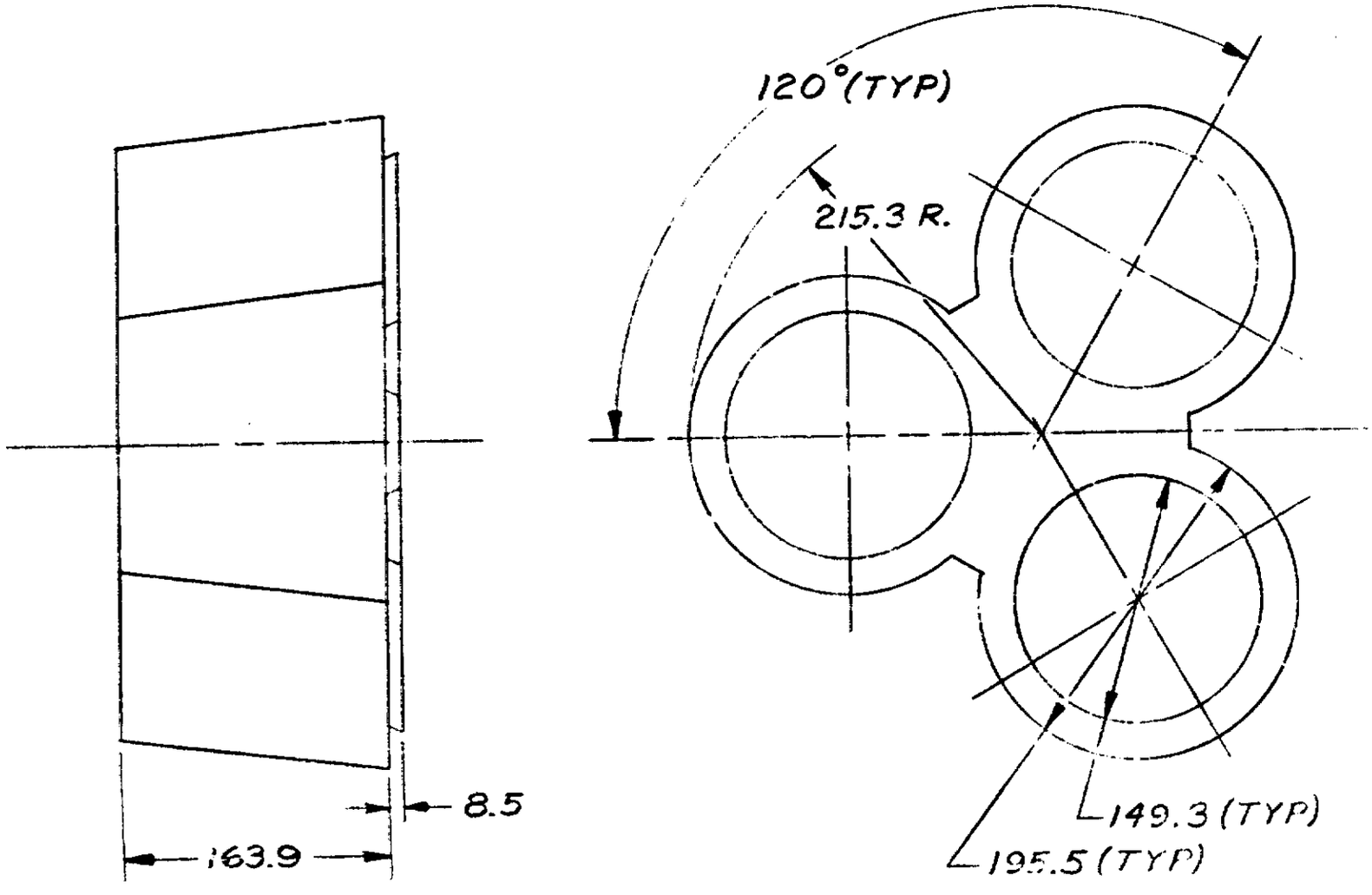

1" = 100"

FIGURE 30

CONFIGURATION I-B

DROGUE PARACHUTE DEPLOYMENT

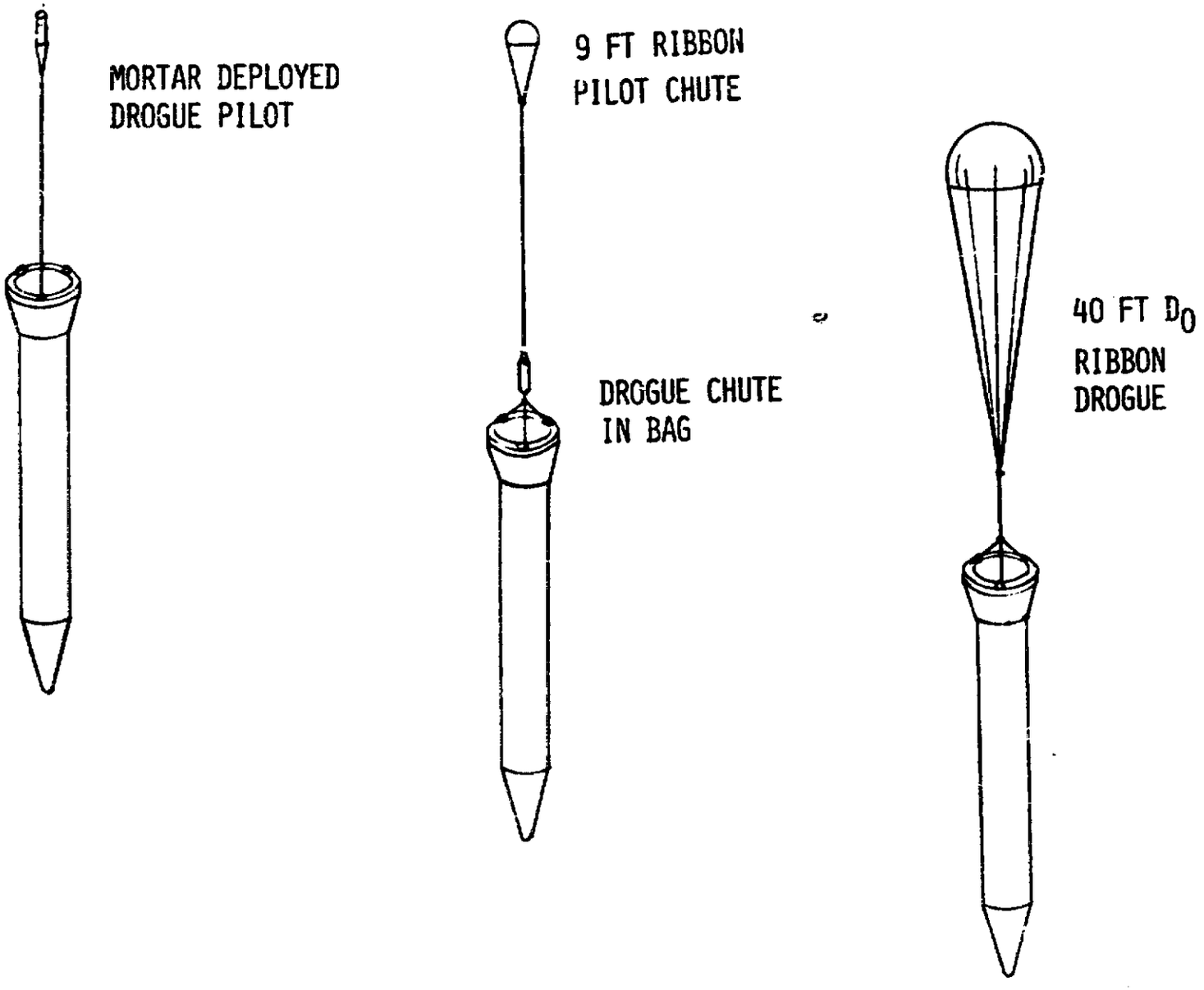

FIGURE 31

CONFIGURATION I-B

MAIN PARACHUTE DEPLOYMENT

2 MORTAR
DEPLOYED
MAIN PILOTS

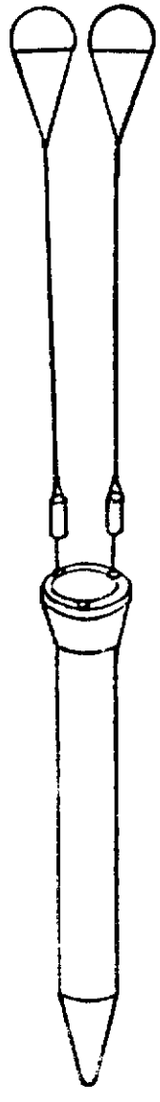

2 - 20 FT D_o
RIBBON
PILOT CHUTES

3 - 81 FT D_o
RIBBON CHUTES
IN EACH BAG

FIGURE 32

MAIN PARACHUTE DEPLOYMENT

CONFIGURATION I

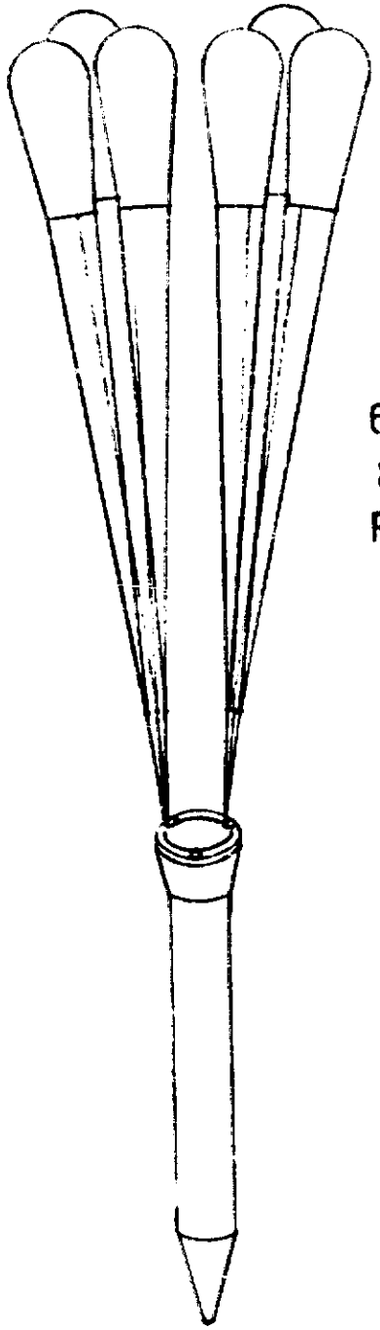

6 REEFED
81 FT D_0
RIBBON CHUTES

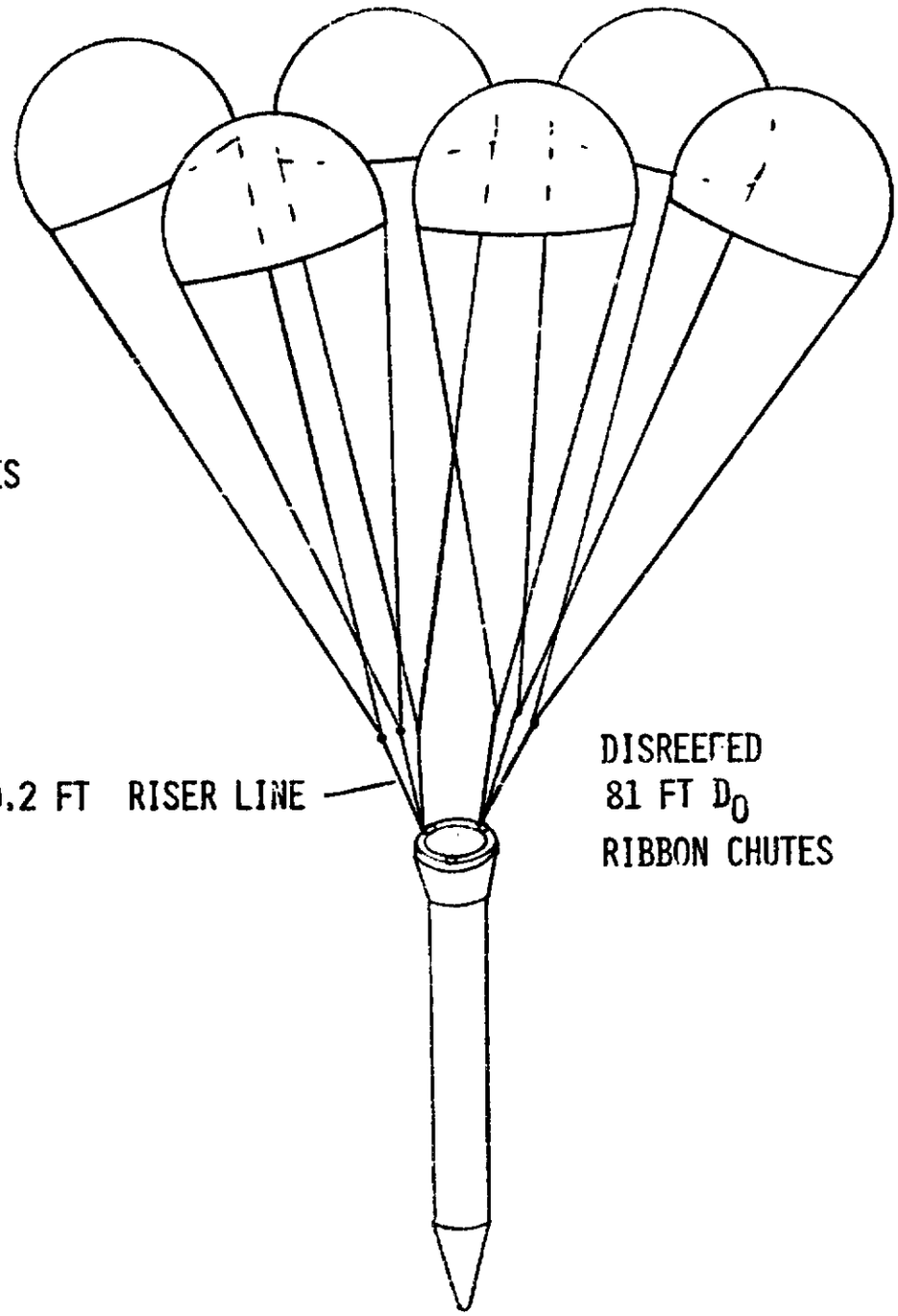

20.2 FT RISER LINE

DISREEFED
81 FT D_0
RIBBON CHUTES

FIGURE 33

CONFIGURATION II-B

DROGUE PARACHUTE DEPLOYMENT

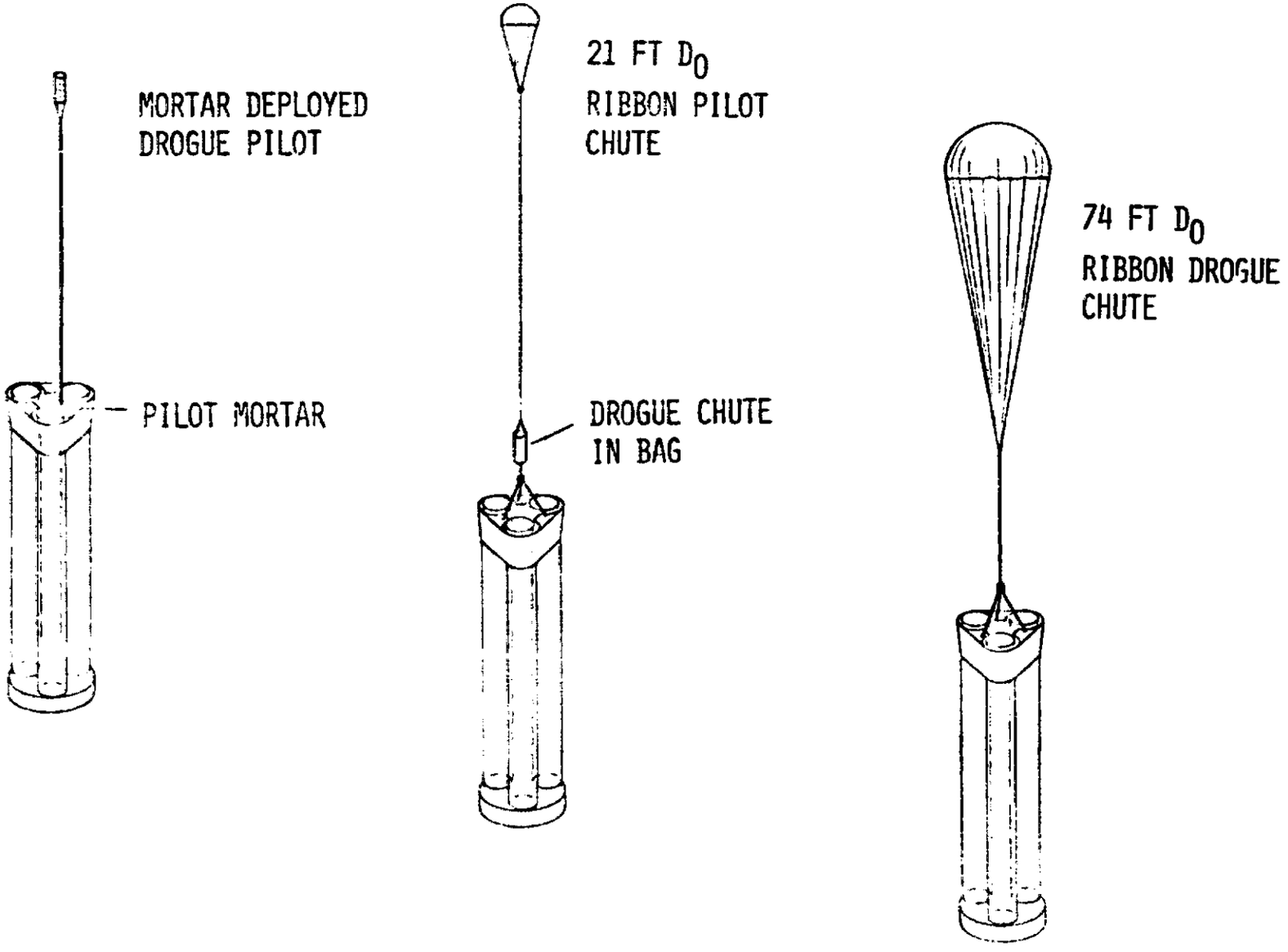

FIGURE 34

CONFIGURATION II-B
MAIN PARACHUTE DEPLOYMENT

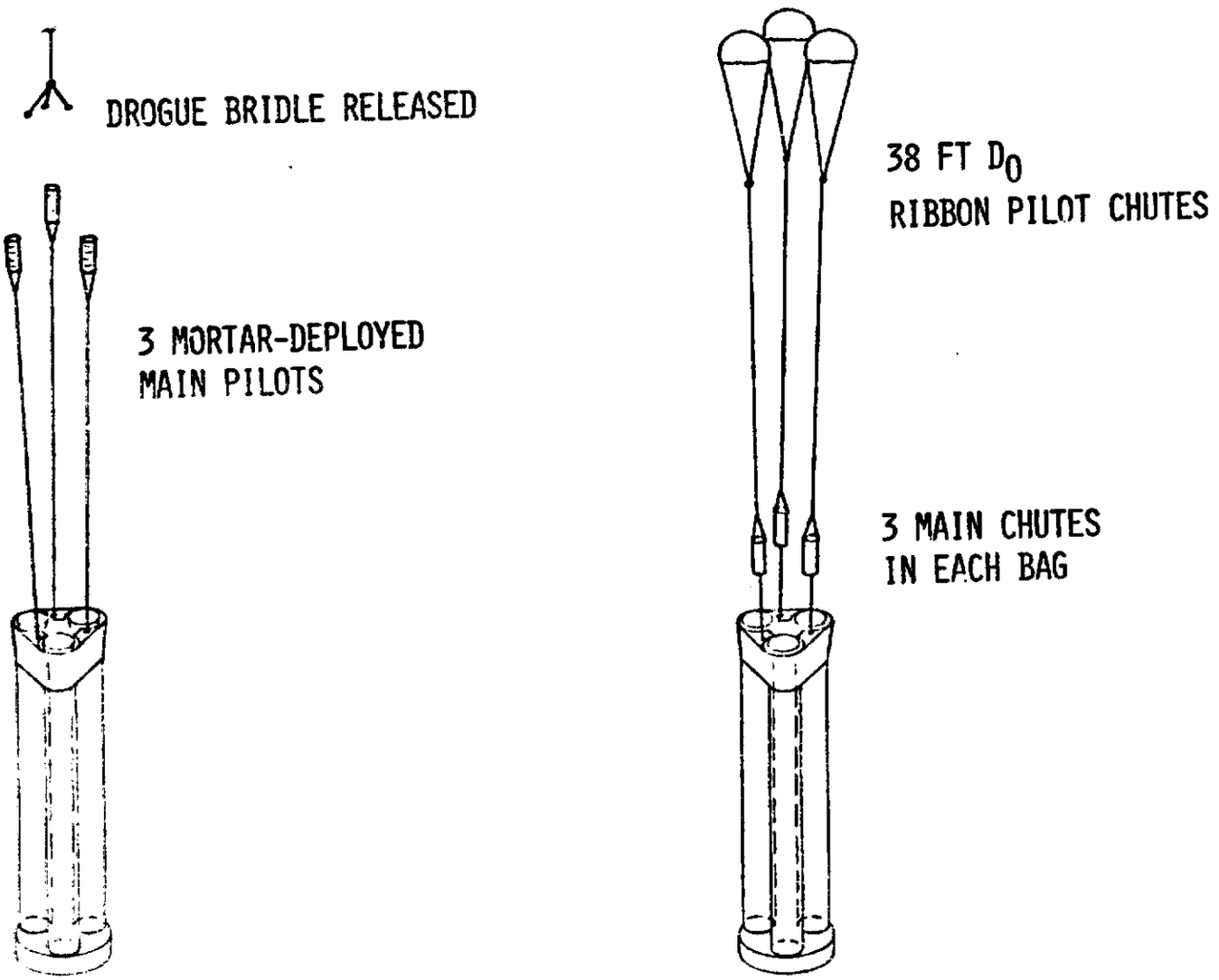

FIGURE 35

CONFIGURATION II-B

MAIN PARACHUTE DEPLOYMENT

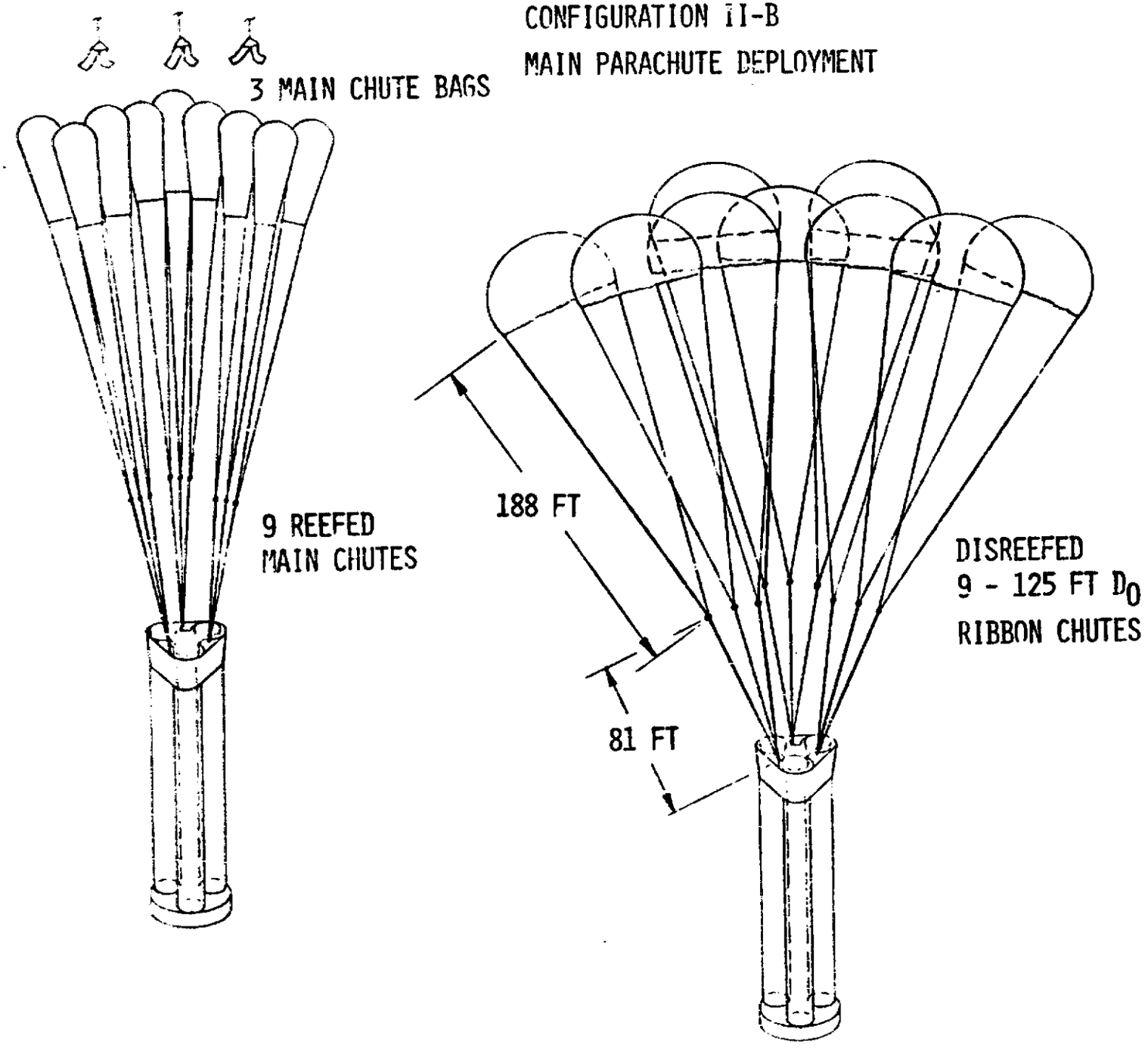

FIGURE 36

CONFIGURATION I-B

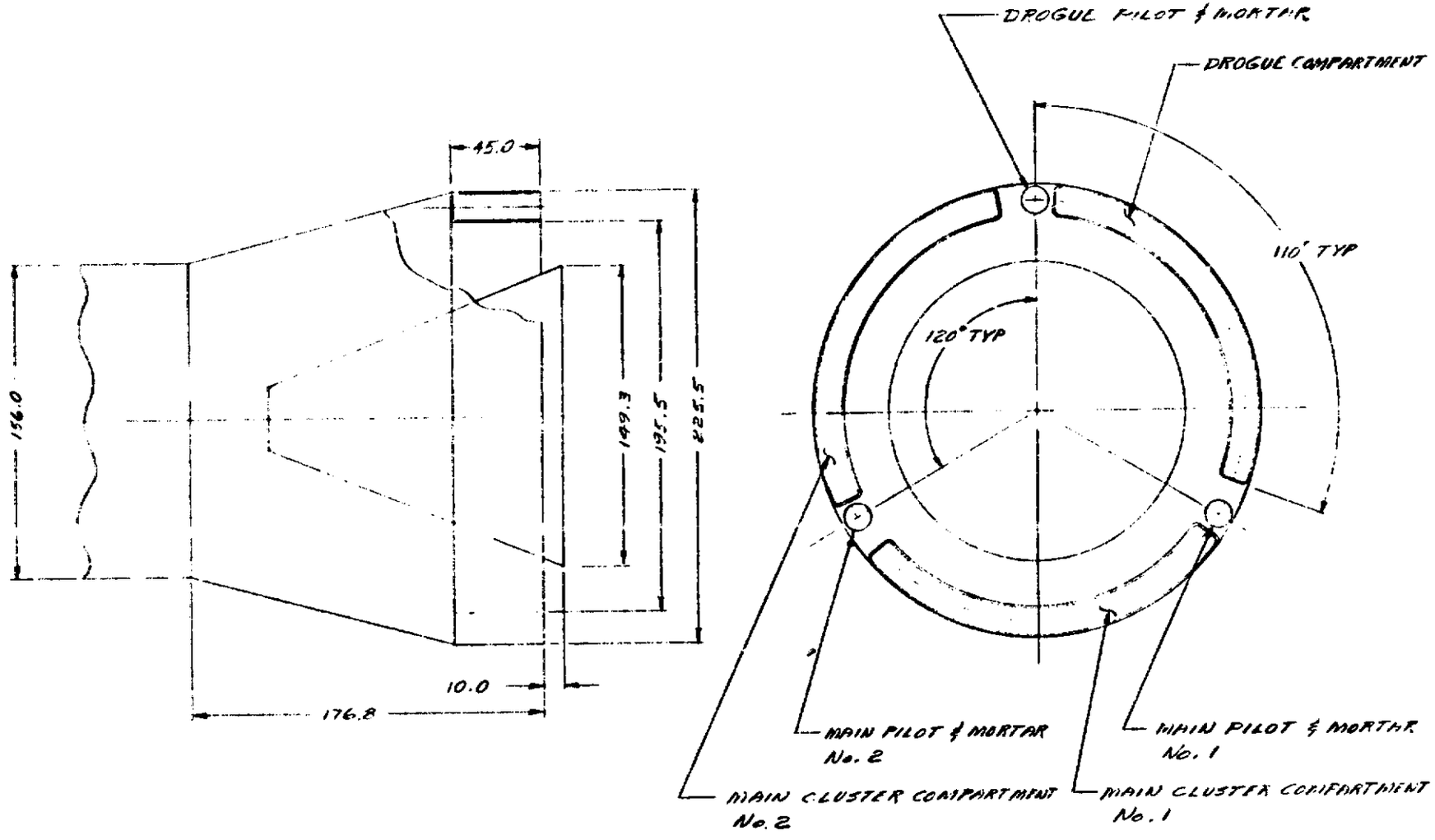

1" = 50"

FIGURE 37

CONFIGURATION I-B

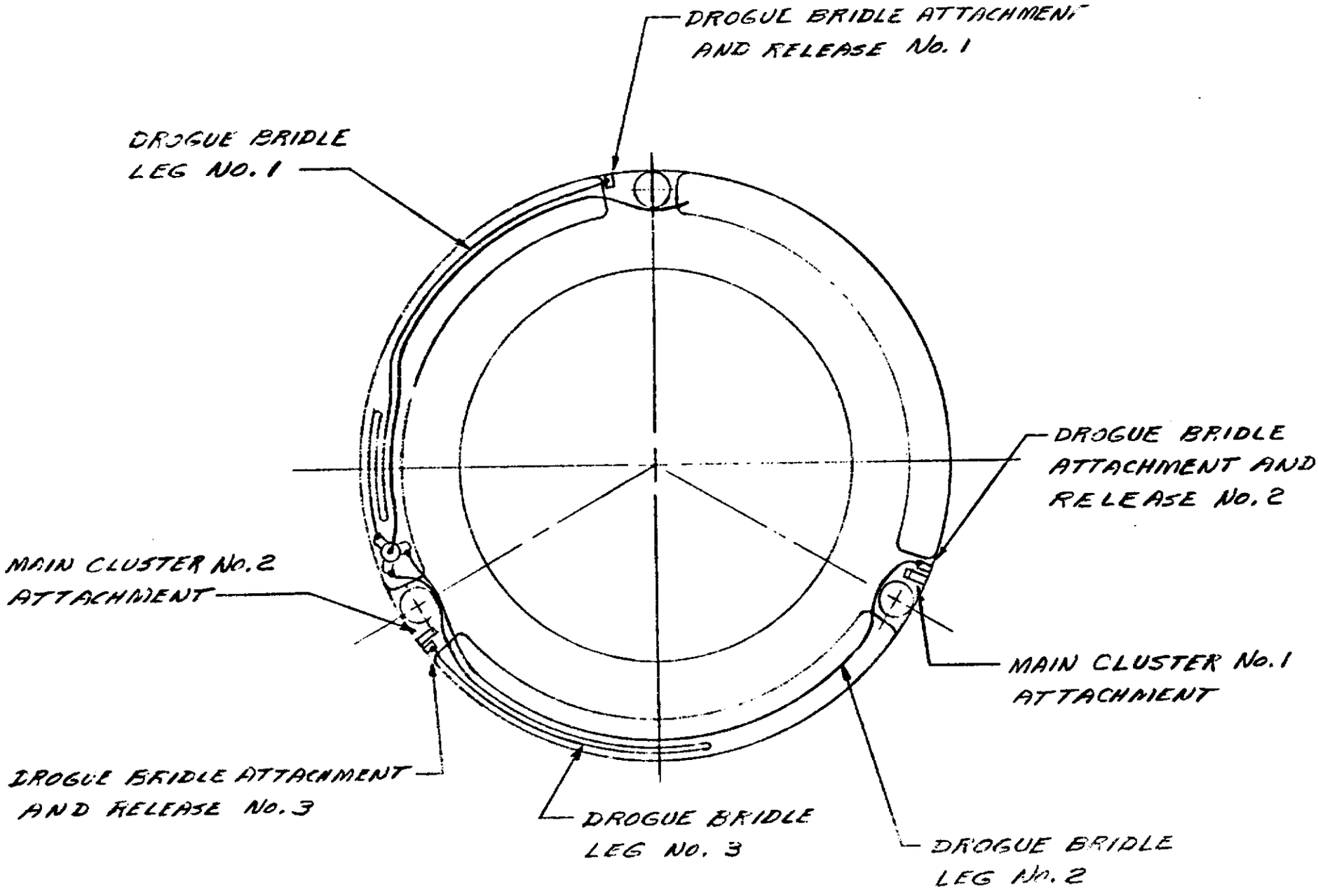

1" = 50"

FIGURE 38

CONFIGURATION IIB

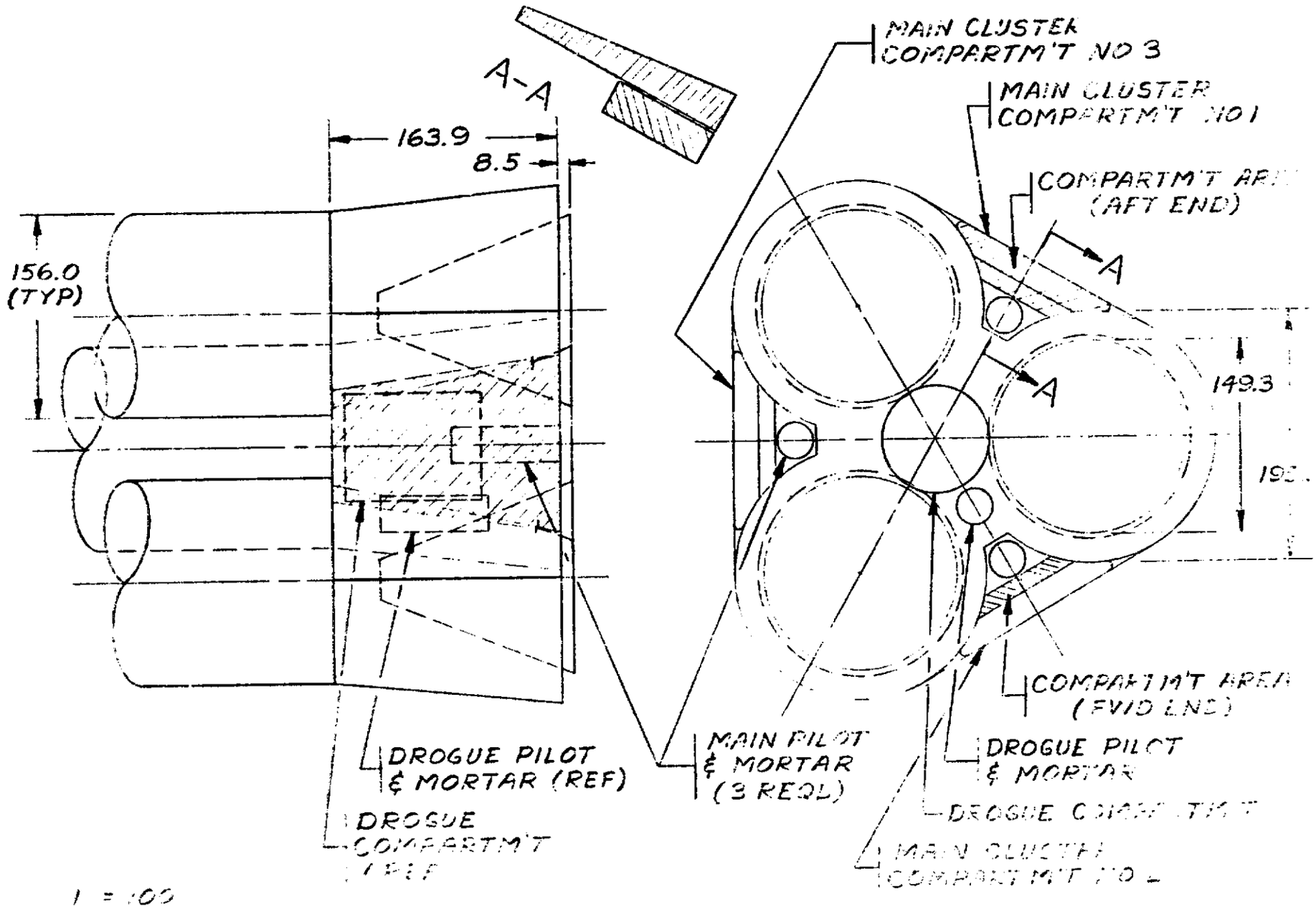

FIGURE 39

CONFIGURATION II-B

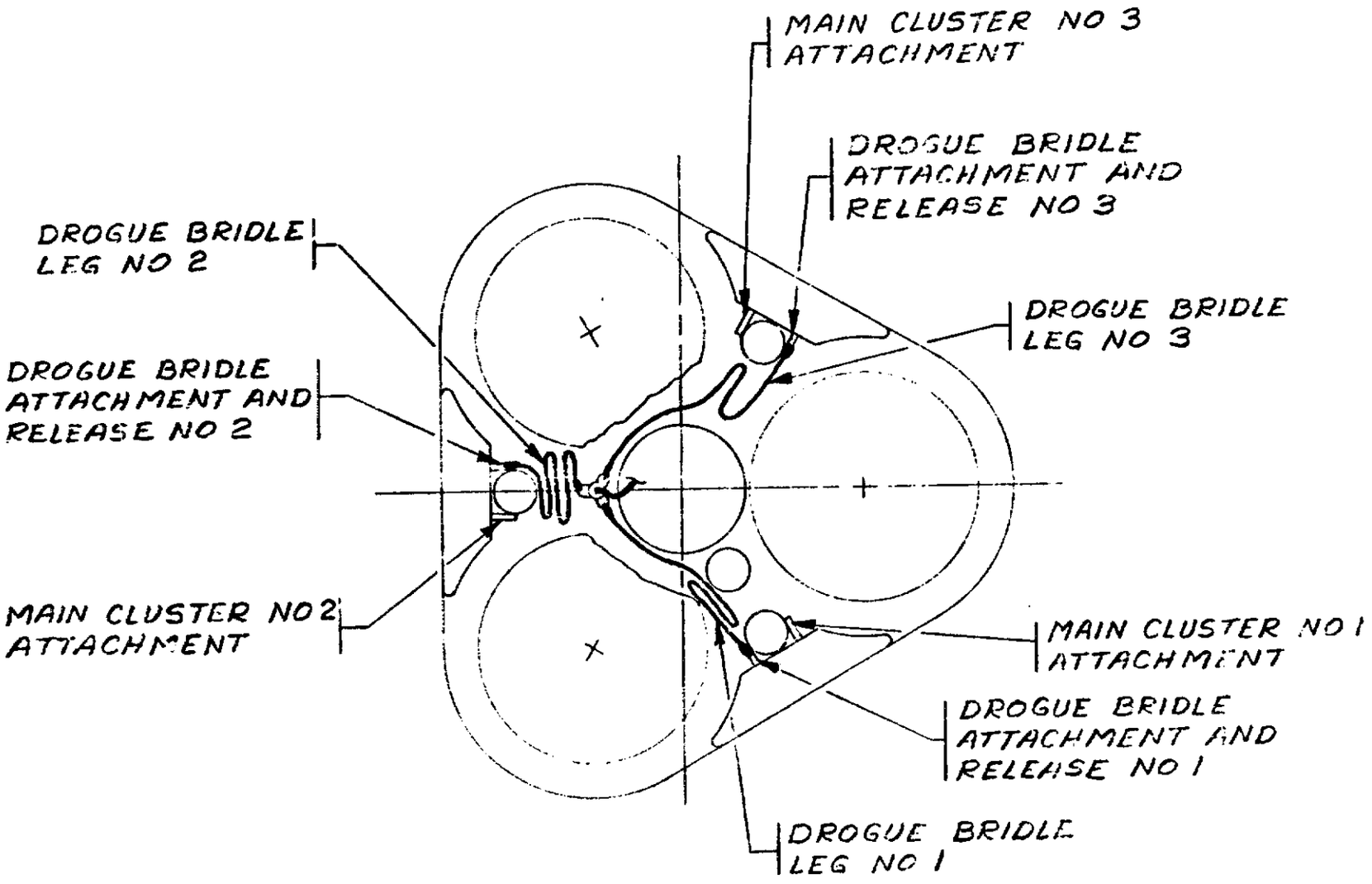

1" = 100"

FIGURE 40

FACILITY FLOOR PLAN

FLOOR PLAN

LEADER IDENTIFICATION

1. Unload Area
2. Defour and separate
3. Wash
4. Dry
5. Monorail System
6. Drop off table
7. Inspection table
8. Repair table
9. Sewing machine depot
10. Chute storage, refurb. and new
11. Packing tables
12. Packing press
13. Parachute pack assy. inventory
14. Main entrance stairs to second level offices
15. Flotation gear, repair and storage
16. Bridle and hardware area
17. Test lab
18. Receiving and material stores
19. office

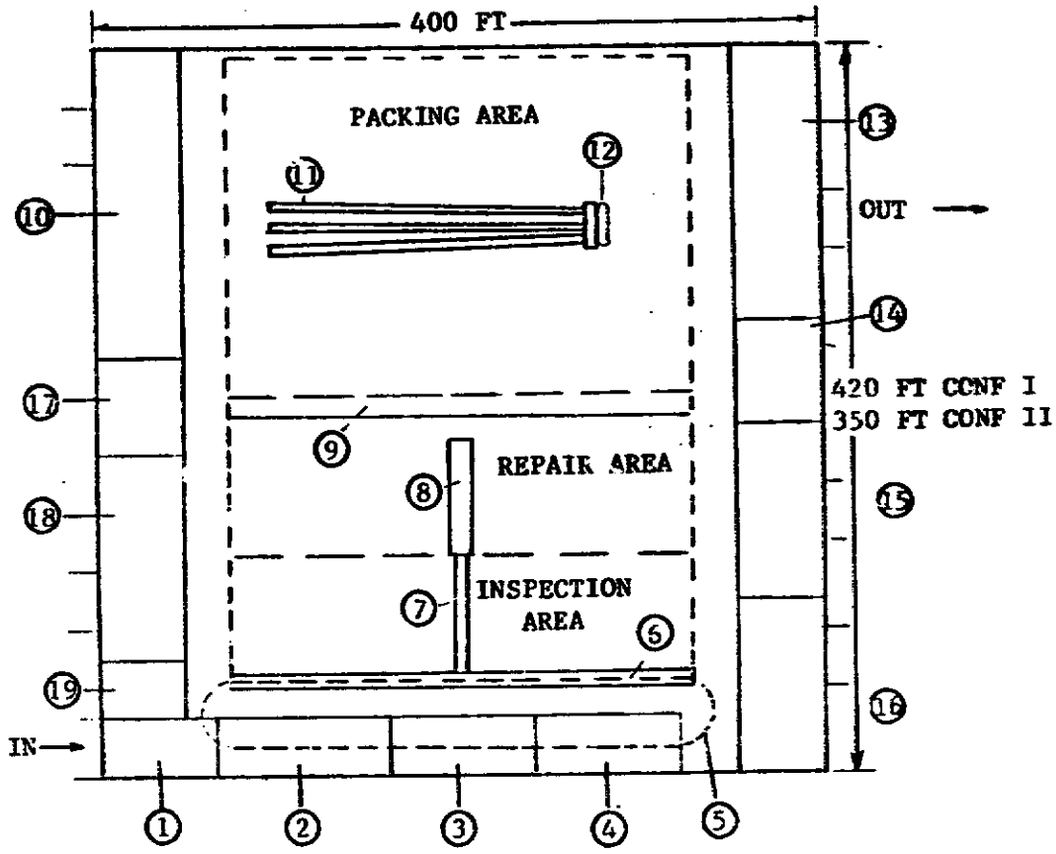

FIGURE 41

LEFT BLANK INTENTIONALLY

FIGUPE 42

PARACHUTE REFURBISHMENT, 81 FT D_o
SCHEDULE FLOW

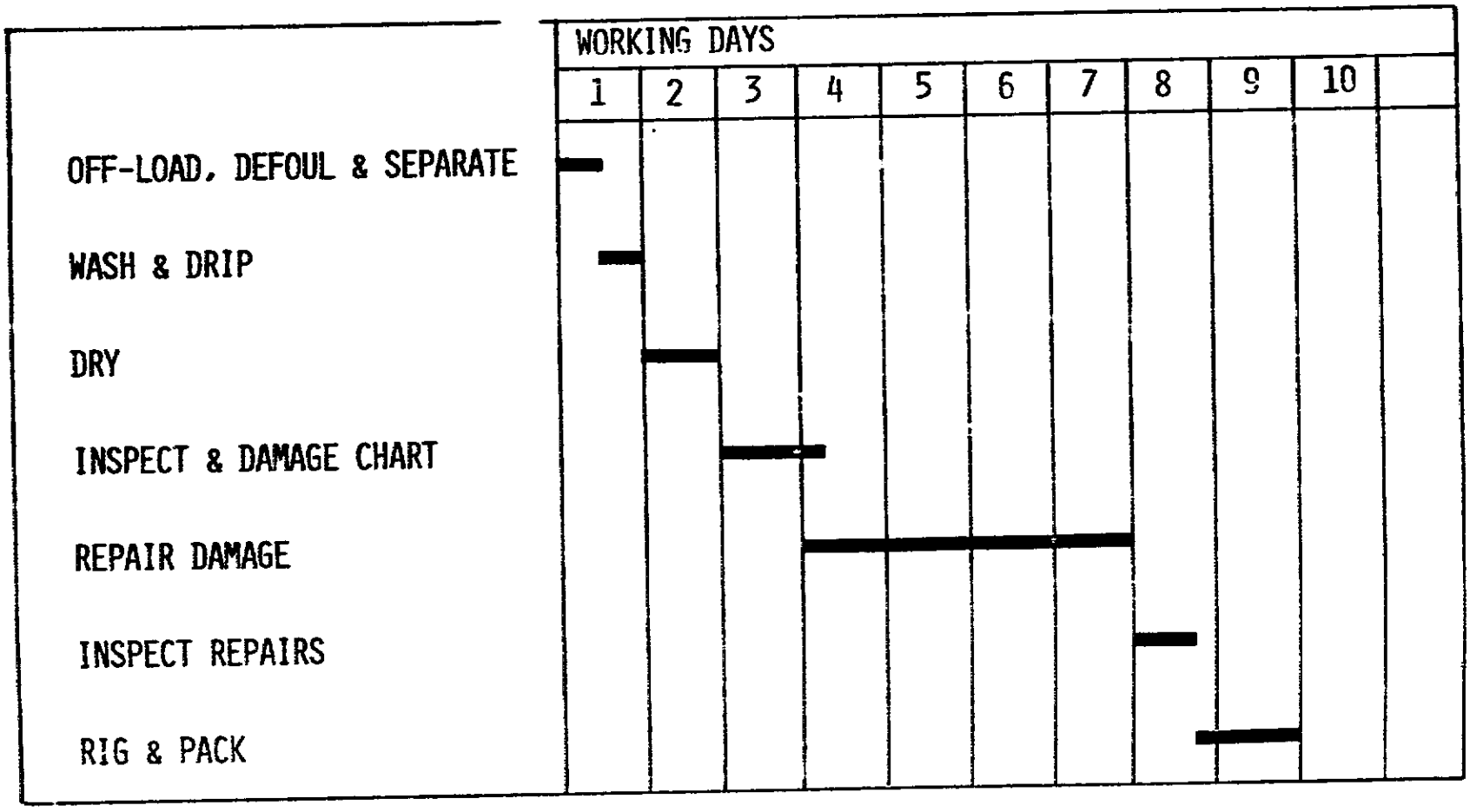

GROUND RULES
(1) TWO SHIFTS /5 DAY
(2) 100TH FLIGHT

FIGURE 43

PARACHUTE REFURBISHMENT, 125 FT D_o

SCHEDULE FLOW

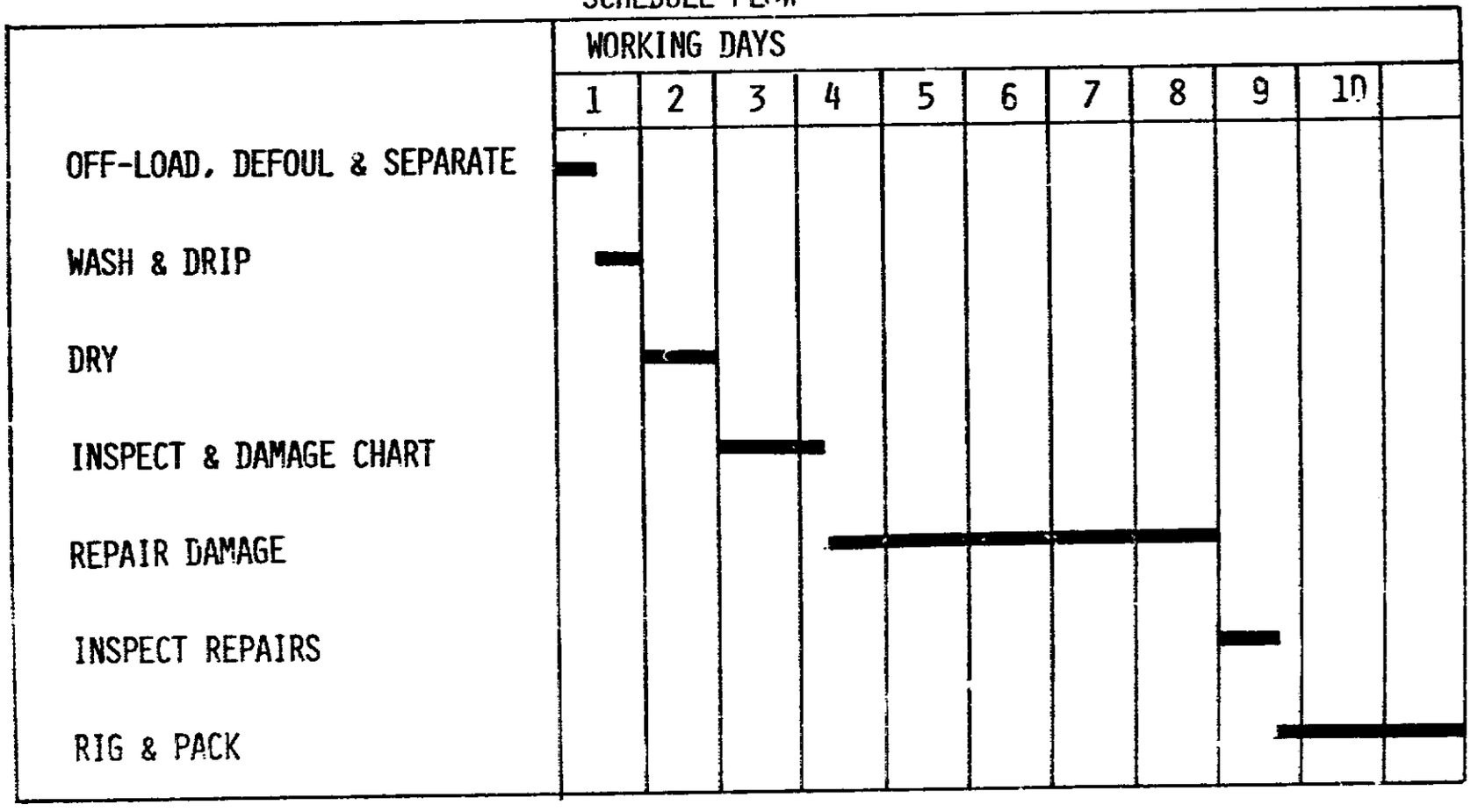

GROUND RULES

(1) 2 SHIFTS/5 DAY

(2) 100TH FLIGHT

FIGURE 44

OPERATIONAL HARDWARE REQUIREMENTS	CONFIGURATION IB 2 BOOSTERS/LAUNCH TOTAL	NEW	REFURB	CONFIGURATION IIB 1 BOOSTER/LAUNCH TOTAL	NEW	REFURB
A) Drogue Sub-System						
1. Drogue Pilot Mortar	890	890	-	445	445	-
2. Drogue Pilot Chute, Lines, Riser & Bag	890	890	-	445	445	-
3. Drogue Parachute Bag	890	890	-	445	445	-
4. Drogue Parachute and Lines	890	178	712	445	89	356
5. Drogue Harness - Parachute Leg	890	178	712	445	89	356
6. Confluence Fitting	890	178	712	445	89	356
7. Drogue Harness - Booster Legs	2,670	535	2,135	1,335	267	1,068
8. Drogue Harness Releases	2,670	535	2,135	1,335	267	1,068
Pyrotechnics	2,670	2,670	-	1,335	1,335	-
9. Flotation and Beacon	890	178	712	445	89	356
B) Main Parachute Sub-System						
1. Main Pilot Mortar	1,780	1,780	-	1,335	1,335	-
2. Main Parachute Release Fitting	1,780	297	1,483	1,335	223	1,112
Pyrotechnics	1,780	1,780	-	1,335	1,335	-
3. Main Pilot Chute, Lines, Riser & Bag	1,780	1,780	-	1,335	1,335	-
4. Main Parachute Bag	1,780	1,780	-	1,335	1,335	-
5. Main Parachute and Lines	5,340	890	4,450	4,005	668	3,337
6. Main Parachute Riser	5,340	890	4,450	4,005	668	3,337
7. Flotation and Beacon	5,340	890	4,450	4,005	688	3,337
8. Reefing System						
a) Reefing Rings	1,068,000	178,000	890,000	1,198,800	199,800	999,000
b) Cutters	42,720	7,120	35,600	31,968	5,328	26,640
c) Reefing Lines	10,680	10,680	-	7,992	7,992	-
C. Booster Orientation and Beacon	890	149	741	445	75	370

Basis: 445 Launches with Re-usable Hardware Being Refurbished (Drogue Sub-System 4 Times and Main Sub-System 5 Times) No Spares Included

FIGURE 45

SOLID ROCKET MOTOR RECOVERY

CONFIGURATION I OR II

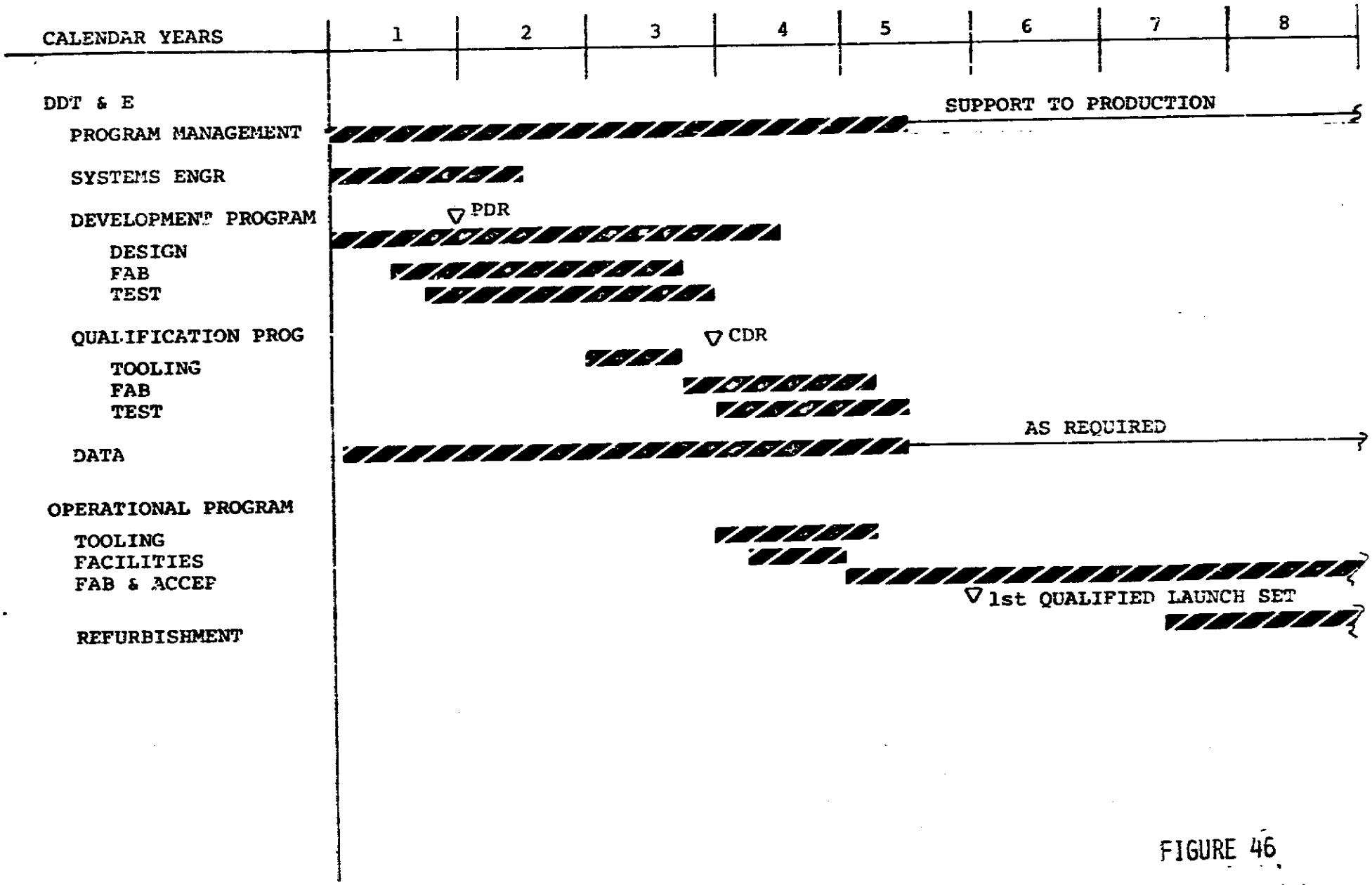

FIGURE 46

2/9/72 (T)

SOLID ROCKET MOTOR RECOVERY

ROM ESTIMATE

	CONFIGURATION IB MILL. DOLLARS		CONFIGURATION IIB MILL. DOLLARS	
DDT&E Estimate				
Program Management	8.0		8.0	
System Engr.	5.0		7.0	
Design, Develop & Test	37.0		45.0	
Customer Components	3.0		4.0	
Hardware for Qualification	11.0		19.0	
Logistic Support & Special Test Equipment	7.0		9.0	
Orientation and Beacon	4.0		4.0	
Data	5.0	80.0	5.0	101.0
Operational Estimate				
Tooling	.9		.9	
Capital Equipment	4.15		4.15	
Facilities	17.35		22.6	
Production:				
Main Chutes 15.1 / 21.8				
Mortars 16.0 / 21.4				
Drogues 4.45 / 3.2				
Orientation & Beacon 4.05 / 4.05	39.6		50.45	
Production Support	4.0		4.2	
Refurbishment:				
Main Chutes 20.4 / 29.1				
Drogues 4.3 / 3.1				
Orientation & Beacon 2.3 / 2.3	27.0	93.0	34.5	116.8
Total ROM Estimate		173.0		217.8

FIGURE 47

APPENDIX F

QUANTITATIVE ASSESSMENT OF THE ENVIRONMENTAL EFFECTS OF ROCKET ENGINE EMISSIONS DURING SPACE SHUTTLE OPERATIONS AT KENNEDY SPACE CENTER

GCA TR-72-8-G

QUANTITATIVE ASSESSMENT OF THE ENVIRONMENTAL EFFECTS OF ROCKET ENGINE EMISSIONS DURING SPACE SHUTTLE OPERATIONS AT KENNEDY SPACE CENTER

H. E. Cramer, R. K. Dumbauld,
A. G. Tingle and J. R. Bjorklund

Prepared for

MR. JOHN THIRKILL
Thiokol Chemical Corporation
P. O. Box 524
Brigham City, Utah 84302

GCA CORPORATION
GCA TECHNOLOGY DIVISION
Environmental Sciences Laboratory
Salt Lake City, Utah

7 February 1972

ACKNOWLEDGMENT

We are indebted to Dr. E. Constantinides, Staff Scientist in the Bedford, Massachusetts Office of the GCA Technology Division, for his assistance in developing the material on the environmental impact of stratospheric emissions contained in Section 5 of the report.

SUMMARY

The purpose of this study is to make a quantitative assessment of the environmental impact of exhaust products emitted by a rocket engine configuration consisting of two solid propellant engines and one LOX engine during launch operations of the NASA Space Shuttle and Booster at Kennedy Space Center. The exhaust products considered in the study are HCl, Al_2O_3, CO, CO_2 and H_2O from the solid propellant engines and H_2O from the LOX engine. Emissions data and other information on the performance of the booster engines were supplied by the Thiokol Chemical Corporation. Toxicity criteria in the form of 10-minute maximum allowable concentrations of CO, HCl and Al_2O_3 were obtained from a recent NASA report. Meteorological data used in the study were obtained from mean monthly vertical profiles of wind speed, wind direction and air temperature for Kennedy Space Center (Smith and Vaughan, 1961) and from selected case studies of meteorological structure at Kennedy Space Center used in previous hazard studies (Record, et al., 1970; Dumbauld and Bjorklund, 1971) by the GCA Corporation Technology Division.

In normal launch operations, the booster engines burn for approximately 135 seconds and the maximum altitude of the burn is about 40 kilometers. Exhaust products are thus emitted in both the troposphere and stratosphere, the base of stratosphere being about 16 kilometers at Kennedy Space Center. Because both the atmospheric processes controlling the transport and dilution of pollutants as well as the receptor effects are different in the troposphere and stratosphere, these two regions of the atmosphere have been treated separately. In estimating the environmental impact of tropospheric emissions, we have used computerized multilayer diffusion models previously developed for NASA by the GCA Corporation Technology Division for calculating toxic fuel hazards (Dumbauld, et al., 1970). In evaluating the possible formation of acid mist in the cloud of exhaust products in the lower troposphere, we have used procedures developed in recent work for Vandenberg Air

Force Base (Cramer, et al., 1970). For the stratospheric problem, we have used a very simple approach based principally on calculations of the time required for the concentrations of exhaust products to reach ambient levels, if the products are normally present in the stratosphere, or levels of the normal trace constituents if the products are not normally present in stratospheric air. The bulk of the tropospheric hazard calculations for this study were made on the UNIVAC 1108 machine at the University of Utah using the computer programs described above in conjunction with the requisite emissions and meteorological data.

The results of the tropospheric hazard calculations are summarized briefly as follows:

- For the three meteorological regimes considered, the ground-level concentrations of HCl, Al_2O_3 and CO are all below the maximum allowable 10-minute concentration levels for both a normal launch and an on-pad abort in which one of the solid propellant engines is completely burned with the vehicle in a hold-down status

- For a low-level vehicle destruct at an altitude of 2 kilometers, the calculations show a stabilized cloud of exhaust products to be formed at an altitude of about 4 kilometers with an approximate diameter of 2 kilometers; average concentrations of CO (50 ppm) and Al_2O_3 (35 mg m^{-3}) within the stabilized cloud are well below the ground-level toxicity criteria and the corresponding HCl concentration (30 ppm) is equal to the ground-level limit

- The formation of an acid mist is possible only in situations where the ambient humidity is close to 100 percent; the production of acid drizzle or rain that will reach the underlying

surface in significant amounts appears to be very unlikely, although the formation of small water drops within the exhaust cloud with an acid content of 1 to 5 percent by weight is likely if a sufficient ambient supply of water is available

- Calculations of the maximum removal of HCl from the exhaust cloud by falling precipitation show that the maximum surface deposition of HCl ranges from about 4.2 to 0.26 grams per square meter, depending on the time after launch at which the precipitation starts; assuming that this amount of HCl is dissolved in 2.5 millimeters of rain, the pH content of the rain water ranges from 1.35 to 2.56; although we are not aware of detailed studies of the effects of HCl acid on vegetation and other receptors, these pH values appear to be potentially capable of producing harmful effects

The results of the stratospheric hazard assessment are:

- Concentrations of CO_2 and N_2 emitted from the rocket engines fall below ambient levels as soon as the exhaust cloud attains horizontal dimensions of a few hundred meters; this occurs within a few minutes after the passage of the vehicle

- Concentrations of H_2O fall below ambient levels as soon as the horizontal dimensions of the exhaust cloud are 1 or 2 kilometers; this is estimated to occur within a few hours after the passage of the vehicle

- Because HCl, Al_2O_3 and CO are not included in the normal constituents of stratospheric air, we have required their concentrations to reach an order of magnitude below the level

for normal trace constituents (10^{11} molecules per cubic centimeter); this criterion requires that the horizontal dimensions of the exhaust cloud be approximately 50 kilometers in extent, which should be achieved after a couple of days of stratospheric residence

- The above criterion for HCl, Al_2O_3 and CO is probably too conservative because there are no established chemical or photochemical reactions in the stratosphere involving these products

The principal conclusion of the study is that the only environmental hazard posed by the rocket engine emissions is the tropospheric washout of HCl by falling precipitation and the consequent surface deposition of acid rain containing from about 1 to 0.01 percent HCl by weight. This phenomenon occurs only if the vehicle is either launched during rain showers or if such showers occur along the first 100 kilometers of the downwind trajectory of the elevated ground cloud of exhaust products. If this trajectory is over water rather than land, the harmful effects are minimized. For overland trajectories, the possible harmful effects of acid rain containing the amounts of HCl indicated above on vegetation and other receptors should be carefully evaluated.

TABLE OF CONTENTS

SECTION 1
INTRODUCTION

1.1 PURPOSE

The Thiokol Chemical Corporation is proposing the use of two solid propellant engines and one LOX engine for the booster of the NASA Space Shuttle. During a normal launch at Kennedy Space Center, combustion products will be emitted from these engines between the launch pad and a maximum height of about 40 kilometers. The purpose of the proposed study is to make a quantitative assessment of the environmental effects of these emissions. The combustion products of concern are: carbon monoxide, carbon dioxide, aluminum oxide, nitrogen, water, and hydrochloric acid. The potential environmental hazards posed by these products fall into three general categories:

- Ground-level concentrations or dosages that exceed established toxicity levels for uncontrolled populations
- Possible damage to vegetation or other receptors through surface deposition of the material by precipitation removal processes
- Possible effects of these products on the chemical and physical balance of the stratosphere

1.2 APPROACH

The quantitative assessment of the first two hazard categories was made principally by means of computerized multilayer diffusion models, previously developed by the GCA Technology Division for NASA and the U. S. Air Force, in conjunction with appropriate emissions data and meteorological data. The emissions data were supplied

by the Thiokol Chemical Corporation and are given in Figure 1-1 and Table 1-1. We have provided the necessary meteorological data representative of the area surrounding Kennedy Space Center which were available from previous work. Toxicity criteria used in the study, which are in the form of maximum allowable 10-minute concentrations for CO, HCl, and Al_2O_3, are presented in Table 1-2.

In calculating the possible environmental effects of stratospheric emissions (above 45,000 feet), we have used simple diffusion models to calculate the time required for concentrations of the combustion products to reach levels of insignificance in terms of ambient concentrations of the normal constituents of the stratosphere.

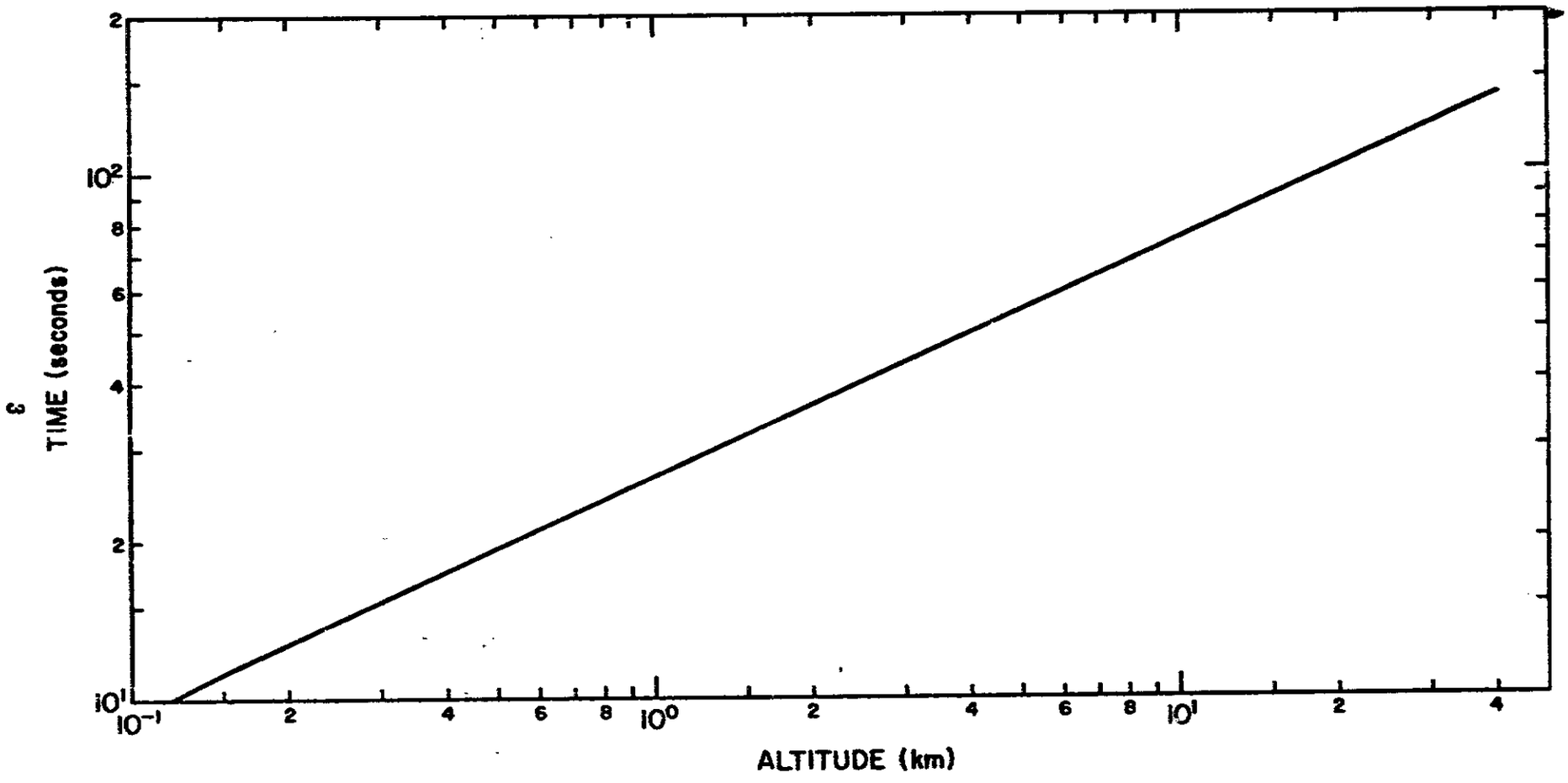

FIGURE 1-1. Booster altitude as a function of time after ignition.

TABLE 1-1

EMISSION RATES OF SELECTED ROCKET ENGINE EXHAUST PRODUCTS

Product	Rate (lb sec^{-1})		Total* (lb)
	2 Solid Engines	LOX Engine	
HCl	3518		4.749×10^5
Al_2O_3	4936		6.664×10^5
CO	3909		5.277×10^5
CO_2	614		8.289×10^4
H_2O	1529	4615	8.294×10^5
N_2	1427		1.927×10^5

*For a 135-second engine burn.

TABLE 1-2

MOLECULAR WEIGHTS AND 10-MINUTE MAXIMUM ALLOWABLE CONCENTRATIONS (MAC_{10}) FOR SELECTED ROCKET ENGINE COMBUSTION PRODUCTS

Fuel Component	Molecular Weight	MAC_{10}* (ppm)
CO	28.01	1500
HCl	36.47	30
Al_2O_3	101.94	50 (mg m^{-3})

*Taken from Table 1-1 of NASA Contractor Report NASA CR-61358 (Dumbauld and Bjorklund, 1971)

SECTION 2

TROPOSPHERIC MATHEMATICAL MODELS

The generalized multilayer concentration models used in the tropospheric hazard calculations were taken from a complete set of computerized multilayer diffusion models developed for use in estimating toxic fuel hazards at Kennedy Space Center (Dumbauld, et al., 1970). Only a brief description of these models is given below. A complete description is available in the above-referenced report prepared by the GCA Corporation Technology Division for the Marshall Space Flight Center. The generalized models are similar in form to the conventional Gaussian plume equations described by Slade (1968, pp. 97-99) and others. However, additional terms have been added to account for the effects of mesoscale factors, such as the depth of the surface mixing layer, vertical wind shear, and precipitation scavenging. The models also contain provision for gravitational settling, decay, and variations in source dimensions, source emission time, and in meteorological structure along the downwind cloud trajectory.

In using the multilayer models, the troposphere is divided into layers in which the meteorological structure is approximately homogenous. Major layer boundaries are placed arbitrarily at the points of major discontinuities in the vertical profiles of wind, temperature and humidity. It is assumed that there is no vertical flux of material across the major layer boundaries due to turbulent mixing; material flux across these boundaries can occur only as a result of gravitational settling or precipitation scavenging. Changes in meteorological structure at some arbitrary time or distance from the point of release can also be accommodated through use of special layer-breakdown models previously developed for this purpose in the work for Marshall Space Flight Center. As explained below, these models were used in the present study when the surface mixing layer was divided into sublayers to accommodate the height dependence of the initial vertical distribution of exhaust products.

The basic formula for the peak concentration in the K^{th} layer at some distance x downwind from the source is given by the expression

$$\chi_p = \frac{Q_K}{2\pi \sigma_{yK} \sigma_{xK}} \tag{2-1}$$

where

Q_K = source strength in units of mass per unit depth of the K^{th} layer

σ_{yK} = standard deviation of the crosswind concentration distribution in the K^{th} layer at distance x

σ_{xK} = standard deviation of the alongwind concentration distribution in the K^{th} layer at distance x

Equation (2-1) above is defined as Model 1 in the report by Dumbauld, et al. (1970), and the subset of equations defining σ_{yK} and σ_{xK} are given on pages 14 through 20 of the report. Briefly, σ_{yK} and σ_{xK} are calculated by means of simple power-law expressions relating turbulence parameters to cloud growth with distance. In this layer model, the source extends vertically through the entire layer; the vertical distribution of the material in the layer is assumed uniform with height and Gaussian along the crosswind (y) and alongwind (x) coordinates. The use of Equation (2-1) requires that material originating in the K^{th} layer is constrained from diffusing vertically beyond the vertical boundaries of that layer, as mentioned above.

In this study, to simplify the calculations of concentrations within the stabilized ground cloud of exhaust products, the major meteorological layers containing the ground cloud were subdivided according to the vertical distribution of material in the ground cloud. Material in the sublayers included in the surface mixing layer (see, for example, Figure 3-3) was permitted to diffuse vertically across the sublayer boundaries. The layer-transition model described as Model 5 by Dumbauld, et al. (1970, pp. 31-33) was used to make these calculations because it provides for the requisite vertical mixing and for identifying the contribution of

the material contained in each initial sublayer to the composite ground-level concentration. In the layer-transition model, material in the original K layers is permitted to diffuse into a new L^{th} layer (in this case the surface mixing layer) starting at a predetermined time t* which was set equal to 1 second. The peak concentration equation for Model 5 is given by the expression

$$\chi_{PL} = \frac{Q_K}{4\pi\,\sigma_{yLK}\,\sigma_{xLK}}$$

$$\left\{ \sum_{i=0}^{\infty} \left[\operatorname{erf}\left(\frac{2i\left(z_{TL}-z_{BL}\right)-z_{BK}+z_L}{\sqrt{2}\,\sigma_{zLK}} \right) + \operatorname{erf}\left(\frac{2i\left(z_{TL}-z_{BL}\right)+z_{TK}-z_L}{\sqrt{2}\,\sigma_{zLK}} \right) \right.\right.$$

$$\left. + \operatorname{erf}\left(\frac{2i\left(z_{TL}-z_{BL}\right)+2z_{BL}-z_{BK}-z_L}{\sqrt{2}\,\sigma_{zLK}} \right) + \operatorname{erf}\left(\frac{2i\left(z_{TL}-z_{BL}\right)-2z_{BL}+z_{TK}+z_L}{\sqrt{2}\,\sigma_{zLK}} \right) \right] \quad (2\text{-}2)$$

$$+ \sum_{i=1}^{\infty} \left[\operatorname{erf}\left(\frac{-2i\left(z_{TL}-z_{BL}\right)-z_{BK}+z_L}{\sqrt{2}\,\sigma_{zLK}} \right) + \operatorname{erf}\left(\frac{-2i\left(z_{TL}-z_{BL}\right)+z_{TK}-z_L}{\sqrt{2}\,\sigma_{zLK}} \right) \right.$$

$$\left.\left. + \operatorname{erf}\left(\frac{-2i\left(z_{TL}-z_{BL}\right)+2z_{BL}-z_{BK}-z_L}{\sqrt{2}\,\sigma_{zLK}} \right) + \operatorname{erf}\left(\frac{-2i\left(z_{TL}-z_{BL}\right)-2z_{BL}+z_{TK}+z_L}{\sqrt{2}\,\sigma_{zLK}} \right) \right] \right\}$$

where

σ_{zLK} = standard deviation of the vertical concentration distribution in the L^{th} layer for the source originating in the K^{th} layer

σ_{yLK} = standard deviation of the crosswind concentration distribution in the L^{th} layer for the source originating in the K^{th} layer

σ_{xLK} = standard deviation of the alongwind concentration distribution in the L^{th} layer for the source originating in the K^{th} layer

z_{TL} = height of the top of the L^{th} layer

z_{BL} = height of the base of the L^{th} layer

z_{TK} = height of the top of the K^{th} layer

z_{BK} = height of the base of the K^{th} layer

z_L = height in the L^{th} layer at which the concentration is calculated

Maximum surface deposition of HCl due to precipitation scavenging in a Layer L through which precipitation is fallir, was calculated by means of a modified version of Equation (3-36) in the report by Dumbauld, et al. (1970):

$$WD_L\{x_L, y_L, z=0\} = \frac{Q_K\,(z_{TL}-z_{BL})}{\sqrt{2\pi}\,\sigma_{yLK}\,\bar{u}_L}\left\{\exp\left[-\Lambda\left(\frac{x_L}{\bar{u}_L} + t^* - t_1\right)\right]\right\} \qquad (2\text{-}3)$$

where

Λ = fraction of material removed from the exhaust cloud by washout per unit time

z_{TL} = height of the top of the L^{th} layer

z_{BL} = height of the base of the L^{th} layer

$\bar{u}_L$ = mean wind speed in the L^{th} layer

σ_{yL} = standard deviation of the crosswind distribution of material in the L^{th} layer at a distance x_L from the source

x_L = distance from the source in the L^{th} layer

t_1 = time precipitation begins

The height of the top of the uppermost layer through which precipitation is falling z_{lim} must also be supplied as input to the computer program. In the washout deposition calculations described in Section 4.4 below, z_{lim} was set equal to 6 kilometers.

SECTION 3

DEVELOPMENT OF SOURCE AND METEOROLOGICAL INPUTS

3.1 METEOROLOGICAL DATA

The three meteorological situations used for the concentration calculations downwind from a normal launch and pad-abort are based on the mean monthly wind speed, wind direction, and temperature profiles for Kennedy Space Center (KSC) published by Smith and Vaughan (1961) and on the work of Record, et al. (1970) and Dumbauld and Bjorklund (1971). Concentrations at ground level are primarily dependent on the depth of the surface mixing layer H_m and the vertical distribution of material in the stabilized cloud of exhaust products. Study of the mean wind speed and direction profiles for KSC showed that for wind flow required to transport the combustion product cloud inland, the average surface mixing layer depth is about 1000 meters. During the spring on some occasions the surface mixing layer depth approaches 2000 meters and during the afternoon sea breeze regime in all seasons, the average mixing depth is about 300 meters. Figure 3-1 shows the wind direction profiles and Figure 3-2 shows the wind speed profiles for the fall, spring and afternoon sea-breeze regimes at KSC. Details of the temperature profiles in the lowest 5 kilometers for these regimes are given by Dumbauld and Bjorklund (1971).

3.2 CLOUD RISE CALCULATIONS

Estimates of maximum cloud rise for the cases of normal launch and pad-abort were obtained from an expression due to Briggs (1969, p. 33; 1970):

$$z = \left[\frac{3F_m}{\bar{u}\,\gamma^2\,s^{1/2}} \sin\left(s^{1/2}\,t\right) + \frac{3F}{\bar{u}\,\gamma^2\,s} \left(1 - \cos\left(s^{1/2}\,t\right)\right) \right]^{1/3} \qquad (3\text{-}1)$$

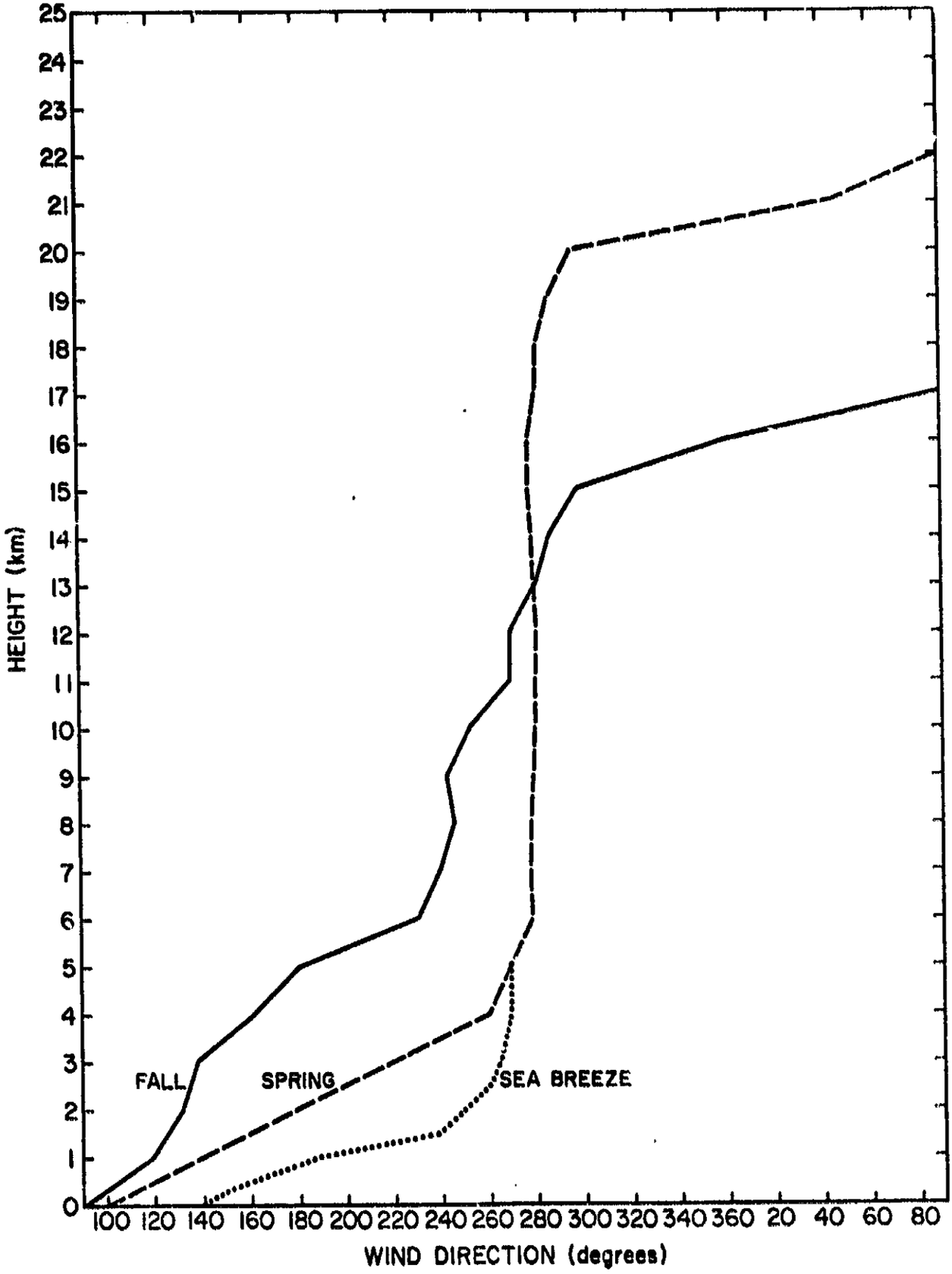

FIGURE 3-1. Wind direction versus altitude for the fall, spring, and sea-breeze meteorological regimes.

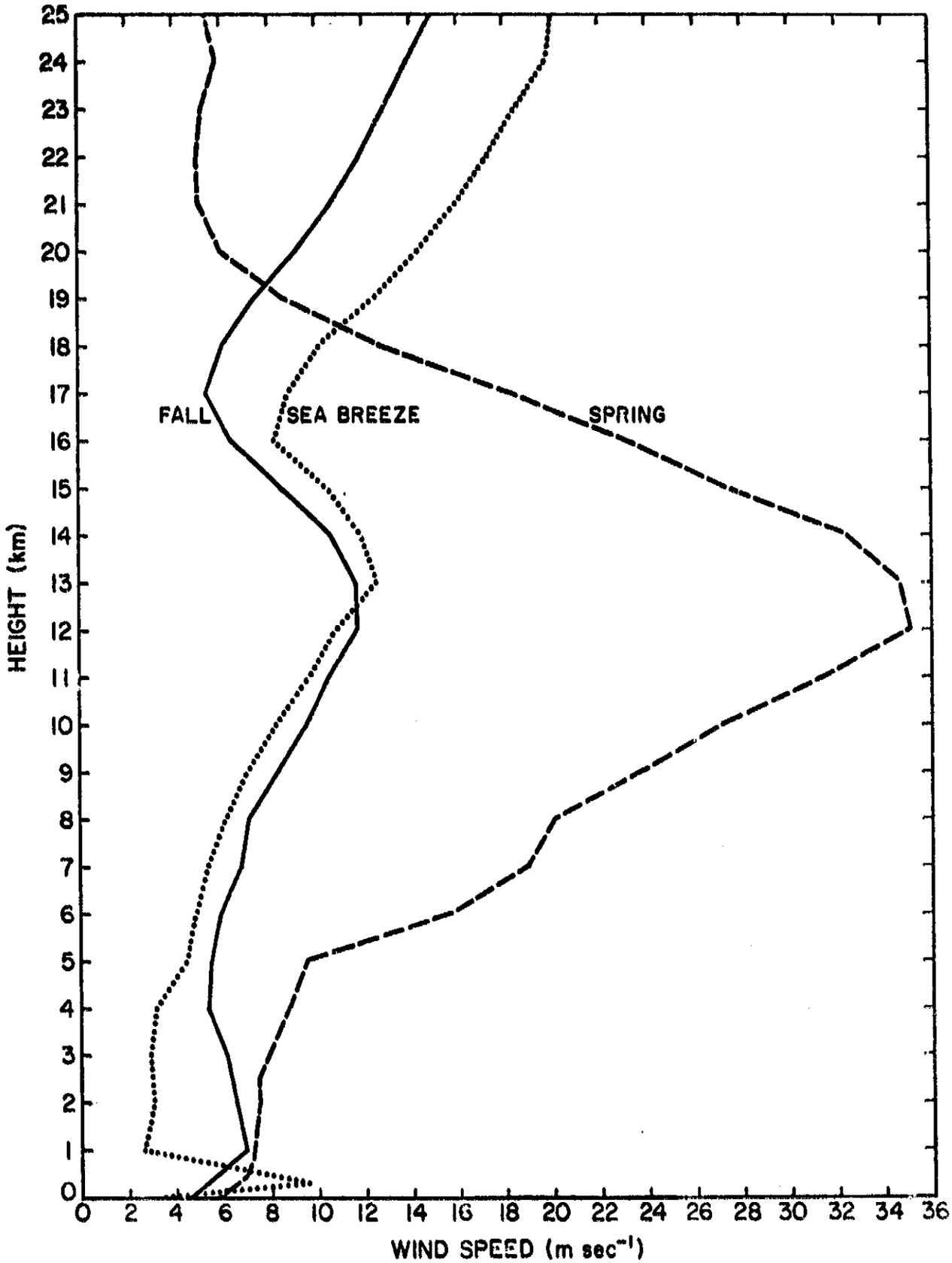

FIGURE 3-2. Wind speed versus altitude for the fall, spring, and sea-breeze meteorological regimes.

where

z = height of cloud at time t

$F_m = w_o^2 r_o^2$

w_o = initial vertical velocity (m sec^{-1})

r_o = radius of area where vertical velocity equals w_o (m)

$\bar{u}$ = mean wind speed (m sec^{-1})

γ = entrainment constant where cloud radius $r(z) = \gamma z$

s = stability parameter $= \frac{g}{T} \frac{\partial \Phi}{\partial z}$

g = gravitational acceleration = 9.8 m sec^{-2}

T = ambient air temperature (^{o}K)

$\frac{\partial \Phi}{\partial z}$ = vertical potential temperature gradient (^{o}K m^{-1})

$F = \frac{g Q_H}{\pi c_p \rho T}$

Q_H = heat emission due to efflux of hot gases (cal sec^{-1})

c_p = specific heat of air (cal g^{-1} ^{o}K^{-1})

ρ = density of air (g m^{-3})

t = time (sec)

The above formula yields cloud rise rates that agree favorably with the observed cloud rise rates from the launch of Saturn vehicles as described by Susko and Kaufman (1971).

According to Briggs (see Slade, 1968, p. 199), the formula for calculating the buoyant rise of nearly-instantaneously generated clouds first given by Morton, Taylor, and Turner (1956) can be written as

$$\Delta h_I = 2.66 \left(\frac{Q'_I}{c_p \rho \, \partial \Phi / \partial z} \right)^{1/4} \qquad (3\text{-}2)$$

where

Δh_I = cloud rise (meters)

Q'_I = heat released (calories)

Briggs compared cloud rises calculated from Equation (3-2) with observed cloud rises from nuclear tests and found that the observed rises were about 30 percent higher. If the formula is adjusted to fit the observations, the expression for cloud rise from nearly-instantaneous sources becomes

$$\Delta h_I = 3.46 \left(\frac{Q'_I}{c_p \rho \, \partial \Phi / \partial z} \right)^{1/4} \tag{3-3}$$

Equation (3-3) also gives results which compare favorably with observations of cloud rise downwind from detonations of high explosives recently reviewed by Church (1969). Equation (3-3) was used to calculate cloud rise for the case in which the booster is destructed at a height of 2 kilometers.

Input parameters used in the calculation of cloud rise are given in Table 3-1. The initial vertical velocity ω_o was calculated from the expression

$$\omega_o = V \cdot \frac{(\pi r_E)^2}{\ell \cdot w} \cdot \sin \alpha \tag{3-4}$$

where

V = exit velocity from rocket engine ($\sim$ 2438 m sec^{-1})

r_E = radius of rocket engine ($\sim$2 m)

ℓ = length of flame trench (137 m)

w = width of flame trench (17.7 m)

α = incline angle at end of flame trench (45 deg, 0 deg)

TABLE 3-1

VALUES FOR INPUT PARAMETERS USED TO CALCULATE BUOYANT CLOUD RISE

Parameter	Type of Hazard Calculation			
	Normal Launch	Pad-Abort	Destruct	Washout Surface Deposition
ω_o (m sec^{-1})	290;0	290;0		290;0
r_o (m)	8.56	8.56		8.56
ρ (g m^{-3})	1190	1190	962	1190
Q_H, Q_I (cal sec^{-1})	6.25×10^9	2.01×10^9	5.54×10^{11}	6.25×10^9
γ	0.50	0.50	0.35	0.50
c_p (cal g^{-1} $^oK^{-1}$)	0.24	0.24	0.24	0.24
T (^oK)				
Fall	299	299		
Spring	300	300		300
Sea-Breeze	294	294		
$\partial\Phi/\partial z$ (^oK m^{-1})				
Fall	0.0044	0.0044	0.0046	
Spring	0.0040	0.0040	0.0057	0.0020
Sea-Breeze	0.0064	0.0064	0.0062	
$\bar{u}$ (m sec^{-1})				
Fall	6.0	6.0		
Spring	7.2	7.2		7.2
Sea-Breeze	4.2	4.2		

Values of ℓ, w, and α were obtained for Launch Complex 39A at KSC from the paper by Susko and Kaufman (1971). Estimates of V and r_E were obtained from Thiokol Chemical Corporation. Note that α equals 45 degrees at one end of the flame trench and 0 degrees at the other. Thus, the cloud rise from the two ends of the flame trench proceeds at a different rate with time. However, the final rise from each end is nearly the same and the results of the cloud rise calculations for both segments were averaged to obtain the estimate used in the concentration calculations.

The value of Q_H shown in Table 3-1 for the normal launch and pad-abort hazard calculations was calculated from the expression

$$Q_H = Q_T + Q_1' - Q_2' \tag{3-5}$$

where

Q_T = total amount of heat available from system exhaust (2 solid engines + liquid fuel engine = 5.58×10^9 cal sec^{-1})

Q_1' = heat required to heat deluge water used to cool trench to boiling point (9.20×10^7 cal sec^{-1})

Q_2' = heat required to vaporize deluge water (6.82×10^8 cal sec^{-1})

The values of Q_1' and Q_2' are based on the assumption that 1.26×10^3 kg sec^{-1} (Susko and Kaufman, 1971) of deluge water are used to cool the flame trench and that the water is vaporized and entrained into the exhaust cloud. The value of Q_I was determined from the amount of solid propellant remaining in the engine after reaching an altitude of 2 kilometers and the assumption that the heat content of the fuel is 691 calories per gram. The parameter γ was set equal to 0.5 in accordance with conservative estimates based on work by Dumbauld (1971) and by Susko and Kaufman (1971) for the normal and pad-abort cases. For the destruct case, γ was set equal to 0.35 for consistency with the derived constant 3.46 in Equation (3-3).

The geometry of the stabilized cloud of combustion products for each of the cloud rise calculations was calculated from the expressions

$$r\{z\} = \left\{ \begin{array}{ll} \gamma (z - z_o + r_R/\gamma & ; \ 0 \leq z \leq z_m \\ z_m - \gamma (z + z_o - r_R/\gamma \geq 200 & ; \ z \geq z_m \end{array} \right\} \qquad (3\text{-}6)$$

where

z_m = height of final rise of ground cloud

z_o = reference height at which plume rise begins (14.6 meters for all cases except destruct where z_o = 2 km)

r_R = reference radius of cloud at height z_o (equal to 68.5 meters for all cases except destruct where r_R = 121 meters)

Note that $r\{z\}$ is not permitted to be less than 200 meters.

3.3 SOURCE INPUTS

Source inputs used in the calculations of ground-level concentrations and washout surface deposition of HCl are given in Tables 3-2 through 3-8.

Table 3-2 gives heights of layer boundaries used in the normal launch and pad-abort calculations. The division of the lowest 5 kilometers of the troposphere into distinct layers was made on the basis of the meteorological structure in the troposphere and the distribution of material in the stabilized ground cloud. For example, Figure 3-3 shows the geometry of the stabilized ground cloud of combustion products for a normal launch during the spring regime. In the figure, the solid lines show the layer structure dictated by the meteorology, while the dashed lines indicate subdivisions of the lowest 2 kilometers made for the purpose of improved definition of the vertical distribution of material. Tables 3-3 and 3-4 present values of the standard deviations of the lateral and longitudinal cloud dimensions for the normal

TABLE 3-2

HEIGHTS OF LAYER BOUNDARIES (z_{BK}, z_{TK}) USED IN THE NORMAL-LAUNCH AND PAD-ABORT CALCULATIONS

Layer (K)	Meteorological Regime					
	Spring		Fall		Sea Breeze	
	z_{BK} (m)	z_{TK} (m)	z_{BK} (m)	z_{TK} (m)	z_{BK} (m)	z_{TK} (m)
1	0	400	0	200	0	300*
2	400	800	200	400	300	1000
3	800	1200	400	600	1000	1500
4	1200	1600	600	800	1500	2000
5	1600	2000*	800	1000*	2000	2500
6	2000	2500	1000	2000	2500	3000
7	2500	3250	2000	3000	3000	4000
8	3250	4000	3000	4000	4000	5000
9	4000	5000	4000	5000		

*Height of the top of the surface mixing layer (H_m).

TABLE 3-3

INITIAL LONGITUDINAL (σ_{xo}) AND LATERAL (σ_{yo}) CLOUD DIMENSIONS FOR THE NORMAL LAUNCH CALCULATIONS

Layer (K)	Meteorological Regime		
	Spring $\sigma_{xo}(m) = \sigma_{yo}(m)$	Fall $\sigma_{xo}(m) = \sigma_{yo}(m)$	Sea Breeze $\sigma_{xo}(m) = \sigma_{yo}(m)$
1	77	52	63
2	168	98	159
3	261	145	319
4	354	191	452
5	448	238	352
6	344	460	235
7	199	335	93
8	93	93	93
9	93	93	

TABLE 3-4

INITIAL LONGITUDINAL (σ_{xo}) AND LATERAL (σ_{yo}) CLOUD DIMENSIONS FOR THE PAD-ABORT CALCULATIONS

($\sigma_{xo}\{K\} = \sigma_{yo}\{K\}$ in meters)

Layer (K)	Meteorological Regime		
	Spring $\sigma_{xo}(m) = \sigma_{yo}(m)$	Fall $\sigma_{xo}(m) = \sigma_{yo}(m)$	Sea-Breeze $\sigma_{xo}(m) = \sigma_{yo}(m)$
1	77	52	63
2	168	98	159
3	261	145	334
4	324	191	233
5	200	238	117
6	95	333	30
7		86	

TABLE 3-5

INITIAL LONGITUDINAL (σ_{xo}) AND LATERAL (σ_{yo}) CLOUD DIMENSIONS AND LAYER BOUNDARY HEIGHTS (z_{BK}, z_{TK}) FOR THE WASHOUT SURFACE DEPOSITION CALCULATIONS

Layer (K)	σ_{xo} (m)	σ_{yo} (m)	z_{BK} (m)	z_{TK} (m)
1	77	77	0	400
2	168	168	400	800
3	261	261	800	1200
4	354	354	1200	1600
5	447	447	1600	2000
6	556	556	2000	2500
7	415	415	2500	3250
8	240	240	3250	4000
9	77	77	4000	5000
10	0	0	5000	6000

TABLE 3-6

VERTICAL SOURCE STRENGTHS (Q_K) IN GRAMS PER METER FOR THE NORMAL-LAUNCH CALCULATIONS

Layer (K)	Meteorological Regime								
	Spring			Fall			Sea Breeze		
	HCl	Al_2O_3	CO	HCl	Al_2O_3	CO	HCl	Al_2O_3	CO
1	1.17×10^2	1.64×10^2	1.30×10^2	4.40×10^1	6.17×10^1	4.89×10^1	8.56×10^1	1.20×10^2	9.51×10^1
2	1.58×10^3	2.22×10^3	1.76×10^3	1.65×10^2	2.31×10^2	1.83×10^2	2.84×10^3	3.99×10^3	3.16×10^3
3	1.04×10^4	1.45×10^4	1.15×10^4	6.49×10^2	9.10×10^2	7.21×10^2	2.22×10^4	3.12×10^4	2.47×10^4
4	3.20×10^4	4.48×10^4	3.55×10^4	2.09×10^3	2.93×10^3	2.32×10^3	5.74×10^4	8.05×10^4	6.38×10^4
5	6.00×10^4	8.42×10^4	6.67×10^4	5.60×10^3	7.85×10^3	6.22×10^3	4.28×10^4	6.00×10^4	4.75×10^4
6	4.15×10^4	5.82×10^4	4.61×10^4	4.56×10^4	6.40×10^4	5.07×10^4	1.73×10^4	2.43×10^4	1.92×10^4
7	1.49×10^4	2.09×10^4	1.66×10^4	3.20×10^4	4.48×10^4	3.55×10^4	9.79×10^3	1.37×10^4	1.09×10^4
8	9.40×10^3	1.32×10^4	1.04×10^4	9.90×10^3	1.39×10^4	1.10×10^4	8.31×10^3	1.17×10^4	9.24×10^3
9	8.31×10^3	1.17×10^4	9.24×10^3	8.31×10^3	1.17×10^3	9.24×10^4			

TABLE 3-7

VERTICAL SOURCE STRENGTHS (Q_K) IN GRAMS PER METER FOR THE PAD-ABORT CALCULATIONS

Layer (K)	Meteorological Regime								
	Spring			Fall			Sea Breeze		
	HCl	Al_2O_3	CO	HCl	Al_2O_3	CO	HCl	Al_2O_3	CO
1	9.85×10^2	1.38×10^3	1.09×10^3	2.32×10^2	3.25×10^2	2.57×10^2	4.21×10^2	5.92×10^2	4.69×10^2
2	1.89×10^4	2.65×10^4	2.10×10^4	1.46×10^3	2.05×10^3	1.62×10^3	2.63×10^4	3.69×10^4	2.92×10^4
3	9.20×10^4	1.29×10^5	1.02×10^5	7.20×10^3	1.01×10^4	8.00×10^3	1.16×10^5	1.62×10^5	1.29×10^5
4	1.16×10^5	1.63×10^5	1.29×10^5	2.66×10^4	3.74×10^4	2.96×10^4	5.83×10^4	8.18×10^4	6.48×10^4
5	3.81×10^4	5.34×10^4	4.23×10^4	6.81×10^4	9.56×10^4	7.57×10^4	4.33×10^3	6.07×10^3	4.81×10^3
6	2.59×10^3	3.64×10^3	2.88×10^3	8.67×10^4	1.22×10^5	9.63×10^4	4.22×10^1	5.92×10^1	4.69×10^1
7				2.06×10^3	2.89×10^3	2.29×10^3			

TABLE 3-8

VERTICAL SOURCE STRENGTHS (Q_{IK}) IN GRAMS PER METER FOR THE WASHOUT SURFACE DEPOSITION CALCULATIONS

Layer (K)	Combustion Product		
	HCl	Al_2O_3	CO
1	5.87×10^{1}	8.23×10^{1}	6.52×10^{1}
2	5.64×10^{2}	7.92×10^{2}	6.27×10^{2}
3	3.50×10^{3}	4.90×10^{3}	3.88×10^{3}
4	1.32×10^{4}	1.84×10^{4}	1.46×10^{4}
5	3.01×10^{4}	4.22×10^{4}	3.34×10^{4}
6	5.35×10^{4}	7.38×10^{4}	5.85×10^{4}
7	3.47×10^{4}	4.86×10^{4}	3.85×10^{4}
8	1.24×10^{4}	1.74×10^{4}	1.38×10^{4}
9	8.37×10^{3}	1.17×10^{4}	9.30×10^{3}

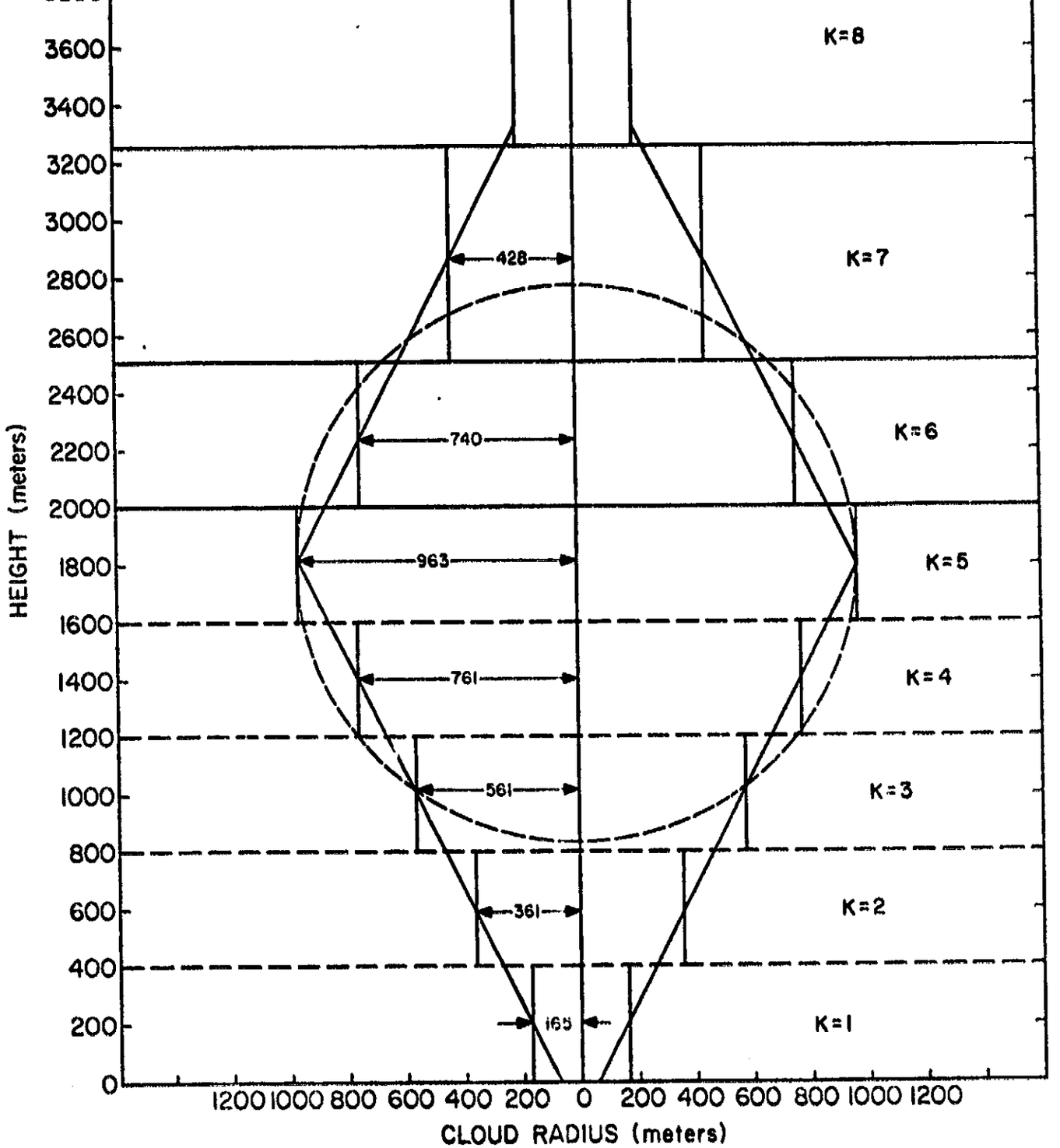

FIGURE 3-3. Layer geometry of the stabilized ground cloud of combustion products for the spring meteorological regime.

and pad-abort calculations. These dimensions were derived on the assumption that at any height the radius of the stabilized cloud equals the 2.15σ limits for a Gaussian distribution. In any layer except the layer containing z_m, the dimensions are given by the expression

$$\sigma_{yo} = \sigma_{xo} = \frac{\bar{r}\{K\}}{2.15} \tag{3-7}$$

where

$$\bar{r}\{K\} = \frac{r\{z_{TK}\} + r\{z_{HK}\}}{2}$$

In the layer containing z_m, the dimensions are given by

$$\sigma_{yo} = \sigma_{xo} = \frac{r\{z_m\}}{2.15} \tag{3-8}$$

Table 3-5 gives the standard deviations of the longitudinal and lateral cloud dimensions and the layer boundary heights for the washout surface-deposition calculations.

Tables 3-6, 3-7 and 3-8 show the vertical source strengths in each layer, respectively, for the normal launch, pad-abort, and washout surface deposition calculations. The total amount of material Q_G contained in the ground cloud for the normal-launch and washout calculations was calculated from the expression

$$Q_G \text{ (lb)} = R \text{ (lb sec}^{-1}) \quad t\{z_m\} \tag{3-9}$$

where

R = emission rate of pollutant (from Table 1-1)

$t\{z_m\}$ = time required for the vehicle to reach the altitude of maximum rise of the ground cloud z_m

$$t\{z_m\} = \left(\frac{z_m}{0.7704}\right)^{0.4545} \tag{3-10}$$

Equation (3-10) was obtained by fitting the vehicle-height curve in Figure 1-1 by a least-squares procedure. For the pad-abort cases, Q_G was set equal to the total emission from a complete burn of one solid-propellant engine. The fraction of material in the K^{th} later contributed by the ground cloud $F_g\{K\}$ is thus given by the expression

$$F_g\{K\} = Q_G\left[P\{z_{TK}\} - P\{z_{BK}\}\right] \tag{3-11}$$

where

$P\{z_{TK}\}$ = integral of the Gaussian (normal) probability function between minus infinity and the top of the K^{th} layer z_{TK}

$$= P\left\{\frac{z_{TK} - z_m}{\sigma}\right\}$$

$P\{z_{BK}\}$ = integral of the Gaussian (normal) probability function between minus infinity and the bottom of the K^{th} layer z_{BK}

$$= P\left\{\frac{z_{BK} - z_m}{\sigma}\right\}$$

$$\sigma = \frac{r\{z = z_m\}}{2.15}$$

The fraction of the rocket exhaust trail in the K^{th} layer $F_E\{K\}$ is given by the expression

$$F_E\{K\} = \left\{ \begin{array}{ll} 0 & ; \quad z_{TK} < z_m \\ R\left[\left(\frac{z_{TK}}{0.7704}\right)^{0.4545} - t\{z_m\}\right] & ; \quad z_{BK} < z_m < z_{TK} \\ R\left[\left(\frac{z_{TK}}{0.7704}\right)^{0.4545} - \left(\frac{z_{BK}}{0.7704}\right)^{0.4545}\right] & ; \quad z_{TK} < z_m \end{array} \right\} \tag{3-12}$$

The source strength in the layer Q_K for use in the model calculations is thus given by

$$Q_K = \frac{F_g\{K\} + F_E\{K\}}{z_{TK} - z_{BK}} \tag{3-13}$$

The values of Q_K in Tables 3-6, 3-7 and 3-8 have been converted to units of grams per meter.

3.4 METEORLOGICAL INPUTS

Meteorological inputs used in the concentration calculations for the normal launch and pad-abort cases are given in Table 3-9. Inputs for the washout surface-deposition calculations are given in Table 3-10.

Values of the mean wind speed $\bar{u}_{BK}$ and wind direction θ_{BK} at the base of the K^{th} layer in Table 3-9 were determined from the vertical profiles shown in Figure 3-2. Values of the standard deviation of the wind azimuth angle at the reference height $z_R = 18$ meters, for a 10-minute sampling period $\{\tau_{oK} = 600$ seconds$\}$, were obtained from the expression

$$\sigma_{ABK}\{\tau_{oK} = 600;\ K = 1\} = \frac{R_d}{6} \tag{3-14}$$

where R_d is the wind direction range at z_R from Figure 2-11 of the report by Record, et al. (1970). The quantity σ_A was assumed to decrease with height according to the expression

$$\sigma_A\{z, K=1\} = \sigma_{ABK}\{z=z_R, K=1\} \left(\frac{z}{z_R}\right)^{-p} \tag{3-15}$$

as suggested by Record, et al. (1970, p. 48).

TABLE 3-9

METEOROLOGICAL INPUTS FOR THE NORMAL-LAUNCH AND PAD-ABORT HAZARD CALCULATIONS

Regime	Parameter	Layer (K)									
		1	2	3	4	5	6	7	8	9	10
Fall	$\bar{u}_{BK}$ (m sec^{-1})	4.7	6.0	6.4	6.7	6.9	7.0	5.6	5.2	5.3	5.5
	θ_{BK} (deg)	90	96	102	107	113	119	131	138	161	180
	$\sigma_{ABK}\{\tau_{oK}\}$ (deg)	12	9.4	8.8	8.5	8.2	8.0	1.0	1.0	1.0	1.0
	τ_{oK} (sec)	600	600	600	600	600	600	600	600	600	600
	τ_K (sec) Normal Launch	240	240	240	240	240	240	240	240	30	30
	τ_K (sec) Pad Abort	229	229	229	229	229	229	229	30	30	30
	α, β	1.0	1.0	1.0	1.0	1.0	1.0	1.0	1.0	1.0	1.0
Spring	$\bar{u}_{BK}$ (m sec^{-1})	6.0	6.9	7.2	7.3	7.4	7.5	7.5	8.2	8.8	9.5
	θ_{BK} (deg)	100	116	133	148	164	180	200	230	260	270
	$\sigma_{ABK}\{\tau_{oK}\}$ (deg)	7.00	6.04	5.85	5.74	5.66	5.60	1.0	1.0	1.0	1.0
	σ_{EBK} (deg)	3.80	3.28	3.17	3.11	3.07	3.05	0.5	0.5	0.5	0.5
	τ_{oK} (sec)	600	600	600	600	600	600	600	600	600	600
	τ_K (sec) Normal Launch	260	260	260	260	260	260	30	30	30	30
	τ_K (sec) Pad Abort	242	242	242	242	242	242	30	30	30	30
	α, β	1.0	1.0	1.0	1.0	1.0	1.0	1.0	1.0	1.0	1.0

TABLE 3-9 (Continued)

Regime	Parameter	Layer (K)									
		1	2	3	4	5	6	7	8	9	10
Sea Breeze	$\bar{u}_{BK}$ (m sec^{-1})	4.5	9.5	2.7	2.9	3.1	3.0	2.9	3.2	4.5	
	θ_{BK} (deg)	140	150	190	240	250	260	265	270	270	
	$\sigma_{ABK}\{\tau_{oK}\}$ (deg)	12	5.7	1.0	1.0	1.0	1.0	1.0	1.0	1.0	
	τ_{oK} (sec)	600	600	600	600	600	600	600	600	600	
	τ_K (sec) Normal Launch	200	200	200	200	200	200	30	30	30	
	τ_K (sec) Pad Abort	185	185	185	185	185	185	30	30	30	
	α, β	1.0	1.0	1.0	1.0	1.0	1.0	1.0	1.0	1.0	

TABLE 3-10

METEOROLOGICAL INPUTS FOR THE WASHOUT SURFACE-DEPOSITION CALCULATIONS

Parameter	Layer (K)										
	1	2	3	4	5	6	7	8	9	10	11
$\bar{u}_{BK}$ (m sec^{-1})	6.0	6.9	7.2	7.3	7.4	7.5	7.6	7.7	7.8	7.9	7.9
θ_{BK} (deg)	100.0	101.3	102.7	104.0	105.3	106.7	108.3	110.8	113.3	116.7	120.0
$\sigma_{ABK}\{\tau_{oK}\}$ (deg)	20.0	17.1	16.5	16.2	16.0	15.8	15.6	15.4	15.3	15.1	5
σ_{EBK} (deg)	10	10	10	10	10	10	10	10	10	10	3.5
α, β	1.0	1.0	1.0	1.0	1.0	1.0	1.0	1.0	1.0	1.0	1.0
τ_{oK} (sec)	600	600	600	600	600	600	600	600	600	600	600
τ (sec)	376	376	376	376	376	376	376	376	376	376	376

The power-law exponent p in Equation (3-15) is given by the expression

$$p = \log\left(\frac{\bar{u}_{TK}\{K=1\}}{\bar{u}_{BK}\{z_R, K=1\}}\right) \Big/ \log\left(\frac{z_{TK}\{K=1\}}{z_R}\right) \qquad (3\text{-}16)$$

Note that a reference height of $z_R = 18$ meters was used for all meteorological parameters in the surface mixing layer. In the next higher layer ($K = 2$), the value of σ_A was linearly decreased from the value at the top of the surface layer to a value of 1.0 degrees at the top of the $K = 2$ layer. In all higher layers ($K > 2$), σ_A was held constant at 1.0 degrees.

The washout surface-deposition calculations were made using the wind speed profile for the spring meteorological regime shown in Figure 3-2. The wind direction profile for the spring meteorological regime was, however, changed and the wind direction shear with height was reduced to reflect a profile more appropriate for a deep layer in which rain showers are occurring. Also, the value of $\sigma_{ABK}\{\tau_o\}$ and σ_{EBK} were increased to reflect the turbulence levels expected in convective activity.

3.5 PROPERTIES OF THE STABILIZED CLOUD

The height, radius, and average exhaust-product concentrations for the stabilized ground cloud are given in Table 3-11. The heights of the ground cloud for the normal launch, pad-abort, and washout cases were calculated from Equation (3-1) and inputs from Table 3-1. For the destruct case, the height of the ground cloud was calculated from Equation (3-3) using inputs given in Table 3-1. The radius of the ground cloud was calculated from Equation (3-6). The average exhaust-product concentrations were calculated by dividing the total amount of each product contained in the ground cloud by the volume of the ground cloud.

It should be noted that ground-level concentrations will not exceed the average concentration in the ground cloud since the cloud will dilute in mixing to the ground.

TABLE 3-11

HEIGHT, RADIUS, AND AVERAGE EXHAUST-PRODUCT CONCENTRATIONS FOR THE STABILIZED GROUND CLOUD USED IN THE HAZARD CALCULATION[a]

Case	Meteorological Regime	Height (m)	Radius (m)	Average Concentration		
					($g\ m^{-3}$)	(ppm)
Normal Launch	Spring	1804	963	HCl	1.76×10^{-2}	14.1
				Al_2O_3	2.47×10^{-2}	
				CO	1.96×10^{-2}	20.4
	Fall	1858	990	HCl	1.64×10^{-2}	13.3
				Al_2O_3	2.30×10^{-2}	
				CO	1.62×10^{-2}	19.2
	Sea Breeze	1820	971	HCl	1.72×10^{-2}	13.9
				Al_2O_3	2.42×10^{-2}	
				CO	1.92×10^{-2}	20.2
Pad-Abort	Spring	1269	696	HCl	7.63×10^{-2}	83.6
				Al_2O_3	1.07×10^{-1}	
				CO	8.47×10^{-2}	83.6
	Fall	1310	716	HCl	7.01×10^{-2}	53.5
				Al_2O_3	9.83×10^{-2}	
				CO	7.78×10^{-2}	77.0
	Sea Breeze	1316	719	HCl	6.92×10^{-2}	53.0
				Al_2O_3	9.71×10^{-2}	
				CO	7.69×10^{-2}	76.5
Destruct	Spring	4779	1095	HCl	2.88×10^{-2}	32.1
				Al_2O_3	1.05×10^{-2}	
				CO	3.20×10^{-2}	46.5
	Fall	4940	1151	HCl	2.48×10^{-2}	27.7
				Al_2O_3	3.48×10^{-2}	
				CO	2.76×10^{-2}	40.2
	Sea Breeze	4729	1077	HCl	3.03×10^{-2}	33.9
				Al_2O_3	4.25×10^{-2}	
				CO	3.38×10^{-2}	49.2
Washout		2208	1195	HCl	1.02×10^{-2}	8.6
				Al_2O_3	1.43×10^{-2}	
				CO	1.13×10^{-2}	12.4

SECTION 4

TROPOSPHERIC HAZARD CALCULATIONS

The tropospheric hazard calculations described in this section principally consist of model estimates of the peak ground-level concentrations of HCl, CO, and Al_2O_3 resulting from the emission of rocket engine exhaust products to the atmosphere during a normal launch and an on-pad abort of the proposed space shuttle-booster vehicle. Hazard calculations are also presented for a low-level destruct of the space shuttle-booster vehicle and consist of model estimates of the dimensions, height and average concentrations of HCl, CO and Al_2O_3 in the elevated exhaust-product cloud resulting from the destruct. Ground-level concentrations are not presented for this case because it is evident that the concentrations of any of these exhaust products that may reach the surface through normal atmospheric diffusion and transport processes will be far below the applicable toxicity criteria. Other tropospheric hazard calculations described below include the maximum surface deposition of HCl by precipitation-removal processes and the formation of acid mist.

4.1 NORMAL LAUNCH

Figures 4-1 through 4-3 show profiles of the calculated ground-level peak concentrations of HCl, CO and Al_2O_3 resulting from a normal launch in each of the three meteorological regimes described in Section 3. The concentrations were calculated by using Equations (2-1) and (2-2) in conjunction with the source and meteorological inputs in Tables 3-2, 3-3, 3-6 and 3-9. Because the depth of the surface mixing layer for the sea-breeze regime is only 300 meters (see Table 3-2), Equation (2-1) was used to calculate the ground-level concentrations. For the spring and fall meteorological regimes, the surface mixing layer was divided into sublayers and Equation (2-2) was used in the calculations.

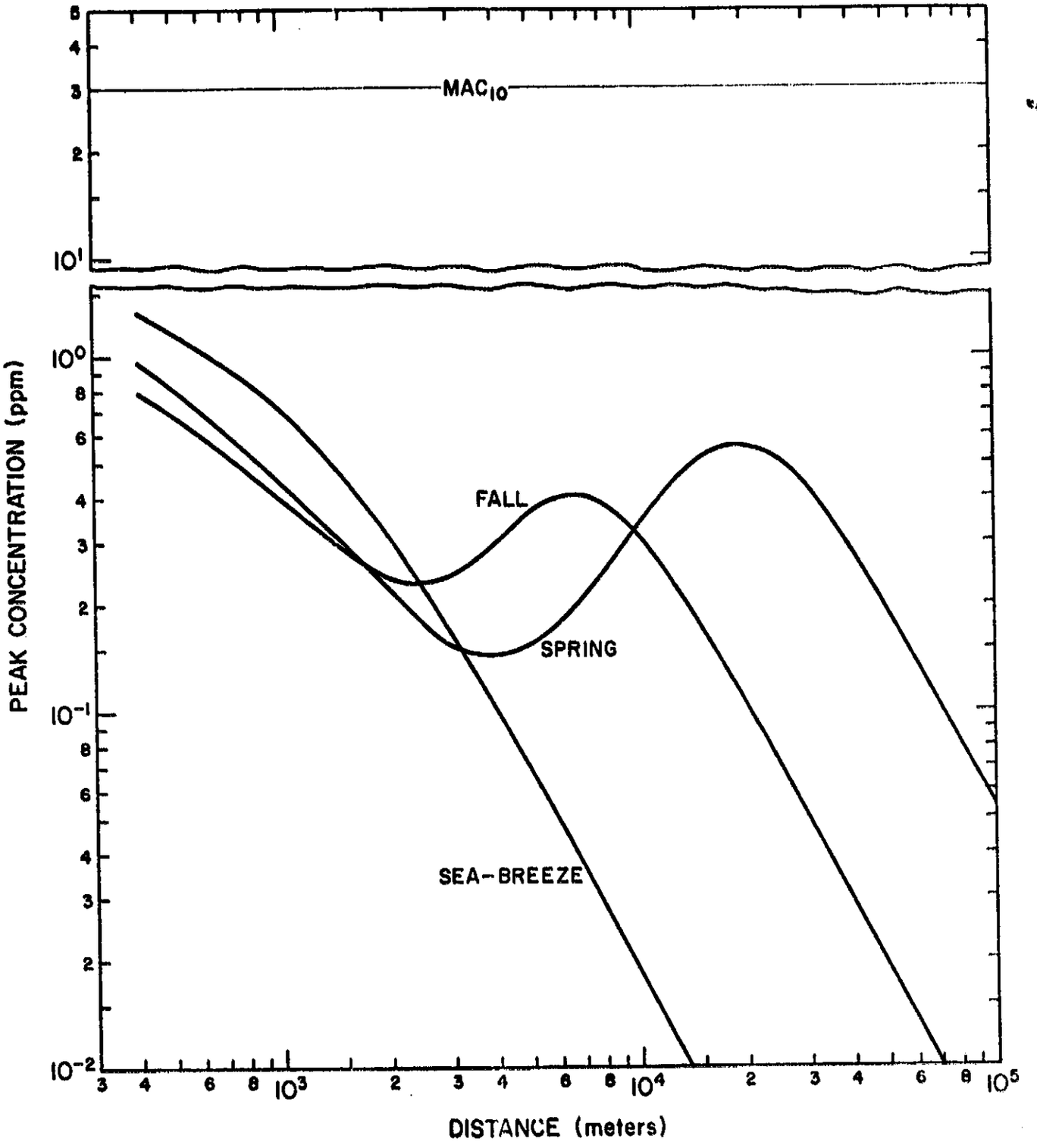

FIGURE 4-1. Peak centerline concentration of HCl at the surface downwind from a normal launch.

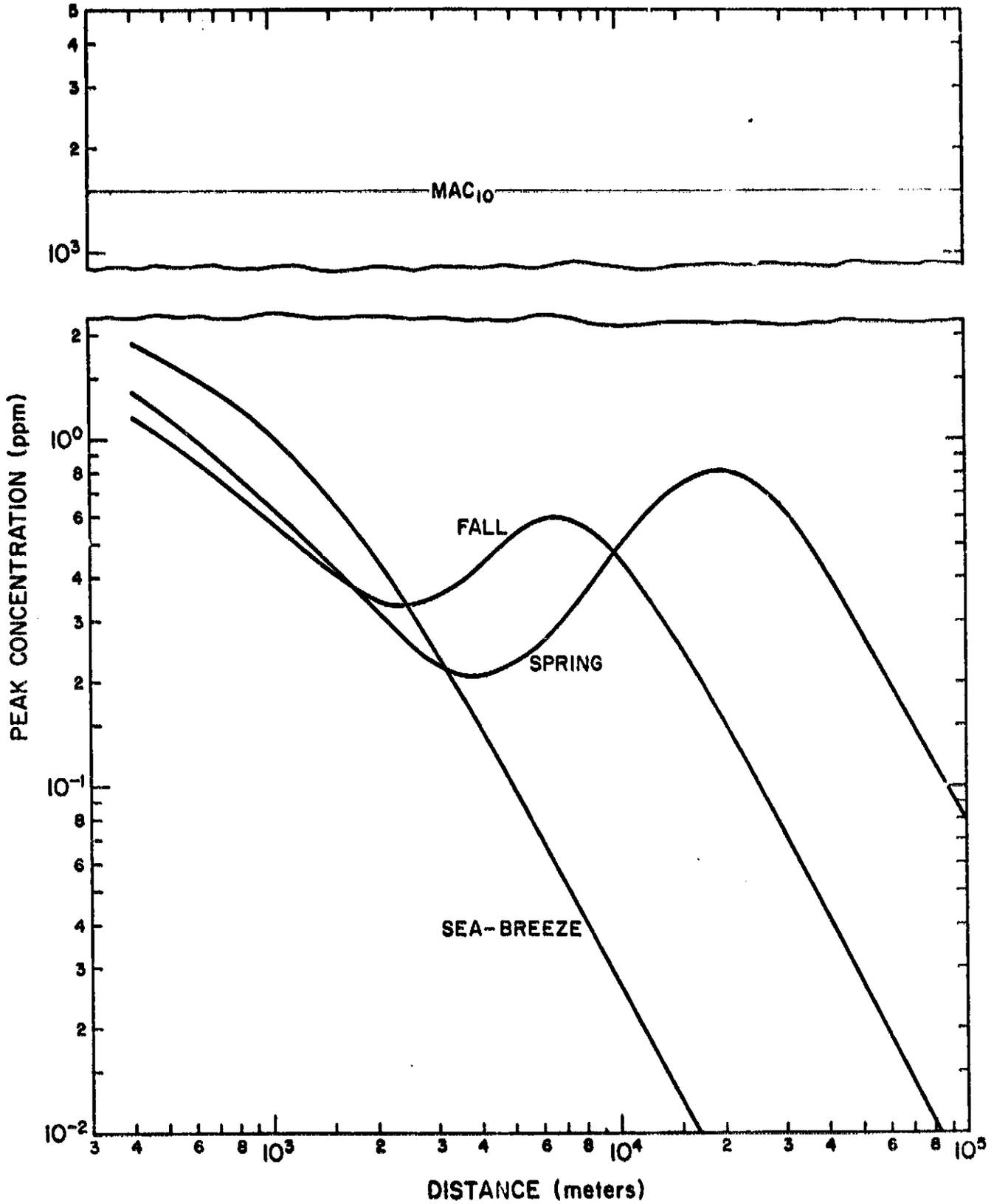

FIGURE 4-2. Peak centerline concentration of CO at the surface downwind from a normal launch.

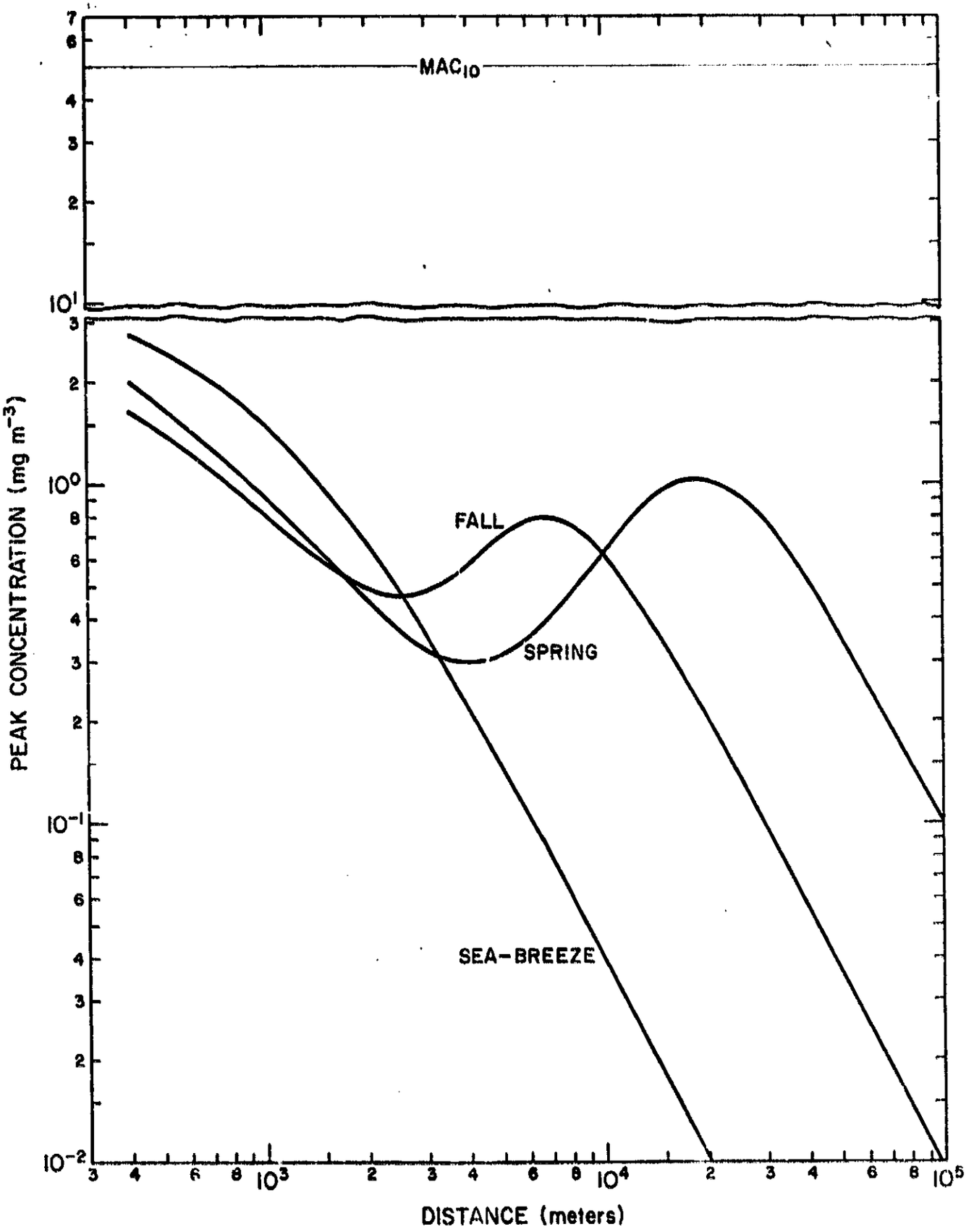

FIGURE 4-3. Peak centerline concentration of Al_2O_3 at the surface downwind from a normal launch.

The maximum allowable 10-minute average concentrations (MAC_{10}) shown by the horizontal lines at the top of the figures are taken from Table 1-2. The peak centerline concentrations plotted in Figures 4-1 through 4-3 are the theoretical maximum concentrations that would be experienced at a particular downwind distance during the passage of the exhaust-product cloud. The average concentration along the cloud centerline at any given downwind distance is approximately six-tenths (0.57) of the calculated peak centerline concentration. For the cloud transport speeds used in the calculations, cloud passage times at distances of 1 kilometer or less downwind from the launch site are of the order of a few minutes. At distances of 10 to 20 kilometers downwind from the launch site, the corresponding cloud passage times are of the order of 10 to 20 minutes. It follows from this discussion that the average 10-minute concentrations indicated by the model calculations at points along the cloud centerline, located at downwind distances less than 1 kilometer from the launch site, are probably only one-fourth to one-fifth as large as the corresponding peak centerline concentrations shown in Figures 4-1 through 4-3. Similarly, the average predicted 10-minute concentrations along the cloud centerline, at downwind distances of 10 to 20 kilometers, are probably about half as large as the corresponding peak centerline concentrations plotted in the figures.

As shown in Figure 4-1, the model estimates of peak centerline HCl concentration are at least one order of magnitude below the maximum allowable 10-minute limit (MAC_{10}) of 30 ppm near the launch site. The secondary maximums for the fall and spring meteorological regimes at respective downwind distances of 10 and 20 kilometers are almost two orders of magnitude below the MAC_{10} value.

The estimated peak centerline CO concentrations shown in Figure 4-2 are approximately three orders of magnitude below the MAC_{10} limit of 1500 ppm. The peak centerline Al_2O_3 concentrations in Figure 4-3 are more than an order of magnitude lower than the MAC_{10} value of 50 mg m^{-3}.

The results of the ground-level hazard calculations for a normal launch thus show that the predicted maximum concentrations of HCl and Al_2O_3 are at least one order of magnitude lower than the applicable MAC_{10} limits while the predicted maximum concentrations of CO are about three orders of magnitude below the applicable MAC_{10} limit.

4.2 PAD-ABORT

The calculated ground-level peak centerline concentrations for HCl, CO and Al_2O_3 resulting from a pad-abort during the three meteorological regimes are shown in Figures 4-4 through 4-6. The assumed source configuration for a pad-abort consisted of a complete burn of one solid-propellant engine with the booster in a pad hold-down status. As in the corresponding normal launch calculations, Equation (2-1) was used for the sea-breeze regime and Equation (2-2) was used for the other two meteorological regimes. Source and meteorological inputs used with these equations are given in Tables 3-2, 3-4, 3-7 and 3-9.

The calculated peak centerline concentrations for the pad-abort cases are about five to ten times larger than for the corresponding normal launch cases. The heat emitted per unit time during a pad-abort is less than during a normal launch, resulting in lower cloud rise, and the total amount of material in the ground cloud is greater for the pad-abort cases. The peak centerline concentrations are in all cases below the applicable MAC_{10} levels.

4.3 DESTRUCT

The calculated buoyant rise, cloud dimensions and average exhaust-product concentrations in the stabilized cloud resulting from the destruct of the booster vehicle at an altitude of 2 kilometers are shown in Table 3-11. As might be expected, the intense heat from the destruct results in about a 3-kilometer buoyant cloud rise

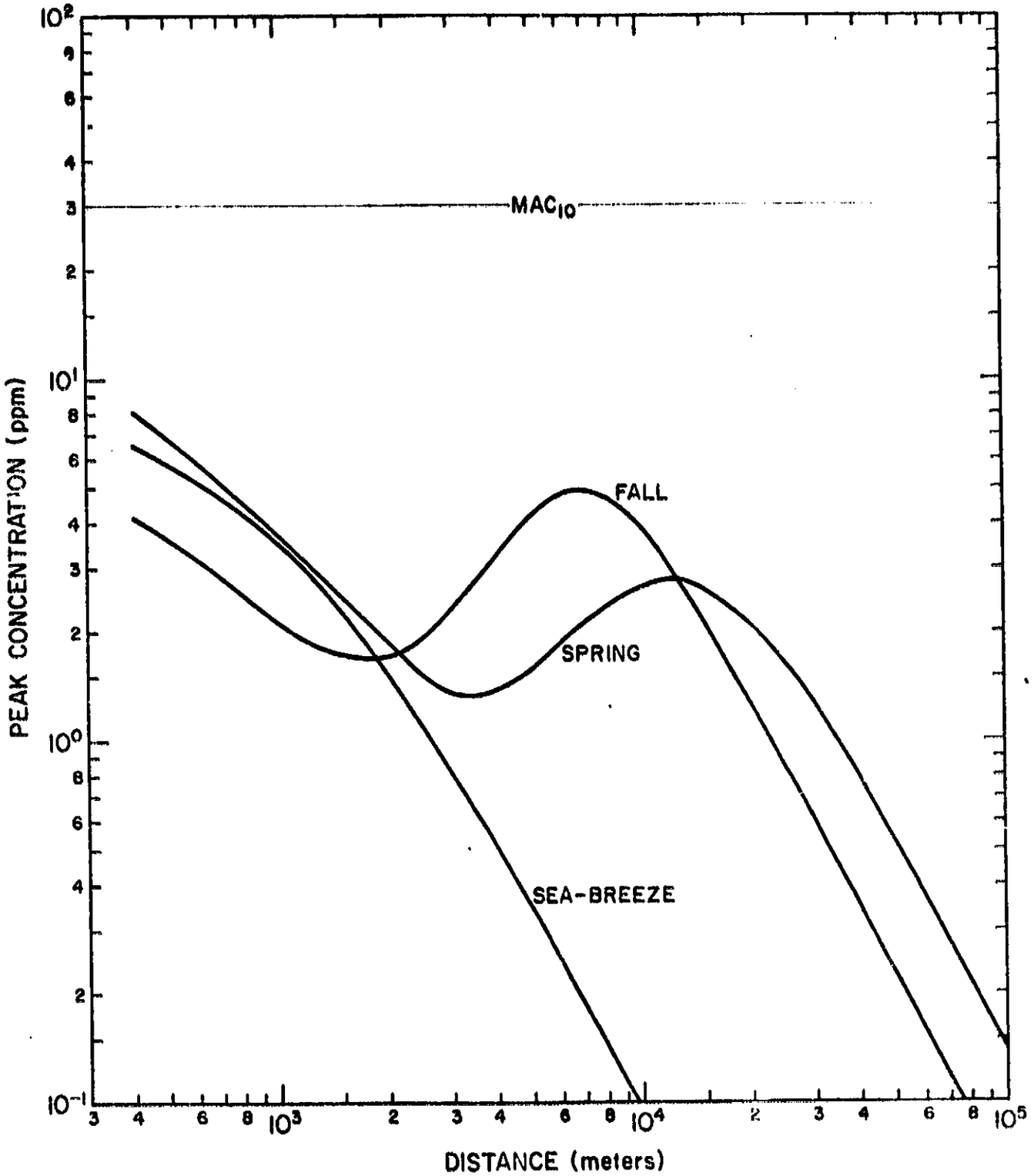

FIGURE 4-1. Peak centerline concentration of HCl at the surface downwind from a pad abort.

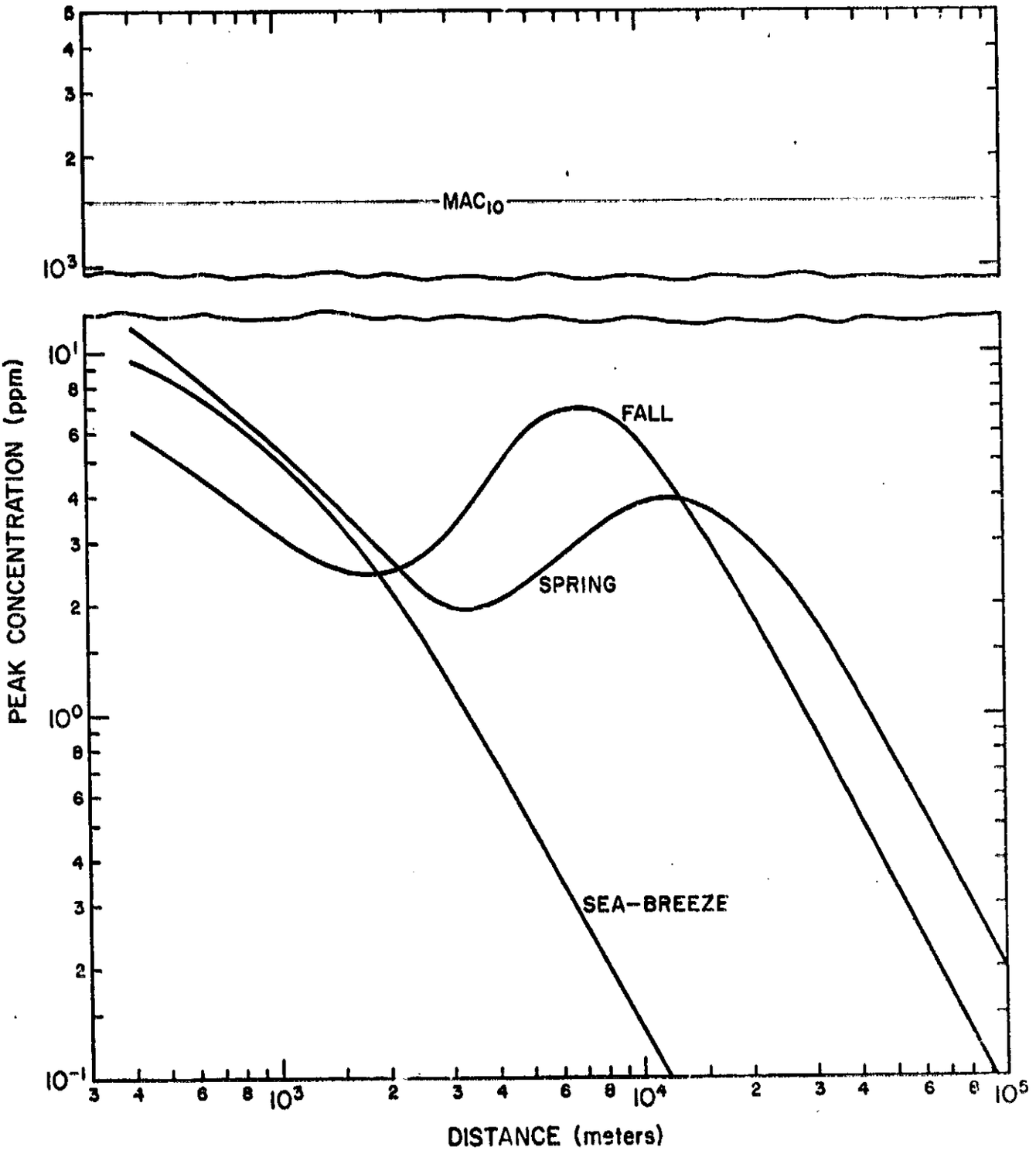

FIGURE 4-5. Peak centerline concentration of CO at the surface downwind from a pad-abort.

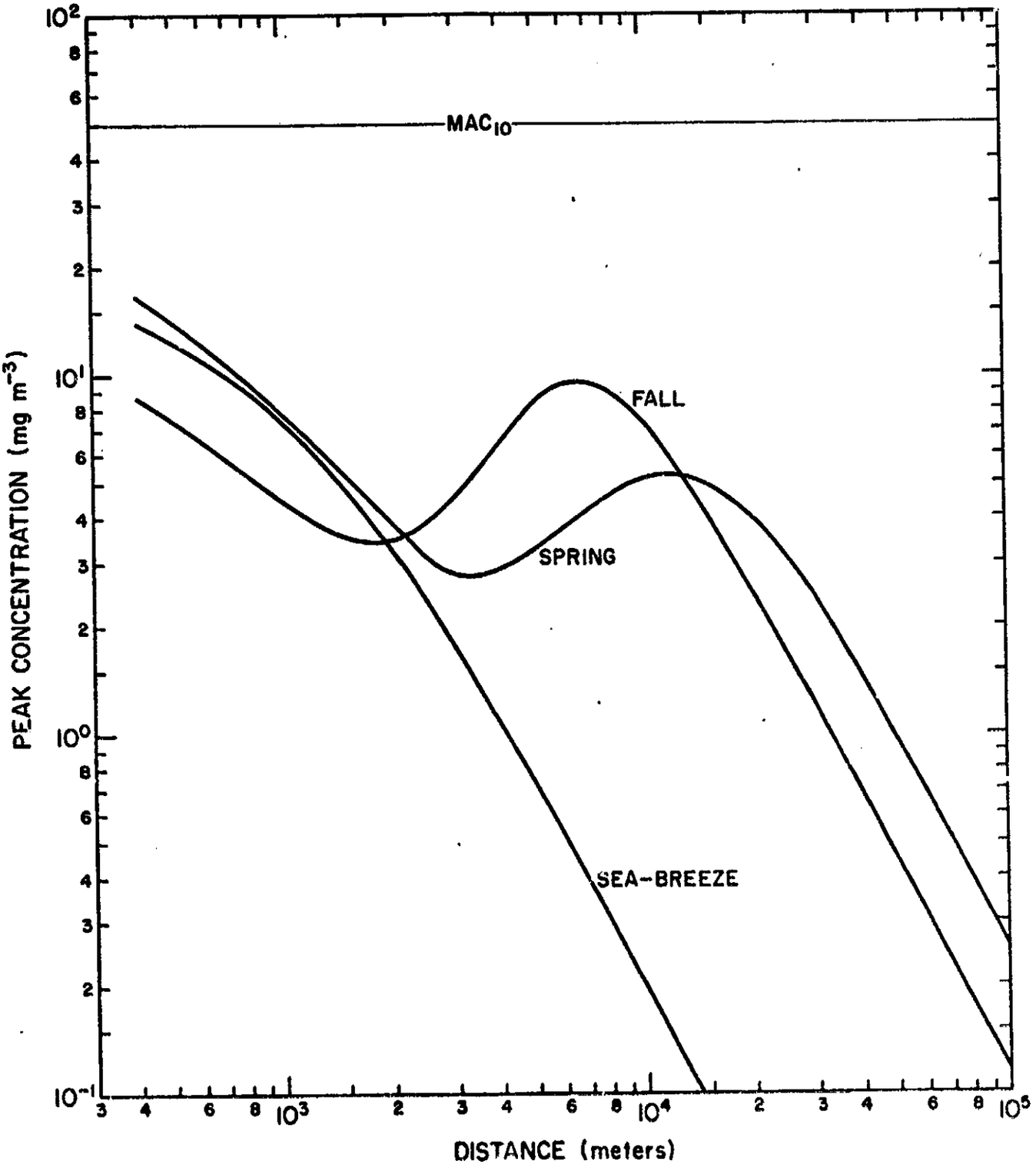

FIGURE 4-6. Peak centerline concentration of Al_2O_3 at the surface downwind from a pad-abort.

after destruct. The final height above the surface of the stabilized cloud is calculated to be 4.5 to 5 kilometers. The average CO and Al_2O_3 concentrations in the stabilized cloud are below the corresponding MAC_{10} levels and the average HCl concentrations are approximately equal to the MAC_{10} value. Any atmospheric transport-diffusion processes acting to bring the cloud to the surface would result in ground-level concentrations much lower than the average concentrations in the stabilized elevated cloud. For this reason, ground-level concentrations were not calculated. It is evident, however, that they would be well below the MAC_{10} levels.

4.4 WASHOUT SURFACE - DEPOSITION OF HCl

Scavenging by precipitation is the primary process by which gaseous and particulate pollutants are removed from the troposphere. The scavenging process is usually described mathematically by simple exponential decay expressions of the form

$$\chi = \chi_o \exp \left[- \Lambda (t^1) \right]$$

The deposition on the ground attributable to scavenging is mathematically described by Equation (2-2). As noted in Section 2, a full description of the multilayer mathematical model used to calculate the amount of material deposited on the surface by precipitation washout is contained in Section 3 of a report prepared for NASA-Huntsville (Dumbauld, et al., 1970) by GCA Technology Division.

The meteorological parameters used in calculating estimates of surface deposition of HCl due to rain scavenging are given in Table 3-10 of Section 3. The meteorological parameters for this case are based on structure in the lowest 6 kilometers of the atmosphere typical of structure in rain shower activity. Values of Λ are not well established. Engelmann (see Slade, 1968, pp. 208-221) cites values of Λ ranging from 10^{-3} to 10^{-5} sec^{-1} for various precipitation rates and other conditions. Makhon'ko (1967) gives values of Λ varying between 10^{-4} and 10^{-5} sec^{-1}.

For the present calculations, a value of Λ equal to 10^{-3} sec^{-1} was selected to provide estimates of maximum expected deposition of HCl due to washout.

According to calculations described in Section 4.5 below, HCl is absorbed very rapidly by water drops. A residence time of a few minutes in the HCl exhaust cloud appears sufficient for cloud drops to absorb the HCl. It follows that precipitation scavenging is efficient in removing HCl from the exhaust cloud.

The results of using the meteorological inputs given in Table 3-10 and the source inputs in Tables 3-5 and 3-8 in the computer program containing the deposition model are graphically presented in Figure 4-7. In the figure, the deposition profiles shown by the dashed lines were obtained assuming that rain begins to fall at, respectively from left to right in the figure, 9, 18, 35, 71, 141 and 283 minutes after launch. The peak deposition value in each profile is the deposition expected on the surface beneath the cloud centerline as the cloud passes over a given point downwind from the launch site. The solid line in Figure 4-7 thus represents the maximum washout surface deposition of HCl that is expected to occur from precipitation scavenging downwind from the launch site under the specified meteorological conditions.

To estimate the HCl content of rain water at the surface due to washout, the total precipitation accumulated at the surface must be known. For this purpose, we have assumed total precipitation amounts of 5 and 2.5 millimeters of rain per square meter of surface. Table 4-1 gives the acid content of rain calculated using these amounts of rainfall and the maximum surface deposition of HCl at various distances selected from Figure 4-7. For convenience, the acid content of rain water is shown in Table 4-1 as HCl content in percent by weight of water and in pH units.

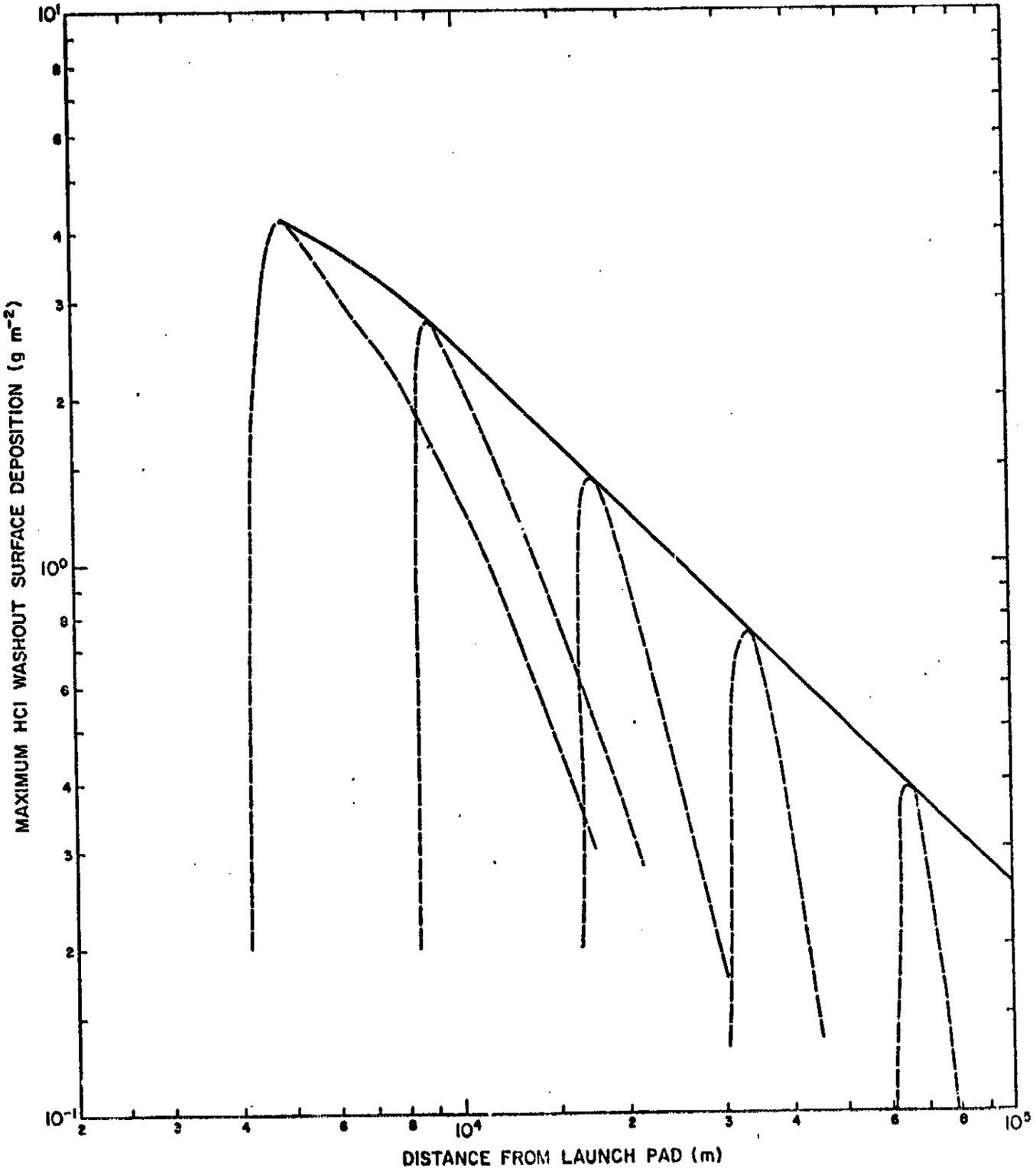

FIGURE 4-7. Maximum washout surface deposition of HCl downwind from a normal launch. Dashed lines represent surface deposition profiles for rain beginning at different distances from the launch pad.

TABLE 4-1

ESTIMATED ACID CONTENT OF RAIN WATER RESULTING FROM THE COMPLETE WASHOUT OF HCl FROM THE GROUND CLOUD

Distance (km)	Maximum HCl Washout Surface Deposition ($g\ m^{-2}$)	Acid Content			
		Percent HCl by Weight		pH	
		Total Rainfall		Total Rainfall	
		5 mm	2.5 mm	5 mm	2.5 mm
5	4.17	8.3×10^{-2}	1.6×10^{-1}	1.64	1.35
10	2.48	5.0×10^{-2}	9.8×10^{-2}	1.87	1.57
20	1.25	2.5×10^{-2}	4.9×10^{-2}	2.16	1.87
50	0.51	0.1×10^{-2}	2.0×10^{-2}	2.55	2.26
100	0.26	5.1×10^{-3}	1.0×10^{-2}	2.85	2.56

4.5 ACID MIST FORMATION

One of the potential environmental hazards associated with the emissions of HCl and water during the burn of the rocket engines is the formation of an acid mist in the stabilized ground cloud of combustion products. Assuming that liquid water droplets are present in the ground cloud, these droplets will very quickly absorb any HCl as long as the acid content of the drops does not exceed 5 or 10 percent. For example, Denbigh (1966, p. 228 and p. 238) cites experimental evidence that the partial pressure of HCl is approximately proportional to the square of the mole fraction or concentration of HCl in very dilute HCl solutions. This relation, which is attributed to the fact that the HCl in solution is almost entirely in ionized form (H^+ and Cl^-), holds for molar HCl concentrations ≤ 0.05. The equilibrium partial pressure of an 0.05 molar HCl solution at a temperature of 15 C is approximately 1 dyne cm^{-2} (see Figure 4-8). As long as the partial pressure of HCl gas in the ground cloud exceeds this value, practically all of the HCl will be absorbed by the liquid water drops as long as the acid content of the drops does not exceed 5 or 10 percent. Fukuta, et al. (1970) reached a similar conclusion in their analysis of the HCl/H_2O problem in the atmosphere of Venus. They point out that a cloud containing liquid water drops serves as a very effective HCl filter because of the negligible partial pressure of HCl at low solute concentrations. The time required for almost complete absorption of the HCl by the water drops is not known with certainty. It appears from the laboratory studies of Terraglio and Manganelli (1967) of the absorption of sulfur dioxide in water, that the maximum time required for almost complete HCl absorption is of the order of a few minutes.

The average properties of the ground cloud generated during a normal launch are given in Table 4-2. The average concentrations of HCl and H_2O were calculated under the assumption that zero concentration levels of these products existed in the ambient air. The total HCl and H_2O contents in the table represent the total rocket engine emissions during the first 40 seconds of engine burn. The

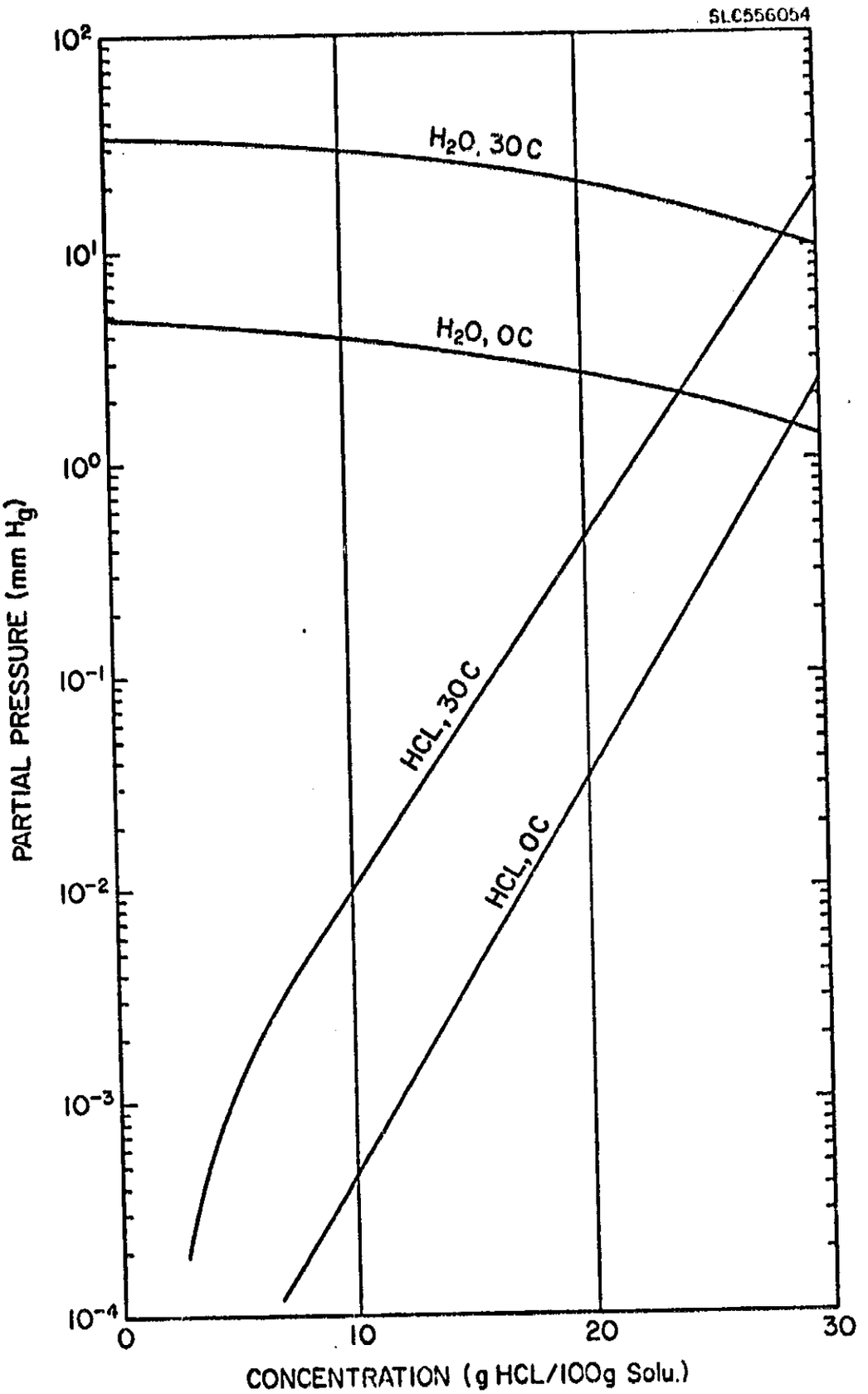

FIGURE 4-8. Partial vapor pressure of HCl and H_2O (after Fukuta, et al., 1970).

TABLE 4-2

AVERAGE PROPERTIES OF THE GROUND CLOUD GENERATED DURING A NORMAL LAUNCH

Cloud Volume	3.7×10^{9} m^{3}
Total HCl Content	6.6×10^{7} g
Average HCl Concentration	2×10^{-2} g m^{-3}
Partial Pressure of HCl	1.3×10^{1} dynes cm^{-2}
Total H_2O Content	1.15×10^{8} g
Average H_2O Concentration	3.1×10^{-2} g m^{-3}
Cloud Temperature	15 C

TABLE 4-3

PROPERTIES OF A CUMULUS CONGESTUS CLOUD

Average Drop Diameter	20 microns
Average Settling Velocity	1.2 cm sec^{-1}
Range of Drop Diameter (Log-Normal Distribution)	7 microns - 65 microns
Liquid Water Content	1.0 g m^{-3}
Drop Concentration	4×10^{7} drops m^{-3}
Cloud Temperature	15 C
Water Vapor Density	1.28×10^{1} g m^{-3}
Partial Pressure of Water Vapor	1.71×10^{4} dynes cm^{-2}

average H_2O concentration of 3.1×10^{-2} g m^{-3} thus calculated for the ground cloud is approximately three orders of magnitude below the saturation value for 15 C. It follows that the ambient humidity content must approach 100 percent before the formation of acid mist can occur in the ground cloud.

We will now consider the possibility of acid mist and acid rain formation under the assumption that the rocket engine emissions during the first 40 seconds of engine burn are injected into a cumulus congestus cloud from which no precipitation is occurring. The assumed properties of the cumulus cloud are shown in Table 4-3 and were obtained from data presented on pages 7-6 and 7-7 of the USAF Handbook of Geophysics (1960). The specific question to be answered is whether HCl absorption by the water drops in the hypothetical cloud, as an isolated process, is capable of producing precipitation from the cloud.

Whether or not precipitation will result is largely dependent upon the drop's fall speed. Table 4-4 gives the terminal velocities for drops of various diameters. This table shows that an 80- to 100-micron drop can be expected to fall out of the cloud as drizzle (the cloud is assumed stable for drops of 7 microns to 65 microns) taking 5 minutes to 10 minutes to fall 100 meters.

The water drops in the cloud will grow if a vapor pressure gradient is created toward the drops. The gradient can be calculated using Raoult's Law in Physical Chemistry (see, e.g., Lange, 1952) which states that the vapor pressure of an aqueous solution is reduced in proportion to the molar concentration of the solute. if $M_H << M_w$, this law may be approximated by

$$\frac{e_s}{e_o} \simeq 1 - \frac{M_H}{M_w} \qquad (4\text{-}1)^*$$

where e_s is the saturation vapor pressure of water at the surface of the drop, e_o is the ambient saturated vapor pressure of pure water, and M_H/M_w is the mole fraction

TABLE 4-4

TERMINAL VELOCITIES FOR FALLING RAINDROPS
(After Johnson, 1954)

Diameter (microns)	Fall Speed (cm sec^{-1})
20	1.24
50	7.72
80	20.0
200	72
400	162

of HCl in solution. The asterisk following the equation number indicates that the derivation of the equation is discussed in Appendix A.

The quantity e_a will approach an equilibrium value e_f as all the HCl is absorbed and the drop grows. The quantity e_f may also be calculated in dynes per square centimeter from the equation

$$e_f = e_o - G\,(a^3 - a_o^3) \tag{4-2}$$

where the second term on the right represents the water vapor used by a drop in growing from diameter a_o to a. The factor G, used for simplicity, is defined in Appendix A. Combining Equations (4-1) and (4-2) and solving for a (assuming $a_o^3 << a^3$) results in the expression

$$a \simeq 374 \sqrt[6]{\frac{e_o M_H}{n^2}} \tag{4-3}*$$

where n is the number of drops per cubic centimeter. Using the cloud properties listed in Table 4-3, this expression yields a = 29 microns, $e_f = 0.97\ e_o$, and $M_H = 0.04\ M_w$ (4 percent by weight HCl solution).

Equation (4-3) shows the drop diameter to be insensitive to large changes in e_o, M_H, and n, forcing the conclusion that precipitation cannot occur without water vapor replenishment. It is interesting to note that if all the water vapor present in the cloud were to condense on the initial number of cloud drops (n = 40), the resulting drops would be about 92 microns in diameter, or the size of drizzle drops. This implies that only about the same amount of water vapor as originally existed must be supplied to the cloud for the HCl to induce drizzle.

We will now consider the growth of cloud drops if a plentiful supply of water vapor is available; i.e., the ambient saturated vapor pressure e_o remains constant during the growth process. In order to isolate the effect of HCl absorption,

we shall use a simplified version of the equation describing drop growth by condensation together with Raoult's Law. The equation for drop growth may be written as

$$a^2 = a_o^2 + \beta e_o \left(1 - \frac{e_s}{e_o}\right) t \qquad (4\text{-}4)^*$$

where β is a coefficient inversely dependent upon temperature and

$$1 - \frac{e_s}{e_o} \simeq \frac{M_H}{M_w} \qquad (4\text{-}5)$$

is Raoult's Law (a rearrangement of Equation (4-1)).

A simplified expression for drop diameter as a function of time t can be derived by substituting Equation (4-5) into Equation (4-4) and by assuming that a fraction f of the HCl is absorbed at a rate sufficient to produce the most rapid drop growth. These steps yield

$$a \simeq 40 \sqrt[5]{f \frac{t}{n}} \qquad (4\text{-}6)^*$$

from which Table 4-5 is constructed showing drop growth for two values of f in an environment in which the supply of water vapor is constantly being replenished.

Since the behavior of HCl at low concentration is such that nearly all of the HCl will dissolve in the initial cloud drops, drops of the order of 80 microns may be expected to form within 20 minutes after launch. Approximately 1.5 hours would be required for drops of this size to fall to the ground from a height of 1 kilometer. If the air below the ground cloud is unsaturated, the drops would evaporate before reaching the ground.

It is emphasized that Equation (4-6) is also insensitive to large changes in the assumed values of the cumulus cloud and exhaust cloud parameters and, thus,

TABLE 4-5

DROP GROWTH BY CONDENSATION AFTER HCl ABSORPTION

Absorption of Available HCl	Time (minutes)	Drop Concentration per cm^3	
		40 Drops	100 Drops
		Drop Diameter (microns)	
f = 1.0	10	67	57
	100	105	90
f = 0.1	10	44	35
	100	69	55

TABLE 4-6

DROP SIZE FROM CONDENSATION AFTER HCl ABSORPTION

Initial Drop Diameter (microns)	Diameter After 250 Seconds (microns)
10	90
20	92
50	102

the formation of acid drizzle is extremely unlikely. However, the cloud drops will probably contain from 1 to 5 percent HCl for the lifetime of the cloud.

In addition to drop growth by condensation, drop size may also be increased as the result of coalescence. This latter process is important in the formation of rain. For drop growth by coalescence to occur, a large drop with a high terminal velocity must fall through a volume containing small drops with a low terminal velocity. The larger drop captures a certain percentage of the smaller drops contained in the air volume swept out in descent, thus increasing the diameter of the large drop.

From the cloud properties given in Table 4-3, assuming a log-normal drop size distribution, the drops may be roughly separated into three size categories:

- 10 drops of 10 microns diameter per cubic centimeter
- 20 drops of 20 microns diameter per cubic centimeter
- 10 drops of 50 microns diameter per cubic centimeter

We will first calculate the drop size distribution produced by condensation resulting from HCl absorption. Using Equation (4-4) for $M_H/M_w = 0.01$ and $\beta c_o = 2600$ gives

$$a^2 = a_o^2 + 26\,t \tag{4-7}$$

for the drop diameter produced by condensation. Table 4-6 shows the drop diameters estimated from Equation (4-7) for t = 250 seconds, resulting from HCl absorption by the three drop size categories. It can be seen that very little difference in drop size exists after 250 seconds. The relative difference of drop terminal velocities in the hypothetical cloud is therefore not adequate to produce precipitation by coalescence. However, if it is assumed that some new drops are formed in the cumulus cloud, or that some of the original drops are unaffected by the growth process, an estimate of growth by coalescence can be made for a cumulus cloud 400 meters deep.

The equation describing coalescence growth is (Johnson, 1954, p. 221)

$$a_2 - a_1 = \frac{\overline{EW}}{2D} (z_2 - z_1) \qquad (4\text{-}8)$$

where $z_2 - z_1$, the fall distance, is considered a positive number; $\overline{E}$ is the collection efficiency; $\overline{W}$ is the liquid water content of the cloud; and D is the density of the drop. The maximum drop size expected by coalescence can be calculated from Equation (4-10) by letting a 100 micron drop fall through the entire 400-meter depth of a cloud of 20 micron drops. The result is a drop diameter of 200 microns. Thus, even for a moderately higher water content, the contribution of coalescence to drop growth within the cloud appears to be minor, except for drops falling from the top of the cloud.

A more appropriate model where the drops are nearly the same size is a stochastic one such as described by Berry (1967). This model produces a growth rate comparable to the coalescence process but transfers more water to the larger drops. It appears that for the low water content of the cumulus cloud, this process will also be unimportant. The computations are lengthy and were not performed for this report.

SECTION 5

STRATOSPHERIC HAZARD CALCULATIONS

The fate of the rocket engine emissions released in the stratosphere, which is defined for present purposes as the altitude range between meters, is determined by three essentially distinct processes:

- Gravitational Settling
- Diffusion
- Photochemical Interactions

These processes are first discussed separately and their relative effectiveness is then assessed in the discussion below.

5.1 GRAVITATIONAL SETTLING

It is our understanding that aluminum oxide (Al_2O_3) is released in particulate form. Thus, gravitational settling in all probability determines the ultimate fate of the aluminum oxide emitted. The fall velocity of particles is given by Junge (1963):

$$w = m_s g(1-\rho/\rho_s)\ \alpha/(6\ \pi\ \eta\ r_s) \qquad (5\text{-}1)$$

where

m_s = particle mass
g = gravitational acceleration
ρ = air density
ρ_s = particle density
α = $1 + \beta\ell/r_s$ (Cunningham's slip correction factor)
β = $1.26 + 0.40 \exp(-1.10\ r_s/\ell)$
ℓ = mean free path

r_s = particle radius

η = dynamic viscosity of the air

Fall velocities for four different Al_2O_3 particle sizes were calculated from this formula in the altitude range of 15 to 35 kilometers. The results are shown in Figure 5-1. The fall velocity increases essentially exponentially with altitude for all particle sizes, and at a given altitude increases very rapidly with particle size. A more informative aspect of the calculation is presented in Table 5-1, which lists the residence time as a function of height for Al_2O_3 particles of 0.1 micron and 1.0 microns. In the present context, the residence time is defined as the time required by a particle of given size to travel from the specified altitude to the bottom of the stratosphere (15 kilometers). It is evident from Table 5-1 that residence times for the smaller particles (0.1 microns) are more than an order of magnitude larger than the corresponding residence times for the larger particles (1.0 microns). Further, the time required to traverse the lowest 5 kilometers (20 to 15) is several times the time required to traverse the top 5 kilometers (35 to 30). Thus, the mechanics of gravitational settling tend to result in an accumulation of particles of all sizes in the lower altitude region, although of course the rate of accumulation varies with particle size. In this region, the particles will be transported into the troposphere by injection into cyclonic storms, as described by Danielsen (1968).

The effect on Al_2O_3 of gravitational settling will be compared with other redistributing mechanisms at the end of this section. None of the remaining rocket engine emission products is in particulate form, and hence, they are not subject to gravitational settling.

5.2 DIFFUSION

To assess properly the importance of diffusion in dispensing rocket engine emissions in the stratosphere, one must first estimate the amount of dilution required

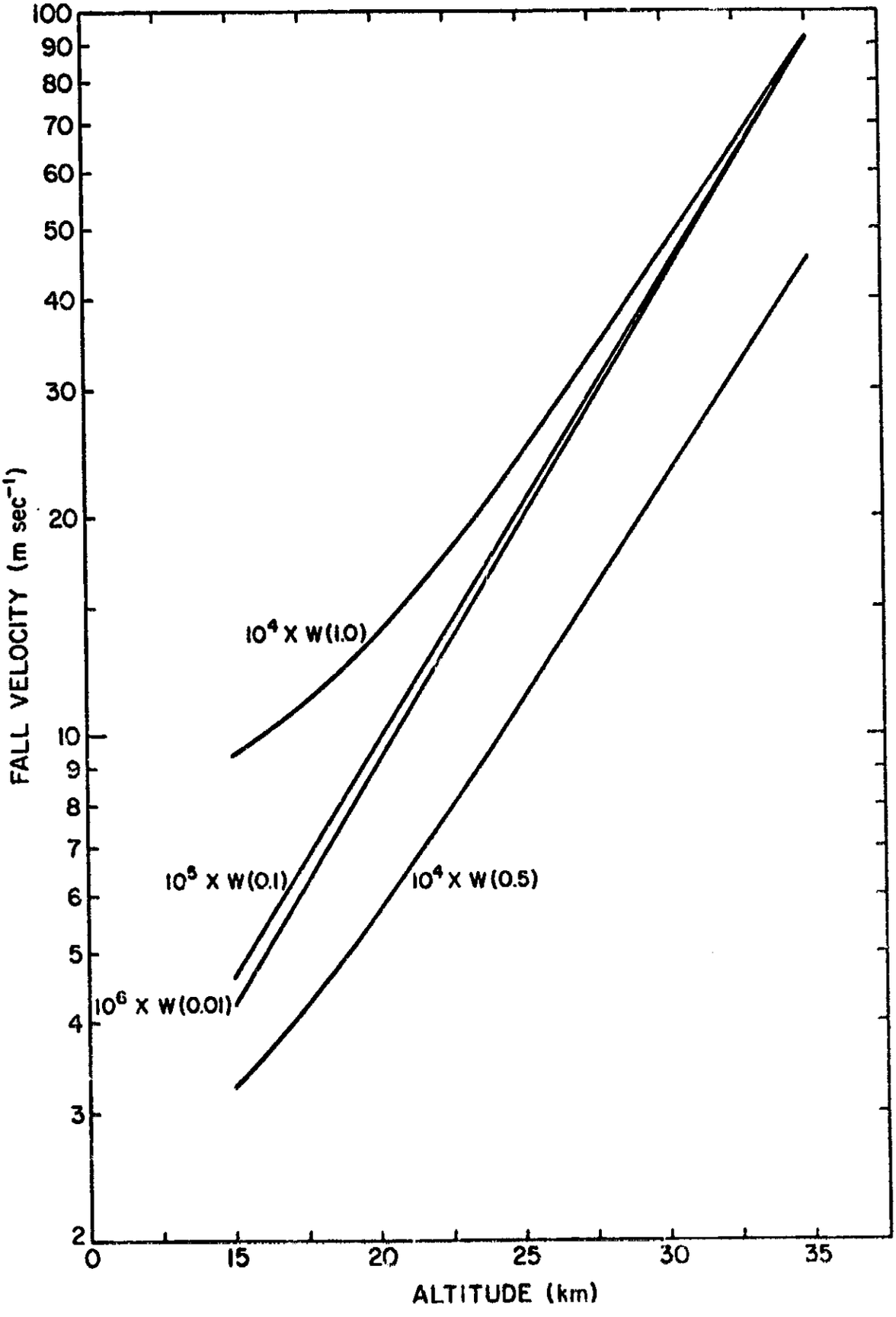

FIGURE 5-1. Fall velocities for Al_2O_3 particles. Numbers enclosed by parentheses indicate the particle size in microns.

TABLE 5-1

RESIDENCE TIMES FOR Al_2O_3 PARTICLES IN THE STRATOSPHERE

Altitude (km)	Radius = 0.1 micron	Radius = 1.0 micron
20	2.43 years	1.82 months
25	3.62 years	2.90 months
30	4.17 years	3.48 months
35	4.43 years	3.78 months

to reduce emission concentration to harmless values. For this purpose, the emissions will be assumed harmless when their concentrations fall below the corresponding normal ambient levels or, for products not usually found in the stratosphere, when their concentrations are at least an order of magnitude less than those of trace elements normally found in the stratosphere.

Figure 5-2, taken from the USAF Handbook of Geophysics (1960, p. 8-3) shows the vertical distribution of the number density of atmospheric constituents. Table 5-2 lists atmospheric composition by percent. Xenon is a very minor constituent at about 25 kilometers and has a number density of 10^{11} molecules cm^{-3}. Therefore, a number density of 10^{10} cm^{-3} for the rocket engine emissions appears to be a very conservative hazard criterion.

The amount of dilution of the emissions required to reach a number density of 10^{10} cm^{-3} is shown in Table 5-3. The first two columns list the products and the emission rates in grams per meter as supplied by Thiokol. In the third column, for calculation purposes, the listed linear density was calculated by assuming the particles to be released in an infinitely thin vertical column. Thus, diffusion occurs only in a horizontal plane. (Although Al_2O_3 is released in particulate form, it will be treated here as if it were released in molecular form, in order to unify the discussion.) The next column lists the number density of the exhaust products in the initial stabilized cloud for a cloud radius of 200 meters. By comparison with Figure 5-2, it can be seen that N_2 and CO_2 number densities are insignificent compared to ambient values and that H_2O reaches ambient values when the cloud has expanded to a radius of about one kilometer. These exhaust products will therefore be eliminated from future consideration. The last three columns of Table 5-3 interpret the number density in terms of the radius to which the cloud must expand to reach values of 10^{11}, 10^{10} and 10^{9} particles cm^{-3}. These values were obtained by uniformly mixing each product throughout the volume. From these figures, it is reasonable to select a value of 50 kilometers as the required radius of dilution.

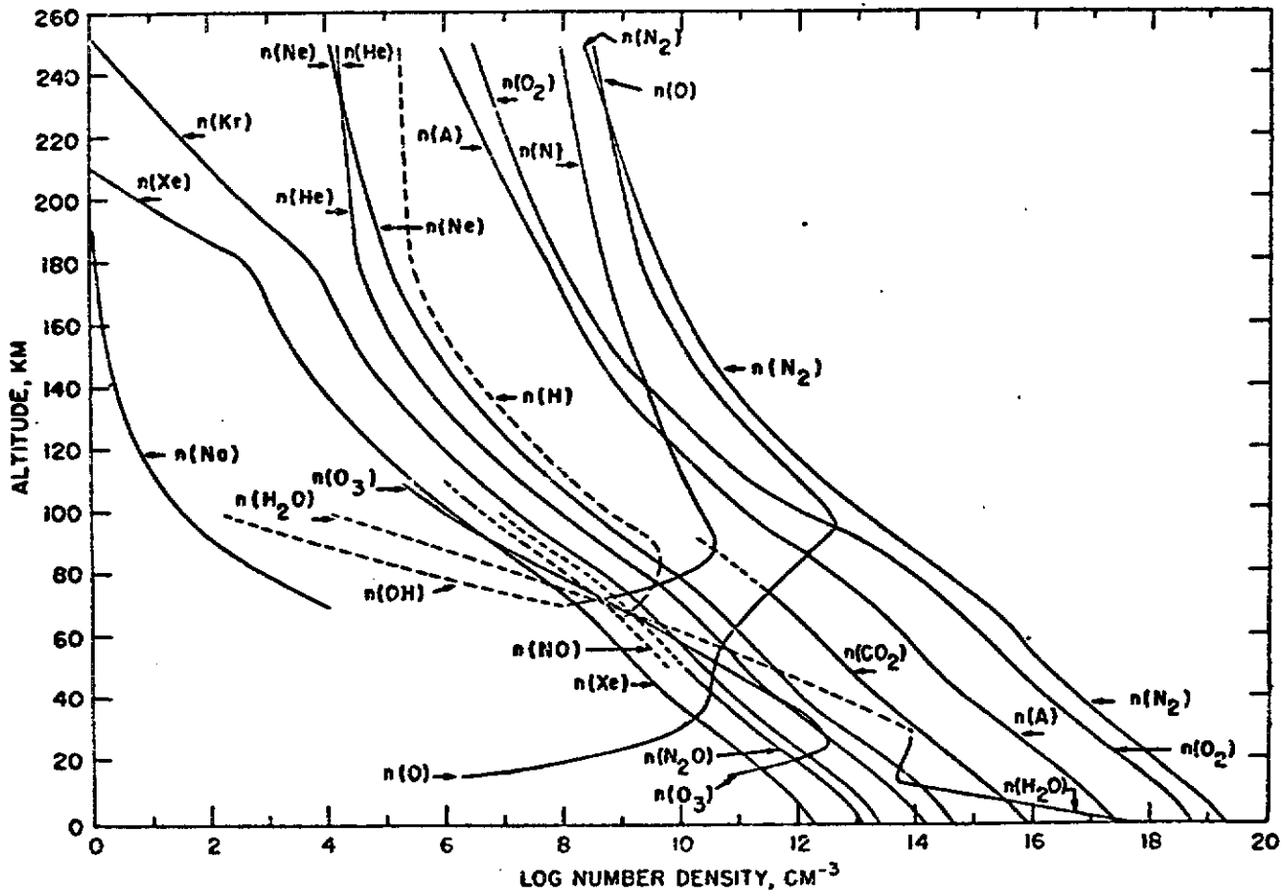

FIGURE 5-2. Vertical distribution of atmospheric constituents from surface to 250 kilometers (from the USAF Handbook of Geophysics, 1970, p. 8-3).

TABLE 5-2

COMPOSITION OF THE ATMOSPHERE (DRY) UP TO ABOUT 90 KILOMETERS*

Constituent	Per Cent by Volume	Per Cent by Weight	Reduced Thickness (atmo-cm, NTP)
Nitrogen	78.088	75.527	624,343.
Oxygen	20.949	23.143	167,495.
Argon	0.93	1.282	7,435.69
Carbon dioxide	0.03	0.0456	239.861
Neon	1.8×10^{-3}	1.25×10^{-3}	14.3817
Helium	5.24×10^{-4}	7.24×10^{-5}	4.18957
Methane	1.4×10^{-4}	7.75×10^{-5}	1.11935
Krypton	1.14×10^{-4}	3.30×10^{-4}	0.911472
Nitrous oxide	5×10^{-5}	7.6×10^{-5}	0.399768
Xenon	8.6×10^{-6}	3.90×10^{-5}	0.068760
Hydrogen	5×10^{-5}	3.48×10^{-6}	0.399768

*From the USAF Handbook of Geophysics, 1970, p. 8-1.

TABLE 5-3

PROPERTIES OF ROCKET ENGINE EMISSIONS IN THE STRATOSPHERE

Exhaust Product	Emission Rate ($g\ m^{-1}$)	Linear Density (cm^{-1})	Density (cm^{-1}) in Stabilized Cloud (r = 200 m)	Diffusion Radius to Reach Number Density of		
				10^{11} (cm^{-3})	10^{10} (cm^{-3})	10^{9} (cm^{-3})
HCl	3215	5.3×10^{23}	4.3×10^{14}	13 km	42 km	130 km
Al_2O_3	4510	2.67×10^{23}	2.1×10^{14}	9 km	30 km	90 km
H_2O	5614	18.8×10^{23}	1.5×10^{15}	*		
CO	3572	7.7×10^{23}	6.3×10^{14}	16 km	50 km	160 km
CO_2	561	0.77×10^{23}	6.1×10^{13}			
N_2	1304	2.8×10^{23}	2.3×10^{13}			

*Reaches background value at a radius of about one kilometer.

In order to estimate the time required for the material to reach this dilution radius, we adopt a simple diffusion model to illustrate what is known about stratospheric diffusion coefficients, which are commonly measured by measuring the dispersion of smoke trails, luminous trails resulting from rockets or of meteor trails.

The simple case of one-dimensional flow with constant diffusivity D, is described by the equation

$$\frac{\partial n}{\partial t} = D \frac{\partial^2 n}{\partial r^2} \tag{5-2}$$

which has the solution

$$n = \frac{\text{const}}{\sqrt{4\pi Dt}} \exp\left[- r^2/4Dt\right] \tag{5-3}$$

Equation (5-3) gives the mean-square dispersion $\overline{r^2} = 2Dt$, although experimental data on cloud expansion for various conditions result in values ranging from $\overline{r^2} \sim t$ to $\overline{r^2} \sim t^3$.

However, we shall use only the term $\exp\left[-r^2/4Dt\right]$ to demonstrate the meaning of the value assigned to D since a reasonable value for r was estimated to be 50 kilometers. Typically, this means that the number density at this distance is 10 percent of the central value. Therefore, $r^2/4Dt = 2.3$ ($\exp\left[-2.3\right] = 0.1$), or solving for t for r = 50 kilometers gives $t = 2.7 \times 10^{12}/D$, where t is in seconds and D is in $cm^2\ sec^{-1}$.

The time required to achieve the required dilution is shown in Table 5-4 for various values of D. Values of the vertical diffusion coefficient in the stratosphere range from 10^3 to 10^4 $cm^2\ sec^{-1}$. Values for the horizontal coefficient are much larger than this and are a function of time.

TABLE 5-4

STRATOSPHERIC INTERPRETATION OF DIFFUSION COEFFICIENTS

Diffusion Coefficient ($cm^2\ sec^{-1}$)	Time to Achieve a 50-km Dilution Radius
10^4	8.7 years
10^5	10.4 months
10^6	1.04 month
10^7	3.1 days
10^8	7.5 hours

The results of the previously-mentioned measurement programs, represented on a time scale from minutes to hours, are shown in Figure 5-3. The scatter in the data is primarily due to the inherent variability of meteorological conditions as well as differences in measurement time scales. Figure 5-4 is more pertinent to the present problem and shows that, for diffusion times on the order of 100 hours, the diffusion coefficient increases by two orders of magnitude despite the broad scatter of the observations. Thus, considering the sketchy information available and the preceding discussion, there appears to be no hazard problem in the stratosphere caused by the rocket emissions—at least after a couple of days.

5.3 CHEMISTRY

As mentioned above, it appears superfluous to consider the chemistry of water vapor, molecular nitrogen and carbon dioxide in connection with the rocket engine emissions under consideration, since the ambient concentrations of these constituents far exceed the contribution of the rocket engine. Of the remaining emission constituents, Al_2O_3 is a stable oxide, insoluble in water, and emitted in particulate form. We are not aware of any stratospheric chemical reactions affecting it.

Most of what little is known about HCl is contained in the report "Preliminary Air Pollution Survey of Hydrochloric Acid" (U. S. Department of Health, Education and Welfare, National Air Pollution Control Administration Publication No. APTD 69-36, October 1969). To quote from the report, "No information has been found on environmental air concentrations of hydrochloric acid." In particular, no observations of HCl in the stratosphere exist, and no information exists as to possible chemical reactions in the stratosphere.

Almost as little is known about the atmospheric chemistry of carbon monoxide (CO). In particular, the reactions

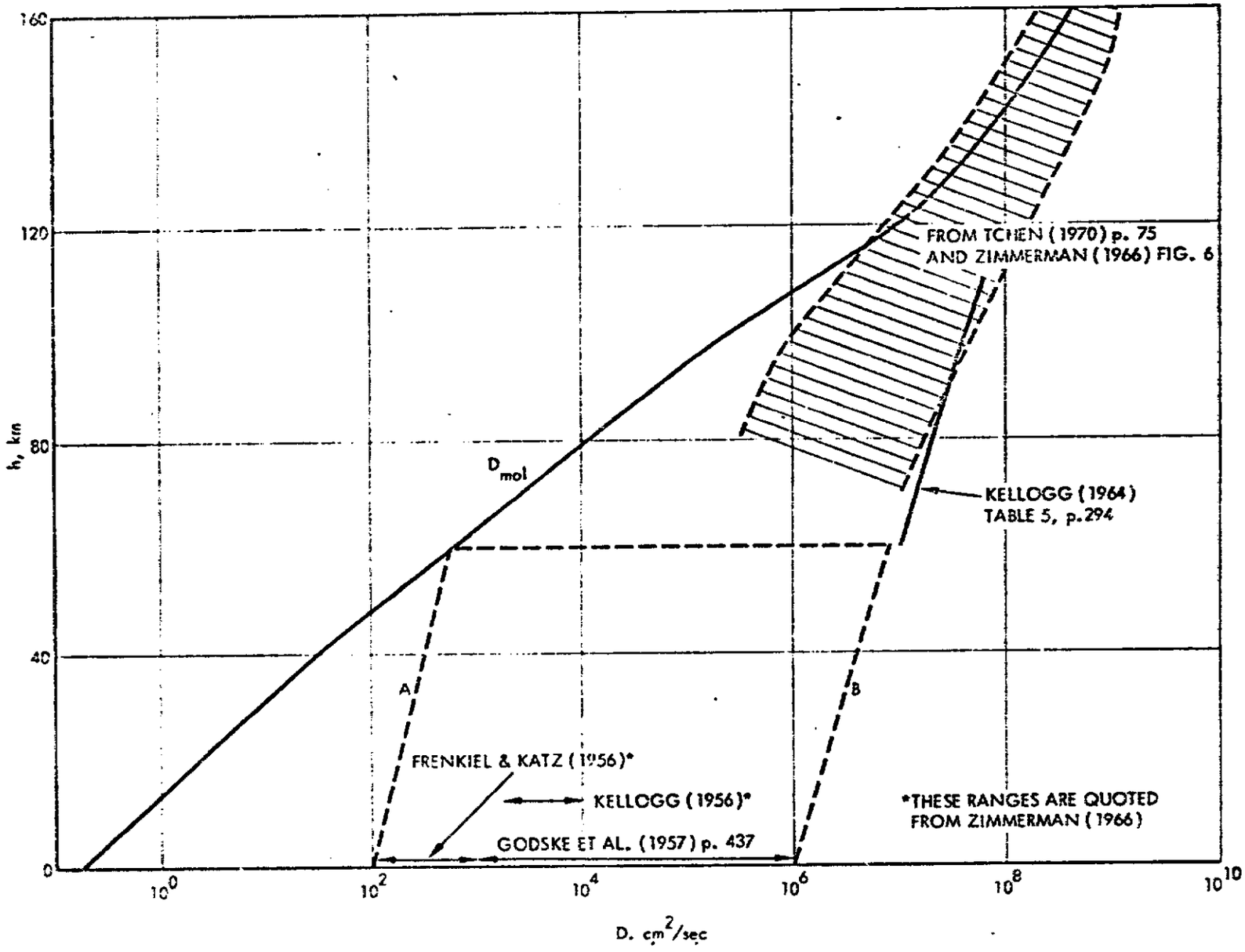

FIGURE 5-3. Effective atmospheric diffusion coefficient D as a function of altitude. (After Bauer, et al., 1971).

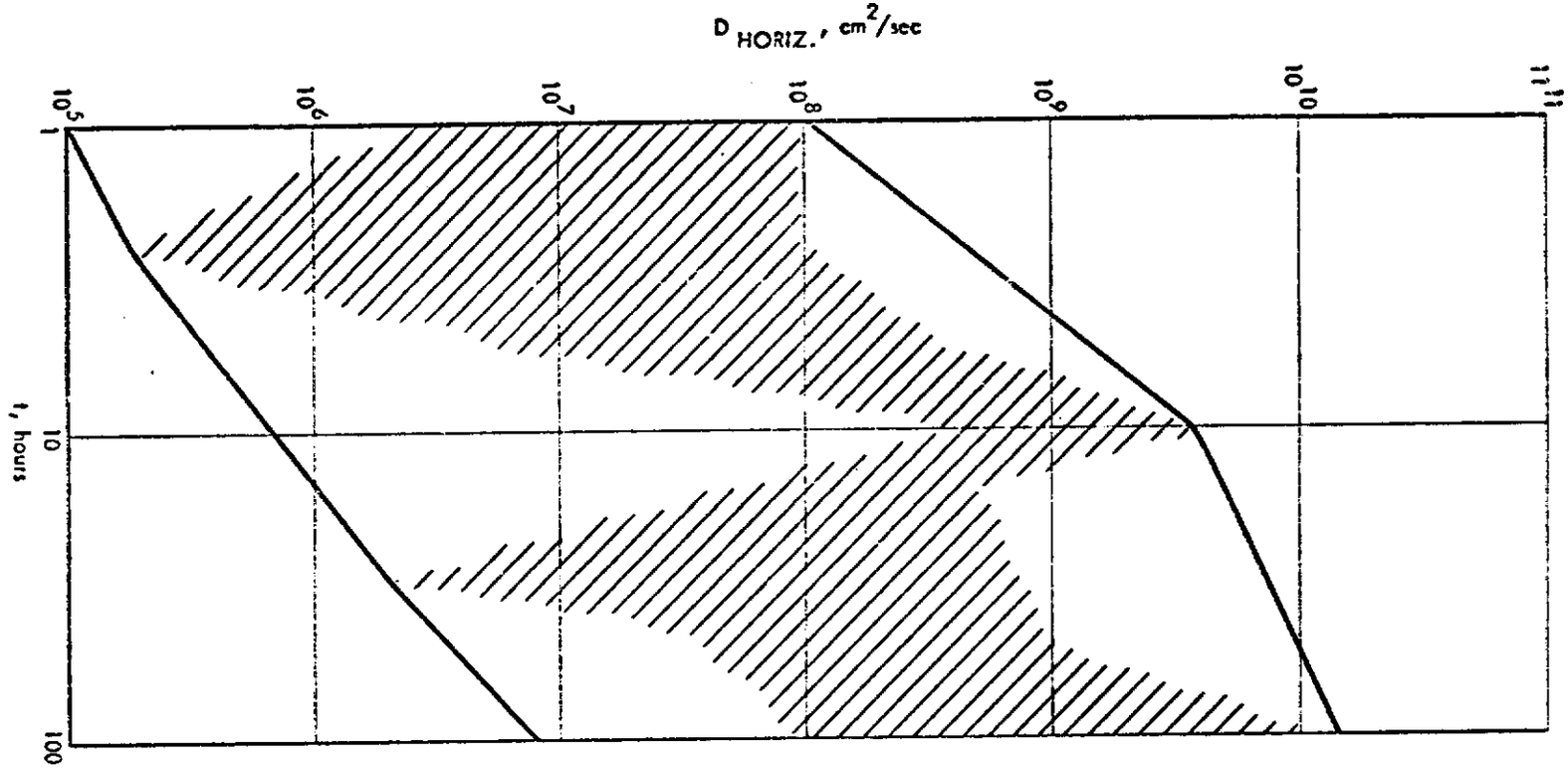

FIGURE 5-4. Change of horizontal diffusion coefficient with time (replotted from Heffter, 1965).

$$2\,CO + O_2 \rightarrow 2CO_2$$

$$CO + O_2 \rightarrow CO_2 + O$$

$$CO + H_2O \rightarrow CO_2 + H_2$$

$$CO + O_3 \rightarrow CO_2 + O_2$$

have been found to be much too slow to appreciably affect the CO concentration ("Air Quality Criteria for Carbon Monoxide," U. S. Department of Health, Education and Welfare, National Air Pollution Control Administration Publication No. AP-62, March 1970). There are possible reactions with NO_2, OH, and HO_2, but no definitive observational or theoretical evidence exists as to their effectiveness. To quote from the aforementioned report, "It must be concluded that no gaseous reactions have been shown to be important scavengers of CO in the atmosphere."

5.4 COMPARISON OF CHEMICAL, DIFFUSIVE AND GRAVITATIONAL EFFECTS

An initial comparison of the relative importance of chemical, diffusive, and gravitational effects can be obtained from the following considerations. Let N be the concentration of a constituent of interest, for which the continuity equation is

$$\frac{\partial N}{\partial t} + \frac{\partial}{\partial z}(WN) - D\nabla^2 N = -\alpha N \qquad (5\text{-}4)$$

where

D = coefficient of diffusion

w = fall velocity

α = a chemical rate coefficient

Using the simple models for diffusion and gravitational settling, we may define

$$F_D \equiv \frac{1}{N} (\partial N/\partial t)_{\text{diffusive}} = \frac{1}{t}\left(\frac{r^2}{4Dt} - 1\right) \tag{5-5}$$

$$F_w \equiv \frac{1}{N} (\partial N/\partial t)_{\text{gravitational}} = \frac{1}{N}\frac{\partial}{\partial z}(wN) \approx \frac{\partial w}{\partial z} \tag{5-6}$$

$$\lambda_c = \frac{1}{N} (\partial N/\partial t)_{\text{chemical}} = -\alpha \tag{5-7}$$

If the relevant parameters are known, a comparison of the relative importance of the three processes can be obtained by comparing the quantities F_D, F_w, and F_c. For example, in the case of Al_2O_3, we can compute $\partial w/\partial z$ quite readily. For 1 micron particles

$$\partial w/\partial z \cong 7 \times 10^{-8} \text{ sec}^{-1} \text{ at 15 kilometers}$$

$$\cong 1 \times 10^{-6} \text{ sec}^{-1} \text{ at 35 kilometers}$$

The ratio $\left| F_w/F_D\,(r=0) \right| = t\,\frac{\partial w}{\partial z}$ indicates that gravitational settling becomes important at $t \cong 10^7$ seconds at 15 kilometers and at $t \cong 10^6$ seconds at 35 kilometers. This in turn indicates that the 1-micron Al_2O_3 population has been significantly diluted before gravitational settling becomes the dominant process.

The preceding discussion indicates that some of the essential information is currently unavailable, whereas in other respects reliable calculations can be made about the effects of rocket engine emissions. It appears from the discussion on diffusion that no credible problem exists in the stratosphere due to the low concentration of emission products relative to ambient trace constituents after a couple of days following launch.

REFERENCES

Bauer, E., et al., 1971: Fluid motions and some of their effects on chemistry in the upper atmosphere. Paper P-756, Institute for Defense Analyses, Science and Technology Division, Arlington, Virginia, 66.

Berry, E. X., 1967: Cloud droplet growth by collection. J. Atm. Sci., 24(6), pp. 688-701.

Briggs, G. A., 1970: Some recent analyses of plume rise observation. Paper ME-8E presented at the Second International Clean Air Congress of the Int. Union of Air Poll. Prevention, Dec. 6-11, 1970, Washington, D. C.

Cramer, H. E., et al., 1970: Titan III D toxicity study. Final Report under Contract No. F04697-70-C-0178, GCA Rpt. TR-70-3-A, GCA Corporation Technology Division, Bedford, Mass., 168.

Danielsen, E. F., 1968: Stratospheric-tropospheric exchange based on radioactivity, ozone and potential vorticity. J. Atm. Sci., 25(3), 502-518.

Denbigh, 1966: The Principles of Chemical Equilibrium. Cambridge University Press, London.

Dumbauld, R. K., et al., 1970: Handbook for estimating toxic fuel hazards. Final Report under Contract No. NAS8-21453, NASA Report CR-61326, Marshall Space Flight Center, Alabama.

Dumbauld, R. K., 1971: Review of cloud rise problem. Technical Note submitted under Contract No. NAS8-26673 to NASA, Marshall Space Flight Center, Alabama.

Dumbauld, R. K. and J. R. Bjorklund, 1971: Hazard estimates for selected rocket fuel components at Kennedy Space Center. NASA Report CR-61358, Marshall Space Flight Center, Alabama.

Fukuta, N., et al., 1970: "Reply" to note entitled "Ice Clouds on Venus?" J. Atm. Sci., 27(2), 334-335.

Heffter, J. L., 1965: The variation of horizontal diffusion parameters with time... J. Appl. Met., 4(153).

Johnson, J., 1954: Physical Meteorology. John Wiley & Sons, N. Y., 208-231

Junge, C., 1963: Air Chemistry and Radioactivity. Academic Press, N. Y., 382.

Lange, N. (ed), 1952: Handbook of Chemistry. Handbook Publishers, Inc., Sandusky, Ohio.

Makhon'ko, K. P., 1967: Simplified theoretical notion of contaminant removal by precipitation from the atmosphere. Tellus, 19, 467-476.

McDonald, J. E., 1953: Erroneous cloud-physics applications of Raoult's law. J. Meteor., 10, 68-70.

Morton, B. R., Sir G. I. Taylor and J. S. Turner, 1956: Turbulent gravitational convection from maintained and instantaneous sources. Proc. Roy. Soc., 234A, 1-23.

Record, F. A., et al., 1970: Analysis of lower atmospheric data for diffusion studies. Final Report under Contract No. NAS8-30503, NASA Report CR-61327, Marshall Space Flight Center, Alabama.

Slade, D. H. (ed), 1968: Meteorology and Atomic Energy. Prepared by Air Resources Laboratories, ESSA, for U. S. Atomic Energy Commission, 445.

Smith, J. W. and W. W. Vaughan, 1961: Monthly and annual wind distribution as a function of altitude for Patrick Air Force Base, Cape Canaveral, Florida. NASA Technical Note D-610, George C. Marshall Space Flight Center, Huntsville, Alabama.

Susko, M. and J. W. Kaufman, 1971: Apollo Saturn engine exhaust cloud rise and growth phenomena during initial launch. Paper presented at MFSC Research Achievements Review, 2 Dec. 1971, Marshall Space Flight Center, Alabama.

Terraglio, F. and R. Manganelli, 1967: The absorption of atmospheric sulfur dioxide by water solutions. J. Air Poll. Cont. Assn., 17, 403-406.

USAF Handbook of Geophysics (Revised Edition), 1960: The MacMillan Company, New York, N. Y.

APPENDIX A

DERIVATION OF EQUATIONS FOR THE HCl ACID MIST PROBLEM (Section 4.5)

A.1 LIST OF SYMBOLS

A summary of symbols used in Section 4.5 and in the derivations of the equations which follow is given in Table A-1.

A.2 DERIVATION OF EQUATIONS

Equation (4-1), Raoult's Law

For application to cloud physics problems, it is convenient to write Raoult's Law as

$$1 - \frac{e_s}{e} = \frac{i\, M_H/m_H}{i\, M_H/m_H + M_w/m_w} \qquad (A\text{-}1)$$

where i is van't Hoff's factor (McDonald, 1953). For the HCl acid drop problem, since the molecular weight of HCl is twice the molecular weight of water and i is approximately 2, Equation (A-1) may be reduced to

$$\frac{e_s}{e} = \frac{1}{1 + M_H/M_w} \qquad (A\text{-}2)$$

For weak acid solutions, M_H/M_w is a small positive number and Equation (A-2) may be expanded by the binomial series to give

$$\frac{e_s}{e} \approx 1 - \frac{M_H}{M_w} \qquad (4\text{-}1)$$

TABLE A-1

LIST OF SYMBOLS

a	=	drop diameter in microns
D	=	density of liquid water = 1 g cm^{-3}
e	=	ambient vapor pressure of pure water = 1.7×10^{4} dynes cm^{-2}
e_s	=	saturation vapor pressure at the surface of the drop containing the HCl
i	=	van't Hoff's factor
m_H	=	molecular weight of HCl = 36.5
m_w	=	molecular weight of H_2O = 18.06
M_H	=	mass of HCl per cubic centimeter = 2×10^{-8} g cm^{-3}
M_w	=	mass of liquid water per cubic centimeter (g cm)
n	=	number of water drops per cubic centimeter = 40
R^*	=	gas constant = 8.31×10^{7} erg $mole^{-1}$ K^{-1}
t	=	time
T	=	absolute temperature = 288 K
μ	=	10^{-4} cm
ρ_w	=	ambient water vapor density = 12.8 g m^{-3}
ρ_{ow}	=	saturated water vapor density at the temperature of the drop surface
K	=	diffusivity of water vapor in air = 0.25 cm^{2} sec^{-1}

• The subscript o refers to t = 0 (initial condition)

Equation (4-3)

Equation (4-3) provides a means of estimating the final drop size that would result from a known concentration of HCl if the amount of water vapor is not replenished. We begin with Equation (4-1); let e_f be the final equilibrium value of the saturation vapor pressure; and express the mass of liquid water per cubic centimeter at final equilibrium M_w as $n\,s\,a^3$, where a is the drop diameter and $s = \frac{D\,\pi\,\mu^3}{6}$.

These substitutions yield

$$\left(e_f - e_o\right) = -\frac{e_o\,M_H}{n\,s\,a^3} \tag{A-3}$$

However, the term $\left(e_f - e_o\right)$ is also the amount of water vapor used in increasing the drop size from a_o to a. Therefore, we may write

$$\left(e_f - e_o\right) = -\gamma\,n\,s\,\left(a^3 - a_o^3\right) \tag{A-4}$$

where, for convenience, $\frac{R^*T_o}{m_w}$ has been set $= \gamma$.

If it is assumed that $a_o^3 << a^3$, Equations (A-3) and (A-4) may be combined to yield

$$a^6 = \frac{1}{\gamma\,s^2}\left(\frac{e_o\,M_H}{n^2}\right) \tag{A-5}$$

or

$$a = 374\sqrt[6]{\frac{e_o\,M_H}{n^2}} \tag{4-3}$$

Equation (4-4)

We begin with the equation describing cloud drop growth as written by Johnson (1954):

$$a^2 = a_o^2 + \mu^{-2} \frac{8K}{D} \left(\rho_w - \rho_{ow}\right) t \qquad (A-6)$$

This equation may be changed to

$$a^2 = a_o^2 + \beta e \left(1 - \frac{e_s}{e}\right) t \qquad (4-4)$$

by using the simplified form of Raoult's Law given by Equation (4-1) and letting

$$\beta = \frac{\mu^{-2} m_w 8K}{D R^* T}$$

For the present problem, we may let T = 288 degrees Kelvin, and e = 1.71×10^4 dynes per square centimeter. The resulting value of 2600 for βe is correct within a factor of 2 for the range of parameters expected within the cloud.

Equation (4-6)

This equation is derived by first substituting Equation (4-5) in Equation (4-4) and then assuming $a_o^2 << a^2$ to obtain

$$a^2 = \beta e_o \left(\frac{M_H}{M_w}\right) t \qquad (A-7)$$

Using the fact that

$$M_w = \frac{D n \pi \mu^3}{6} a^3 \qquad \text{(A-8)}$$

and substituting Equation (A-8) into Equation (A-7) gives

$$a^5 = \frac{6 \beta e_o M_H}{D \pi \mu^3} \left(\frac{f}{n}\right) \qquad \text{(A-9)}$$

where the quantities outside the parentheses are held constant. Letting f ($0.1 \leq f \leq 1$) represent the fraction of gaseous HCl absorbed by the liquid water and solving for a yields

$$a = \sqrt[5]{\frac{6 \beta e_o M_H}{D \pi \mu^3} \left(\frac{ft}{n}\right)} = 40 \sqrt[5]{\frac{ft}{n}} \qquad \text{(4-6)}$$

where $\beta e_o = 2600$ and $M_H = 2 \times 10^{-8}$ g cm^{-3}.

APPENDIX G

THIOKOL SOLID PROPELLANT ROCKET ENGINE NOISE PREDICTION

BOLT BERANEK AND NEWMAN INC

CONSULTING • DEVELOPMENT • RESEARCH

THIOKOL SOLID PROPELLANT ROCKET ENGINE NOISE PREDICTION

Hanno H. Heller
Eric E. Ungar

4 February 1972

Report No. 2326
BBN Job No. 152000
Contract No. 72-00-441

Submitted to:

Thiokol Chemical Corporation
Wasatch Division
Brigham City, Utah 84302
Attention: Mr. D.C. Mecham

I. INTRODUCTION

NASA's office of Manned Space Flight is currently studying two booster concepts for the space shuttle system: (1) the pump-fed ballistic recoverable booster with an expendable pressure-fed booster and (2) the solid-propellant recoverable (or expendable) booster as "thrust augmenter" for the orbiter. The Thiokol Chemical Corporation, Wasatch Division, is developing solid-propellant propulsion systems that can be used in either of two modes:

1. Series Burn Mode: The booster consists of a cluster of either five or six 120-in.-diameter motors or three 156-in.-diameter motors. These motors are arranged as shown in Fig. 1. The booster engines fire simultaneously; the orbiter takes over at liftoff and ascent, until after separation.

2. Parallel Burn Mode: Four 120-in. diameter or two 156-in. diameter motors are mounted symmetrically on the sides of the orbiter propellant tank (Fig. 2). The booster motors and orbiter engines fire simultaneously.

In either case, the orbiter engine uses liquid hydrogen/oxygen as propellant. The booster units are driven by a solid propellant whose exhaust product contains CO_1, CO_2, $HC\ell$, H_2O, H_2, and N in gaseous form, and $A\ell_2O_3$ in either liquid or solid form.

One important consideration in the solid-propellant propulsion concept is the noise generated. In the following, we predict both the nearfield and the farfield noise produced in both the series and the parallel burn modes.

II. JET AND ROCKET NOISE PREDICTION

A. Rocket-Exhaust Flow

In general, the rocket-exhaust characteristics that influence the radiated sound are determined primarily by the rocket engine configuration, the dynamics of combustion and flow within the engine, and the ambient conditions. Rocket-exhaust characteristics vary over the flight regime of a launch vehicle: When the rocket engine fires on the launch pad and immediately subsequent to lift-off, the exhaust jet contracts in response to an ambient pressure that is higher than the pressure in the exit plane of the rocket engine. As illustrated in Fig. 3a, this overexpanded nozzle condition (or, equivalently, underexpanded jet condition) creates – within the flow – shock cells that continue to repeat in the downstream direction. Viscous effects modify this flow, slowing it to a subsonic turbulent jet. During this process, shock-dependent noise-producing mechanisms are present.

As the rocket gains altitude, the engine design condition is reached – i.e., ambient and exit plane pressures are substantially identical (see Fig. 3b). The flow is essentially shock-free (very weak shocks may actually be present because of second-order effects), and the mechanisms of noise generation dependent on shock interactions essentially vanish.

As the launch vehicle climbs and passes into a region for which the engine nozzle is underexpanded, the ambient pressure continues to decrease. As shown in Fig. 3c, the exhaust jet expands immediately downstream of the nozzle exit plane and

generates a shock cell structure in a manner similar to the over-expanded nozzle conditions. Again, the shock-dependent noise-producing mechanisms are present.

The exhaust continues to expand with increasing altitude and such phenomena occur as a shock wave detached from the exhaust and attached to the vehicle. However, for these conditions, vehicle speed is typically supersonic and the atmosphere is quite rarified; therefore, this regime is unimportant with regard to sonic excitation.

B. Noise-Generating Mechanisms

The aerodynamic properties of a rocket-exhaust jet are intimately related to its acoustic behavior. A subsonic jet consists of three distinct flow regimes (Fig. 4): a mixing region (with a potential core and a highly intense, surrounding, shear layer), a transition region, and a fully developed region. The process of the turbulent mixing of the high-speed exhaust with the surrounding medium represents the dominant noise source of subsonic jets.

A supersonic jet has a complex flow field, providing a multitude of noise sources. Figure 5 schematically illustrates – in more detail than Fig. 3 – the flow field of a supersonic jet. The most important distinction between subsonic and supersonic jet flow is the occurrence of oblique and normal shock waves in the supersonic flow. Figure 5 illustrates an underexpanded jet condition, such as exists at lift-off.

Figure 6 illustrates several well-known noise sources in rocket exhaust flows:

1. Instabilities in the combustion process may result in a fluctuating mass flow through the nozzle of the engine. This *monopole* type of noise source behaves much as if the entire exit plane of the nozzle were a piston which moves back and forth rapidly.

2. Lip noise is generated when vortices or intense turbulence passes through the nozzle and interacts with the nozzle lip, generating fluctuating forces on this nozzle lip; this mechanism is a *dipole* source of noise.

3. The subsonic mixing region of slightly supersonic jets is the most important mechanism of noise generation. This source of noise is associated with the fluctuating velocities created when the jet mixes with the ambient air. As most of the energy of a supersonic jet is lost in the subsonic mixing region, this noise source may be dominant even in supersonic jets.

4. Mach wave radiation, which results because the air in the jet is moving supersonically with respect to the ambient air, is completely analogous to the shock waves which are a characteristic of a supersonically moving body. Mach waves may be important sound generators, particularly in hot jets.

5. Shock-turbulence interaction noise is the last source of noise generation. The normal shocks associated with an under or overexpanded supersonic jet are normally very stable and do not generate sound. However, noise may be generated when a density or temperature fluctuation associated with turbulence passes through the pressure discontinuities associated with the

stationary shocks. (This discussion excludes "jet screech", which is a very singular and distinct type of noise resulting from a severe instability.)

Figure 7 shows the radiation efficiency of the various noise sources illustrated in Fig. 6, plotted against jet Mach number. The radiation efficiency is proportional to the first power of the Mach number for fluctuating mass flow noise, to the third power for lip noise, to the fifth power for subsonic mixing noise, and independent of Mach number for Mach wave radiation.

Mach wave radiation is the dominant source of noise for large rockets where the exhaust is highly supersonic and very hot. The shock-turbulence noise source has been studied very little and its radiation efficiency is not known.

It should be noted that implicit in Fig. 7 is the well-known dependence of the acoustic power of monopole (fluctuating mass flow), dipole (flow/rigid body interaction), and quadropole (turbulent mixing) sources upon the fourth, sixth and eighth power, respectively, of the flow speed V. Since the Mach number contains a V-term, multiplication of this number by V^3 from the jet kinetic energy term $[1/2\rho V^3 A]$ yields the stated dependences.

As evident from Fig. 7, subsonic mixing noise (for a supersonic exhaust jet) is the dominant noise source for exhaust Mach numbers of 1 to 3, in which range the sound producing turbulent eddies are still convected at subsonic speeds. Above a Mach number of 3, these eddies are convected at supersonic speeds, and the Mach wave radiation becomes the dominant noise source.

The efficiencies (ratio of acoustic to mechanical jet power) shown in Fig. 7, have been substantiated experimentally. For large rocket engines it has been found that up to 1% of the jet's kinetic energy is radiated as sound.

The above discussion illustrates the complexity of supersonic jet noise generation and radiation. For this reason, attempts at predicting supersonic jet noise on a purely theoretical basis have not been very fruitful, and corresponding empirical or semi-empirical prediction schemes have been developed.

C. Empirical Prediction Schemes

Farfield Noise

We consider here only the noise from large supersonic rocket exhausts. Empirical prediction schemes are based on data from measurements taken over the last 15 years.

It has been found that for modern large-scale rocket-exhaust flows a fraction of the kinetic energy is converted and radiated as acoustic energy. The ratio of the acoustic to kinetic energy – i.e., the *acoustic efficiency* – depends basically on the exhaust speed, as qualitatively indicated in Fig. 7. Modern large boosters convert up to 1% of their mechanical energy into acoustic energy.

To determine the overall sound power radiated from a rocket exhaust flow, one simply calculates its kinetic energy W_m

$$W_m = 0.676\ T\ V \quad , \tag{1}$$

where W_m = kinetic energy (watt), T = thrust (lb), and V = exhaust velocity (ft/sec). Then, one assumes an acoustic efficiency η, which for large boosters — such as those contemplated for the shuttle — is between 0.5 and 1%.

Hence, the overall acoustic power W_a is calculated

$$W_a = \eta W_m \quad . \tag{2}$$

The acoustic power level L_W is defined as

$$L_W \equiv 10 \log \frac{W_a}{10^{-12}} \tag{3}$$

with W_a in watts.

The spectral distribution of acoustic power can be presented in nondimensional form by plotting the power in each octave band, referenced to the overall power level, as a function of a nondimensional Strouhal frequency

$$S = f\ D/V \tag{4}$$

where f = octave band center frequency, Hz, D = nozzle exit diameter (ft), and V = exit velocity (ft/sec). A nondimensional power spectra is shown in Fig. 8.

The sound power spectrum is converted into a sound pressure spectrum at a distance R by assuming spherical spreading of acoustic energy. If both observer (at distance R) and sound source are located on the ground, then radiation occurs into a half sphere, with an area

$$A = 2\pi R^2 \quad .$$

If the source is at altitude h, then radiation occurs into a spherical space, with a cut-off segment; its area is given by

$$A = 2\pi R(R+h) ,$$

as illustrated in Fig. 9. The sound pressure level (SPL) spectrum relates to the sound power level (PWL) spectrum as

$$SPL\ (f) = PWL\ (f) - 10 \log A + 10.5 \qquad (5)$$

where SPL (f) = octave band sound pressure level at center frequency f, dB, PWL (f) = octave band sound power level at center frequency f, dB, and A = area (ft^2), as defined above.

As evident from Eq. 5, sound pressure decreases as $1/R_h^2$ — i.e., with 6 dB per doubling of distance. However there is additional attenuation due to atmospheric absorption. This attenuation is frequency dependent, and can be obtained from Table I.

TABLE I. EXCESS ATTENUATION DUE TO ATMOSPHERIC ABSORPTION IN dB PER 1000 FT DISTANCE

Frequency, Hz	Attenuation, dB/1000 ft
1	0.02
5	0.05
10	0.08
50	0.15
100	0.3
500	0.8
1000	1.0

Jet and rocket exhaust flow noise is highly directive. In general, most of the energy will be concentrated in the space between 50° and 70° from the exhaust flow centerline.

The effect of directivity can be expressed in nondimensional form as a "directivity index" vs the angle to the exhaust flow direction (Fig. 10). Each frequency, normalized with the ratio of exhaust diameter and flow speed, has its own directivity curve. The directivity index, in dB, is then added to the space-averaged value of the sound pressure level at the given location. It should be noted that the angle α under which the observer sees the source is complementary to the angle θ (used in Fig. 9), the directivity angle of interest with respect to the exhaust flow.

The frequency of the acoustic signal for a distant observer differs from the original frequency due to the Doppler effect. Simple geometric considerations show that the frequency at the observer f_p must be corrected with the forward speed of the vehicle U, and the angle θ between the exhaust flow direction and the observer; thus,

$$f_U = f_0 \left(\frac{c}{c + U \cos\theta} \right) .$$

Nearfield Noise

The most practical general method for predicting the noise field near rockets is the source location method, summarized in Ref. 1 for straight exhaust flows, and applied to deflected flows in Ref. 2. This method considers that the source of rocket exhaust noise in a given frequency band is confined to

a limited region of the exhaust stream, and assigns positions and strengths to the sources in terms of their dimensionless Strouhal frequency on the basis of empirical data.

References 2 and 3 present plots of the ratio x/D versus fD/V where x is the distance of the noise source aft of the exit plane (along the flow axis), D is the effective nozzle exit diameter,* f is the center frequency of the band of interest, and V is the exit velocity of the flow. Such plots may be used to predict the source locations.

Similarly, one may obtain estimates of the strengths of these sources from plots of the dimensionless spectrum function $GV/\rho cW_m D$ versus fD/V, such as appear in Ref. 3 and (in somewhat different form) in Refs. 2 and 4. Here, G(f) is the spectrum function (which is proportional to the acoustic power radiated by the source per unit bandwidth), ρ is the density of the ambient air, c is the velocity of sound in that air, and W_m is the mechanical power of the exhaust flow (which one may readily determine from the thrust and mass flow rate, or from related information).

Once one has determined the source locations and strengths, one may readily estimate the acoustic pressures at any given point by taking account of the appropriate geometry and assuming that the mean-square sound pressure varies inversely as the square of the distance from the source.

---

*For single nozzles, the effective diameter is equal to the actual diameter. For multiple nozzles, the effective diameter is that of a single nozzle that would pass the total flows.

The dimensionless source-location and spectrum function plots given in Refs. 2-4 are based on rather old data, which were obtained from rockets that are small by current launch vehicle standards. Fortunately, MSFC has recently undertaken an analysis of all available Saturn V data, and has developed corresponding source-location and spectrum functions. Test calculations have shown that use of these new functions permits one to calculate sound pressures that agree rather well with corresponding experimental data. These new functions [1], extrapolated toward lower Strouhal frequencies in accordance with trends illustrated in Refs. 2-4, are used for the present predictions.

III. THIOKOL ENGINE NOISE PREDICTION

A. Shuttle Configurations

For the series burn and the parallel burn configurations shown in Figs. 1 and 2, the following predictions will be restricted to the 156-in. diameter engines.

In predicting noise from a narrowly spaced cluster of engines, one must consider the clustered engines as one engine, with an effective nozzle diameter

$$D_{eff} = \sqrt{n} \cdot D_i \quad ,$$

where n is the number of (closely spaced) engines and D_i the nozzle diameter of each engine.

Thus, in the *parallel burn* situation, we have treated the four orbiter engines as one engine of twice the diameter of the individual engines, while the booster engines – being separated by about 50 ft – were considered as radiating independently. In the *series burn* situation, the three booster engines were treated as one of 1.7 times the diameter of the individual engines. These assumptions are considered valid for farfield noise predictions where the sound from all engines "merge".

B. Engine Parameters

The following parameters were used for the calculations:

	Booster	Orbiter
Nozzle Exit Diameter (ft)	12.4	6.42
Weight Flow (lb/sec)	8889	1154
Exhaust Speed (ft/sec)	8000	9500
Thrust (lb)	2.2×10^6	0.2×10^6

C. Farfield Noise

Series Burn

The mechanical power of 3 clustered booster engines is

$$W_m = 35.7 \times 10^9 \text{ watt} \quad .$$

For an assumed acoustic efficiency of

$$\eta = 0.6\% \quad ,$$

the overall acoustic power is

$$W_{ac} = 215 \times 10^6 \text{ watt} \quad .$$

However, since 1/3 of the exhaust flow has condensed by the time it leaves the nozzle, one can assume that only 2/3 of the exhaust flow is actually participating in the noise fluctuation process. Hence, the acoustic power must be reduced by 1/3, yielding

$$W_{ac} = 143 \times 10^6 \text{ watt}$$

or, in terms of sound power level

$$L_W = 201.5 \text{ dB re } 10^{-12} \text{ watt} \quad .$$

The octave band sound power level spectrum is shown in Fig. 11.

An effective diameter of 21.5 ft was used for the cluster of three engines. For purposes of comparison, the spectrum from a single engine is also shown in Fig. 11. Figure 12 presents the sound pressure level spectra for the following conditions.

	Observer distance at ground level (miles)	Shuttle Flight Altitude (feet)
1	1	100 to 1000
2	5	100 to 1000
3	1	10,000
4	5	10,000

Source directivity and atmospheric absorption were accounted for. A frequency shift due to the Doppler effect is negligible for flight altitudes up to 1000 ft. At 10,000 ft altitude (vehicle speed about 500 ft/sec), frequencies change for a ground-located observer by a factor of 0.73 at a 1-mile ground level distance and by 0.88 at a 5-mile ground level distance.

Parallel Burn

Following steps similar to those described above gives the sound power level spectra for the two separated booster engines, and the four clustered orbiter engines shown in Fig. 13. Sound pressure level spectra are shown – again for four different distances – in Fig. 14.

Shuttle Configuration on Launch Pad at Ignition

Two additional effects must be considered for the shuttle on the launch pad. First, the exhaust flow impinges on either a flame splitter or an exhaust deflector. In the former case, the exhaust flow is divided evenly into two portions, streaming horizontally in two opposite directions. In the latter case, the entire flow is deflected in one horizontal direction. The

launch configuration for the shuttle employs a flame deflector, resulting in a nonrotationally symmetrical directivity pattern in the ground plane.

Second, in addition to the attenuation caused by spreading, there is "excess attenuation" over the ground. A ground-located observer at some distance will thus be exposed to levels that are substantially reduced by ground absorption. However, as always, wind and temperature gradients affect the propagation characteristics, and it is next to impossible to predict, with any accuracy, acoustic levels in a ground-to-ground situation over large distances.

Using Fig. 15, we will attempt to predict the sound pressure level spectra at one- and five-mile radii for the launch configuration at ignition – i.e., at zero altitude. Figure 15 provides the excess attenuation over and above the spreading attenuation. From this figure, we read for frequencies below 400 Hz, typical excess attenuations of 12 dB for a one-mile radius and 8 dB for a five-mile radius.

It has been found that, in comparison to undeflected exhaust flow, sound pressure levels are about 7 dB higher at locations facing the deflected exhaust stream and about 7 dB lower at locations away from the deflected exhaust stream.

Hence, we take the sound pressure level spectrum that would exist at one- and five-mile radii for the shuttle several hundred feet above the ground, there is (a) no exhaust deflection and (b) no excess ground attenuation, and apply the following corrections.

	Correction, dB	
Distance from Launch Pad	1 mile	5 miles
Facing Deflected Exhaust Flow	-12 + 7 = -5	-8 + 7 = -1
Away from Deflected Exhaust Flow	-12 - 7 = -19	-8 - 7 = -15

Figures 16 and 17 show the sound level spectra, for the shuttle on the launch pad at the instant of ignition, for ground distances of 1 and 5 miles, facing and away from the deflected stream. It should be re-emphasized that this data is valid only for the shuttle on the launch pad. As soon as the shuttle clears the tower, the effect of exhaust deflection and ground attenuation disappears, and levels, as observed from a distance, will quite suddenly increase to those presented in Figs. 12 and 14.

There is an indication that exhaust deflectors decrease the total acoustic power of a rocket exhaust flow by about 5 dB at the spectral peak and by as much as 10 dB one decade below the spectral peak. Due to the uncertainty of the actual deflector configuration, the levels in Figs. 16 and 17 were not adjusted for this effect.

The accuracy of the farfield noise data for the shuttle on the launch pad is estimated to be no better that $\pm$ 10 to 15 dB, due to the many unknowns that affect near-ground propagation.

D. Nearfield Noise

Figures 18 and 19 show the results of nearfield prediction calculations for the series and parallel-burn modes, respectively. For both of these cases, the booster nozzle exit plane was assumed to be 87 ft above a flame splitter (wedge-shaped flame deflector), approximating the Saturn V launch configuration at NASA/KSC Launch Complex 39. For each of the two modes, calculations were carried out for two locations on the orbiter — at the crew compartment location (near the orbiter's nose) and at the cargo compartment location (near the midpoint of the orbiter's upper surface). For each of the two modes, two flight conditions were considered: The full-thrust condition just prior to lift-off, where the exhaust impinges on the flame splitter, and a condition where the vehicle has risen high enough above the launch pad so that the exhaust essentially extends straight out behind the vehicle.

For the series burn mode, in which only the solid-propellant engines fire, the flame splitter was assumed to split the exhaust into two oppositely directed horizontal streams of equal size. For the parallel burn mode, the flame splitter was assumed to direct the orbiter engine exhaust in one direction (horizontally, in the direction of the orbiter fin) and the solid-propellant motor exhaust in the other.

As evident from Figs. 18 and 19, the acoustic environments of the cargo and crew compartments are similar, because their distances from the noise sources do not differ by significant factors. Only at the highest frequencies, for which the noise sources are located very near the nozzle exit planes, is there any noticeable effect.

Similarly, the differences between the "on pad" and the "after lift-off" conditions are insignificant. The greatest differences here occur around the middle of the range indicated in the figure. The lowest frequency sources are so far away from the exit plane that the turning of the exhaust stream barely affects their distances from the observation points on the vehicle surface. The highest frequency sources, on the other hand, are so near the exit plane that they are still in the undeflected exhaust stream; thus, the location of these sources, with respect to the vehicle, does not change as the vehicle lifts off.

Changes in the effective frequencies and sound propagation distances occur as the vehicle gains speed. However, for vehicle Mach numbers that do not exceed 0.2, these changes are negligible.

REFERENCES

1. Personal communication from W. Gruner, Teledyne Brown Engineering, Huntsville, Alabama, Jan. 1972.

2. P.A. Franken, *et al.*, "Methods of Space Vehicle Noise Prediction". WADC Technical Report 58-343, Vol. II, Sept. 1960.

3. J. Dyer, "Estimation of Sound-Induced Missile Vibration", Chap. 9 of *Random Vibration*, Ed. by S.H. Crandall, Technology Press of MIT, Cambridge, 1958.

4. L.C. Sutherland, *et al.*, "Sonic and Vibration Environments for Ground Facilities – A Design Manual". Prepared for NASA-MSFC under NAS8-11217. (March 1968).

APPENDIX A – EFFECT OF SOME GEOMETRIC AND GAS DYNAMIC PARAMETERS ON ROCKET NOISE GENERATION AND RADIATION

In relating a sound power to a mechanical power (of the exhaust stream), one avoids the need to consider individual gas dynamic and geometric parameters of the rocket engine, although these undoubtedly affect the exhaust flow. In the following, we will briefly discuss the effect of pressure ratio and temperature on jet noise.

1. Nozzle geometry and pressure ratios – A nozzle is designed to operate optimally at a particular pressure ratio. In this case a certain exhaust Mach number will occur, which (together with the weight flow) determines the thrust of the rocket motor. The thrust together with the exhaust speed determines the kinetic energy, a fraction of which is radiated as acoustic energy.

If the nozzle geometry (i.e., the ratio of the thrust to the exit area) is not correct for a given pressure ratio, or equivalently, if a nozzle is operated at a nondesign pressure ratio the jet will either under or over-expand whereby shock waves occur, which in conjunction with turbulence generate sound. Shock waves by themselves, which are quasi-stationary, would not generate noise. It should be noted that a (slight) off-design operation of rocket-engine nozzles is the rule, rather than the exception, since the ambient pressure for an ascending rocket changes continually.

2. Exhaust temperature – The empirical prediction scheme advanced in the bulk of this report was based on data from existing large boosters. Exhaust temperatures of such boosters are always of the same order, and, within the possible accuracy

of noise prediction it is unnecessary to consider temperature effects for this class of boosters.

Model tests on subsonic and supersonic jets, conducted by GE several years ago, indicate that for constant thrust and velocity the total acoustic power emitted from the jet being independent for temperatures between 450°R and 3000°R.

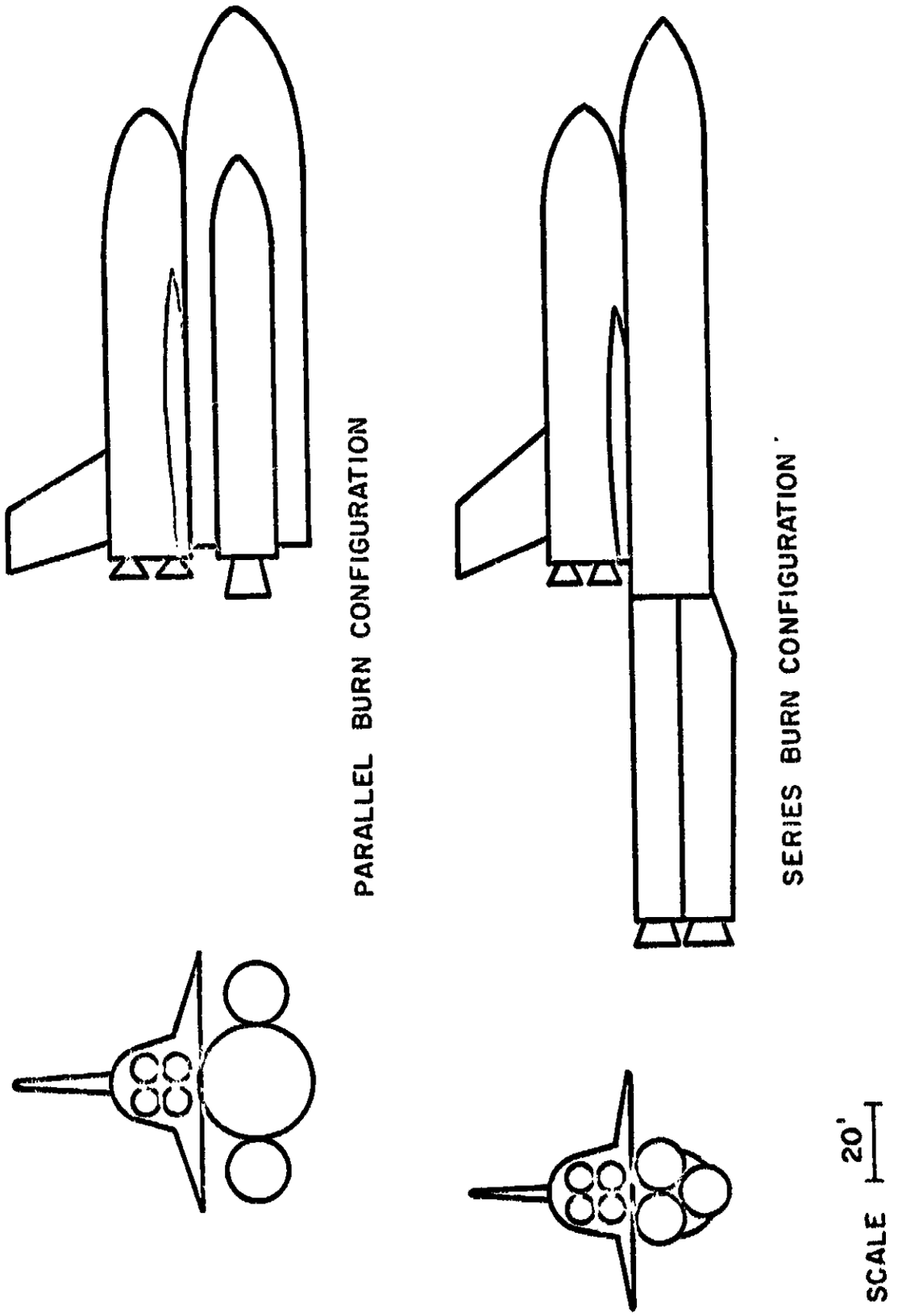

FIG. 1&2 SPACE SHUTTLE CONFIGURATIONS

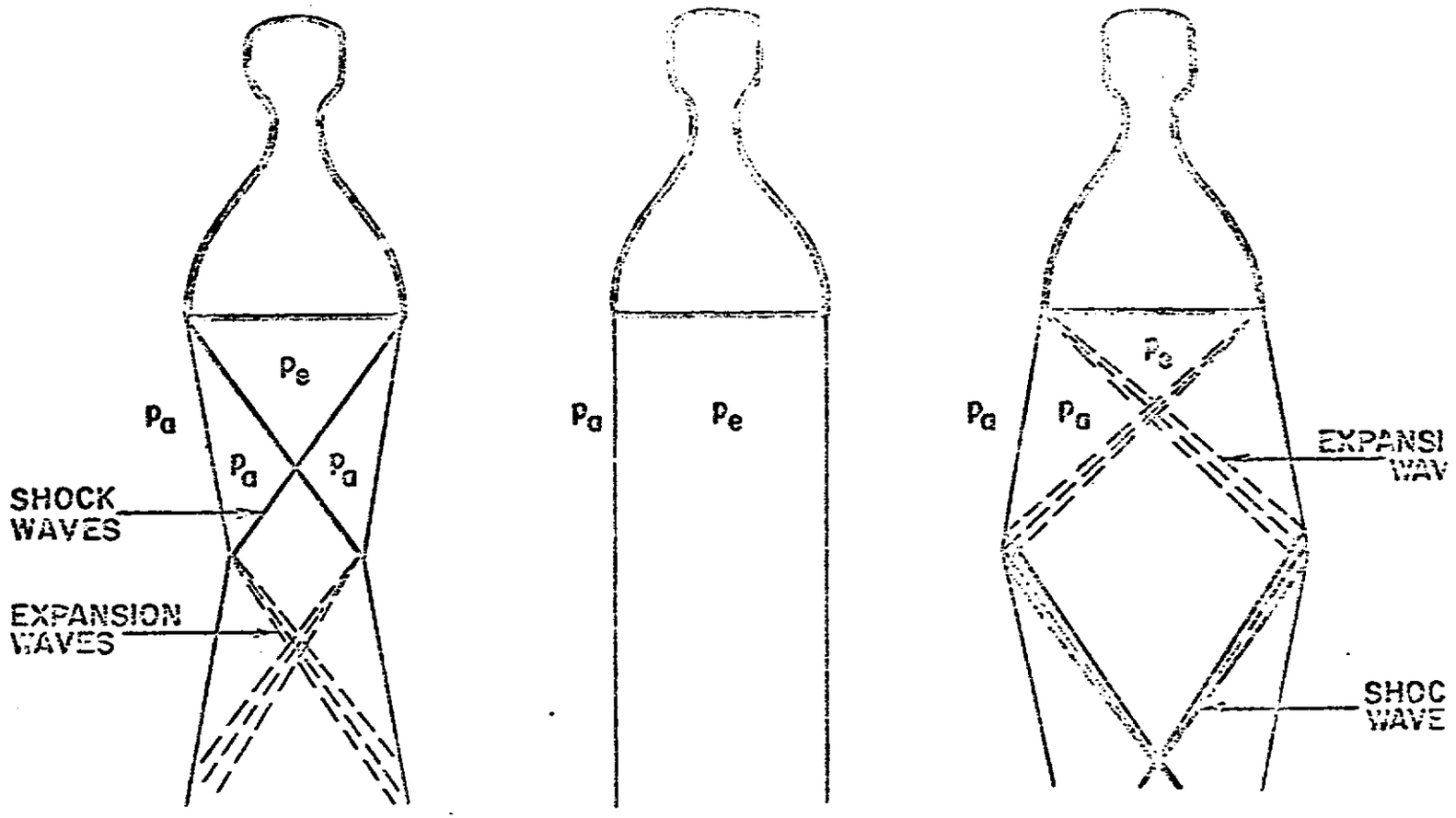

a) over expanded nozzle-lift-off condition $p_a > p_e$

b) design condition-low altitude $p_a = p_e$

c) under expanded nozzle-higher altitude $p_a < p_e$

FIG. 3. SIMPLIFIED ILLUSTRATION JET EXHAUST FLOW PATTERNS CORRESPONDING TO SEVERAL STAGES OF FLIGHT AND AMBIENT PRESSURES

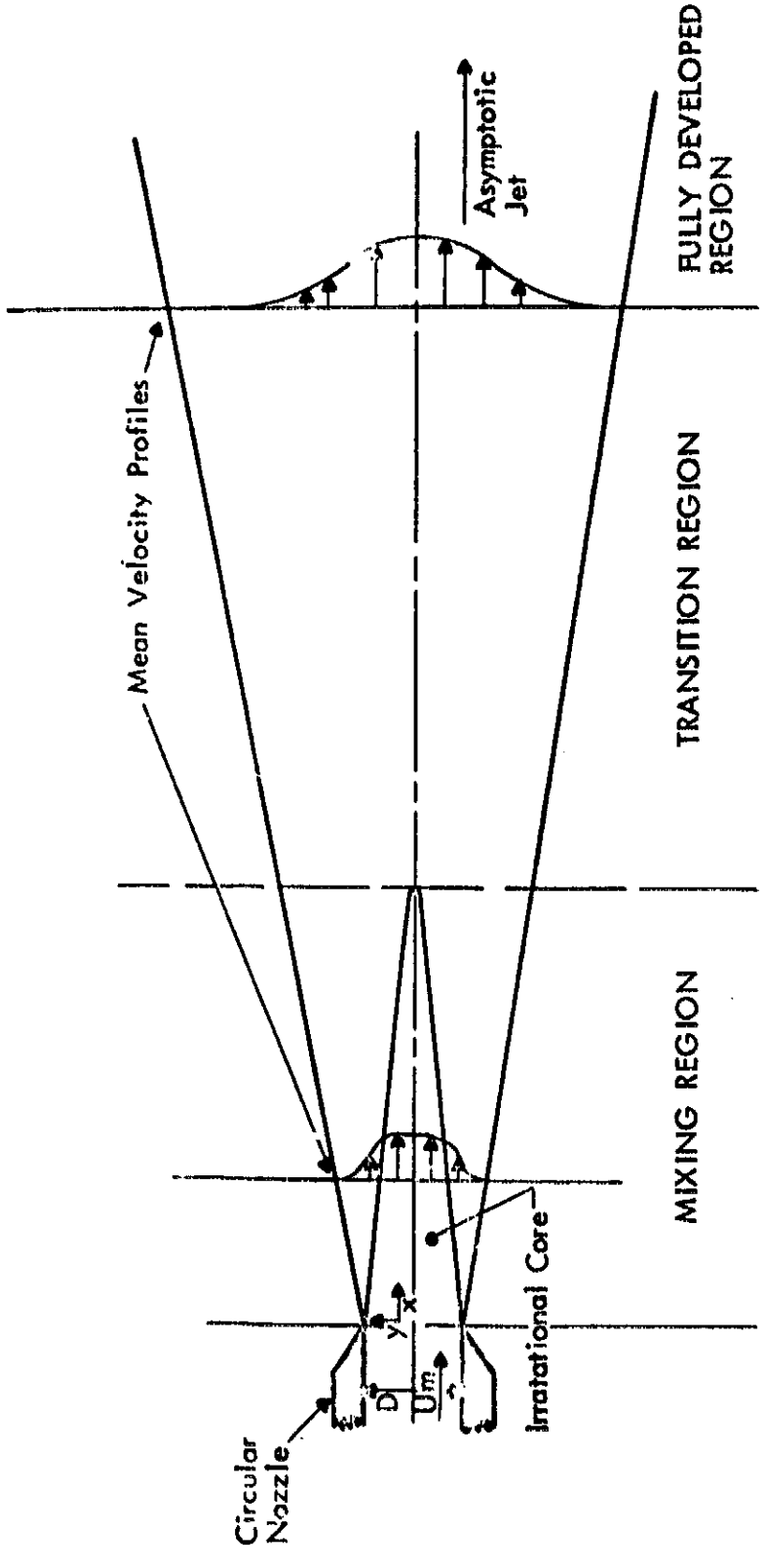

FIGURE 4. IDEALIZED MODEL OF A SUBSONIC JET ENGINE

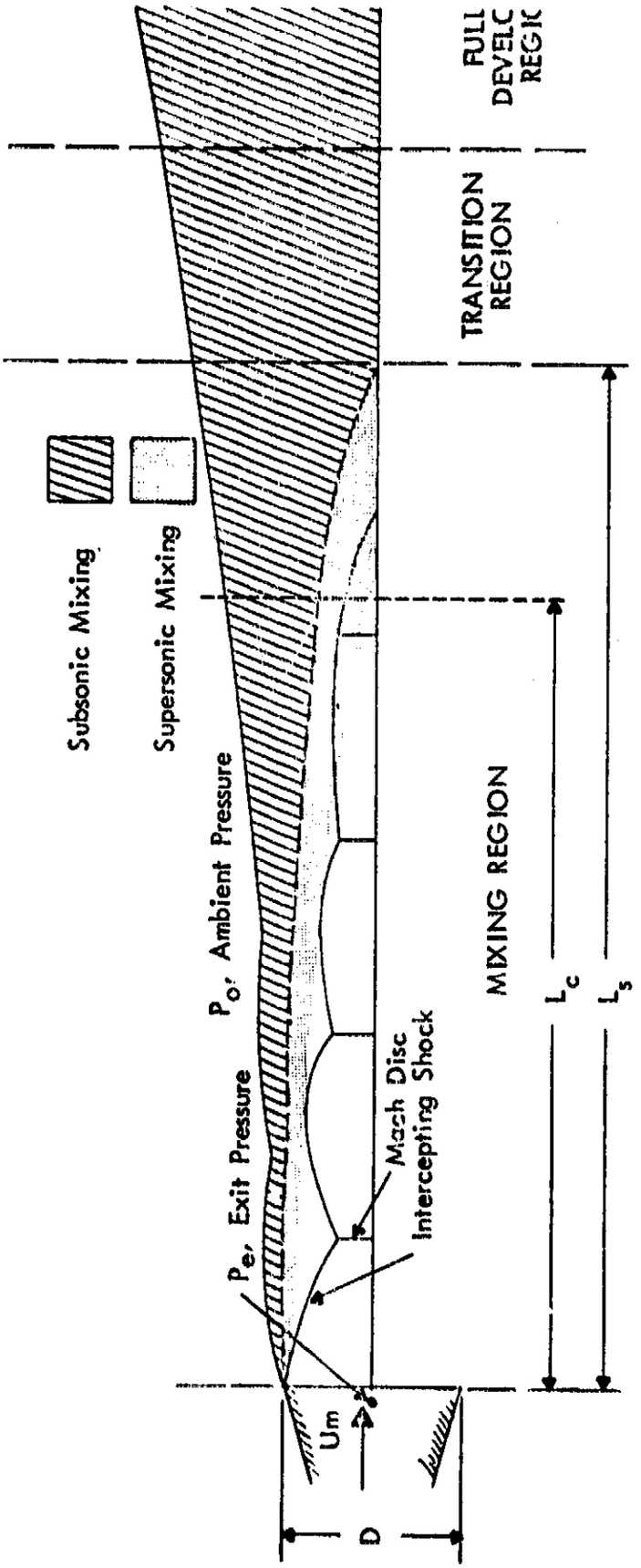

FIGURE 5. SCHEMATIC OF SUPERSONIC JET EXHAUST

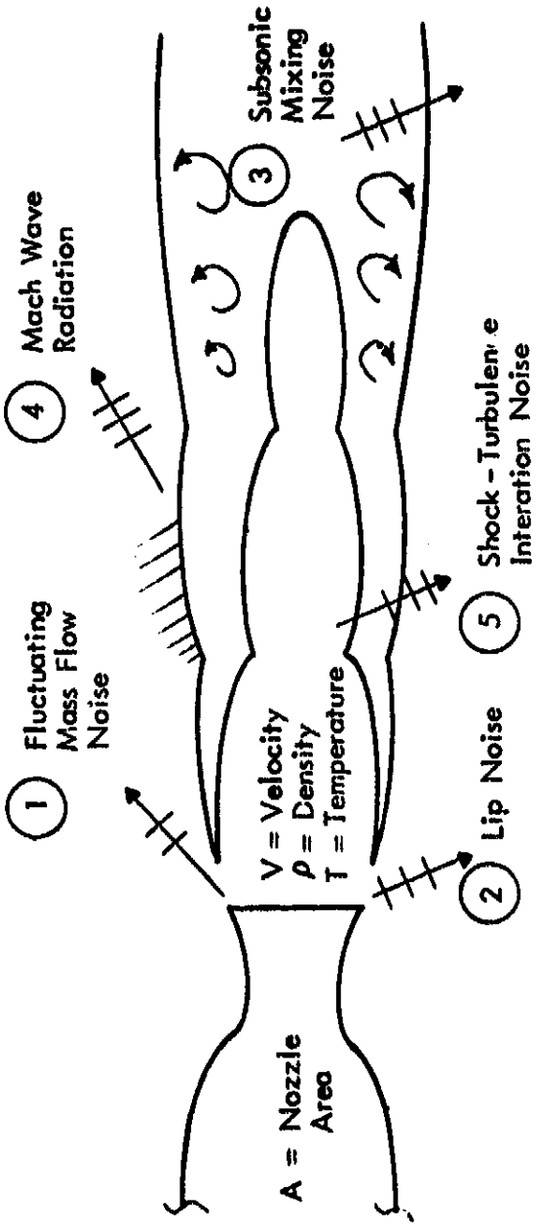

FIGURE 6.
SUPERSONIC JET EXHAUST NOISE SOURCES

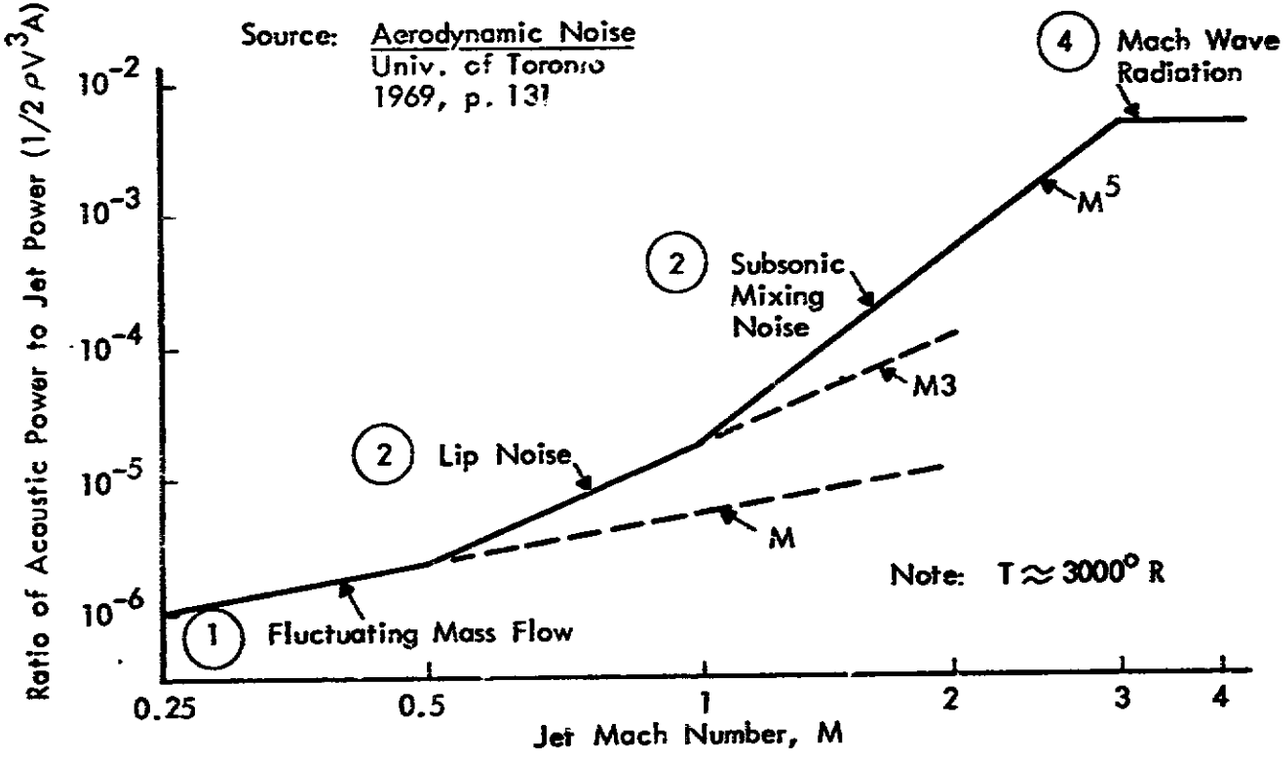

FIGURE 7.
RADIATION EFFICIENCY OF NOISE SOURCES IN THE JET EXHAUST

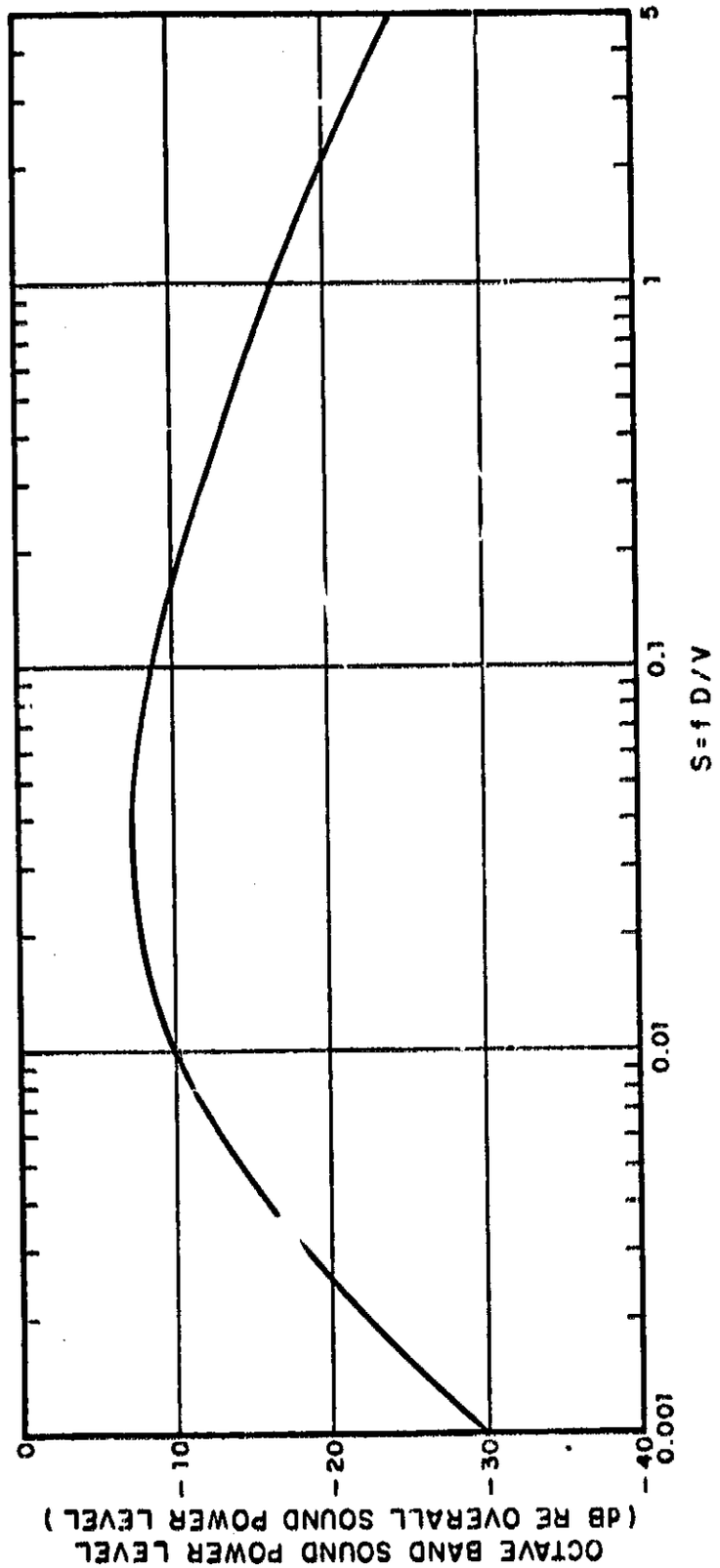

FIG. 8 NON-DIMENSIONAL ROCKET EXHAUST NOISE SPECTRUM.

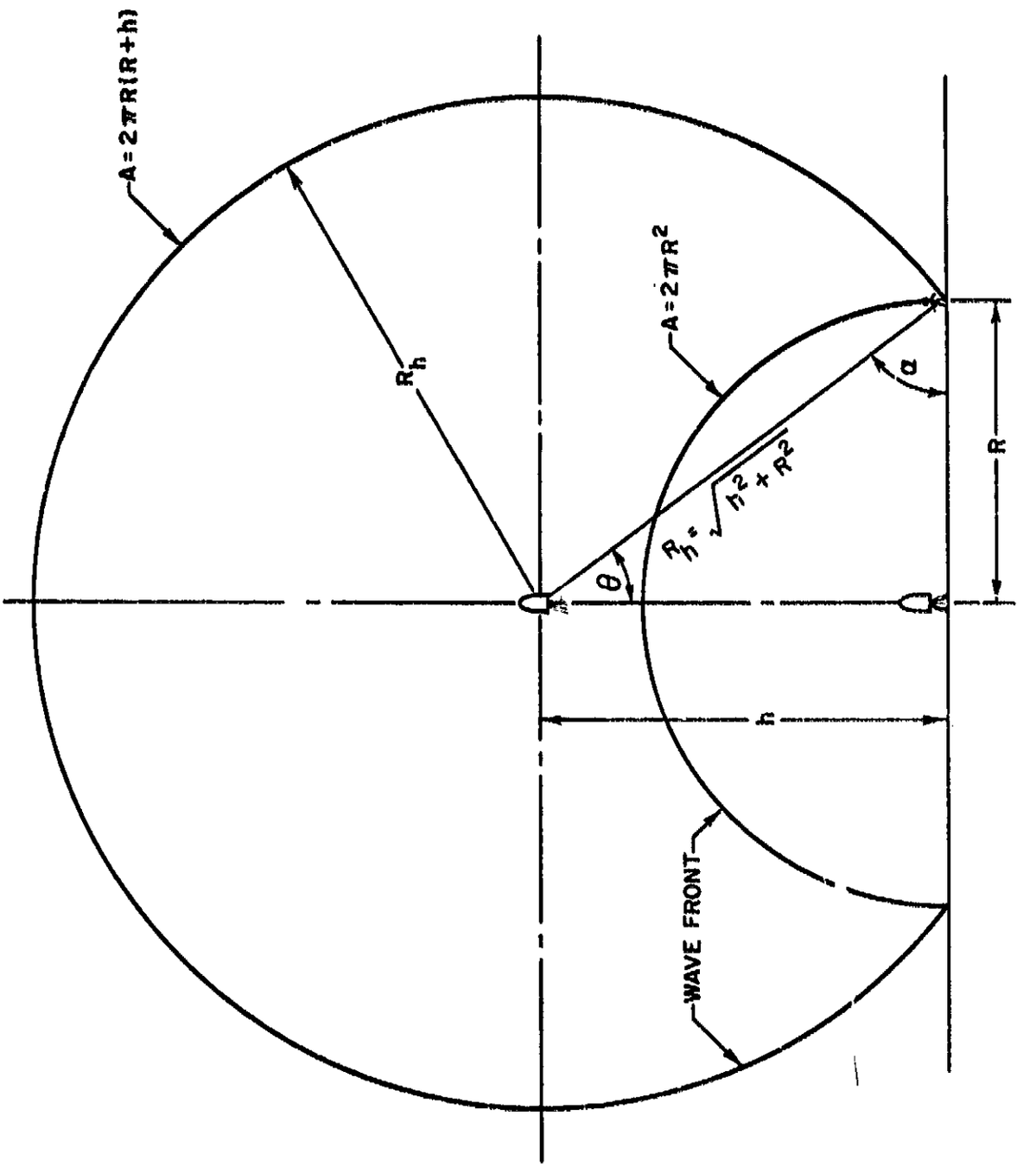

FIG. 9 ACOUSTIC RADIATION GEOMETRY FOR SHUTTLE ON LAUNCH PAD AND AT ALTITUDE.

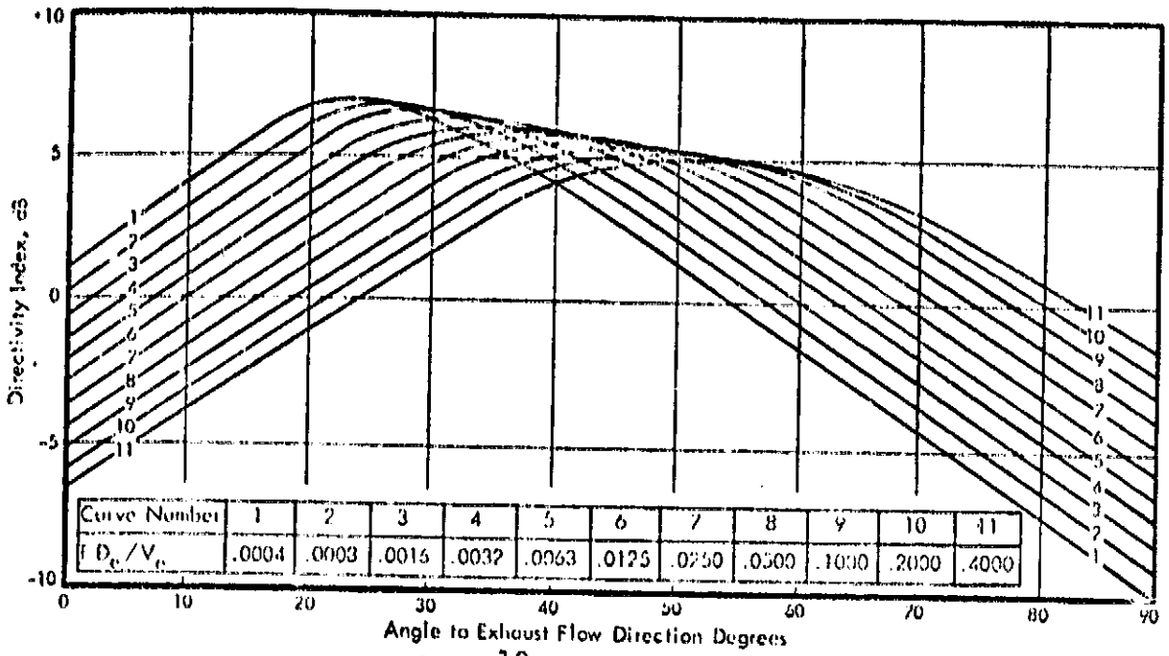

Curve Number	1	2	3	4	5	6	7	8	9	10	11
fD_e/V_e	.0004	.0003	.0016	.0032	.0063	.0125	.0250	.0500	.1000	.2000	.4000

FIGURE 10 Directivity Curves

FIG. 10 DIRECTIVITY CURVES (From Ref. 4)

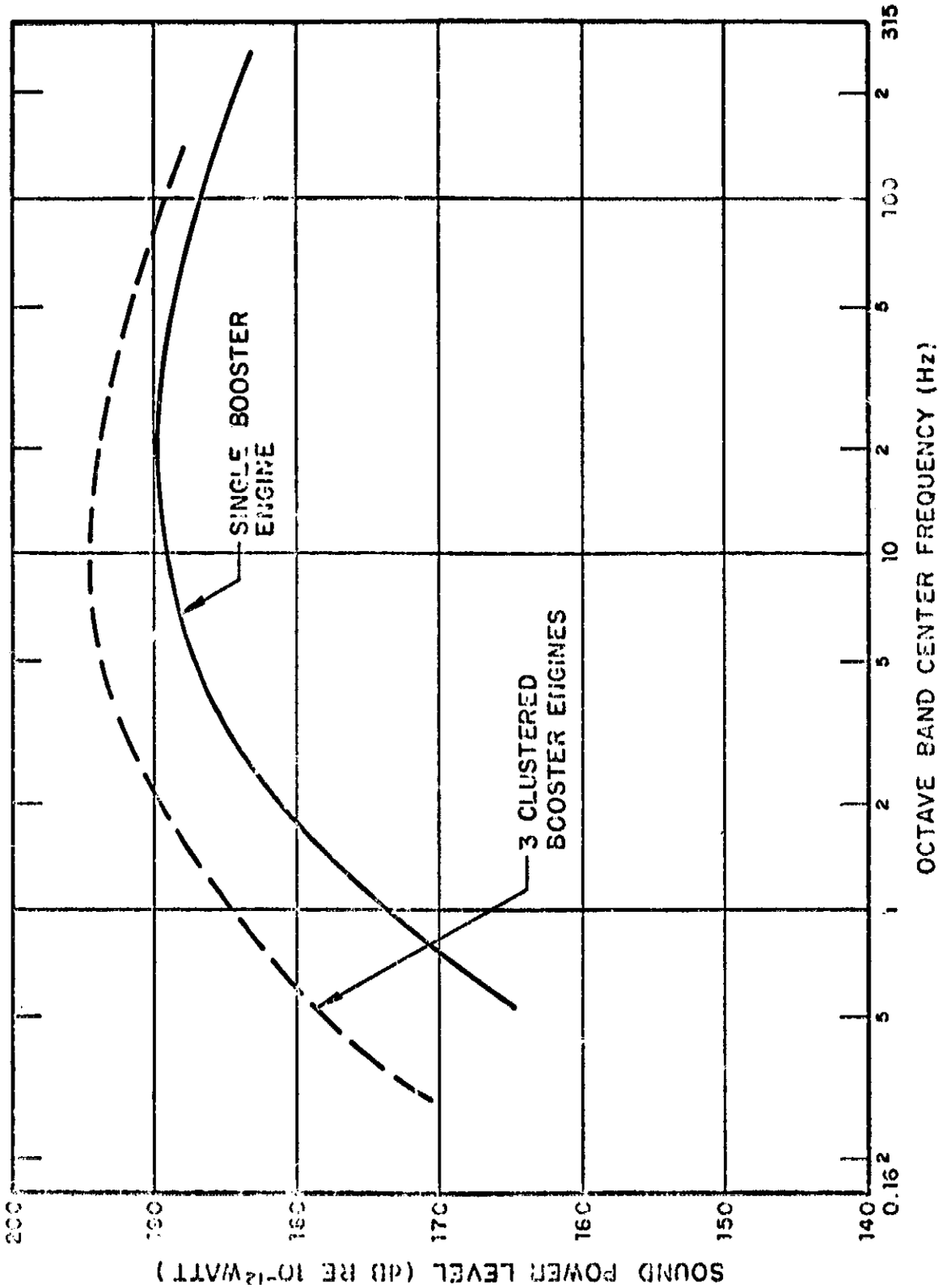

FIG. 11 OCTAVE BAND SOUND POWER LEVEL SPECTRA. SERIES BURN CONFIGURATION.

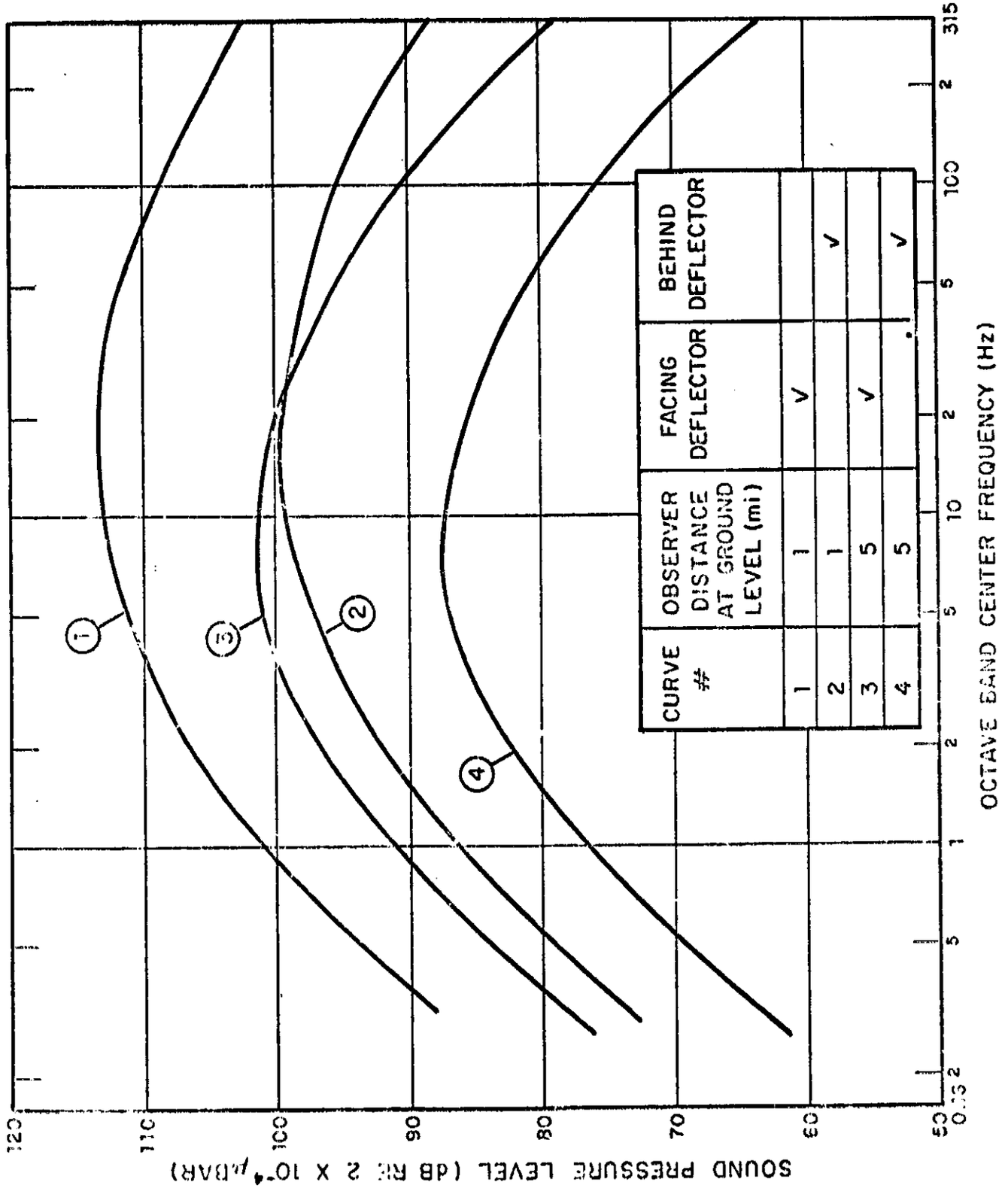

FIG. 12 OCTAVE BAND SOUND PRESSURE LEVEL SPECTRA.
SERIES BURN LAUNCH CONFIGURATION ON LAUNCH PAD.

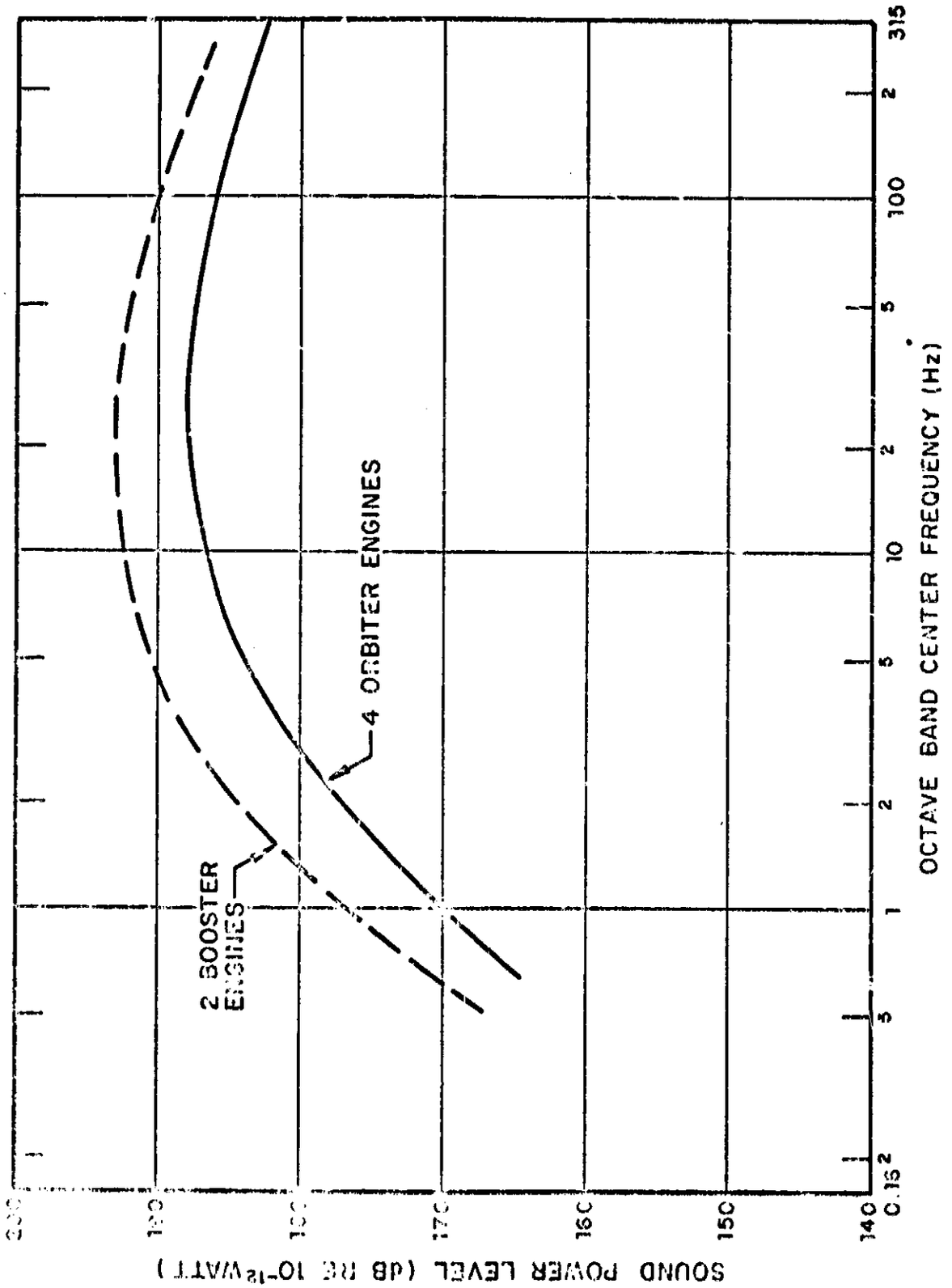

FIG. 13 OCTAVE BAND SOUND POWER LEVEL SPECTRA. PARALLEL BURN CONFIGURATION.

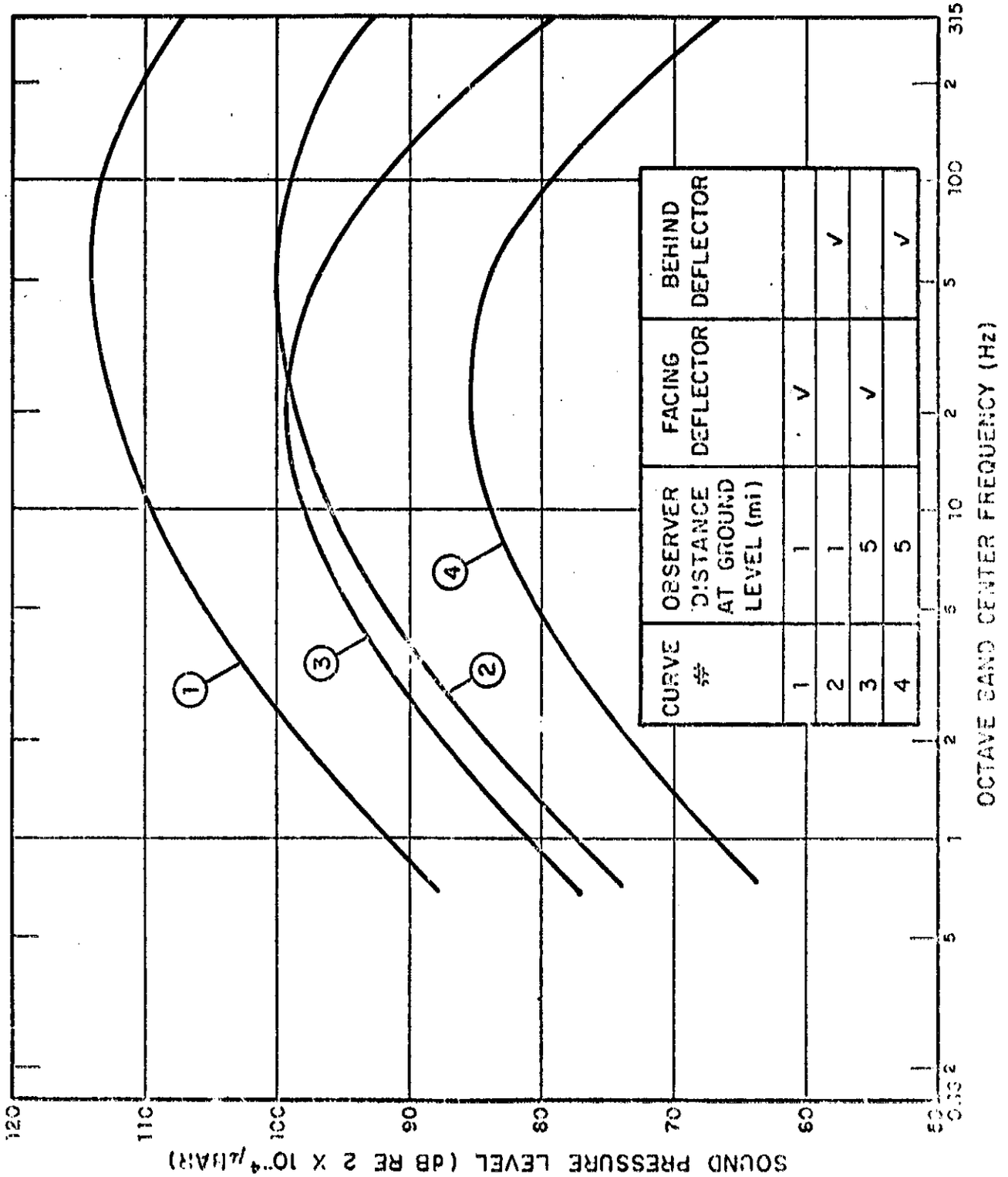

FIG. 14 OCTAVE BAND SOUND PRESSURE LEVEL SPECTRA. PARALLEL-BURN LAUNCH CONFIGURATION ON LAUNCH PAD.

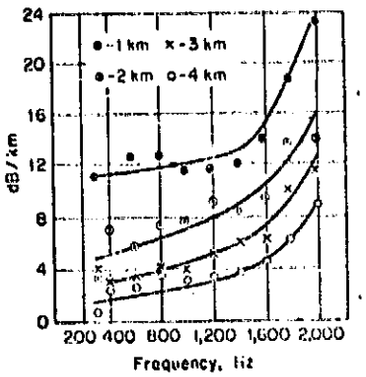

FIG.15 EXCESS ATTENUATION IN dB/km (dB/3280 ft) IN THE ABSENCE OF ACOUSTIC SHADOWING FOR FLOW PATH LENGTHS.

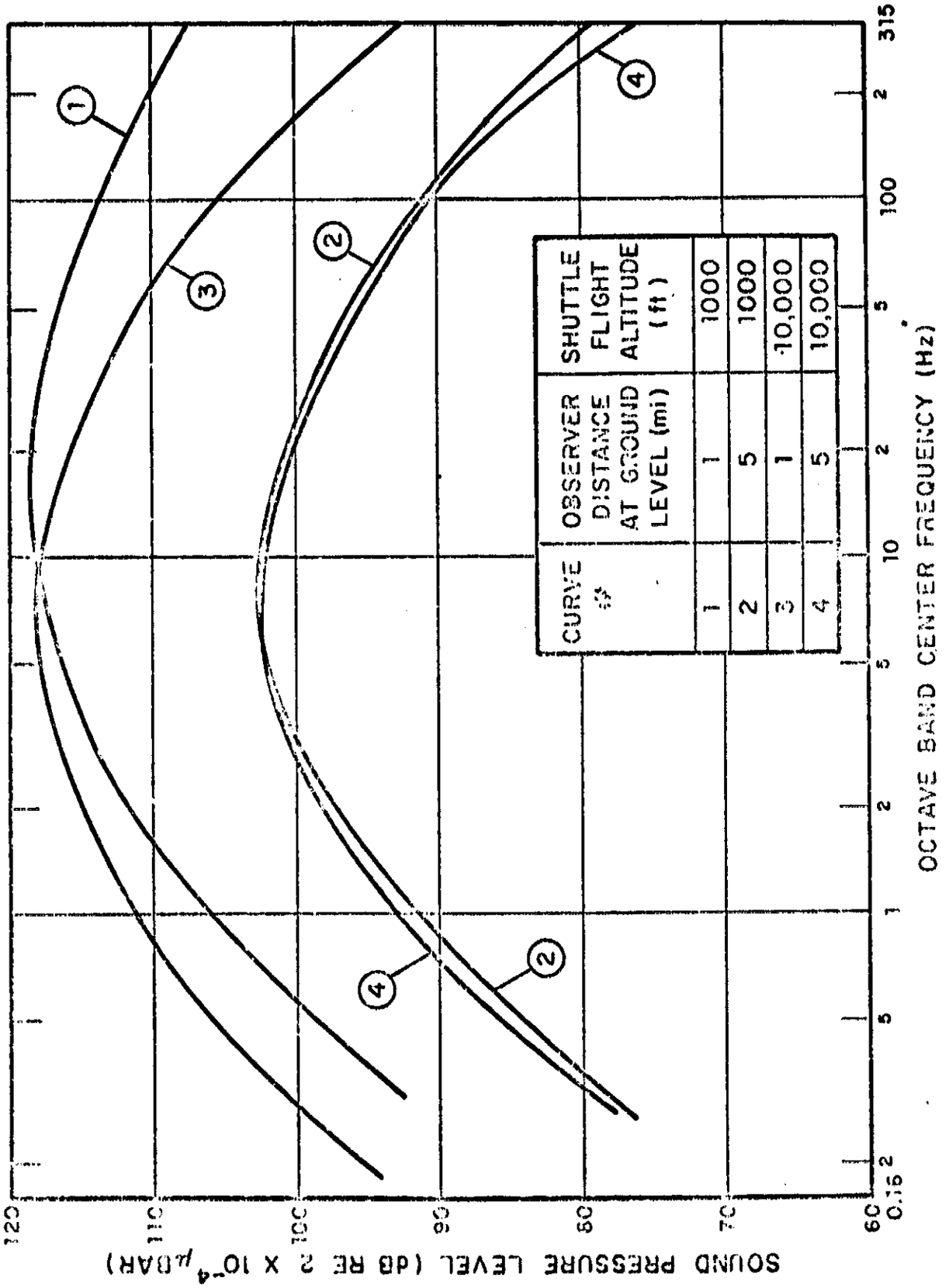

FIG. 16 OCTAVE BAND SOUND PRESSURE LEVEL SPECTRA. SERIES BURN CONFIGURATION.

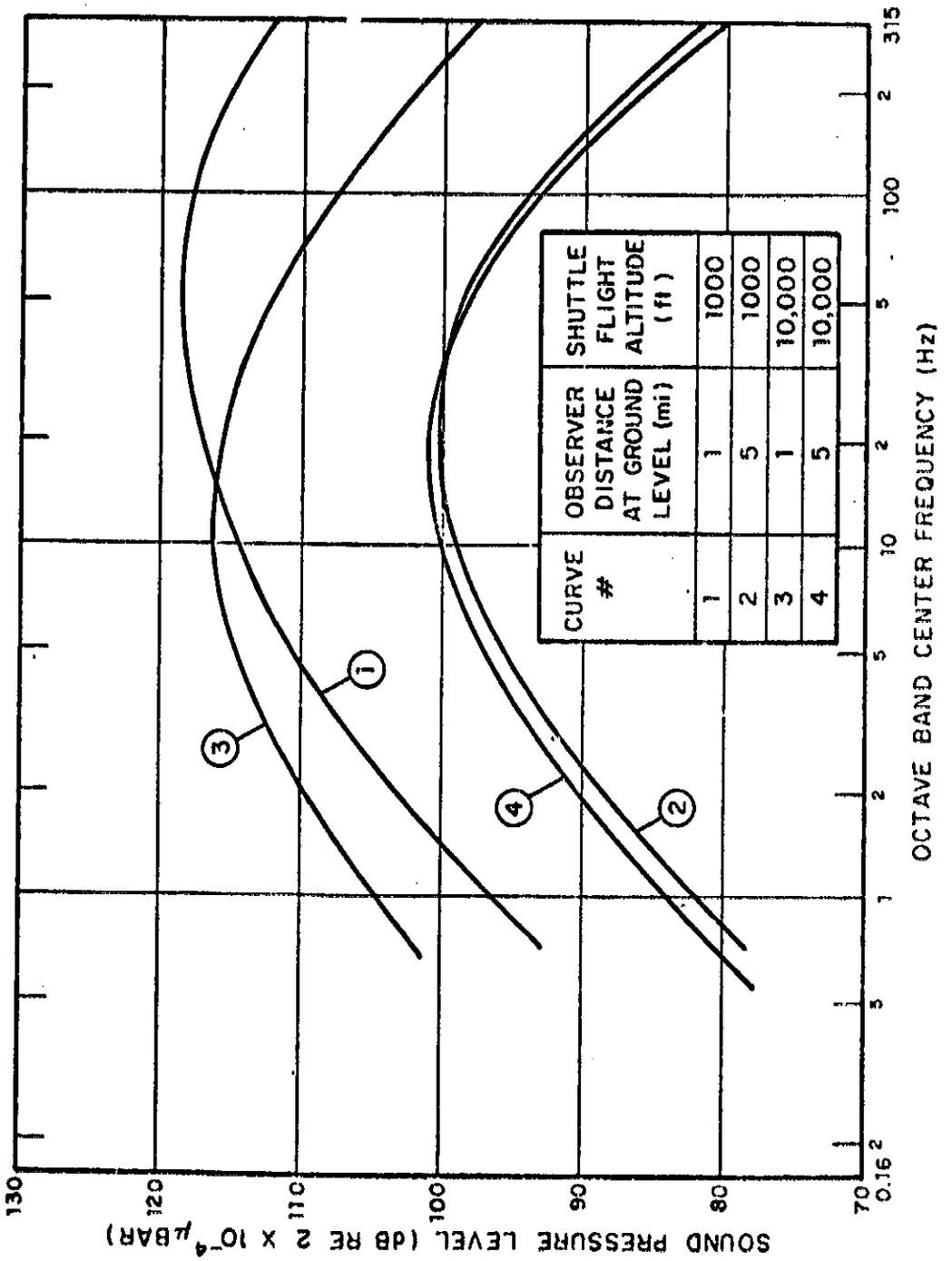

FIG. 17 OCTAVE BAND SOUND PRESSURE LEVEL SPECTRA. PARALLEL-BURN CONFIGURATION.

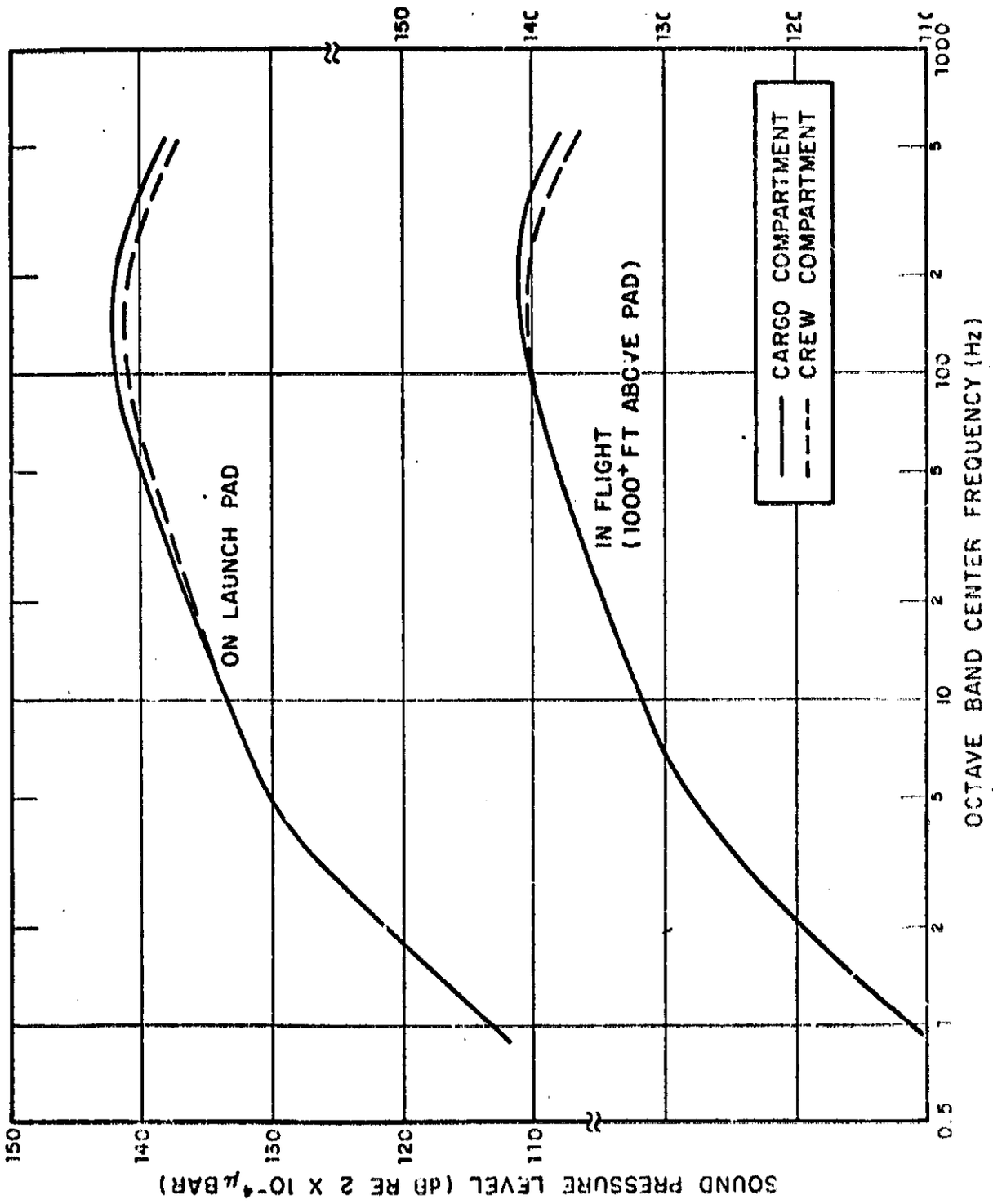

FIG. 18 SERIES BURN CONFIGURATION
EXTERNAL ACOUSTIC ENVIRONMENT

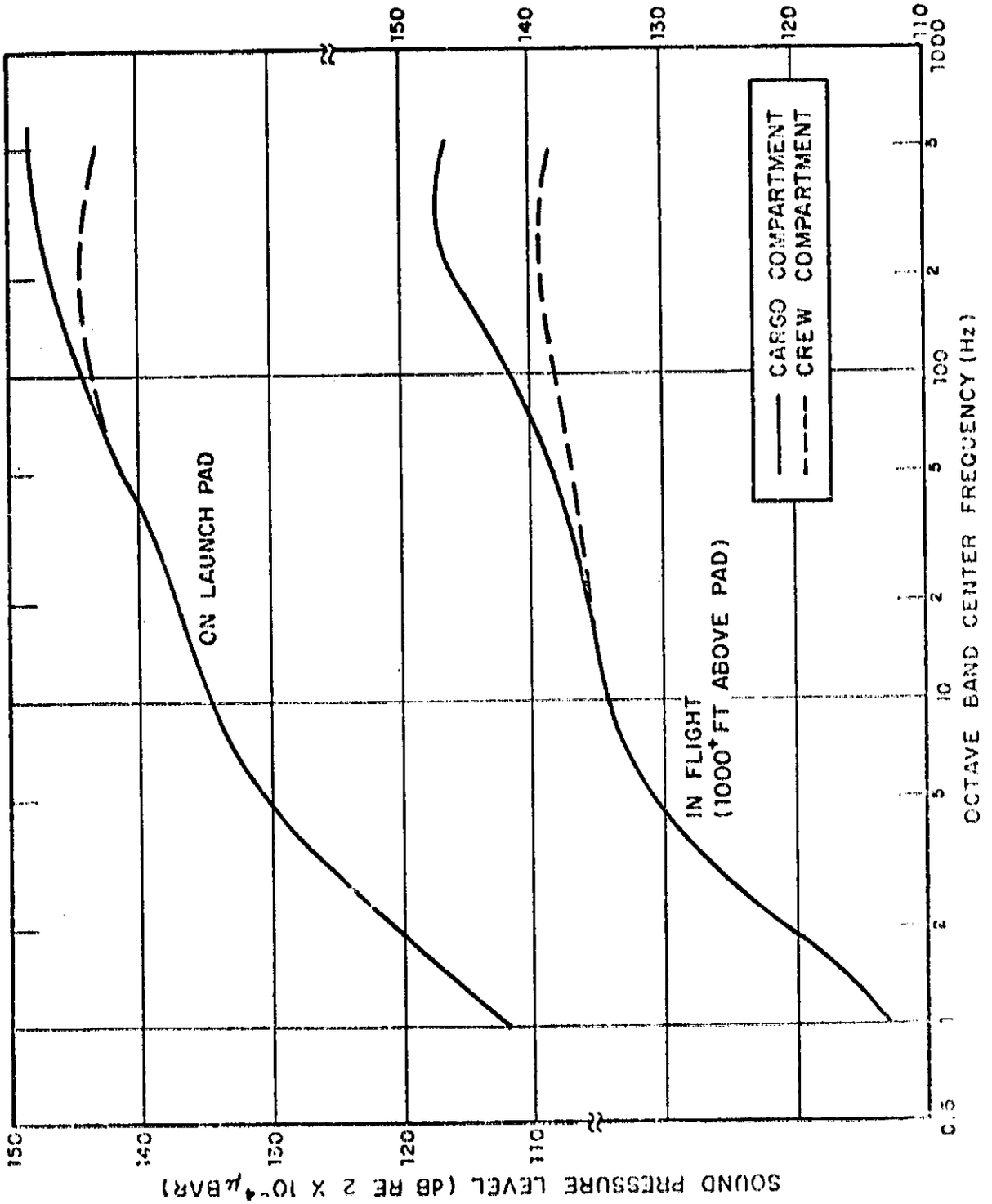

FIG. 19 PARALLEL-BURN CONFIGURATION
EXTERNAL ACOUSTIC ENVIRONMENT

APPENDIX H

SRM STAGE RECOVERY

APPENDIX II - SRM STAGE RECOVERY

This supporting technology plan is presented in three parts.

1. Free Flight Dynamics
2. Water Impact
3. Environmental and Cyclic Effects

These three elements of the total recovery sequence which includes staging, free flight, captive flight, water impact (entry-submergence-rebound-slap-flotation), recovery, and refurbishment are considered the most critical to the SRM Stage development program scheduling. The indicated programs are required to establish the design requirements and/or constraints on the captive flight reentry system and the motor case. Because of interaction between the design of these two items, long lead time for the case, and significant development testing for the reentry system, the design requirements, concepts and materials must be defined at an early date.

1.0 SRM STAGE RECOVERY-FREE FLIGHT DYNAMICS

1.1 STATUS

The anticipated mode of SRM reentry is to force the body into an autorotation flat spin motion. No physical testing of cylindrical models in the supersonic regions has been performed to date. The dynamics of spinning bodies at large angles of attack have been theoretically analyzed by J. E. Brunk of the Advanced Technology Division, Electronic Communication, Inc., Santa Barbara, California, for the Air Force Office of Scientific Research, Office of Aerospace Research, Holloman Air Force Base, New Mexico, under Contracts AF 24(600)-2936, Project No. 7856, Task No. 78535, and AF 99(638)-1158, Project No. 7856, Task 7856-01. The aerodynamic characteristics of a cone-cylinder-frustrum of cone with autorotation spin fins at high angles of attack at supersonic speeds must be evaluated. In addition, the free-free dynamics of such a body must be analyzed, tested and evaluated.

1.2 JUSTIFICATION

This test program is intended to develop the data required for selection of the system design concepts for initiation and maintenance of the autorotational mode of free flight.

1.3 TECHNICAL PLAN

1.3.1 Objectives

This program should evaluate the complete aerodynamic and dynamic characteristics of the SRM configuration, aerodynamic parameters such as axial and normal force coefficients, pitch, yaw, and roll moment coefficients, and damping coefficients need to be evaluated.

These coefficients should be evaluated for body angles of attack from 0 to 180 deg, roll attitude angles of 0 to 180 deg for various fin sizes, fin dihedral angles, and radial and longitudinal fin location for Mach numbers of 1 thru 6. It is further desired to evaluate the body external ballistic dominant tumble modes and spin rates for reentry conditions.

1.3.2 Technical Approach

To characterize the body autorotation dynamics, detailed theoretical analysis of the aerodynamic configuration must be performed. Verification or rejection of this analysis must be accomplished by model testing. Anticipated is a three phase testing program. The first phase would evaluate the static aerodynamic characteristics in a supersonic wind tunnel. A static balance model with forward, normal at projected center-of-gravity, and aft mounted sting attachments will be required. The test configuration should be capable of varying the angle of attack and roll attitude and should be capable of varying the angle of attack and roll attitude orientation.

After the first phase static testing is complete and the data are analyzed, the second phase testing could be initiated. This phase would involve the supersonic wind tunnel testing of a spin model gimbaled and sting mounted at the configuration center-of-gravity. This test would evaluate the aerodynamic damping coefficients, and the dynamic spin modes at high angles of attack. The third phase would test the free fall dynamics by use of a scale model boosted to speed and altitude with use of a sounding rocket.

To assess the test results, the model must contain: (1) a beacon for use in radar tracking, (2) rate gyro to sense spin rates, (3) pressure transducers to evaluate altitude and dynamic pressure, and (4) a telemetry system to transmit the collected data.

If a 1/25 scale model were used, its size would be 63 in. long, 6-1/4 in. in diameter and weigh 240 lb.

1.4 RESOURCES REQUIREMENTS

1.4.1 Manpower

	Manhours
Analysis - 3 men 1 year	6,240
Balance model wind tunnel testing - 5 men 1 month	867
Spin model wind tunnel testing - 5 men 1 month	867
Sounding rocket testing - 5 men 1 month	867
	8,841

1.4.2 Specialized Facilities

Supersonic wind tunnel - AEDC

Rocket test range - White Sands MTR

1.4.3 Funding

Direct labor charge	$135,000
Equipment and materials	
Wind tunnel models (2)	100,000
Sounding rocket (3)	150,000
Sounding rocket test payloads models (3)	30,000

1.4.4 Facilities

AEDC supersonic wind tunnel	
48 hr at 4K/hr	192,000
Missile range time	
8 hr at 5K/hr	40,000
Total	$647,000

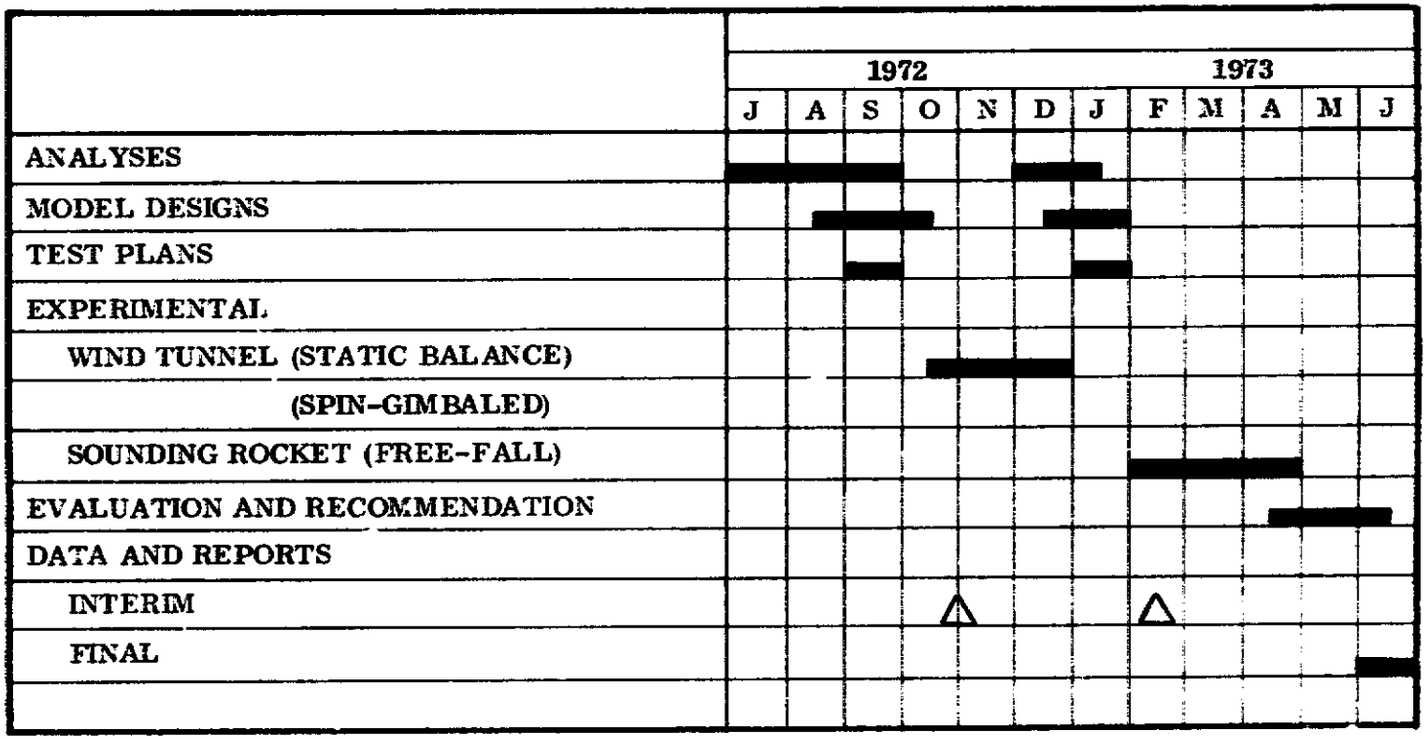

Target Schedule: SRM Stage Recovery, Free Flight Dynamics

2.0 SRM STAGE RECOVERY - WATER IMPACT

2.1 STATUS

Analytical and experimental techniques are available that are applicable, in general, to the evaluation of hydrodynamic loading and structural response of an SRM Stage during the water impact phase at recovery. However, the adaptation of particular analytical techniques must be verified by model or subscale experiments. Then through analysis and from experimental data the requirements and/or constraints will be developed for the selection of structural design and reentry system concepts and materials selection.

2.2 JUSTIFICATION

Since the recoverability and number of reuses of the SRM Stage has a significant impact on program cost, the critical condition of water impact on component survival must be studied in depth. Both the case and reentry system (chutes and, if required, energy absorbing or deceleration techniques) are long lead time development items. Hydrodynamic loadings from impact through submergence, rebound, slap, and flotation will be developed as a function of reentry flight dynamics. Structural response and failure criteria will be developed and evaluated relative to design concepts, materials, and constraints or requirements for reentry.

Substantial bodies of literature are available on the water entry of various geometries and the response of stiffened and nonstiffened shells to hydrodynamic loads. Sophisticated analytical techniques have been developed for the evaluation of blast effects on similar structures and should be adaptable to the subject problem. However, as was identified in the NASA report (NAS7-394, April 1967, National Engineering Science Co) on "Recovery of Boosters at Sea," the particular problem has not been studied in depth and significant experimental verification is required. It is understood that MSFC and some system contractors have initiated experimental programs of this nature.

2.3 TECHNICAL PLAN

2.3.1 Objectives

The objective of this program is to define the design requirements and/or constraints for the SRM Stage structure (case, nose cone, attach hardware, aft skirt) and/or the recovery system (initial conditions of water impact). Failure criteria for the stage structure will be established as a function of initial conditions so that the indicated trade study between stage and recovery system component design concepts and requirements can be performed. Inherent in this work will be the selection of requisite analytical and design techniques.

2.3.2 Technical Approach

Because of the nature of the application, the objectives of this program must be developed on a subscale or structurally and dynamically simulated model basis. The validity or accuracy of analytic and design techniques will be verified through model test such that they can be applied with confidence in the definition of requirements and constraints for and the design of the full scale components and systems.

The program is planned in four major tasks: (1) analytical techniques; (2) subscale experiments; (3) evaluation and definition of requirements; and (4) program support, data, and reporting.

Only the adaptation of existing analytical techniques and codes will be required. Current planning envisions the adaptation of blast effects codes such as SABRE for loads and elastic response predictions and the use of NASTRAN. However, other current and applicable work will be surveyed and evaluated. Significant consultant service by experts in particular aspects of the problem is planned.

The experimental program would be conducted in two parts. Two dynamically simulated models and approximately 50 tests will be required to define the various hydrodynamic loads as a function of initial impact conditions. The application of instrumentation must be studied in detail to minimize a possible interaction with results; telemetry techniques are a possible solution. One can also postulate and should evaluate that the prediction of rigid body dynamics will validate the analytic techniques and, thus, the prediction of dynamic loads and their distribution.

Structural response testing will require structurally simulated models and 15 replacement components to perform approximately 50 tests. Again, instrumentation interaction may be a problem; however, the test conditions can be planned to close on the fixture conditions. In this manner, the limiting criteria can be reasonably defined. No static tests are planned since a wealth of applicable structural stability data exists.

The experimental program will use existing drop tank facilities and experimental capabilities such as those as MSFC.

Experimental results will be evaluated and the most applicable analytical techniques for the prediction of hydrodynamic loadings and structural response will be selected. Those techniques and experimental data will be used to evaluate the interaction between requirements and/or constraints to be applied to the design of stage structure and the reentry system. In turn, recommendations can be made on the selection of stage structure design concepts and materials.

2.4 RESOURCES REQUIREMENTS

2.4.1 Manpower

The program will require 6.8 man-years of effort over fiscal year 1974.

2.4.2 Specialized Facilities

The program will require the use of an experimental drop tank facility such as that at MSFC.

2.4.3 Funding

Direct labor	$155,000
Equipment and materials	$130,000
Facilities	--
Other - Computer usage	$ 10,000
Consultants	$ 50,000
Total	$345,000

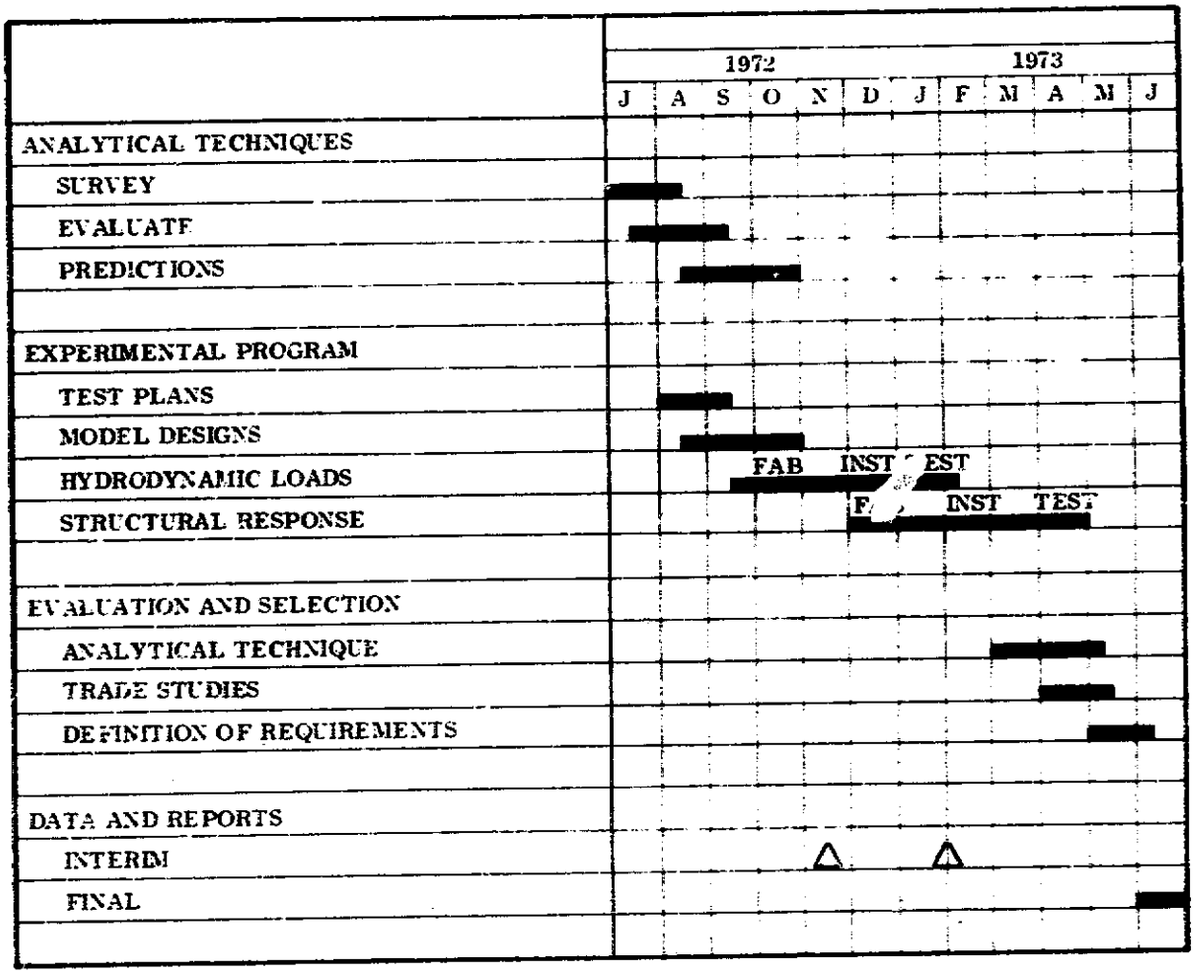

Target Schedule: SRM Stage Recovery, Water Impact

3.0 SRM STAGE RECOVERY - ENVIRONMENTAL AND CYCLIC EFFECTS

3.1 STATUS

While the materials under consideration for the SRM recoverable components are state-of-the-art, they have not, in total, been evaluated for the particular process and short term cyclic and environmental requirements. The test results will be used to select materials and, thus, in a somewhat removed context, system design concepts.

3.2 JUSTIFICATION

The recoverability and reuse of SRM components has a significant impact on program cost. Development program lead time constraints, particularly for the case, require predetermination of materials. To avoid undue design conservation the material characteristics for the particular conditions must be established. The subject materials are continually evaluated in support of various programs, but not necessarily for the particular conditions.

3.3 TECHNICAL PLAN

3.3.1 Objectives

The objective of this program is to establish the effects of the particular SRM Stage recovery environment and reuse (short term cyclic) history on critical material design characteristics and then recommend the best material for each component. The planned goal is a minimum of 10 uses and the necessity or reproof testing must be established.

3.3.2 Technical Approach

The program will initiate with an indepth survey of applicable data on the candidate materials. Current planning includes three case materials [D6AC (200 ksi), 18 Ni (200 ksi), HY-140] and three stage structural materials (6061-T6 aluminum, a standard structural steel, HY-140). The primary factors of evaluation will be corrosive mechanisms, the effect on strength and toughness, and requirement for and types of protection. The variables to be studied are time of exposure, component temperature during exposure, residual stresses, refurbishment techniques, cyclic effects, and inherent initial fabrication constraints.

The testing will be so planned that the materials are evaluated for the anticipated value of the variable and at a value toward either extreme. Baseline parent and welded material data will be established relative to the applicable processes. Exploratory testing will be performed relative to the mechanism and rate of material degradation and the value of various protective techniques. Based on the results of the survey, and exploratory tests, a detailed parametric test matrix will be planned and implemented.

The test results will be used to recommend the most suitable materials for the motor case, nose cone, stage attachment hardware, and aft skirt. The requirements or constraints on recovery and refurbishment techniques, protective coatings or techniques, and component retest relative to the materials studied will be determined.

3.4 RESOURCES REQUIREMENTS

3.4.1 Manpower

The program will require 4.5 man-years of direct effort.

3.4.2 Specialized Facilities

No special facilities are required.

3.4.3 Funding

Direct labor	$135,000
Equipment and materials	$ 75,000
Facilities	--
Other	--
Total	$170,000

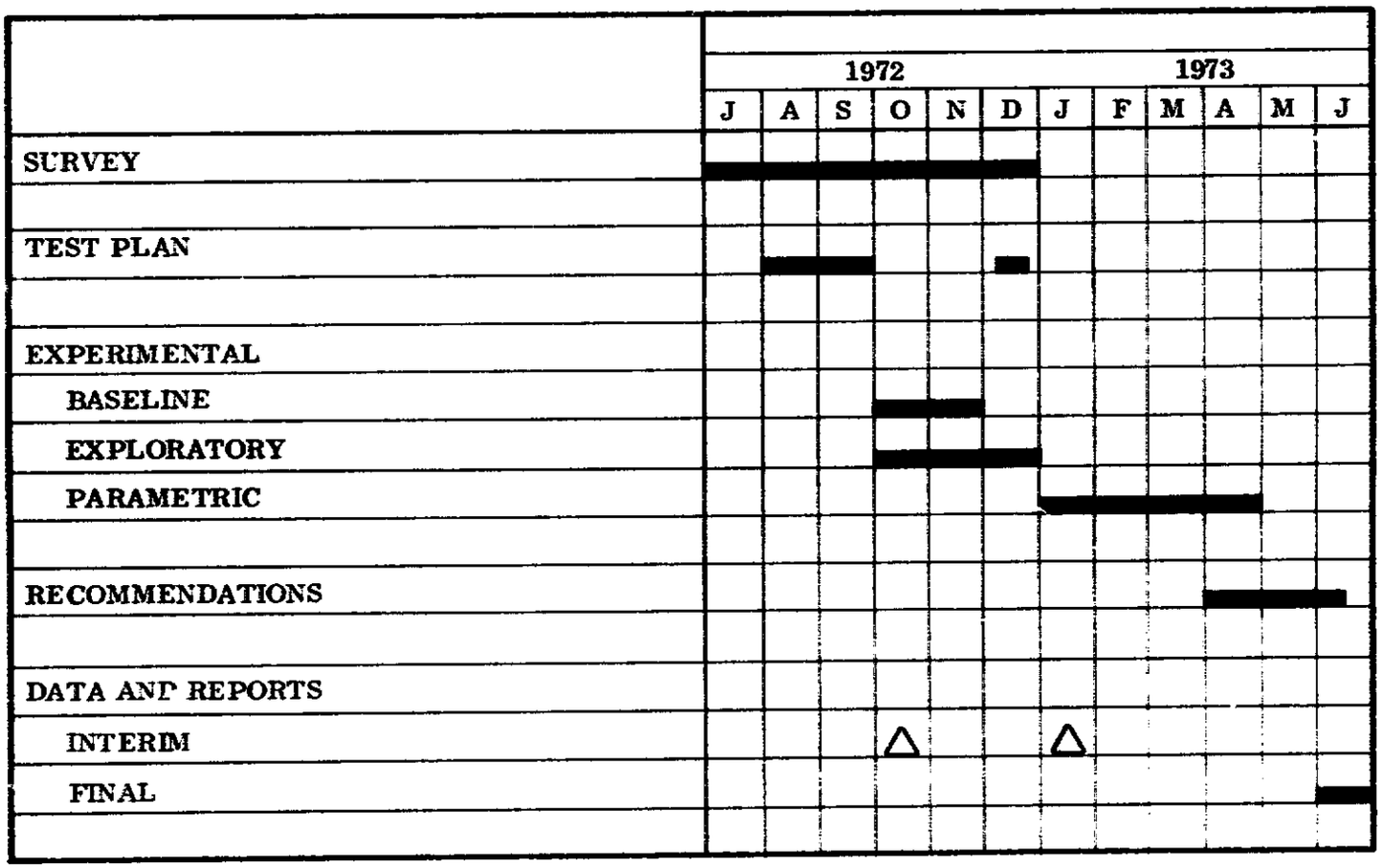

Target Schedule: SRM Stage Recovery,
Environmental and Cyclic Effects